Mineralogie

The Bond-valence deficiency model

A new application to describe mineral surface reactions

Inaugural-Dissertation

zur Erlangung des Doktorgrades

der Naturwissenschaften in Fachbereich Geowissenschaften

der Mathematiscch-Naturwissenschaftlichen Fakultät

der Westfälischen Wilhelms-Universität Münster

Vorgelegt von

Andreas Mutter

aus Pirmasens,

Bundesrepublik Deutschland

-2007-

Dekan	Prof. Dr. Hans Kerp
Erster Gutachter	Prof. Dr. Andrew Putnis
Zweiter Gutachter	Prof. Dr. Wulff Depmeier
Tag der mündlichen Prüfung	11.04.2007
Tag der Promotion	

Contents

1. Introduction

Since the early times of human history, mankind has been fascinated by the beauty of minerals. This curiosity has not changed since, but besides their attribute of pure beauty, crystals and minerals provide the resources without which the cultural and social evolution of the modern ages would not have been possible.

Minerals, crystals and stones in general are used among many other applications as building stones, fertilizers, cleaning agents, isolators, electric conductors and so on. Their field of application is manifold as they satisfy many of our daily needs.

In the beginning of the technical application only the most visible attributes of minerals, such as hardness and durability or their metal content was of interest. Today, in modern technology “secondary” attributes such as conductivity, magnetic properties and the reactivity of crystal surfaces play a vital role.

Especially the interest on the reactivity of minerals has increased, as our understanding of the interaction of minerals and the environment evolved. This curiosity has lead to the development of a new side branch in mineralogy, broadly referred to as Mineral Surface Science.

The understanding of the reactivity of crystal surfaces, the growth of crystals, their dissolution or inhibited growth, the ability of surfaces to adsorb heavy metals or other pollutants and the understanding and control of bio-mineralization, are only some of the new aspects research is focused on.

Increasing this knowledge, together with the development of new models, describing principal mechanisms and processes influencing the growth and morphology of crystals, and hence the reactivity of their surfaces, will have influence on our daily lives, as well as it may change our attitude towards our environmental setting.

The intent of the research presented is to develop a methodology, which can easily be referred to while describing crystal growth processes, as well as mineral surface reactions. This model is proposed to be a tool, a method to be applied when approaching mineral surface reactions for the first time. It may to some extent be an alternative to molecular dynamic simulations, in so far as predictions of crystal morphologies and minerals surface reactions are possible and can be obtained in relatively short time periods. The strength of this model is its fundamental concept based on the principles of the bond-valence theory.

The bond-valence theory has proven to be a valuable tool and is readily applied in order to refine internal crystal structures, by surveying for example the number and "strengths" of bonds formed between the constituents of a crystal. Diverging bond-valence sums around an atom within the crystal structure are treated as an indication of possible defects in the crystal structure, or even worse, indicate an insufficient crystal structure analysis.

On the other hand, missing bond-valences or insufficient bond-valence sums are natural to atoms at mineral surfaces, and to a large extent these unsatisfied bonds control the readiness of a crystal surface to participate in chemical reactions. The number and thus the "strength" of these bonds can easily be calculated and is addressed as the "bond-valence deficiency" of an atom, ion, molecule or crystal surface. Obtained bond-valence deficiencies of different crystal faces of a mineral are comparable, and can be used as indicators to predict the crystal morphology. This new concept of the bond-valence theory can be applied to crystal surfaces and solvents alike, and it can be used to interpret the processes and interactions occurring at crystal surfaces, the interfaces between a solid and a solution.

Chapters 2 and 3 are to be considered as historical overviews about various different methods, which have been applied to described crystal growth processes. Chapter 4 is a general introduction into the bond-valence theory, while Chapter 5 considers the newly

developed bond-valence deficiency model. The usefulness of this approach is tested in Chapter 6, concerning morphological surface features of uranium-minerals.

Further developments of the bond-valence deficiency model are stated in Chapter 7, in which the synthesis of internal crystal factors and the bond-valence deficiency model is demonstrated. This combination is based on different aspects of the theories described in Chapter 3 and concludes that internal crystal factors, such as crystal symmetry, lattice density and reticular density can be incorporated into the bond-valence deficiency model. This combined approach can be applied to predict the “abstract crystal form ” of crystals and is discussed for several crystal structure types in Chapter 8. In Chapter 9, the bond-valence aspects of liquids and solvents are outlined and some considerations about the interaction of aqueous solutions and mineral surfaces are given in Chapter 10, while Chapter 11 is dedicated in detail to the influence of impurities on the crystal morphology interacting with a crystal surfaces.

2. The morphology of polyhedral crystals

All the various morphological features of crystals, such as polyhedral, hopper, dendritic and spherulitic can be described as being the results of the interplay of internal structural and external factors, involved during crystal growth.

If, for example the physico-chemical conditions of the environment change, growing faces may disappear and new faces develop. Such changes lead to variations in the Tracht and Habitus of a polyhedral crystal. Therefore it is worth not only to address the morphology as a whole, but to distinguish between Tracht and Habitus of a crystal, because such changes give hint of differences of the external factors involved during crystal growth. While the term Tracht describes the number and combination of the faces (e.g. hexahedron, octahedron), the term Habitus relates to the size and development of these faces (e.g. prismatic, platy).

Tracht and Habitus may change during growth and it is necessary to mention the "stage of growth" concerned. Therefore, terms such as "structural form", "abstract form", "equilibrium form" and "growth form" have been introduced, to provide a better understanding of the origin of polyhedral crystal morphology.

Even though it seems reasonable to distinguish between changes in Tracht and changes in Habitus, these terms are mainly used in the German literature. On the international level, both terms Tracht and Habitus are compiled within the term "crystal morphology", as a more general approach.

2.1 Different "forms" of polyhedral crystals

It is known empirically that the order of morphological importance of crystal faces is closely related to the lattice type of the crystal. Historically the habit of polyhedral crystals was predicted by neglecting the influences of the growth conditions (BRAVAIS 1866, NIGGLI 1920, DONNAY & HARKER 1937). The theoretical crystal forms obtained were called "*structural forms"* or *"abstract forms"*, as they were derived considering only the internal crystal factors, such as symmetry and lattice types.

The thermodynamic approach is to analyze the habit of polyhedral crystals when they have reached their equilibrium state and the "forms" obtained by this method are called *"equilibrium forms"*. GIBBS (1906) considered that a crystal, should, at equilibrium, take a form in which the product of the total surface area times the surface free energy is at a minimum. A crystal in this state has an "equilibrium form", which is unique for a given temperature and pressure condition (SUNAGAWA 2005).

The term *"growth form"* of a polyhedral crystal is used when the attention is focused on external factors controlling the growth. Tracht and Habitus vary greatly depending on the growth environments and conditions. Habitus and Tracht may change during the growth process of a particular crystal, or they may be different among crystals of the same species formed under different conditions.

The growth form of polyhedral crystals appears as a result of different normal growth rates termed "R", of different crystal faces or among different, crystallographically equivalent, faces. Crystal faces with large "R" will disappear; only those with small "R" will survive. When a crystal reaches an equilibrium state, the crystal will be bound by crystal faces with the smallest surface free energy called "γ", namely with the smallest "R". This is the equilibrium form. However, before reaching such a state, the crystal will exhibit different Tracht and Habitus determined by the relative ratio of "R" values (Fig.: 2.1). These intermediate "forms" will be called the "growth forms" of a polyhedral crystal (SUNAGAWA 2005).

The structural and equilibrium forms of crystals can be predicted by assuming that the crystal is perfect and that the ambient phase is isotropic. Growth forms, however, describe real crystals containing lattice defects growing in a real ambient phase. (SUNAGAWA 2005).

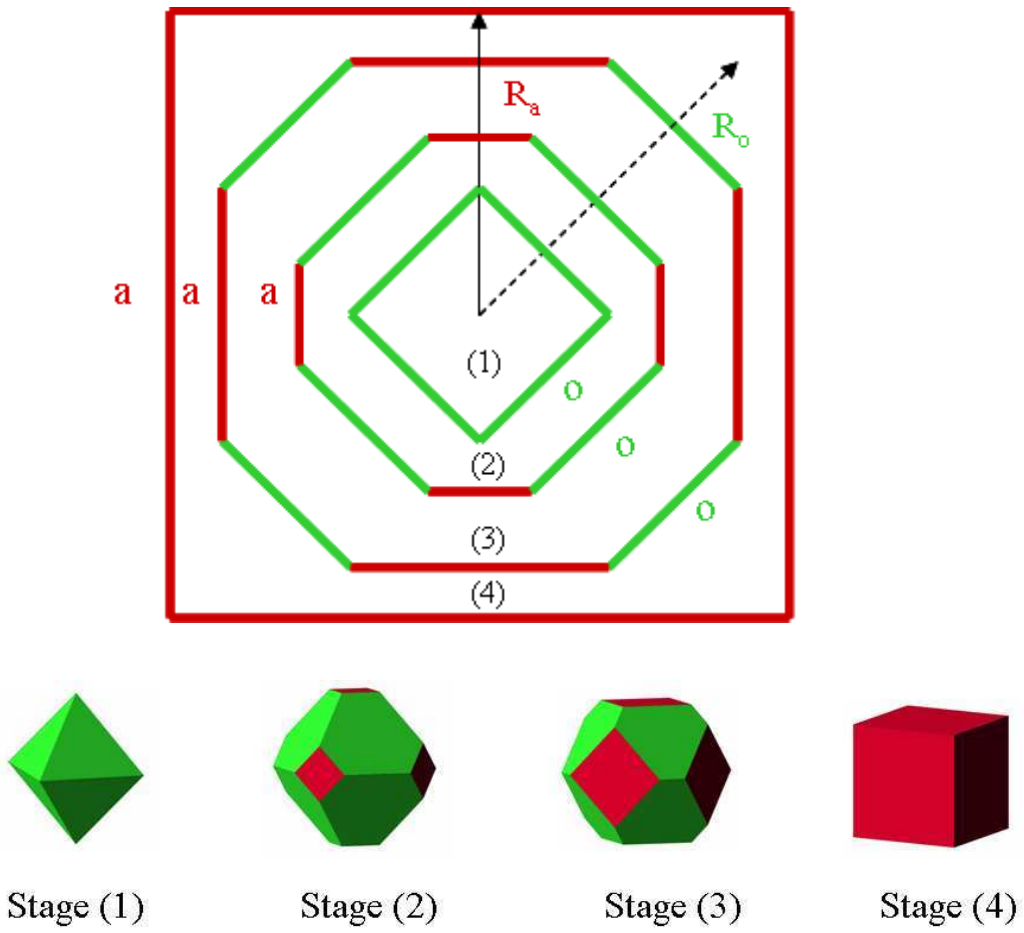

Fig.: 2.1 The influence of different growth rates "R" for different crystal faces is given in this figure. In this example the growth rate of the face "o", marked green is higher than the growth rate of the face "a", marked red. Starting at the initial stage (1) the influence of the different growth rates can be observed as the crystal grows in size (stages 2 and 3) until it reaches the end form stage (4). Stages (2) and (3) may be addressed as the "growth forms" of the crystal, while stage (4) represents the "equilibrium form" or "final form"

2.2 Mineral surface features

As mentioned earlier we have to distinguish between internal and external factors controlling the growth and hence the shape or habit of a crystal. In this sense, it is the interaction between different external factors and the mineral surface, which controls the growth rate "R" of a crystal face. Therefore, the crystal surface can be addressed as the interface where both internal and external factors meet, and it is necessary to describe this interface exactly.

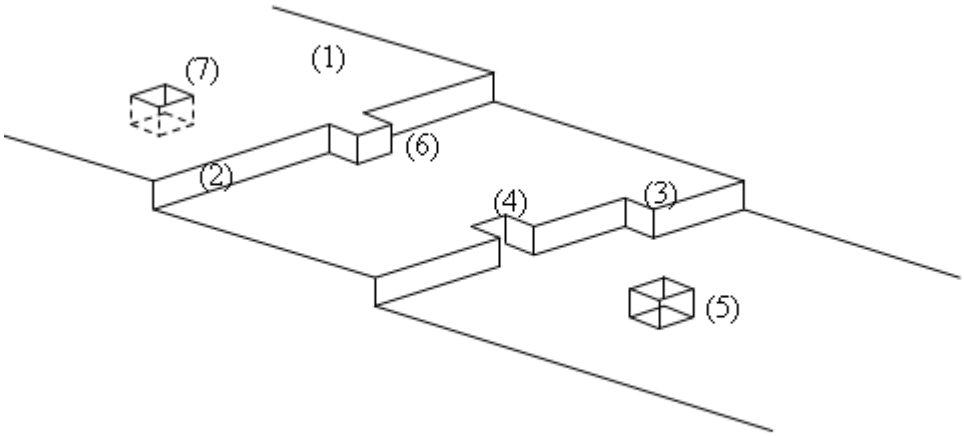

Fig.: 2.2 Diagram illustrating some of mayor topological features of a mineral surface. (1) terrace, (2) step, (3) kink-site, (4) vacancy at a step, (5) adatom on a terrace, (6) adatom at a step, (7) vacancy on a terrace (modified from LASAGA, 1990).

With the development of new techniques to investigate mineral surfaces in more detail, the interest in the microtopography of mineral faces increased. A general model of microtopography of a crystal surface was proposed and is shown in Fig. 2.2 (LASAGA, 1990). This general model, which was introduced first by BURTON et al. (1951), has

been developed from growth, dissolution, and other surface studies, and compiles most of the common features of crystal faces.

According to this model the surface consists of flat areas, called “terraces”, which are separated by “steps”. In their simplest form, steps are one atomic layer high, although they can be considerably higher than this. “Kink-sites” appear where there is a corner on a step, and the step changes direction. An atomic or molecular-size hole in a terrace is called a “vacancy”, which as it grows in size, can develop to an “etch-pit”. The opposite of this, that is an atom or molecule sitting on top of a terrace, is called an “adatom” or “admolecule”, respectively.

Considering only surface atoms, the atoms that make up the terrace have the greatest number of surface neighbors. At the edge of a step, the number of nearest neighbors is reduced, and atoms at the outer corners of kink-sites have even fewer neighbors. Adatoms generally have the fewest nearest neighbors of all surface sites, and adatoms sites are potentially, but not always, the most reactive sites on a surface (LASAGA, 1990).

The given description relates well to the bond-valence model, mainly with the approach of bond-valence deficiencies (Chapter 5). For example, atoms on a terrace of the surface, having the greatest number of neighbors, will have a low bond-valence deficiency, while edges or steps, having less neighbors, have a higher bond-valence deficiency.
Therefore, flat faces will show different surface reaction mechanism compared to stepped faces or kinked steps, and as a result, special attention has to be given to the overall topology of the crystal faces concerned.

2.3 Changes in "Crystal morphology"

While the internal crystal factors, such as symmetry, reticular density and lattice spacing can be applied to describe the "abstract forms" of minerals, the influence of external factors needs to be taken into account to describe the "equilibrium" and "growth forms". External factors are numerous (such as pressure, temperature, supersaturation, impurities), and their impact on the crystal morphology plays a fundamental role in determining the crystal morphology. These external factors either enhance or inhibit the growth rate of crystal faces. The use of inhibitors to hinder, the growth of barite crystals during offshore oil-explorations, is an example of the technological relevance of the research on external factors controlling crystal growth processes (PINA et al., 2004).

When a crystal is bounded by many faces, it can be observed that a face with a lower order of morphological importance will show a roughening transition at a lower temperature than a face with higher order of morphological importance (SUNAGAWA 2005).

The roughening transition can be related to changes in the growth mechanism of a crystal face. HUMAN et al. (1981) found a correlation between the temperature at which a crystal is growing, its growth rate and its driving force (e.g. the concentration of the solution). They argued that :

> When a face on a crystal is growing at a temperature, having a certain value, the so called "roughening temperature" (T_R), the face will be rough on an atomic scale. This face will then grow "continuously", and a linear dependence of the growth rate and the driving force will be found. When the face is growing at a temperature below T_R and below a certain value of the driving force, the face is smooth on an atomic scale and a non-linear relation between the growth rate and the driving force will be found.

Cooling or heating of a solution can therefore change the morphology of a crystal, according to whether the solubility and/or the supersaturation is increased or decreased. Pressure will also have an effect as well as the degree of impurity concentration (SUNAGAWA 2005). Besides temperature and pressure, the composition of the solution in contact with the mineral surface is one, if not at the end the mayor key factor controlling the relative growth rates of minerals.

The first step of crystallization is nucleation. Nucleation can only occur when the solution is supersaturated with the crystal forming solute. This stage of supersaturation can be reached by manipulation of the solution. Common methods to achieve supersaturation are cooling or heating of the solution (see above), evaporation, pH changes, mixing different solutions containing different soluble species and many combinations of these methods.

Such manipulations of the solution in respect of changing the saturation affect not only the nucleation, but are as important during the further growth of the crystal. This is due to the fact that different crystal faces do not have the same behavior in highly or weakly supersaturated solutions. An overview of crystallization mechanisms in solution starting from the point of supersaturation until to the point when habit modifications take place, is given by BOISTELLE & ASTIER (1988) and their references stated.

Each of these external factors leaves a trace in the morphology of the crystal, and each new process or coupled process identified helps to interpret the settings of crystal growth or dissolution processes.

3. Theories of crystal growth (Historical overview)

Historically one of the first theories that gained serious consideration by crystallographers was that of CURIE (1885). He proposed that there is a close connection between the crystalline form and the surface energy of the solid. This assumption was derived from the capillarity theory of GAUSS (1830) elaborated for liquids (BUCKLEY, 1951). Wherein GAUSS stated that the virtual work in capillary phenomena should be separated into a "volume" function and a "surface" function.

CURIE´s analogy between a liquid and a crystalline solid is far from complete, as a liquid can change its shape (e.g., be deformed in a manner incompatible with a crystal). He assumes that the equivalent of "deformation" in a crystal is that of transferring a quantity of crystalline matter from one type of crystal face, to another. Therefore in crystals, since they are practically incompressible, the volume function becomes negligible and the virtual work due to capillary forces is proportional to the change of the surface alone. This led to the assumption, that the "end form" of a crystal will be consistent with its minimum sum of total surface energies (BUCKLEY, 1951).

As an introduction to the bond-valence deficiency model, outlined in this thesis, some of the most common crystal growth theories are described in short in the following chapters. This introduction is intended to give on overview about some of the basic principles of crystal growth theories known today. While most of these profound concepts have been incorporated into the bond-valence deficiency model it is necessary to refer to their historical background and setting to recognize their impact on the development of this new approach to describe crystal growth processes.

3.1 Wulff extensions to the theories of Curie and Bravais

In 1901 Wulff published a paper about crystal growth and dissolution of crystal faces, which today can be regarded as a summary or extension of different crystal growth theories known by that time.

He recognized that there are two aspects of crystal growth. One being the extension of a face sideways (called “extension”), the other being the growth along the face normal (called “growth) The former largely depends on the latter. Wulff concluded, for example, that the speed of “extension” of a crystal face is larger while its “growth” speed is low, or, that crystals will promote such faces having the lowest growth rate. He derived these considerations by a graphical assumption given in Figure. 3.1.

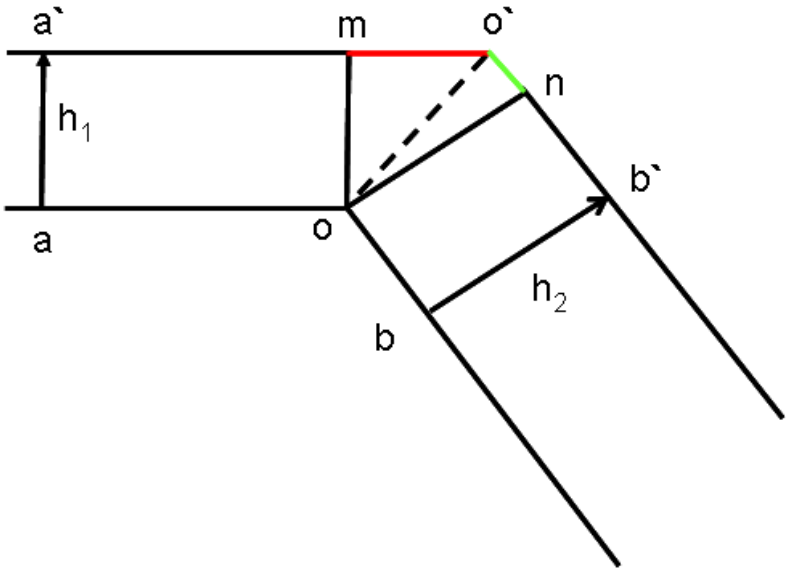

Fig.3.1 This figure, form WULFF (1901), illustrates the correlation between the “extension” of a crystal face and the ”growth” velocity parallel to the face normal. Given are two faces “a” and “b”, joined at point “o”. After a given time “t_i” the faces have advanced to the positions a` and b`, now joining at point o´. During time “t”, face “a” has advanced at the rate h_1 and face “b” at the rate h_2 ($h_1 < h_2$). After time “t”, the extension of the slow growing face “a” equals the distance m – o` (red), while the extension of face “b” equals the distance n – o´ (green). The length ratio being m-o` > n-o`. This graphic clearly indicates the correlation between a slow growing face having a high rate of extension compared and a faster growing face having a low rate of extension.

From this graphical approach (Fig. 3.1) it is possible to derive the consideration that the amount of extension of a face sideways ("ε_i"), can be considered proportional to the vector ("h_i") of its growth rate in the direction of its face normal. This can be formulated as:

$$\frac{\varepsilon_1}{h_1} = \frac{\varepsilon_2}{h_2} = \frac{\varepsilon_3}{h_3} = ...const. \qquad [3.1]$$

WULFF (1901) further showed that it was possible to combine his theory of the relative growth rates of crystal faces (WULFF, 1901; WEYBERG, 1901), with the theories of CURIE (1887) and BRAVAIS (1866). This application is discussed in detail by LAUE (1943) and is summarized below:

In 1878 (GIBBS) and 1885 (CURIE) derived an equation to describe the "equilibrium form" of a given crystal:

$$\Phi = \sum_{[i=1]}^{N} \sigma'_i F_i \qquad [3.2]$$

The total free energy Φ of a given crystal, can be described by the total sum of the free energies σ_i of the number (N) of faces F_i.

Similar to this, CURIE (1987) considered the capillary constants of crystal faces to be crucial to decide which faces will determine the morphology of a crystal. Curie argued that the capillary constant (k_i) is a characteristic energy at the interface of two media, such as e.g. the crystal surface (s_i) and a solution. This energy has to be dissipated before the interface can be promoted any further. He concluded that the most "stable form", e.g. for a given body with the faces $s_1 + s_2 + s_3 + \ldots$, and these faces having the capillary constants $k_1 + k_2 + k_3 + \ldots.$, is such that the sum $s_1k_1 + s_2k_2 + s_3k_3 \ldots$tends to have a minimum value.

WULFF (1901) observed that by measuring the relative growth rates of crystal faces the capillary constant of these faces may be determined directly. Therefore, he concluded that there is an analogy of his concept of crystal growth rates and the theory of CURIE (1887) considering the influence of the capillary constant of a crystal surface. WULFF (1901) concluded that the concept of Curie could be simplified by introduction of the growth vector (h_i), of the length of the face normal.

As these assumptions of Wulff have proven to be crucial for the further development of crystal growth theories, the example given by WULFF (1901), correlating the growth rate of crystal faces with the capillary constant of crystal faces, and hence with the surface energy, is given here as a summary, starting with the assumptions of CURIE (1887):

CURIE (1887) argued that: *if one considers the capillary constants A and B of the surface of a cube and octahedron of a regular crystal, "x" being the length of the edge cut of the hexahedron by the octahedral face, and "b" the residual length of the edge of the hexahedron the cube-octahedron would be in equilibrium with the solution if:*

$$x = \left(\frac{3}{2} - \frac{B}{A} \frac{\sqrt{3}}{2} \right) b \qquad [3.3]$$

From this relation (equation 3.3), CURIE deduced that the cube would stand alone if:

$$\frac{x}{b} = \frac{3}{2} - \frac{B}{A} \frac{\sqrt{3}}{2} \qquad [3.4]$$

$$\frac{A}{B} < \frac{1}{\sqrt{3}} \qquad [3.5]$$

Analogue, the octahedron would be the equilibrium form if:

$$\frac{A}{B} > \sqrt{3} \qquad [3.6]$$

WULFF (1901) summarized these observations in a formula to describe the general conditions of stability of these two faces present at the cube-octahedron:

$$\frac{x}{b} = \frac{3}{2} - \frac{B}{A}\frac{\sqrt{3}}{2} \qquad [3.7]$$

He deduced that equation [3.7] can be simplified by substitution of "x" and "b", by the vectors "ω" and "γ", representing the values of the faces normal (h_i) for the octahedron (ω) and the cube (γ), and he defined the equation:

$$\frac{\omega}{\gamma} = \frac{B}{A} \qquad [3.8]$$

leading to the formulation: that the distances of the faces of the octahedron and the cube from the center of the crystal ("Wulff-point) are proportional to the capillary constant of the respective faces.

Finally, WULFF (1901) interpreted this law graphically. No matter if one considers the capillary constant or the total free energy of a crystal (Φ), a "central point" within a crystal can be detected referred to as "Wulff´s point". The distances of the face normals (h_i) of the faces (F_i) and this point are proportional to the free surface energies σ_i, or the capillary constants. Considering the free surface energies (σ_i) this relation can be written as:

$$\frac{\sigma_1}{h_1} = \frac{\sigma_2}{h_2} = ... = \frac{\sigma_N}{h_N} \qquad [3.9]$$

In order to construct the "equilibrium shape" or the form of minimum free energy of a given polyhedral crystal graphically (Fig. 3.2), one needs to construct from the Wulff-point the face normal (h_i), with the length $p\sigma_i$. At the end of the line $p\sigma_i$, the face F_i perpendicular to h_i is drawn. If the faces F_i belong to the "equilibrium form" of the

polyhedron, the shape of the closed form of the polyhedron is described by these faces. If the surface free energies σ_i of all possible faces turns out to be equivalent to:

$$\frac{\sigma_1}{h_1} = \frac{\sigma_2}{h_2} ....const \qquad [3.10]$$

the "equilibrium form" constructed resembles a sphere.

In those cases where σ_i differs, only such faces, leading to the smallest possible closed polyhedral form are regarded to be part of the "equilibrium shape" (Fig. 3.2).

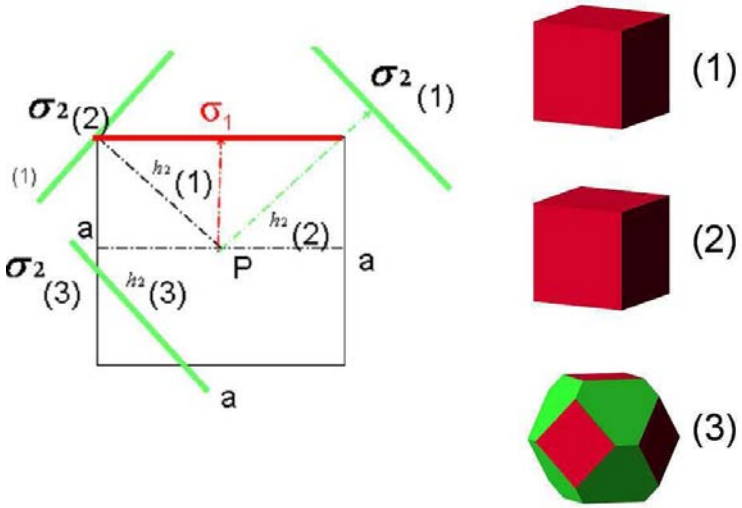

Fig.: 3.2 Schematic Wulff construction of a polyhedral crystals. Starting from the center of a polyhedral crystal (P = Wulff´s point) the face normals to (001) in red and (111) in green are plotted. The length of the vectors h_i is proportional to the measured velocity of growth (see text). Given are three cases with different growth velocities for (111). In the first case (1) the growth velocity of the (111) face is much faster than the growth velocity of the (001) face. Hence the construction line of the (111)-face is beyond the (001)-polygon. The resulting "equilibrium form" is a cube. In case (2) the growth velocity of (111) is lower, but the construction line of the (111)-face is just barely out off the (001)-polygon. Hence the "equilibrium form" is a cube. In case (3) the growth velocity of (111) is very slow. In this case a cube-octahedron resembled the "equilibrium form".

During the decades the Wulff-equation and the graphical Wulff-plot have proven to be applicable to fit the needs of different crystal growth theories (TOSCHEV, 1973; BENNEMA, 1973). No matter which method has been applied, even up to the extent of modern thermodynamic approaches, the results obtained are still cross-checked by construction of a Wulff-plot. This is due to the general concept of the Wulff-equation, by which it is possible to compare different attributes of crystal surfaces by considering the surface properties as a reciprocal functions plotted as the length of a face normal.

3.2 The Reticular-Density Theory of Bravais

Developments in crystal-growth theories led to the effort to associate the observed crystal habit with prevailing crystal structure theories. BRAVAIS (1866) was the first to account for a relation between the unit-cell geometry and the origin of different faces exhibited by different crystal species. He connected the habit of crystals with the particle density of net planes in a crystal-lattice. This approach can be summarized as the Bravais´ laws:

1. Observed crystal faces are parallel to the net planes with the highest reticular density.

2. The greater the reticular density the more important the corresponding crystal face.

The importance of a crystal face is estimated from its size, frequency of occurrence, and the presence as a cleavage face. The reticular density of a net plane (hkl) is defined as the number of lattice points per unit surface. It is inversely proportional to the reticular area, or area “S” of the smallest mesh in the net, and directly proportional to the interplanar distance “d”.

This correlation can be written as:

$$S \times d = V \tag{3.11}$$

where V, the volume of the smallest unit cell, is a constant for any lattice (DONNAY & HARKER, 1937).

According to Bravais´ laws, planes of maximum density (highest reticular density) are those, which during growth move forward (normally to themselves) at the slowest rate. Consequently they extend tangentially to exclude more rapidly depositing planes with a lower reticular density (3.3).

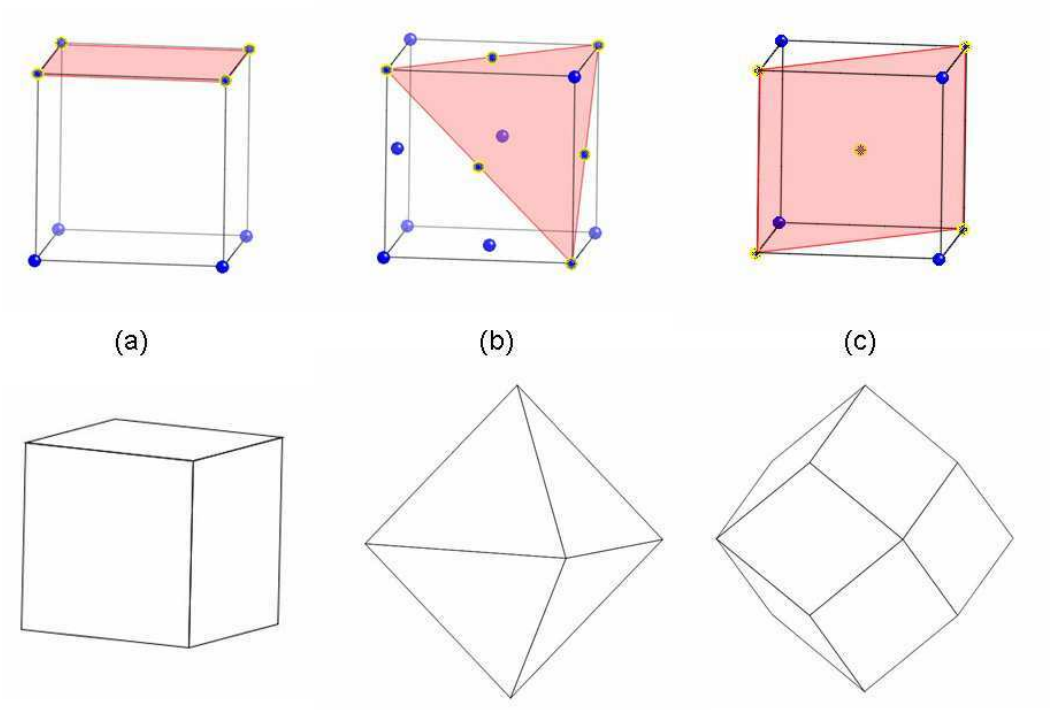

Fig.: 3.3 Given are the constructions of (a) Pm3m, (b) Fm3m and (c) Im3m Bravais-lattices. Marked in red are the planes with the highest reticular density of lattice points in the given Bravais-lattice. Below, polyhedrons corresponding to these faces with the highest reticular density of lattices points are plotted.

WULFF (1901) referred to this theory of BRAVAIS (1866), proposing that the surface energies, and therefore the rates of crystal growth, are inversely proportional to the reticular densities of the planes of the crystal (BUCKLEY, 1951). Those faces "surviving" at the end would be those having the greatest density of atoms.
SOHNKE (1888) deduced that the ions or atoms of faces with a high reticular density are not capable of promoting any further work to move closer together, and therefore the potential energy of such a face must be at minimum. Further he stated that reducing the packing of a face, lowering its reticular density, will increase the surface energy, which as well can be described by an increase of the capillary constant of the respective face. From these observations WULFF (1901) derived his correlation between the reticular density of a crystal face and the respective capillary constant on the one hand and the capillary constant and the growth velocities of crystal faces on the other.

The theory of Bravais´ was the first method to consider the particular crystal structure to attribute for the morphology of a crystal, but after some time the restrictions of his theory came to be noticed and further amendments had to be made. First the influence of the planar spacing was considered by NIGGLI (1920). Then DONNAY & HARKER (1937) extended the law of Bravais to include not only simple symmetry operations such as rotation–axis and mirror-planes, but also screw-axis and glide-planes. Their intention was to introduce a new law for crystal morphology, which considered all different symmetry operations present in the 230 space groups

3.3 Niggli´s extension to the Law of Bravais

NIGGLI (1920) developed a model of crystal growth, which is a logical consequence of the view´s of Bravais. Considering Bravais´ approach, and as a result the relation that the velocities of growth of various faces are inversely proportional to their reticular densities, Niggli regarded the density of lattice spacing of these faces (net planes), as being an additional factor to be considered.

The density of planes in a lattice is related to the width of separation (e.g., to the "spacing," $\delta_{(hkl)}$). From this NIGGLI (1920) concluded that a higher spacing of $\delta_{(hkl)}$ will correspond with slower rates of normal extension. A narrow spacing implies that, over a given distance in a direction normal to (hkl), there will be more planes upon which the atoms are strung, so that there will be fewer atoms per plane (Fig. 3.4).

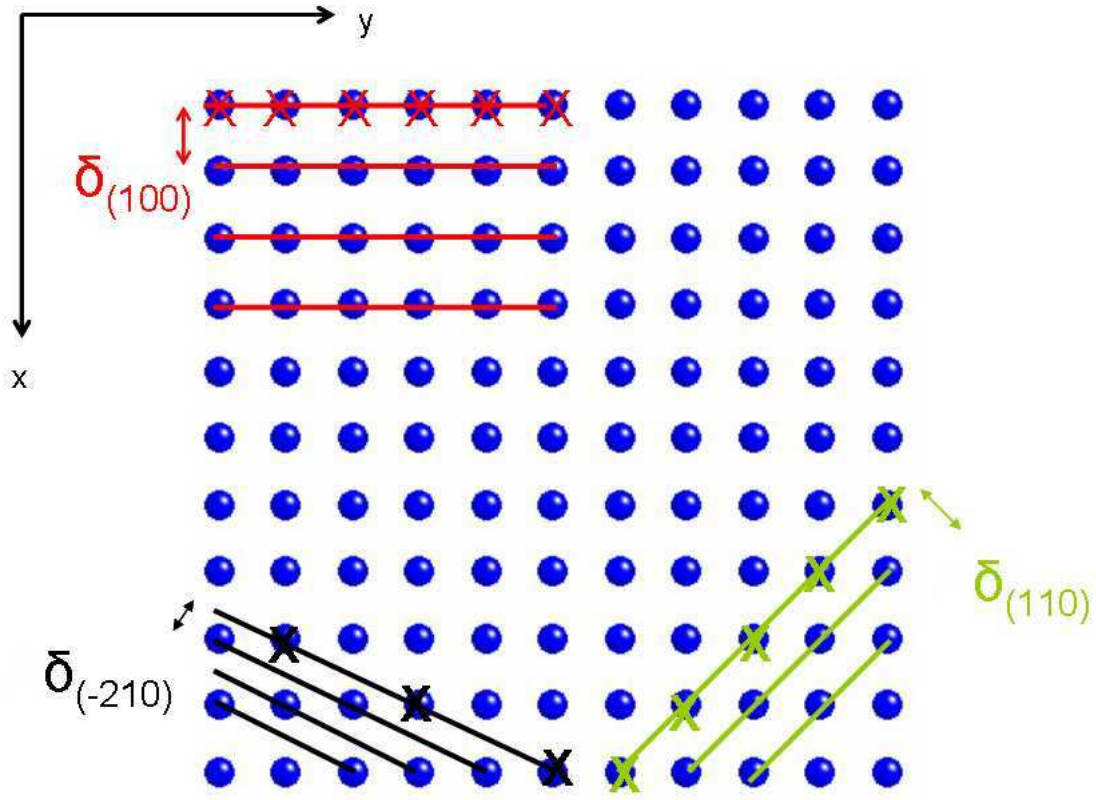

Fig.: 3.4 View perpendicular to a Primitive cubic lattice. Planes running parallel to (100) have a higher reticular density (number of lattice points marked X) as planes running parallel (110) or (-210). Further the planes parallel to (100) have a higher spacing $\delta_{(hkl)}$ compared to the planes parallel to (110) and (-210). The application of the Law of Bravais and the extension of Niggli would therefore state, that the order of importance of these faces will be (100) < (110) < (-210).

3.4 The Donnay and Harker Theory

DONNAY & HARKER (1937) expanded the Bravais´ law based on the geometry of 14 lattice types to include the symmetry operations defining the 230 space groups. Basically the effects of translation symmetry operations such as screw axis and glide planes were now taken into consideration (Fig.: 3.5). This method proved to be fertile as most of the discrepancies noted between the observed forms and the calculated forms based on Bravais´ law diminished. In addition the theory of DONNAY & HARKER (1937) pays attention to the lattice spacing density theory proposed by NIGGLI (1920).

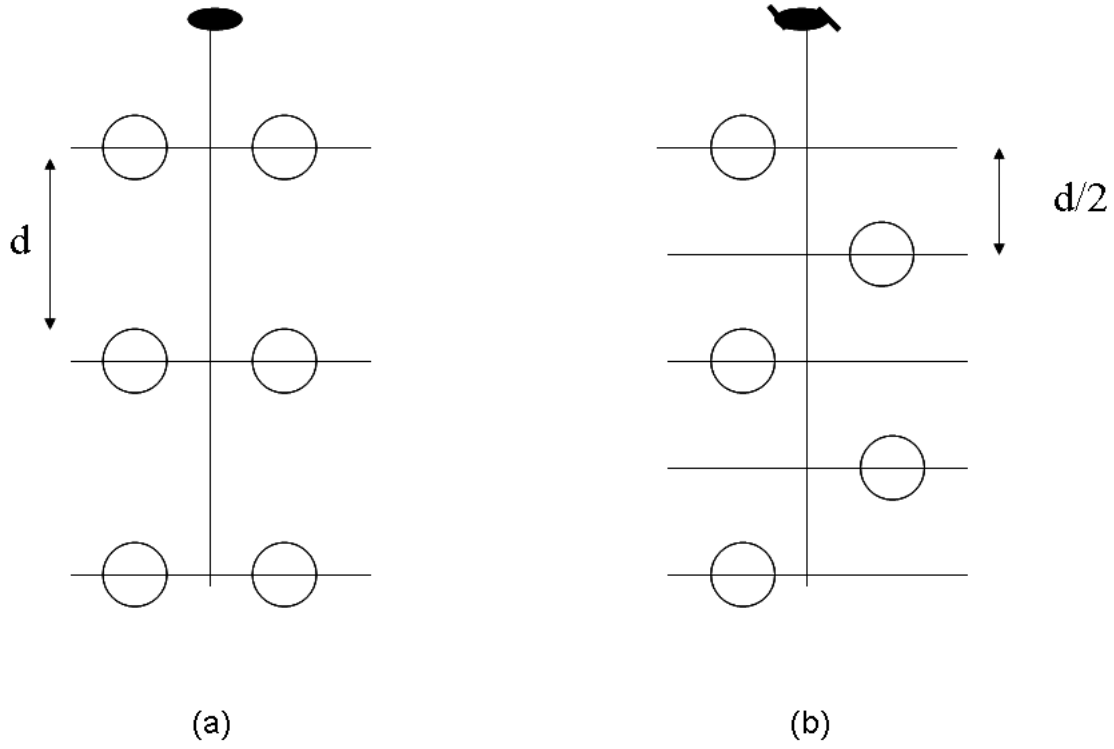

Fig.: 3.5 Comparison of a 2-fold rotation axis (a) with a 2-fold screw axis (b) and their influence on lattice spacing. Due to the translation vector of ½, additional lattices at a distance d/2 are formed perpendicular to the 2-fold screw axis, compared to the lattice distance d of the 2-fold-rotation axis.

Quartz and pyrite are two common examples to show that predicting the morphological ordering of crystal faces according to DONNAY & HARKER (1937) correlates better with observations of natural samples.

The polyhedral form of quartz, considering its lattice type only (Bravais´-law), should be bounded by three equally developed faces {0001} = {$10\bar{1}0$} = {$10\bar{1}1$}. However the {0001} face appears only exceptionally rarely in real quartz crystals. This discrepancy can be explained by the Donnay & Harker theory due to the presence of a three-fold screw axis perpendicular to {0001}. Recalculation of the reticular density of the basal pinacoid considering the screw component, transforms {0001} into {0003}, lowering its morphological importance drastically.

According to Bravais´ law, the sequence of morphological importance of the faces of pyrite should be {100}, {111}, {110}. In natural samples faces parallel to {110} are rarely observed. Instead faces parallel {210} seem to be dominant instead. This difference can be explained by the approach of Donnay & Harker due to the presence of a glide plane, transforming {110} into {220}.

3.5 The Periodic Bond Chain Theory (PBC)

One of the most known theories to predict crystal morphologies is the Periodic Bond Chain Theory (PBC-Theory) of HARTMAN & PERDOK (1955 a,b,c). Their approach is based upon similar ideas as those of Bravais and Donnay-Harker, but instead of paying attention to the importance of planes, Hartman-Perdok focused on "zones". They classified the crystal faces into three different types (Fig.3.6), F-faces (flat faces), S-faces (stepped faces) and K-faces (kinked-faces). This differentiation depends on the number of PBC´s (periodic-bond chains) involved in the respective faces (SUNAGAWA, 1999).

The PBC´s are uninterrupted chains of strong bonds between building units (atoms, ions) of the crystal and these bonds belong to the primary coordination sphere of an atom or molecule. PBC chains that contain only strong bonds between atoms or molecules define the direction of major growth of a crystal, and PBC chains containing weaker bonds between atoms define directions of minor growth. F-faces contain two or more types of PBCs parallel to the face. S-faces have only one type of PBC parallel to the face, and K-faces have no PBCs parallel to the face.

The prediction of morphology from the crystal structure involves (1) determination of PBCs, and (2) classification of (*hkl*) layers as F, S or K faces. The morphology so obtained is controlled by the occurrence of F-faces, which tend to grow to large faces. S and K faces develop small or do not appear at all.

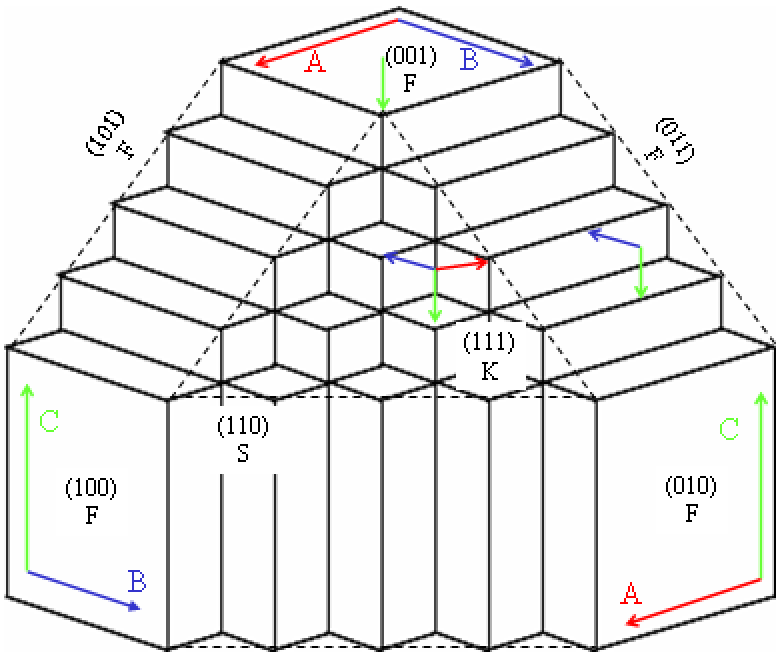

Fig.: 3.6 Hartman-Perdok model of F,S and K-faces defined by PBC´s. The arrows A,B and C are PBC vectors in a simple cubic crystal (Kossel-crystal). F-faces: (100),(010),(001); S-faces: (110),(011), (101); K-face: (111) (image modofied from SUNAGAWA 1999).

There have been a few downsides to the PBC theory: the first is that a certain arbitrariness is unavoidable in finding PBC´s in real crystal structures, and the second is that PBC analysis is difficult in complicated structures. Both can be overcome by application of the net model proposed by BENNEMA (1993). The PBC theory has developed since and methods have evolved to calculate attachment energies of PBCs (SUNAGAWA , 1999).

3.6 The atomistic models of crystal growth

The methods outlined in the previous chapters, starting with Bravais and Niggli, followed by Donnay-Harker and Hartman-Perdok, are directed to an ideal crystal form. These theories assume that the crystal form can be determined by considering the internal structure of a crystal only, entirely neglecting the effect of external growth parameters. Such crystal forms are called “structural forms” or “abstract forms”. They may be related to thermodynamic parameters such as temperature or pressure as driving forces, or the free surface energy or capillary constants as surface properties, but they mostly neglect various other growth mechanisms, such as kinetic processes involved during the attachment or detachment of crystal building-blocks.

Today, kinetic processes correlated for example to the attachment of inhibitors to crystal surfaces play a vital role in Mineral Surface Science. But it was not until VOLMER (1926) published his theory of nucleation and crystal growth by the formation of two-dimensional nuclei, that these processes were recognized and they further obtained much attention after KOSSEL (1927) and STRANSKI (1928) developed their atomistic model of crystal growth processes.

KOSSEL (1927) and STRANSKI (1928) picked up on the ideas of VOLMER (1926) and were the first to introduce an atomistic approach, considering molecular-kinetic methods. Their theories are based on a particular crystal model known as the Kossel-

Crystal (Fig.3.7). A theoretical crystal based on the simple cubic lattice. With this Kossel-Crystal it was possible to calculate the separation energy of ions which occupy different sites on the crystal surface.

KOSSEL and STRANSKI showed that by following the successive attachment or detachment of individual building elements (ions, atoms, molecules), it became possible to describe crystal growth and dissolution processes from a more dynamic perspective. By application of this semi-quantitative approach, conclusions about the stability of a crystal face as well as the equilibrium structure of different crystal face can be obtained (SUNAGAWA, 1999).

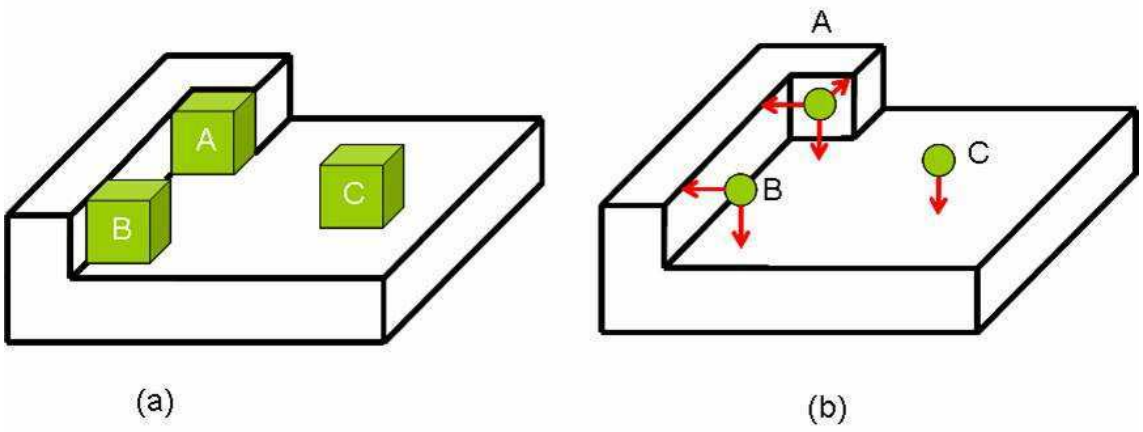

Fig.: 3.7 Left: Kossel-crystal showing three possible attachment sides (A,B,C) for building elements such as ions, atoms or molecules. Right: Atoms attaching to a kink site (A), a step (B) and a terrace (C). Bonds forming between the nearest neighbors and the attaching ions are marked in red (for further explanation see text).

The basic principles of the theories of Kossel and Stranski are schematically given in Fig.: 3.7). They are focused upon a model of a homöopolar crystal with a simple cubic lattice and the interaction of the first (nearest) neighbors of an atom. The energies calculated with this model are derived from the "work of separation" of two atoms. This

"work of separation" for a given atom is equal to the number of its first neighbors times the work (Φ) needed to break a bond between the two neighboring atoms (SUNAGAWA, 1999). Figure 3.7 shows that atoms occupying different sites on a crystal surface have different binding energies and therefore different values of the work of separation. The atom "C" in Figure.3.7 bonds only to one neighbor on the terrace. Its work of separation is 1Φ. The atoms at the sites "B" and "A" bond to two and three atoms of the surface. Their work of separation is 2Φ and 3Φ respectively. Consequently atoms having a low work of separation can be detached from the surface more easily. On the other hand, sites such as the kinked site "A" in Figure. 3.7 offering a high number of neighbors are preferred sites for atoms to attach themselves. The lattice energy gained by atoms attaching to this position, is much higher, compared to the energy gained at the sites"B " or "C".

The kinked site "A" is one of importance in the molecular-kinetic model of Kossel and Stranski and is called "half-crystal position". The position "A", having three nearest neighbors, and consequently a work of separation of 3Φ, is indeed special. The number of full-neighbors in the bulk would be 6 and at site "A" it is half of this value. The work of separation at that site is equal to the lattice energy gained by adsorption of a building particle (ion, atom , molecule). In their works Kossel and Stranski showed that if the crystal surface is large enough the attachment or detachment of a building unit to the half-crystal position is a repeatable step, producing similar positions with the same energy of attachment and detachment (SUNAGAWA, 1999). Therefore, a crystal can be built or be destroyed merely by attaching or detaching building particles from these half-crystal positions.

This basic theory was later applied to various minerals and a list of the numerous works of KOSSEL and STRANSKI, as well as some other authors who applied this concept (KAISCHEW, HONIGMANN) are listed in the references.

3.7 Modern approaches

Molecular modeling models are modern approaches to predict the morphology of crystals. These models refer to either empirical or quantum-mechanical models in order to calculate surface energies or step energies. In these models, the surface energy is the difference in energy between the bulk structure and the surface structure; thus, the lower the surface energy, the more stable the face. The step energy is the difference in energy between the surface and the corresponding step; thus, the lower the step energy, the more stable the step. Using such calculations, one can categorize different faces or steps. It is possible, but very time consuming, to calculate the energy of every face or step that might occur in a crystallization or dissolution process, but these calculations only work well as long as accurate interacting potentials are available for the constituent species.

Examples of such computer based *ab initio* calculations are far too numerous to be considered in detail in this short summary. Mostly every month new Monte Carlo simulations of many mineral surfaces are published in the various journals, and many of them exhibit slight changes in the formulation of equations or potentials used to compute these simulations.

As an example of recent computer simulations applied to reproduce experimentally observed crystal growth, refer to PIANA et al. (2005). The authors have combined several computer based models such as atomistic molecular dynamics simulations and kinetic Monte Carlo simulations, to describe the growth of urea crystals observed *in situ* with an atomic force microscope.

4. Introduction to the Bond-Valence Theory

The basis of bond-valence theory was established, upon several ideas of PAULING (1929). In his rules about the nature of "coordinated polyhedrons" he had defined that the number of bonds formed by a cation are equal to its anion coordination number. The length of such bonds are determined by the sum of the cation-anion radii. The "electrostatic valence principle" states that the electric charge of each anion compensates the strength of electronic valences of bonds reaching to it from the cation in the center of the coordination polyhedron. First quantitative bond-valence parameters and empirical correlations between bond-strength and bond-length were introduced by BROWN & SHANNON (1973). Later, BROWN (1981) introduced bond-valence theory. This approach and further investigations cumulated in his work about chemical bonds in inorganic chemistry (BROWN, 2002).

4.1 Bond-Valences

In mineralogy the term "bond valence" concerns the bonding power (strength and length of a bond) between two atoms or ions. Further, we have to distinguish between "e*xperimental bond-valences"*, "*theoretical bond valences"* and "*effective bond valences"*. Historically bond valences have been calculated from atomic valences of atoms and their coordination numbers. This approach comes from Paulings ´s first rule about "the nature of coordinated polyhedrons":

The nature of coordinated polyhedrons:

> *A coordination polyhedron of anions is formed around each cation, the cation-anion distance being determined by the radius sum, and the coordination number of the cation by the radius ratio.*

We can address a crystal as a network of atoms or ions connected to each other by bonds. The bond valences obtained correlate well with the model of ionic crystals and the concept of Lewis acids and Lewis bases. For example, an ionic crystal can be described as a network of bonds, having a Lewis acid (cation) at one end, and a Lewis base (anion) at the other end of the bond (BROWN 1981). All such compounds having an acid-base network must obey "the rule of stoichiometry".

> *The total valence of the Lewis acids is equal to the total valence of the Lewis bases.*

BROWN (1981) transformed the empirical stoichiometry rule into one of the fundamental principles of bond-valence theory, designating it "equal valence sum-rule":

> *The sum of bond valences at each atom is equal to the atomic valence*

It is worth mentioning that the "equal valence sum-rule" is another form of stating Pauling´s second rule, "the electrostatic valence principle":

> *In a stable coordination structure the electric charge of each anion tends to compensate the strength of electrostatic valence bonds reaching to it from the cations at the centers of the of the polyhedra of which it forms a corner; that is, for each anion*:

$$\varsigma = \sum_i z_i / \nu_i = \sum_i s_i \qquad [4.1]$$

> ς = anion charge, z = cation charge, ν = cation coordination number,
> s =(Pauling) bond strength

The electrostatic valence principle is represented by the equal valence rule (or loop rule), equation [4.2], where the summation is over the bond valences around any closed

loop in the bond network considering the direction in which the loop is traversed, S_{ij} being taken as positive if the bond is traversed from the anion to the cation and negative otherwise (BROWN 2002).

$$0 = \sum_{loop} S_{ij} \qquad [4.2]$$

The bond valences approach proved to be useful, when BROWN & SHANNON (1973), showed that bond valences correlate very well with bond length. This has been determined for many different types of bonds in a large number of crystal structures, and is accurate to 0.05 valence units (BROWN, 1981). Bond-valences can be determined in many compounds using crystal structure information calculating the bond-length between the ions or atoms. Bond valences obtained in this way are called "experimental bond-valences".

Bond valences can be calculated using the following equations if the bond-lengths are known:

$$S_{ij} = \exp\left(\frac{R_0 - R_{ij}}{B}\right) \qquad [4.3]$$

$$S_{ij} = \left(\frac{R_{ij}}{R_0}\right)^{-N} \qquad [4.4]$$

where R_{ij} is the length of the bond between atom i and j, and S_{ij} is its "*experimental valence"* in valence units (vu). R_0, B, and N are parameters that are chosen to ensure that the sum of the bond valences around all the ions in a large number of well-determined structures are the same as their atomic valences or formal charges (BROWN 2002).

The experimental error in the measured bond lengths ensures that the sum of experimental bond-valences around any particular ion will never exactly equal the atomic valence. There are cases where this discrepancy gives important information about the crystal chemistry. The *valence sum rule*, which states that the sum of experimental bond valences around each atom is equal to the atomic valence V_i , is much better obeyed than Pauling´s second rule (BROWN 2002). Equation [4.5] is the mathematical expression of this valence sum rule:

$$V_i = \sum_j S_{ij} \qquad [4.5]$$

Equation [4.2] represents the condition that each atom distributes its valence equally among its bonds considering the constraints of equation [4.5]. Both equations are known as the *network equations* and provide sufficient information to determine the bond valences, given a knowledge of the bond graph and the valences of the atoms. The solutions of the network equations are called *theoretical bond valences* (BROWN 2002).

Some problems with this simplistic model are stated by BROWN (2002):

> For example, the difficulty of determining precise values for atomic or ionic radii. The radii are determined from observed bond lengths, but which distance is to be used? Different bond lengths are often found between the same pair of atoms even in the same coordination polyhedron, and the average bond length varies systematically with the coordination number (SHANNON and PREWITT 1969; SHANNON 1976).
>
> In a hard-sphere model each cation is assumed to be surrounded by the maximum possible number of anions in order to form the most densely packed structure. The factor that determines the coordination is determined by the ratio of the cation radius and the anion radius, as expressed by Pauling´s first rule.

The problem with the hard-sphere model is that it predicts a single coordination number for each ion pair and is therefore unable to account for the behavior of cations such as Cs^+, which are observed with a wide range of coordination numbers (BROWN 2002).

One reason for the failure of the radius ratio rules is that ions do not behave like hard spheres. This is clearly seen in the way that bond length varies with the bond valence. If cation-anion bonds can be compressed, so can the distance between the O^{2-} ions in a first coordination sphere of a cation. The stronger the cation-anion bonds, therefore, the closer the anions in the first coordination sphere can be pulled together (SHANNON et al. 1975).

As a result of this the angle, α , between two oxygen and a cation (O – X – O) can vary depending on the strength of the cation –anion bond. The factor therefore that determines how close the two oxygen atoms can approach is the *effective valence*, s´, defined by equation [4.6].

$$s` = s \cos \alpha \qquad [4.6]$$

More detailed analyses of these problems, are given by BROWN (2002) and citations therein.

4.2 Theoretical Bond-Valences (Applications)

As a first approach it is appropriate to consider the theoretical bond-valences that can be calculated via the solution of the valence sum rule (eqn. 4.5), if the bond-lengths can be measured. They may as well be derived for any cation by dividing its atomic valence by its coordination number. The latter approach is more general, and the bond-valences obtained can be refined later, after the bond-lengths measurements.

Depending on the coordination number, we will obtain a certain valence unit (vu) for each individual bond around an atom or ion. For example, the Mg^{2+} ion has an atomic valence of 2 and a coordination number CN = 6, forming an octahedral coordination polyhedron (Fig. 4.1), resulting in a theoretical bond valence of ~ 0.33 valence units (vu).

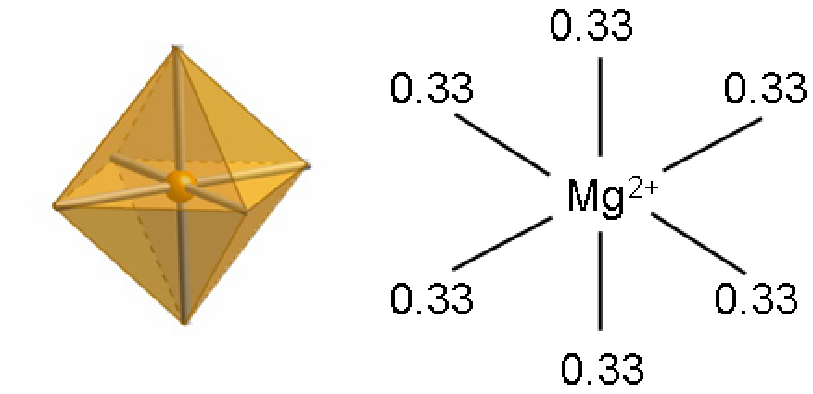

Fig.: 4.1 The left image shows an octahedral coordination polyhedron around a central Mg^{2+}-cation. The right image is a bond-graph around the Mg^{2+}-cation. Bond-valences are stated in valence units (vu), obtained by the division of the atomic valence of the Mg^{2+}-cation by its coordination number (CN = 6).

The calculation of the more common ionic-complexes such as $(CO_3)^{2-}$, $(SO_4)^{2-}$ or $(SiO_4)^{4-}$ is done going from the central cation outwards. Bond valences are attributed to the first anion neighbours, satisfying the atomic valence of the central cation first. But these valences are insufficient to satisfy the atomic valence of the anions. Therefore the remaining valences are calculated and depending on the coordination number of the anions, distributed evenly among the residual anion bonds. This is shown schematically in Fig. 4.2 for the complex-ion or $(SiO_4)^{4-}$.

In the case of $(SiO_4)^{4-}$,we have to start with the central Si^{4+} cation (Fig.: 4.2). The Si^{4+} cation is coordinated by 4 O^{2-} ions. Each of the four bonds from the Si^{4+}-ion to the oxygen will have a bond-valence of 1.0 vu, because the atomic valence of the Si^{4+}- cation has to be divided by its coordination number (4 : 4 = 1.0).

Now the atomic valence of the Si^{4+}-cation is satisfied and each of the four oxygen atoms already receives a theoretical bond-valence of 1.0 vu from the central cation of the coordination polyhedron. In order to satisfy the valence of 2^- of each of the oxygen, some more bonds have to be considered (Fig. 4.2).

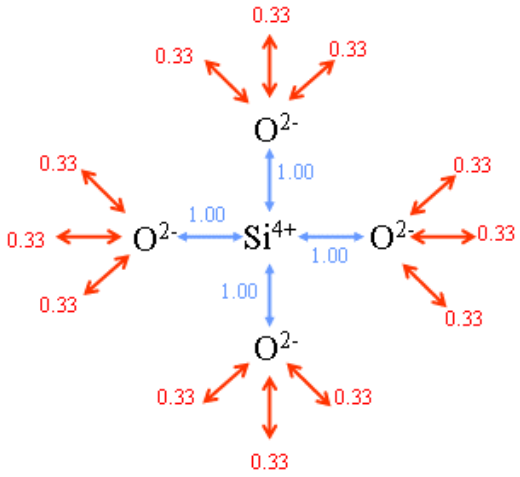

Fig.: 4.2 This Bond-graph shows the distribution of bonds an their corresponding bond-valence (vu) of an $(SiO_4)^{4-}$-anion complex. In blue the four bonds with a valence unit of 1.0 vu each emitting from the central Si^{4+} - cation to the tetrahedral coordinated polyhedron of oxygen. The residual bonds (see text) of the oxygen and their corresponding bond-valences (vu) are given in red.

Lets consider that each of the oxygen atoms has a coordination number of CN = 4. One of these bonds is already taken by the Si^{4+}-cation, leaving three more bonds to be calculated.

After calculating the influence of the Si^{4+} -cation, there is only a valence of 1.0 vu left which has to be divided among the three residual bonds of each of the four oxygen

atoms. Therefore, the residual bond-valence of 1.0 vu must be distributed to these three bonds and we will receive a bond-valence of 0.33 vu for each of this bonds (1 : 3 = 0.33). For reasons of simplification the anion-complex of $(SiO_4)^{4-}$ will be stated to have an average theoretical bond-valence of 0.33 vu.

4.3 The valence matching principle

One of the major consequences from the calculation of bond valences is the possibility to determine which atoms will form stable compounds. BROWN (2002) stated that the cation bonding strength is an estimate of the valence of bonds formed by a cation, and the anion bonding strength is an estimate of the valence of the bonds formed by an anion. Therefore most stable bonds between the two will occur when the bonding strength of the cation is equal to the bonding strength of the anion. This statement is in conjunction with the electrostatic valence principle of PAULING (1929) and can be summarized as the "*valence matching principle*":

> *The most stable compounds are formed between cations and anions that have the same bonding strength.*

A number of examples are quoted in BROWN (1981, 2002), but good examples are again the Mg^{2+} cation and the SiO_4^{4-} complex. Both form bonds with valences of 0.33 vu and therefore, having the same bond valences, readily form the mineral Mg_2SiO_4 (forsterite), which is a common mineral of the earth´s upper mantle (Fig. 4.3).

Although stable compounds are formed when the bonding strengths of the cation and the anion exactly match, a certain degree of mismatch is allowed. BROWN (2002) states that compounds can exist if the ratio of the two bonding strengths does not exceed 2.0. While it may be possible to prepare materials that are more poorly matched, it requires extreme methods and the resulting compounds are generally unstable (BROWN 2002).

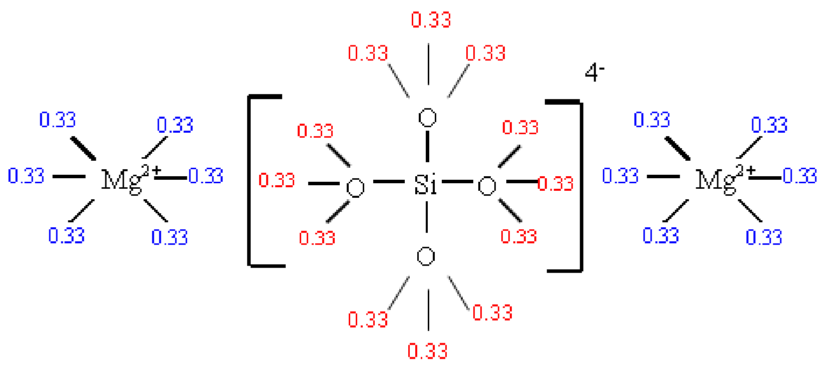

Fig 4.3 This bond-graph illustrates the principles of the valence matching principle. The bond-valences of the Mg^{2+} -cations, given in blue, match the bond-valences of the SiO_4^{4-} -anion complex, given in red. Therefore a stable compound such as forsterite is expected to form.

4.4 Bond-length, bond strength and bond-valences

BROWN (1981) states that there is a correlation between the length of a bond and its strength. Different charged ions can approach each other until their attractive forces reach a maximum. Further approach of the ions will lead to a repulsive force because the electron shells of the ions will begin to overlap. On the other hand ions can be separated from each other and in this case the strength of the bond decreases until the ions are separated from each other completely.

A correlation between the length of a bond and its strength can be found (Fig 4.4). Short bonds have a higher bond-valence (vu) than longer bonds between the same ions. Bonds with a relatively higher bond valence are stronger than equivalent bonds with a lower bond-valence, and in turn bonds with a high bond-valence are shorter than equivalent bonds with a lower bond-valence.

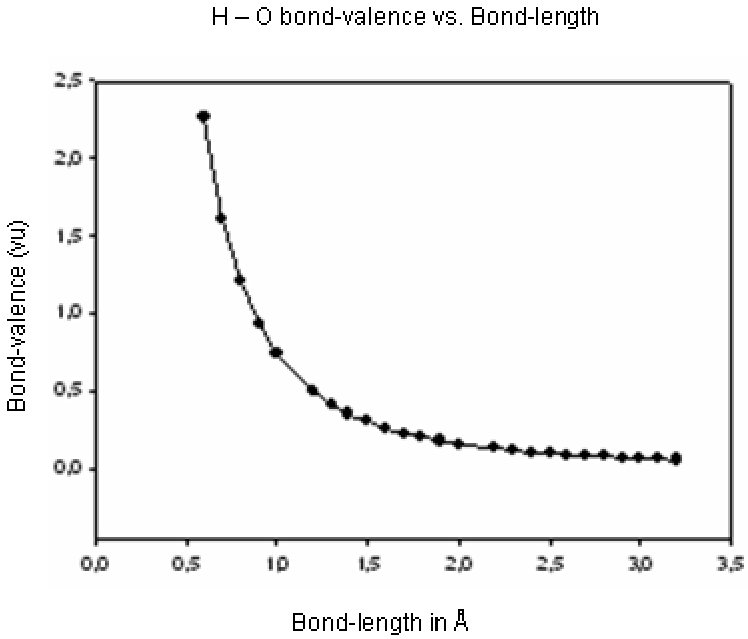

Fig.: 4.4 The correlation between the bond-length and the bond-valence of H-bonds calculated by equation. [4.4]., illustrating the decrease in bond-strength as bond-valences (vu), while the bond-length increases. The parameters for calculating the bond-valences have been taken from BROWN (1981). $R_0 = 0.87$; $N = 2.2$

It has been noted that the bond-valence of a bond depends on the coordination number of the ions. This is due to the fact that the central ion within a coordination polyhedron distributes its bonds as equally as possible to its surrounding ions (eqn. 4.5), in order to satisfy its atomic valence. As a result, the higher the coordination number, the more bonds will be formed and the lower the bond valence of each individual bond.

Furthermore, if the surrounding coordination polyhedron should be too large there also might be a shift of the central ion out of the centre of the coordination polyhedron. As a consequence the central ion will still form bonds to each of the surrounding ions, but these bonds will not have equal bond-valences because they differ in bond length. The shorter bonds will have a higher bond-valence than the longer ones. The sum of all bond-valence will be equal to the atomic valence of the central ion (Valence Sum Rule).

The shift of the central ion is described by the "*Distortion Theorem"* of BROWN (2002):

> *For any ion, lengthening some of its bonds and shortening others, keeping the bond valence sum the same, will always increase the average bond length.*

This rule has a certain impact on how we approach crystal structures. The bond-valences of bonds within a crystal which is built up of highly symmetric polyhedrons, having bonds of equivalent length, can be calculated by considering the ratio between atomic valence and coordination number only. All the bond-valences calculated will be equal. In cases where a distortion of the coordination polyhedron is to be expected or observed special care has to be given to the length and the direction of the bonds in the coordination polyhedron. In such cases the bond-valences must be calculated via the equations [4.3] and [4.4].

4.5 Latest developments of the bond-valence theory

The bond-valences parameters described in the previous chapters (4.1 – 4.4) have been determined straight forwardly from the assumption that the bond-valence sum of a central atom is determined by the interaction of the atom and its first coordination sphere. These assumptions led to the formulation of the equations [4.3] and [4.5], with the parameters R_0 and B chosen to ensure that the sum of the bond valences around all ions is as close as possible to their atomic valences or formal charges.

For many inorganic crystal structures these assumptions are sufficient and the bond valence sums calculated deviate by less than 0.1 *vu* from the atomic valence of the ion. Nevertheless examples are known (BURNS et al, 1997), in which deviations from up to 1.0 vu are reported (LIEBAU & WANG, 2005). In the past, such rather large deviations, have been interpreted merely as experimental errors or inaccuracies of the bond valence parameters applied.

New investigations (WANG & LIEBAU, 1996; MOHRI, 2000; LIEBAU & WANG, 2005; ADAMS, 2001; GIBBS et al, 2005; BICKMORE et al 2006), hint that these variations are not merely statistical errors, but include additional information about the relationship between bond-valences and the properties of the bonds formed between the atoms or ions.

One approach to sustain an accurate bond-valence sum, which is in concordance with the atomic valence of a central ion, is given by the "distortion theorem" in Chapter 4.4 (BROWN, 2002). According to this approach a central ion can be shifted from the central position within a coordination polyhedron, until the bond-valence sum is close to is atomic valence. As a consequence the individual bond-lengths between the central atom and its coordinated atoms varies.

Considering the distortion of a polyhedron LIEBAU & WANG (2005) introduced a new bond-valence parameter, called the "structural valence" ($^{struct}V_i$), a bond-valence which is distinct from the classical stoichiometric bond-valence, referred to by the authors as $^{stoich}V_i$. This new "bond-valence" $^{struct}V_i$, accounts for a variety of deviations between the bond-valence sum expected and the bond-valence sum calculated in distorted coordination polyhedrons. The authors argue that the values of the classical bond-valences ($^{stoich}V_i$) are governed by the group number of the elements and therefore are not influenced by the specific structure of the compounds. In contrast to this, the value of the structural valence ($^{struct}V_i$) of an atom depends mainly on the eletronegativities of its coordination partners and thus does depend on the structure of the coordinated polyhedron. As a conclusion LIEBAU & WANG (2005) specify that a distinction needs to be made between the classical stoichiometric bond-valences derived from chemical analysis and those bond-valences derived from structural analysis. For the bond-valences so obtained for $^{stoich}V_i$ and $^{struct}V_i$ may be similar for undistorted coordination polyhedrons of a central atom but may as well deviate conspicuously in the case of a distorted environment.

ADAMS (2001) proposed that the bond-valence parameters R_0 and B have to be refined by considering the hardness and/or softness (Parr & Pearson, 1983) of the bonds formed between ions or atoms. He showed that even the weak interactions of a central atom with its second coordination sphere may influence the bond-valence sum of the central atom significantly. This approach tends to incorporate the effect of electronegativity, ionization potential and electron affinity into the bond-valence calculations, as these factors definitely influence the bond-length between two atoms, ions or molecules.

These examples are only an extract of many efforts undertaken to render the bond-valence parameters more precisely, improving the capability of the bond-valence model to be used in *ab inito* calculation of crystal surfaces. Lately, BICKMORE et al. (2006) demonstrated how a bond-valence approach together with electrostatic calculations and molecular dynamic simulations can be combined to predict pK_a values of molecules.

5. The Bond-valence deficiency

In Chapter 4.3 it has been stated that stable compounds will form if cations and anions have a similar bonding strength, being able to satisfy their bond-valences as much as possible. One major consequence of the definition of the valence matching principle is its relation to bonds already formed and bonds still unsatisfied. Those bonds not yet formed, are the missing bond valences of the compound or its deficiency.

5.1 The definition of the bond-valence deficiency (BVD)

The bonding-strength of bonds formed by an ion depends, besides its charge, mainly on its coordination number. For example, a cation with an atomic valence of 1 *vu* and a coordination number of 4 will extend 4 bonds, each having a theoretical bond valence of 0.25 *vu*. The same cation having a coordination number of CN = 8, will have 8 bonds each of which having a bond-valence of 0.125 *vu*. According to the valence matching principle a coordination polyhedron around the cation can form consisting either of four anions donating bonds of 0.25 vu, or eight anions donating bonds of 0.125 vu.

Whatever the circumstances may be, it clearly can be stated that each cation has the tendency to satisfy its atomic valence as well as possible. This leads to the statement that each ion possesses a certain bonding power, which it is able to share and this bonding power is in return related to the atomic valence of the ion.
Before the complete coordination polyhedron around an ion is formed, and all the valences are shared, the ion possesses a number of unsatisfied bond-valences (Fig 5.1), called the *bond-valence deficiency (BVD)* of the ion.

The incomplete polyhedron is an unstable state of high energy. When it is overcome and all the possible bonds are satisfied the compound reaches equilibrium with its

surrounding and has reached a state of low energy. In a mineral the state of equilibrium is accomplished within the bulk, where all the bonds are satisfied and cations are surrounded by anions. The state of imbalance can be found on the surface where only the bonds reaching to the interior are satisfied, while those extending out of the bulk into the environment are incomplete.

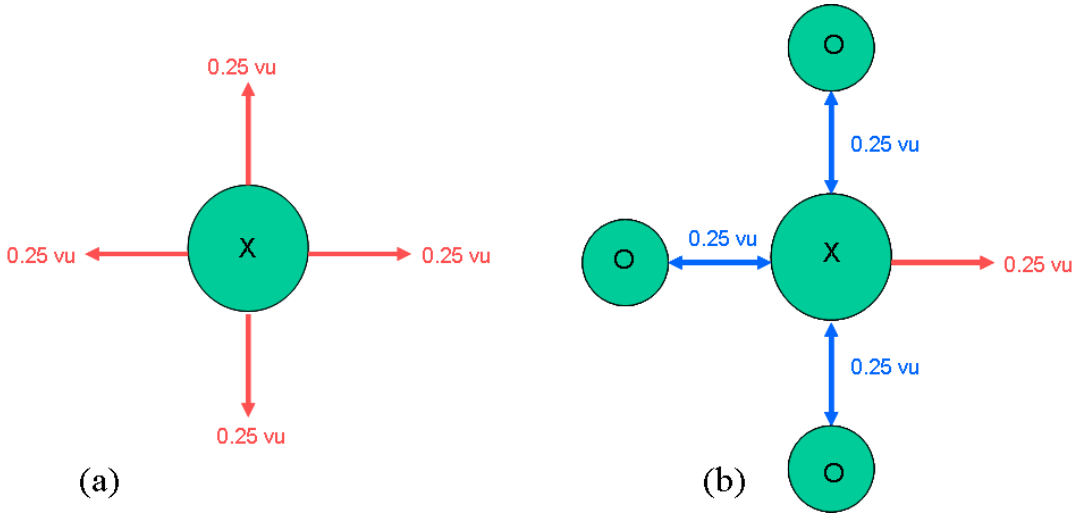

Fig.: 5.1 (a) The cation marked X has an atomic-valence of 1, and a coordination number of CN = 4. Therefore each bond (marked in red) has a bond-valence of 0.25 vu. If none of the bonds is taken by a coordinating anion, the bond-valence deficiency (BVD) is 1.0 vu. (b) Considering the same cation as in (a) it is now coordinated by three anions (marked O), and each of the bonds formed has a bond-valence of 0.25 vu (marked blue). The residual bond-valence or bond-valence deficiency (BVD) is therefore 0.25 vu, (red arrow), respectively.

This concept allows to calculate "surface energies" in terms of bond-valence deficiencies (Chapter 5.3). Researchers using thermodynamic based computer-models to calculate surface energies yield excellent results, that can be used to predict mineral growth and dissolution processes anticipating the reactivity of mineral surfaces. However, these calculations are very time consuming.

To look at a mineral surface from the perspective of the bond-valence deficiency is another way to assess relative surface energies. Different from computational-modeling, the calculation of missing bond-valences can be achieved very quickly, as it is only necessary to calculate the number of bond-valences still to be satisfied.

If the BVD approach is transferred to mineral surfaces, e.g. to an edge of a terrace from an atomistic point of view, we notice that the edge of a terrace is built from of a “chain” of atoms, that is exposed along the edge (Fig. 5.2). Not all possible bonds along this chain are satisfied, when compared to an equivalent “chain” within the bulk. Calculating the number of unsatisfied bonds (dangling bonds) along this chain and normalizing them to a certain chain length will give the bond-valence deficiency of the edge.

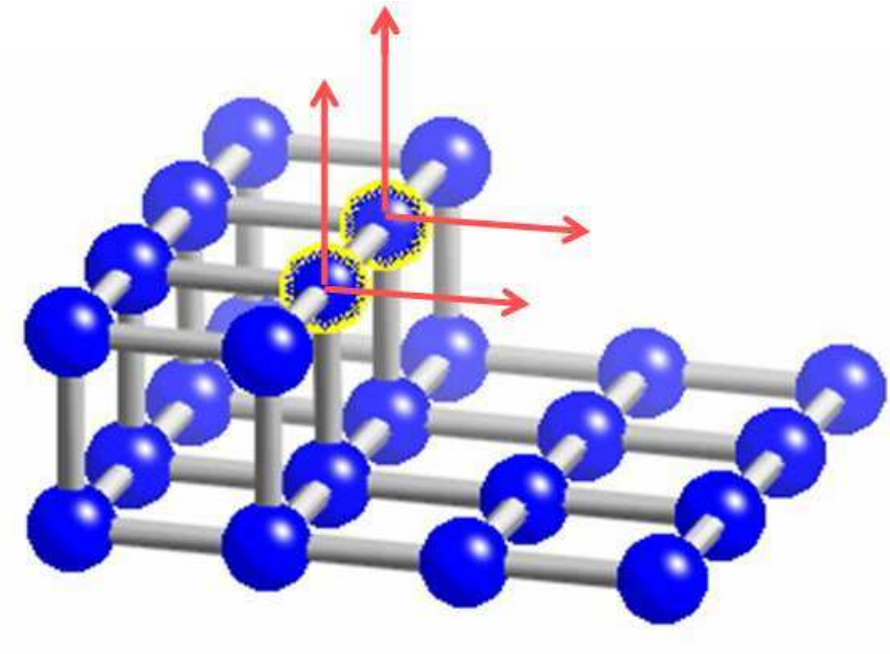

Fig.: 5.2 Atomistic representation of an edge terminating a terrace. For two of the atoms (yellow cricles) terminating the edge, the number of missing bonds (two each) is marked with red arrows.

5.2 The bond-valence deficiency of crystal faces

SCHINDLER et al. (2004 a, b) have shown that polyhedral-chains in sheet-like minerals can be compared by calculating the bond-valence deficiency of anions terminating these chains. They deduced that edges having a lower bond-valence deficiency than others will be more stable than edges with a higher bond valence deficiency. As a consequence they concluded that it is possible to predict the relative morphology of sheet like uranium-minerals by comparing the bond-valence deficiencies of different anion terminations, only.

The investigations of SCHINDLER et al. (2004 a, b) focussed on "two-dimensional" structures, of crystal surfaces, such as edges and terraces. We now apply this approach to predict the morphology of crystals more generally. The aim is to describe the "three-dimensional" morphology of a polyhedral crystal, because at the end of a reaction or in the state of equilibrium only faces with a low bond-valence deficiency will terminate the crystal.

SCHINDLER et al. (2004 a, b) defined the bond-valence deficiency for chains of polyhedrons. We now define the BVD more generally:

> *The bond-valence deficiency of an ion, chain of polyhedrons or crystal face is the difference between the amount of bond-valences reaching to the ion, chain or face and the amount of bond-valence still needed to satisfy the atomic valence of the ion, chain or face*.

5.2.1 The BVDF-approach

Atoms terminating a surface are bonded to atoms within the bulk, as well as to neighbouring atoms within the same layer. In addition, unsatisfied bonds, called "dangling bonds", are extending out of the surface and are directed towards the surrounding liquid or gas phase. "Dangling bonds" can be described as broken bonds

and occur when an atom is missing a neighbour. They can be “found” on mineral surfaces due to the absence of lattice atoms above them, or at defect sides of a crystal. The sum of such extending bonds over a specific area will be called the bond-valence deficiency of the face (BVDF), and is expressed as valence unit per area (vu/Å^2).

As an example of calculating the BVDF of a face we will treat a double-layer-lattice (Fig. 5.3) as a theoretical crystal. The lattice points are occupied by atoms, their coordination number is CN = 6.

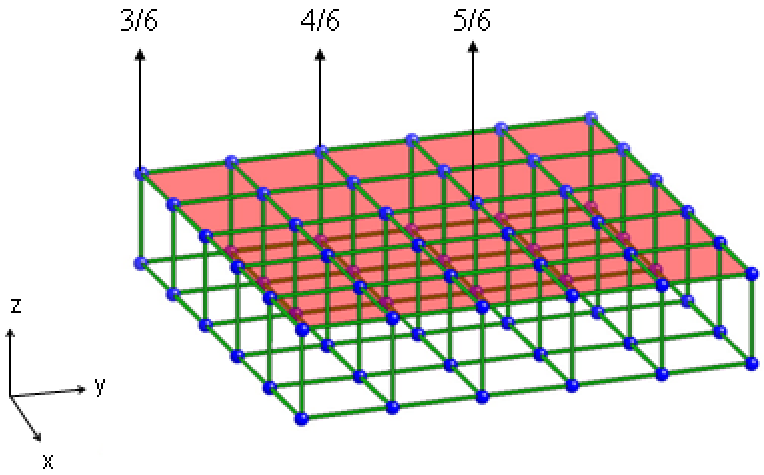

Fig.: 5.3 A double-layer of a theoretical crystal, with the space group symmetry Pm3m. The (001) surface is marked in red. The coordination number of the atoms is CN = 6. The atoms of this crystal are placed at the positions of the lattice points (blue spheres). Marked with arrows are atoms at the corner, edge and within the (001) face. These atoms bond to fewer atoms, compared to atoms within the bulk of a larger crystal. E.g. atoms at the corner of the (001) face bond to 3 neighbours having satisfied only 3 from 6 possible bonds.

The main objective of this approach is to define a crystal faces as a two-dimensional lattice and the atoms occupy the positions of lattice points of the given lattice type. Implications of symmetry factors concerning these “special” atom positions will be discussed in Chapter 7.

In our example (Fig.: 5.3), atoms at the corner of the (001)-face have three “dangling bonds”; three bonds are to atoms along the edges of the crystal and three are extending to the surrounding, later are the so-called “dangling bonds”. Atoms along an edges, have two “dangling bonds”, atoms within the face have only one “dangling bond”, respectively.

Calculation of the number of “dangling bonds” over a specific area will give us the BVDF-value of this face, and the comparison of the BVDF-values of different faces will result in the prediction of the morphology of a polyhedral crystal (Chapter 5.4).

5.3 Correlations between BVDF and surface energy

The ability to compare the BVDF-values of different faces in a short period of time by calculating the number of dangling-bonds, seems to be compensated by the disability to obtain thermodynamic data about the crystal surface.

Solving even one of the basic thermodynamic equations (eqn. 5.1), in order to calculate the energy gained during nucleation, is not possible if the BVD-theory is applied.

$$\Delta G = -\Delta G_V + \Delta G_S \qquad (5.1)$$

ΔG = nucleation energy; ΔG_V = energy required to attain volume; ΔG_S = surface free energy

The nucleation energy ΔG is the sum of energy spent in forming a particle by coagulating atoms. $-\Delta G_V$ reflects the cohesive forces between close-packed ions or atoms in the interior and is proportional to r^3. $+ \Delta G_S$, refers to the reactivity of unsatisfied bonding potential on the surface and is proportional to r^2. The factors r^2 and r^3 correspond the surface area and the volume of the particle. In Figure 5.4 changes in nucleation energy ΔG are given as the size of crystal nucleus changes. The energy

required for nucleation to occur, increases as “r” increases, reaches a maximum and decreases thereafter.

Among clusters that form, those exceeding the critical size do not dissociate and can grow larger. This is caused by the density of dangling bonds per unit area of the surface. The relative number of “dangling bonds” decreases as the size increases (SUNAGAWA 2005).

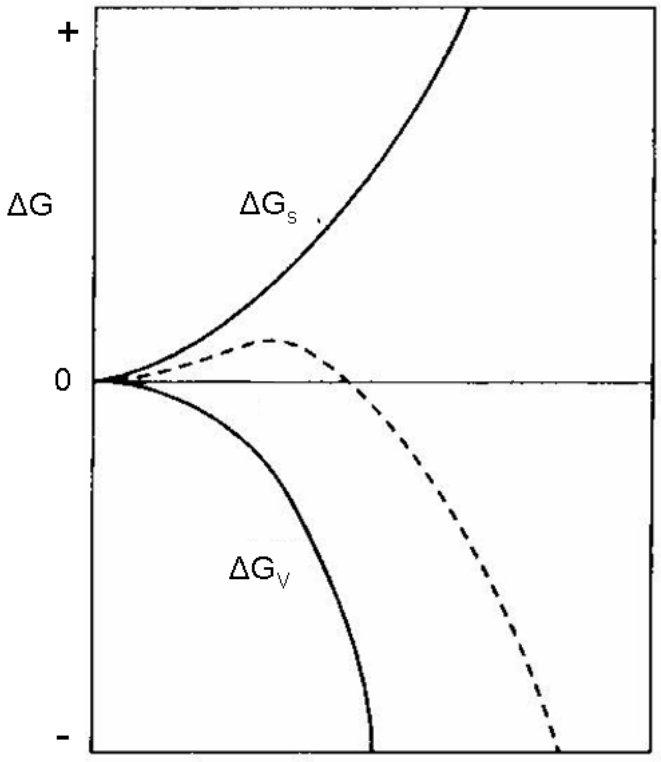

Fig.: 5.4 Changes in nucleation energy ΔG (dashed lines) depending on changes in ΔG_S and ΔG_V (Figure changed after SUNAGAWA, 2005).

Taking a closer look at equation (5.1) some similarities between the BVD-theory and thermodynamic models can be obtained. As an example we refer to a theoretical crystals (Fig. 5.5) having the space group symmetry Pm3m. The atoms occupy the positions of lattice-points and have a coordination number CN = 6, and a_0 = 5 Å.

Calculating the total number of dangling-bonds of the different growth steps of the (001)-faces in (Fig. 5.5), we notice that the total number of dangling-bonds increases as the size of the face becomes larger (Tab. 5.1). This observation can be compared to changes of ΔG_S in the thermodynamic approach. Calculating the BVDF of the (001) surface of the growing crystals (Fig. 5.5, Tab.5.1) shows the opposite trend. As the crystal size increases the BVDF of the face decreases.

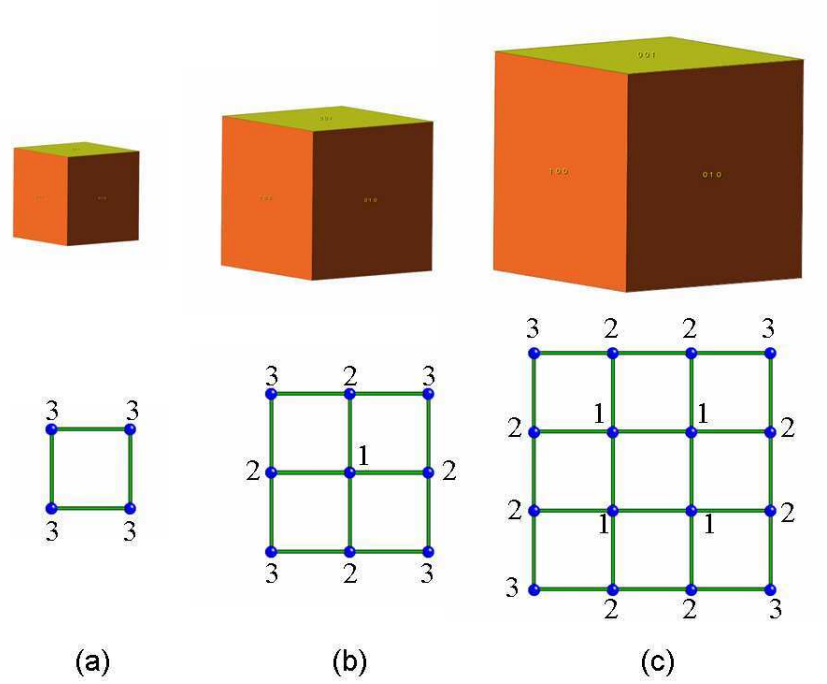

Fig.: 5.5 Shown is a growth sequence of a cube, represented in "growth steps" a - c. The space group of this theoretical crystal is Pm3m a_0 = 5.0 Å. The coordination number of the atoms is CN = 6. Below the images of the hexahedrons the corresponding (001)-surface termination is given. The blue balls represent atoms on the crystal surface and the numbers given indicate the amount of dangling bonds.

The results obtained are not surprising as they represent some fundamental coherences known in crystal growth theories. But they are worth to be mentioned, as they prove the applicability of the BVD-approach to describe crystal growth processes.

(DB)	Surface area ($Å^2$)	BVDF ($vu/Å^2$)
12	25	0,480
21	100	0,210
32	225	0,142
45	400	0,113
60	625	0,096
77	900	0,086
96	1225	0,078

Tab.: 5.1 This table corresponds to Fig. 5.5. Given are the number of dangling-bonds (DB), the size of the surface area (001) and the BVDF-values of a theoretical crystal with space group symmetry Pm3m, a_0 = 5 Å , atoms having a coordination number CN = 6. Two trends are visible. First the increase in the number of dangling bonds as the crystal grows in size, second the decrease of the BVDF-value while the surface area increases.

Concluding we can say, even though the BVD-theory is not able to provide specific thermodynamic data for calculating crystal surface energies, the BVD-approach yields to some extent results, which are comparable to known thermodynamic properties of crystals.

5.4 Application of the BVDF-model for primitive cubic lattices

As an example how the BVDF-model can be applied, the “abstract form” of a theoretical crystal having a primitive cubic lattice will be calculated. The space group symmetry is Pm3m, the coordination number of the atoms CN = 6, the number of lattice points Z = 1, and a_0 = 5 Å.

The results obtained by calculating the BVDF-values for the faces (100),(110) and (111) are quoted in Table (5.2) and visualized in the diagrams of Figure (5.6).

Face (100)	(DB)	Surface area (Å^2)	BVDF (vu/Å²)
	12	25	0,180
	21	100	0,210
	32	225	0,142
	45	400	0,113
	60	625	0,096
Face (110)	(DB)	Surface area (Å^2)	BVDF (vu/Å²)
	18	70,71	0,255
	38	282,84	0,134
	66	636,39	0,104
	102	1131,36	0,090
	146	1767,75	0,083
Face (110)	(DB)	Surface area (Å^2)	BVDF (vu/Å²)
	15	21,65	0,693
	27	86,6	0,312
	42	194,85	0,216
	60	346,4	0,173
	81	541,27	0,150

Tab.: 5.2 Summary of the results obtained for a Pm3m-lattice by application of the BVDF-method. First column states the face (hkl) considered. Column 2 states the number of dangling bonds. Column 3 represents the size of the two-dimensional face (hkl) concerned and column 4 gives the BFDF-value obtained by dividing the number of dangling bonds by the surface area. The list has been cut off after five "growth steps"

The diagram in Figure (5.6 a) gives the correlation between the increase of the total number of dangling bonds and the increase of the crystal size, given as growth steps. The "growth steps" resemble the increase (extension) of the surface area of a given face (hkl). The gradient of the graphs shows differences in the increase of the number of dangling bonds as the faces advance, indicating changes in the relative surface energies of the faces as they grow in size.

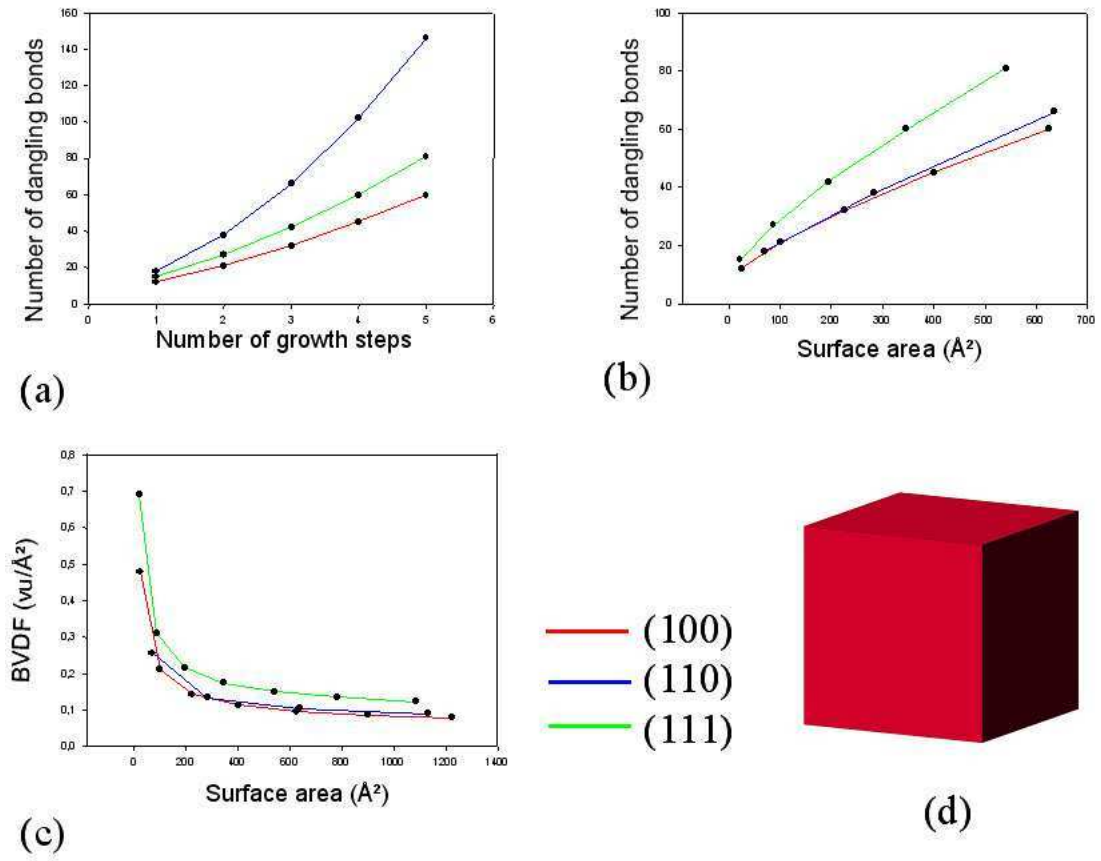

Fig.: 5.6 Plotted in these diagrams are the results from Tab.5.2. Fig. (a) shows the increase of the total amount of dangling bonds vs. the number of growth steps. The "growth steps" represent the extension of the crystal surface. Fig. (b) shows the correlation between the total number of dangling bonds and the increasing size of the growing faces. Fig. (c) shows the decrease of dangling bonds per area as the size of the faces increases. (Details see in text). Fig. (d) represents the predicted "abstract form" of a crystal having a space-group symmetry Pm3m.

Figure.(5.6b) is similar to Figure. (5.6a), showing the increase in the total number of dangling bonds. Here the total number of dangling bonds is plotted against the actual size of the corresponding faces. Comparing both diagrams (Fig. 5.6a and 5.6b), it is possible to deduce that the increase in the total number of dangling bonds, and thus the "surface energy", is compensated by the size of the crystal faces. This correlation is more obvious in Figure (5.c).

The gradients of the graphs as well as their progression indicate a close relation between free energy of a face (BVDF-value) and its actual size. The (110)-face having a high number of dangling bonds (5.6a) now proves to have a lower "surface energy" (BVDF-value) than the (111)-face.

The graphs in the diagram (Fig. 5.6b) are cut off after the faces have reached a size of approximately 600 Å² (see Tab.5.2). The (100)-face needs 5 "translations" steps to reach a size of 625 Å². Only 3 translations are needed by the (110)-face to reach a size of 636 Å². The (111)-face increased to 541 Å² after 5 translations. The different number of translations needed to reach a similar size hint to the approaches of NIGGLI (1920) and DONNAY-HARKER (1937) considering the lattice density as a factor to be recognized while predicting the morphology of a crystal (Chapters 3 and 7).

The diagram of Figure (5.6c) shows a negative gradient of the graphs. Here the "surface energy" of the faces, calculated as the total number of dangling bonds, is normalized to the size of the faces, namely the BVDF-value of the face given as vu/ Å². This BVDF-value is plotted against the increase in surface area. This diagram indicates that the relative surface energy of a crystal face decreases as the size of the face increases, due to the decrease in the BVDF-values.

Having reached a certain size, the BVDF-values of all crystal surfaces tends to reach a minimum. This is due to the decreasing influence of the bond-valence deficiencies of the edges on the overall BVDF-value of the surfaces, as the surfaces size increases. For each surface this minimum is expected to be equivalent to the number of "dangling bonds" present in the respective unit-cell. In our example the minimum BVDF-value of the (100) surface is 0.04 *vu* / Å². The unit-cell of the (100)-face has a size of 25 Å², and the number of dangling bonds is one, therefore: 1 / 25 = 0.04.

This minimum, being characteristic for each face, can be used to establish a relative ordering of morphological importance of these faces (see Chapter 8). In this example the (100)-face, showing the lowest BVDF-value, would dominate the morphology of the macro-crystal, followed by the (110) and (111) faces.

It is worth to be mentioned that at the start of nucleation, at the time when the surface areas of the crystal faces are still small, a “cross-over” of the BVDF-values of the (100) and (110) faces occurs. It is not until the crystal, and therefore the surfaces, have reached a certain size that the (100) faces turn out to having the lowest BVDF-value.

As a result from these observations we can deduce that at the early stages of nucleation, before the nucleus of the crystal has reached a critical value, faces later being only of minor importance to the morphology of the macroscopic crystal, have a larger influence on the habit and therefore on the reactivity of the crystal surfaces at nano-scales.

6. First applications of the BVD-theory

The following chapters are a selection of results obtained by application of the bond-valence deficiency approach, concerning the morphology of uranyl-sheet minerals. These results have been obtained in the progress of this study and have been published (Appendix V). The results obtained had a major impact on the further development of the BVD-theory, as they have been the first attempts to describe mineral surface reactions via the calculation of bond-valence deficiencies.

6.1 Bond valence deficiency calculations on steps and edges

Uranyl-sheet minerals are very useful when approaching the BVD-theory for the first time. These minerals have been described in terms of bond-valence models, since the 1980´s by different authors FINCH (1996), HAWTHORNE (1985, 1986). Even though the mineral structure of uranium minerals seems to be very complex, and the atomic interactions are numerous; the structures of uranyl-sheet like minerals can be simplified as described by HAWTHORNE (1985,1986,1990) and SCHINDLER & HAWTHORNE (2001a).

The basic idea of SCINDLER & HAWTHORNE (2001 a) was to factor the crystal structure into two components (Fig.6.1): the structural unit (an array of uranyl polyhedrons with high-bond-valences, which are usually anionic in character) and the interstitial complex (an array of cations, simple anions and (H_2O) groups, with low bond-valences, which are usually cationic in character.

It can be noticed that the structural unit, in the example given for becquerelite (Fig. 6.1), consists of a layer of uranyl-polyhedrons. This structural unit dominates the crystal morphology and edges terminating the structural unit define the morphology of the minerals, respectively.

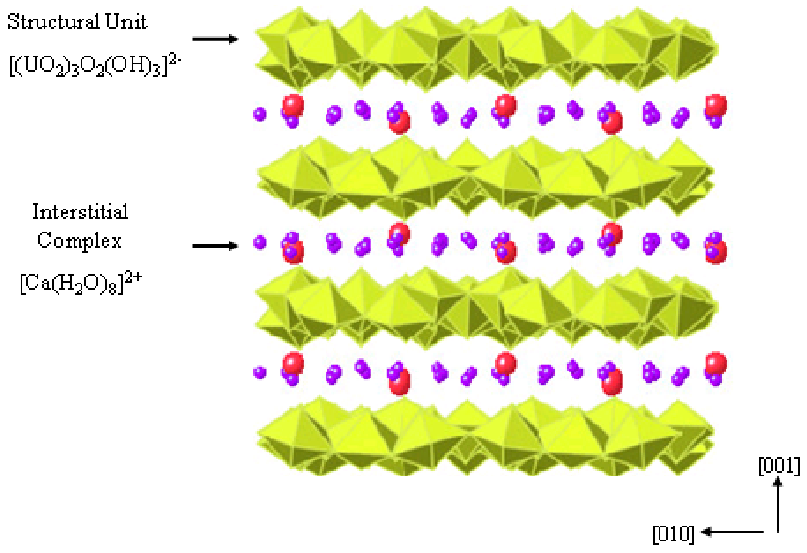

Fig.: 6.1 The crystal structure of becquerelite $Ca[(UO_2)_3O_2(OH)_3]_2(H_2O)_8$. This structure can be separated into a structural complex $[(UO_2)_3O_2(OH)_3]^{2-}$ as well as an interstitial complex $[Ca(H_2O)_8]^{2+}$.

The edges of the basal faces and the basal surfaces (structural unit) themselves vary in reactivity owing to differences in the local stereochemistry of their constituent uranyl-polyhedrons. In general, uranyl-sheet minerals contain layers of polymerized uranyl-polyhedrons with uranium in [6], [7] and [8]-coordination as tetragonal, pentagonal and hexagonal bipyramids, respectively (Fig 6.2). In these polyhedrons, the strong U–O uranyl bonds (U_{ur}) are not involved in linkage between uranyl polyhedrons. They extend orthogonal to the sheet, whereas weaker equatorial U–φ bonds [φ = O^{2-}, $(OH)^-$, (H_2O)] link the polyhedrons in the plane of the sheet.

The reactivity of the basal surface is determined primarily by the reactivity of the apical oxygen atoms of the uranyl-group (U_{ur}). These oxygen atoms receive an average of 1.6–1.7 valence units (*vu*) from the U–O bond, and hence they cannot be protonated (by H^+), as each O–H bond has an average bond-valence of 0.80 *vu*, and the aggregate incident bond-valence at the uranyl O-atom would be 1.6 + 0.8 = 2.4 *vu*, which is in conflict with the valence-sum rule (Brown 1981, Hawthorne 1994, 1997). Apical oxygen atoms of the uranyl group are therefore not involved directly in any acid–base reactions at the surface.

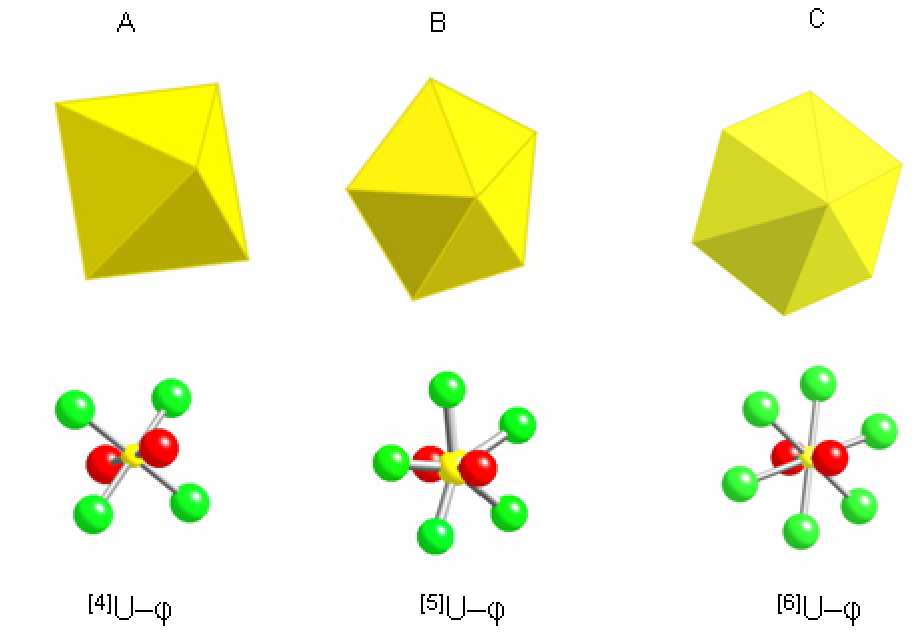

Fig.: 6.2 Three different uranyl-polyhedron (above) and their atomic representation (below). The uranium atoms (yellow) are coordinated by oxygen atoms (red and green) in either [6], [7] or [8]-coordination. The oxygen atoms of the strong uranyl-group (U_{ur}) are marked red. The equatorial oxygen atoms (U–φ) are marked in green. The notation concerning only the equatorial oxygen atoms (U–φ) can be given as $^{[4]}$U–φ for the polyhedron-type "A" , or as $^{[5]}$U–φ and $^{[6]}$U–φ for the polyhedron "B" and "C".

In contrast to the uranyl-bonds (U_{ur}), equatorial U–O bond lengths vary over a larger range, with average bond valences between 0.2 and 0.8 *vu*. Thus, equatorial O-atoms (U–φ) at basal and edge surfaces can participate in acid–base reactions through protonation and deprotonation. Hence, edged surfaces are much more reactive than basal surfaces because equatorial O-atoms on the edged surface almost always bond to fewer atoms of U^{6+} than O-atoms in the sheet, and hence must satisfy their individual bond-valence requirements through a higher degree of protonation. Equatorial oxygen atoms in the sheet of polyhedrons commonly bond to two or three U^{6+}-atoms.

One of the basic uranyl-sheet minerals is schoepite. The interstitial complex consists only of H_2O- molecules and the structural sheet is made out of uranyl-polyhedra which all have $^{[5]}$U–φ bonds. One approach to the structural unit of schoepite would be the

Periodic Bond-Chain theory (Hartman & Perdok 1955a, b, c), by which the basal face can be defined as an F face, because the sheet contains more than one periodic bond-chain of strong bonds. In our approach, however, we consider polyhedrons instead of bonds, a linear periodic bond-chain is therefore part of a linear periodic chain of polyhedrons. Such a chain of polyhedrons we call a *polyhedron chain* or *chain*, (Fig. 6.3).

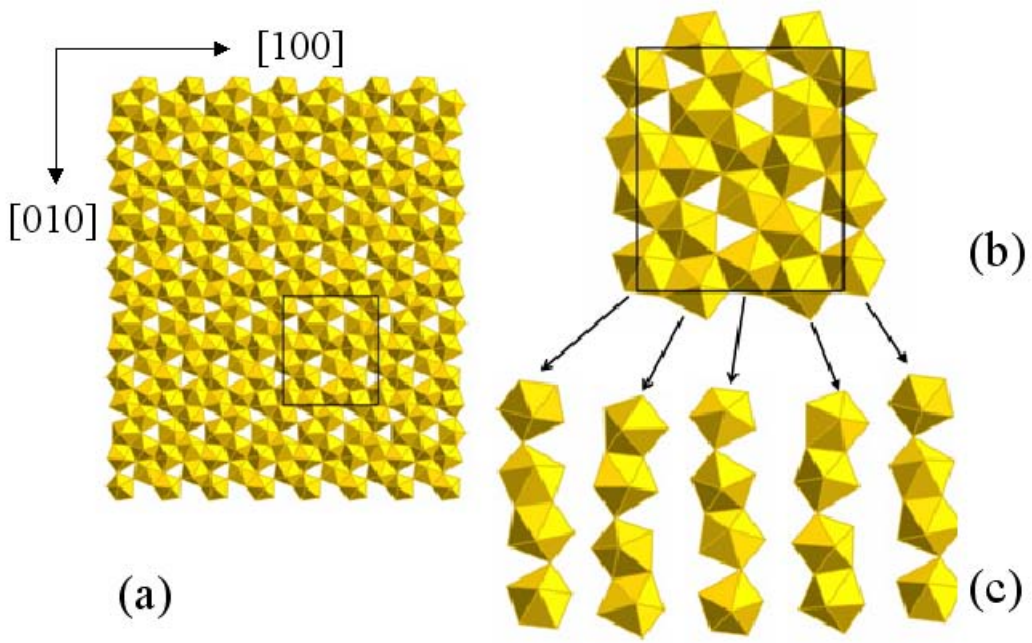

Fig.: 6.3 (a) Shows the structural-sheet of schoepite parallel to the (001)-face, consisting of uranyl-polyhedrons. This view is parallel to the c-axis of the mineral. The unit-cell dimension is framed. (b) and (c) show that the unit-cell, as well as the whole structural-sheet of schoepite, can be thought of being composed of chains of polyhedrons (polyhedron chain).

Even though we will later arrange polyhedron chains parallel to distinct crystallographic directions, the idea to subdivide a structural sheet in "chains" was first mentioned by Miller et al. (1996) and Burns et al. (1996). Their intention was to reconstruct and predict sheet anion topologies of sheet minerals, in order to develop a method to compare and classify the numerous uranyl-mineral structures which are based upon sheets of polyhedrons of higher bond valence (BURNS, 1999).

As the structural sheet dominates the morphology of uranyl-sheet minerals and polyhedron chains can be determined terminating the edges along the structural sheet, our interest will be focused on how to compare these different terminations and how they influence the final morphology of the crystal.

A polyhedron chain in schoepite, terminating a structural-sheet contains ligands that bond either to U^{6+} cations and/or ligands which bond to U^{6+} cations *and* to species in the adjacent gas phase or aqueous solution. The linearity of the chain of polyhedrons requires that the polyhedrons should have a small number of U– φ terminations. Figure 6.4 shows chains of polyhedra parallel to [100], [010], [120], [210] and [110] in the structural unit of schoepite, $[(UO_2)8O_2\ (OH)_{12}](H_2O)_{12}$, after Finch *et al.* (1996).

Figure 6.4 refers to the following question: which periodic bond-chains in uranyl-sheets define the morphology of the corresponding F-faces? Application of PBC theory requires categorization of different types of bonds in these bond chains. Bonds between U6+ and O^{2-} or $(OH)^-$ can have similar strengths in all these chains, and therefore one must consider the distances to the central $U6^+$ cations. PBC theory does not consider the type of equatorial ligands in the chain [O^{2-} or $(OH)^-$], the arrangement of interstitial cations, the change in morphology with pH or the degree of supersaturation. Further the PBC-theory can not distinguish between a left and a right termination of a polyhedron chain, which is important if parallel edges show an anisotropic behaviour. Those are the reasons why we use chains of polyhedra instead of chains of bonds, as required by the PBC-theory.

To predict the occurrence of different edges, we must consider the different types of linear periodic chains of polyhedra parallel to an edge. Figure 6.5 shows linear periodic chains of polyhedra parallel to [100] in schoepite. Depending on whether one considers the surface on the right or left side of the figure, one can construct (linear periodic) chains of polyhedra with different types of terminations (Fig 6.6). Terminations of linear periodic chains that terminate the layer to the right or left side are called *right terminations* or *left terminations*, respectively.

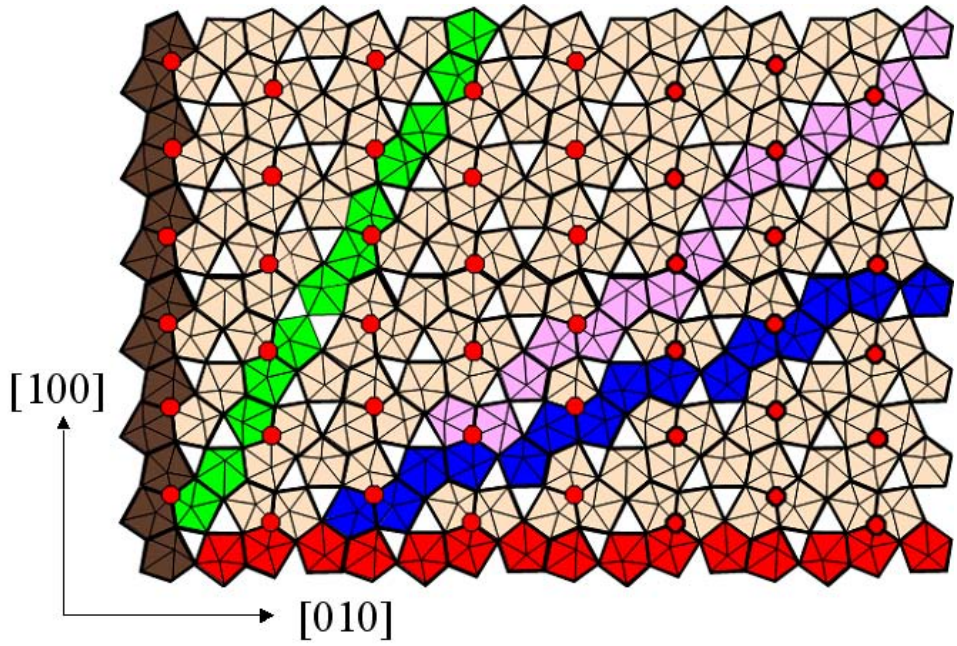

Fig.: 6.4 Structural sheet of schoepite. Marked in different colors are edges of terraces running parallel to distinct crystallographic directions. Brown [100], red [010], pink [110], green [210] and blue [120]. (Figure modified from SCHINDLER et al. 2004 a). Red balls indicate the position of equatorial O^{2-}anions.

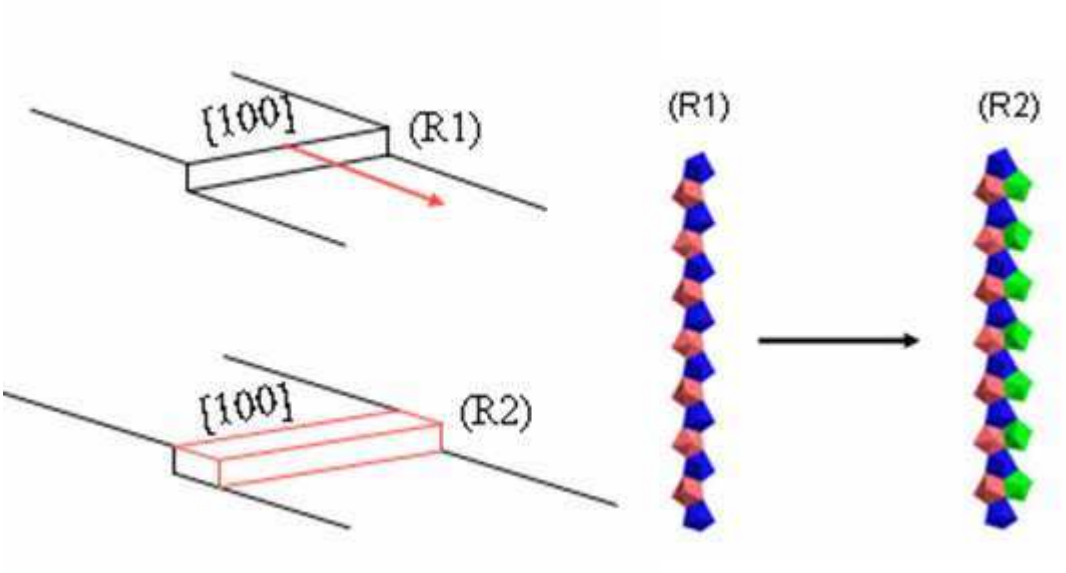

Fig.: 6.5 Shown on the left is the advancement of a stepped terrace. The step is oriented parallel to the [100] direction. On the right the different termination of this step R1 and R2 are shown. The advancement of the step occurs due to adding an additional chain of polyhedrons (marked in green).

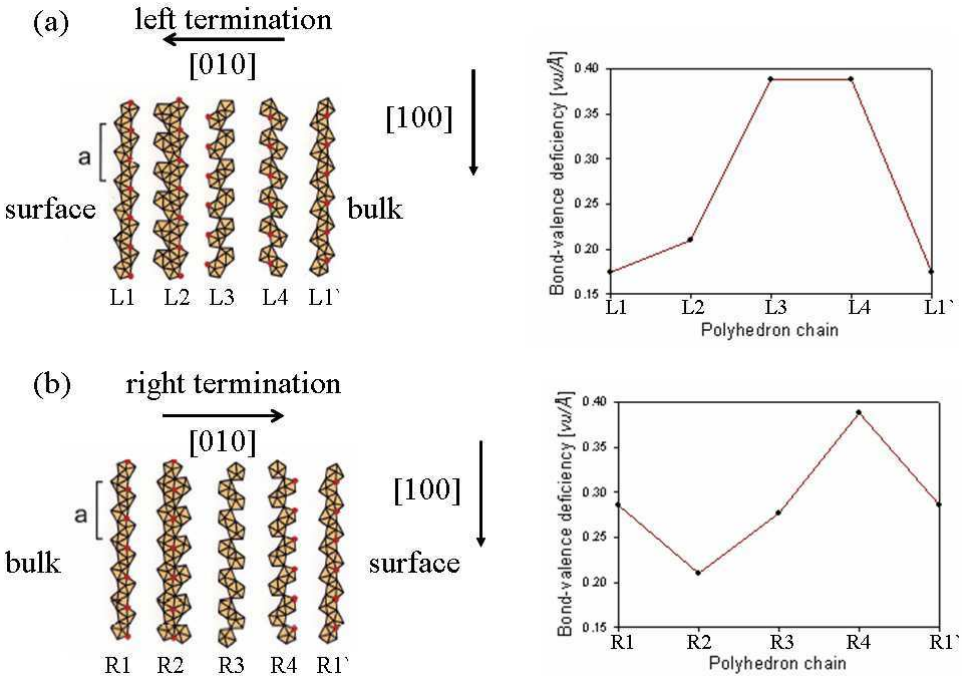

Fig.: 6.6 This figure shows the differences in the bond-valence deficiency of [100]-edges of the structural-unit of schoepite. Above the advancement of the step is shown schematically. Fig. 6.6a demonstrates the step advancement from right to left (left termination). In Fig.: 6.6b the steps advance from left to right (right termination). The diagrams apply to the changes in the BVD-value as the steps advance (modified from SCHINDLER et al. 2004a).

The linear periodic chain of polyhedra parallel to [100] in schoepite has a repeat distance of 14.377 Å. Let us designate the right termination of this chain as *R1*: there are two $^{[7]}$U–OH terminations and four $^{[7]}$U–OH– $^{[7]}$U terminations (Fig. 6.7). The average bond-valence of $^{[7]}U6^{+}$–O in schoepite is 0.47 *vu*, and the average O–H bond-valence is 0.80 *vu* (Brown 1981). The oxygen atoms of the two [1]-coordinated and the four [2]-coordinated (OH) groups receive (2 x 1 x 0.47 + 2 x 0.8) = 2.54 *vu*, and (4 x 2 x 0.47 + 4 x 0.8) = 6.96 *vu*, respectively. The resulting bond-valence deficiency at the oxygen atoms in the chain is the difference between their formal valence and their incident bond-valence sum.

For example, the oxygen atoms of the two [1]-coordinated (OH) groups in the repeatunit of the chain have a formal sum charge of 4^-, and they accept 2 x 0.47 *vu* from equatorial U–O bonds and 2 x 0.80 *vu* from O–H bonds. The sum of the incident bond-valence is 2.54 *vu*, resulting in an aggregate bond-valence deficiency of 4 – 2.54 = 1.46 *vu*. The bond-valence deficiency of the four [2]- coordinated oxygen atoms is 1.04 *vu*. The bond-valence deficiency of the oxygen atoms in the repeat distance of the chain of polyhedrons is 1.46 + 1.04 = 2.50 *vu*, and normalized to the length of the chain: 2.50 / 14.337 = 0.1744 *vu* / Å. The bond-valence deficiency of such a chain depends on the type and number of anion terminations.

A high bond-valence deficiency occurs where the chain contains a high number of negatively charged terminations, such as U–OH, U–O–U or U–O, and a low bond-valence deficiency occurs if the chain contains a high number of the formally neutral U–OH–U terminations. Here, the number of kink sites along the chain controls the number of U– φ and U– φ –U terminations.

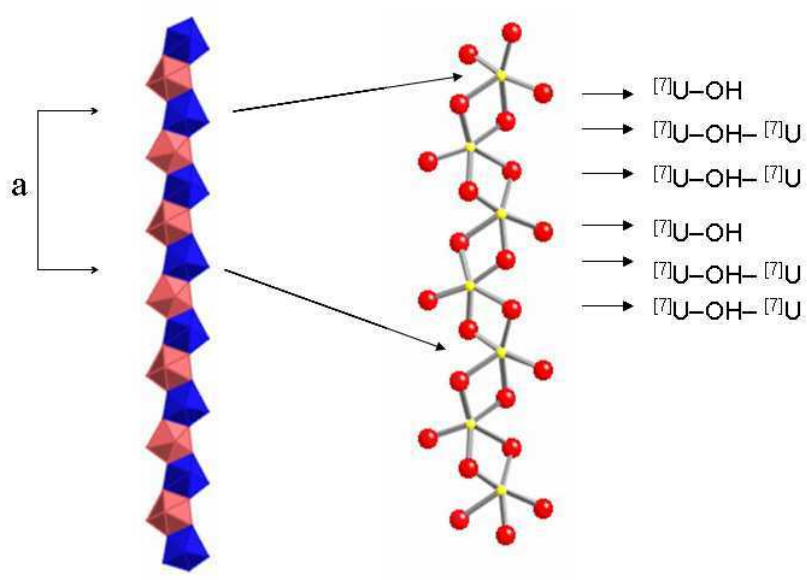

Fig.: 6.7 This image shows a chain of polyhedrons parallel to the [100] direstion. The repeat unit "a" is 14.377 Å. On the right side the same chain is given in an atomistic construction and the coordinated environment of the terminating oxygen atoms is given.

6.2 Prediction of the morphology of dehydrated schoepite

The previous Chapter (6.1) has outlined how the BVD-model can be applied to calculate bond-valence deficiencies of polyhedral chains terminating a stepped terrace. This method will now be applied to predict the morphology of synthetic dehydrated schoepite crystals.

Dehydrated schoepite has been chosen as an example because of its simple crystallographic structure. The structural unit of dehydrated schoepite consists of $^{[7]}$U- and $^{[8]}$U- uranyl polyhedrons and there are no H_2O-molecules present in the interstial-complex (FINCH et al. (1998). Therefore, dehydrated schoepite is a good example to test the BVD-model and its capability to predict crystal morphologies of sheet-like minerals. Focusing on the bond-valence deficiencies of different polyhedral chains terminating the structural-unit of dehydrated schoepite, predictions about the morphology of the crystals and predictions about certain crystal surface features, such as the shape of etch-pits for example, are possible.

FINCH et al. (1997) reported that dehydrated schoepite, with the general formula $[(UO_2)\ O_{0.25\ -\ 2x}\ (OH)_{1.5\ +\ 2x}]$, occurs in natural samples as a corrosion ring around schoepite crystals $[(UO_2)_8\ O_2\ (OH)_{12}](H_2O)_{12}$. But, dehydrated schoepite has not been observed as larger single crystals in nature so far. Nevertheless, single crystals of dehydrated schoepite can be synthesized under laboratory conditions.

In our experimental setting dehydrated schoepite was synthesized under hydrothermal conditions in Teflon-vessels at 120°C for 3 days, with a molar ratio of 1 : 2.5 uranyl-acetate and (H_2O). Besides microcrystalline powder, the residual contained idiomorphic crystals of up to 60 µm in size (Fig.6.8). This solid phase was characterized by X-ray powder diffraction, SEM, EDX and DTA analysis and the crystals have been identified as dehydrated schoepite having a $[(UO_2)\ O_{0.2}(OH)_{1.6}]$ composition.

6.2.1 The "theoretical" structural sheet of dehydrated schoepite $UO_3 \cdot 0.8\ H_2O$

Despite the knowledge of the chemical composition of our sample [$(UO_2)\ O_{0.2}(OH)_{1.6}$] and the lattice parameters derived by singly-crystal diffraction [a = 4.2799, b = 6.8971, c = 10.1946, α = 90.0496, β = 09.0279, γ = 89.9991), the topology of the structural sheet of the dehydrated schoepite phase synthesized [$(UO_2)\ O_{0.2}(OH)_{1.6}$] is not known in detail so far.

Based on the observations that schoepite [$(UO_2)\ O_2\ (OH)_{12}](H_2O)_{12}$ transforms slowly in air at ambient temperatures to metaschoepite $UO_2 \cdot n\ H_2O$ (n = 2), and metaschoepite can be further altered to "dehydrated schoepite" [$(UO_2)\ O_{0.25\ -\ 2x}\ (OH)_{1.5\ +\ 2x}$], FINCH et al. (1998) proposed a model about the structural relation ship of these phases.

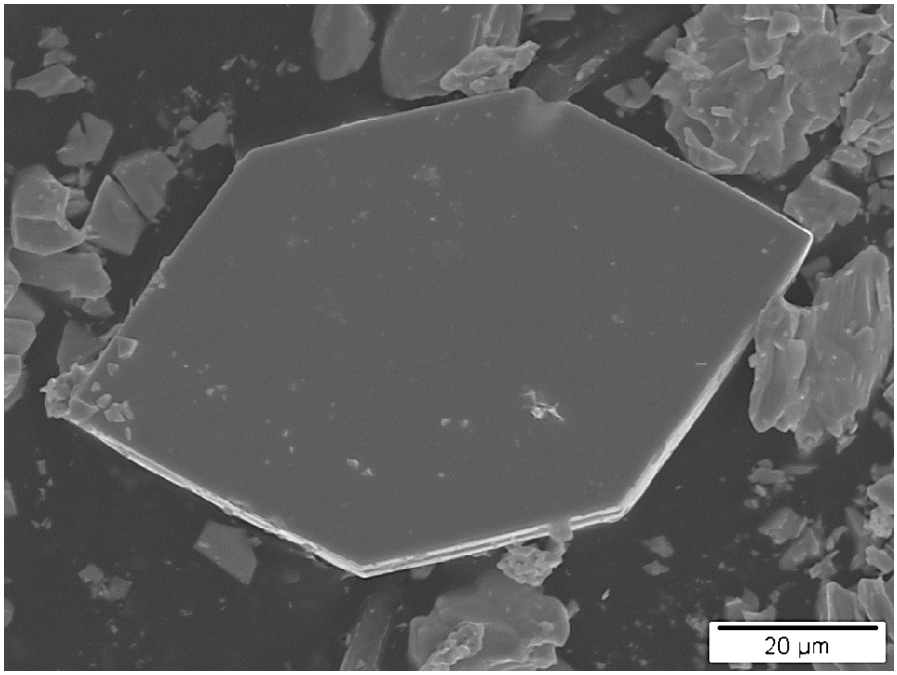

Fig.: 6.8 SEM-image of a synthesized dehydrated schoepite crystal.

According to this model (FINCH et al., 1998), the alteration of schoepite to dehydrated schoepite occurs in three steps: (a) loss of all interlayer H_2O from schoepite, causing a collapse of the layers, (b) atomic rearrangement within the structural sheet to a

configuration that may be similar to metaschoepite, and (c) further re-arrangement to a defect α-$UO_2(OH)_2$-type sheet.

These structural rearrangements can be described by two equations. The first resembles the loss of all interlayer H_2O-goups, equation 6.1 (FINCH et al., 1998):

$$[(UO_2)_8\ O_2\ (OH)_{12}](H_2O)_{12} \Rightarrow [(UO_2)_8\ O_2\ (OH)_{12}] + (H_2O)_{12} \qquad (6.1)$$

the second equation (eqn. 6.2) refers to the relaxation of the structural sheet and can be formulated as proposed by FINCH et al.(1998) as:

$$[(UO_2)_8\ O_2\ (OH)_{12}] \Rightarrow 8\ [(UO_2)\ O_{0.25}\ (OH)_{1.5}] \qquad (6.2)$$

The right-hand side reaction of equation 6.2 represents a structural-derivate of α-$UO_2(OH)_2$ in which anion vacancies are disordered with a composition similar to "dehydrated schoepite" ($UO_3 \cdot 0.75\ H_2O$) . The structural relationship between schoepite, dehydrated schoepite and α-$UO_2(OH)_2$ obtained by (FINCH et al., 1998) is illustrated in Figure (6.9).

The ball-and- stick model (Fig.: 6.9b) is a theoretical structural sheet with a stoichiometric schoepite composition on the left, "dehydrated schoepite" composition in the middle and α-$UO_2(OH)_2$ – composition on the right.

According to MILLER et al. (1996), uranyl-sheet minerals can be classified by their sheet anion topologies, which can be separated into different chains of polyhedrons (Fig. 9.6 d,f). The structural sheet of schoepite, contains three types of such chains, all of which consist of uranyl-pentagons. The P-chain is composed of edge-sharing pentagons, the D- and U-chains are composed of arrowhead chains of pentagons with opposite orientation. The structural sheet of α-$UO_2(OH)$ is composed of H-chains, which contain edge-sharing hexagons.

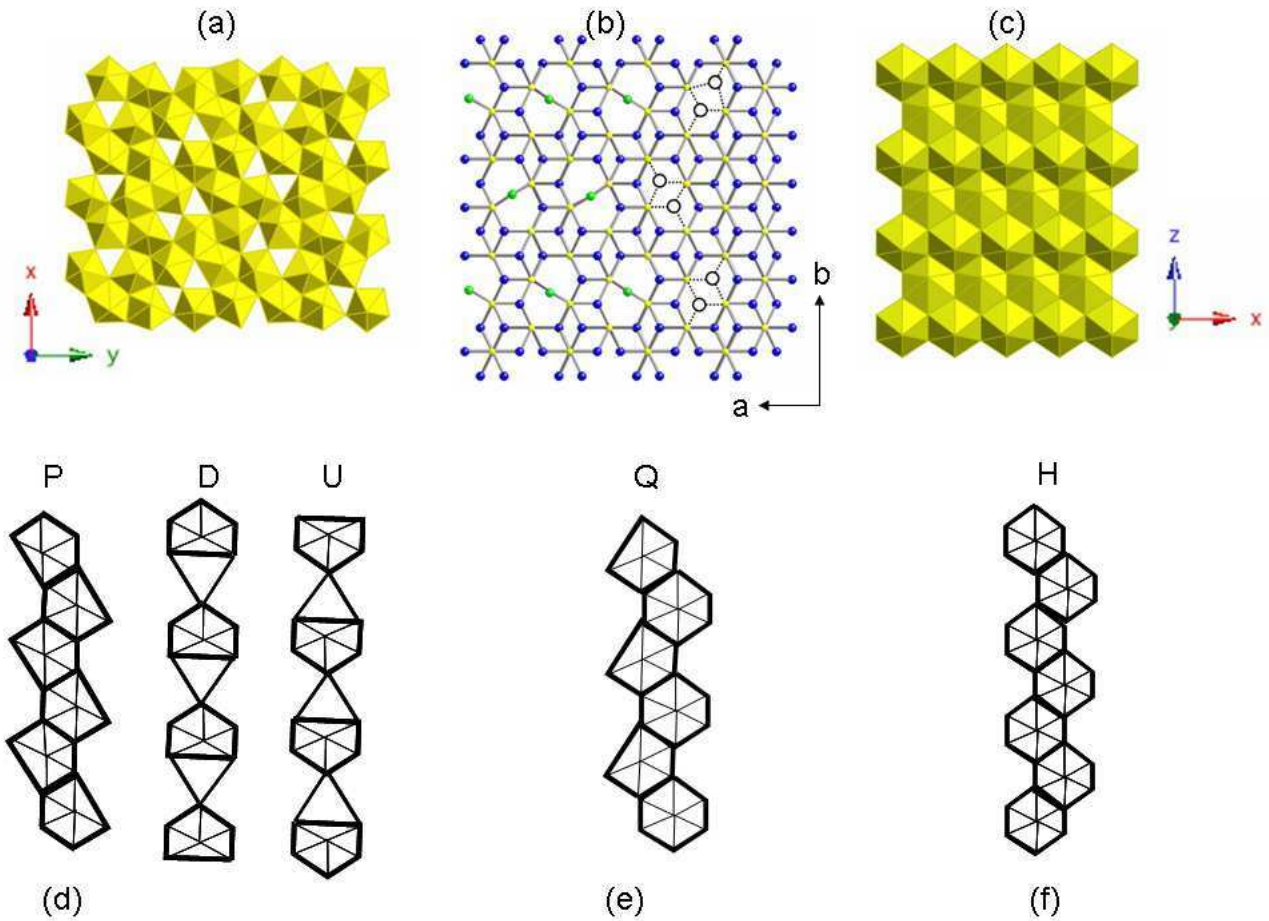

Fig.:6.9 (a) Polyhedral representation of the structural sheet of schoepite [$(UO_2)\ O_2\ (OH)_{12}$]. (c) Polyhedral representation of the structural sheet of α-$UO_2(OH)_2$. (b) Ball-and stick model of a structural sheet of "schoepite", showing the structural relationship between schoepite (left), dehydrated schoepite (middle, with open circles) and α-$UO_2(OH)_2$ on the right (FINCH et al., 1998). Yellow spheres are uranyl ions (uranyl O atoms not shown). Blue and green spheres are O atoms of the structural sheet (O^{2-} and OH). The open black spheres represent possible vacancies of O positions in the α-$UO_2(OH)_2$ structure, representative for a sheet with a dehydrated schoepite composition. (d) Anion chains in of schoepite (e) Additional anion chain in dehydrated schoepite (F) Anion chains in of α-$UO_2(OH)_2$.

The structural sheet of dehydrated schoepite is similar to the structural sheet of α-$UO_2(OH)$ but contains anion vacancies. This gives rise to a new theoretical chain (Q) shown in Figure (9.e), composed of edge sharing pentagons and hexagons.

Acknowledging the circumstance that the anion vacancies in dehydrated schoepite are disordered, this chain represents a theoretical chain of short-range order and is an additional chain implemented to reconstruct the theoretical structural sheet of the synthetic dehydrated schoepite crystals (Fig. 6.10).

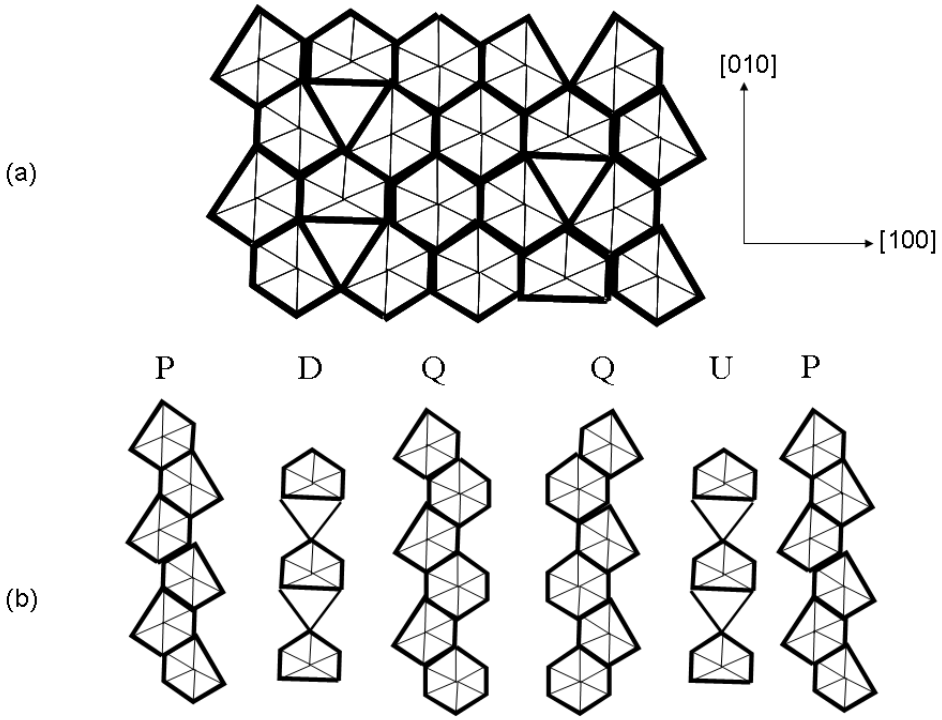

Fig.: 6.10 (a) Theoretical anion sheet topology of dehydrated schoepite with the composition $UO_3 \cdot 0.8\ H_2O$. (b) Stacking sequence of anion chains present in the dehydrated schoepite structure.

The lattice parameters of dehydrated schoepite [a = 6.86, b = 4.26, c = 10.20] given by FINCH et al.(1997), are similar to the lattice parameters of the dehydrated schoepite phase synthesized in our experiments [a = 4.2799, b = 6.8971, c = 10.1946]. Further, the chemical composition of the schoepite phase $[(UO_2)\ O_{0.2}(OH)_{1.6}] = UO_3 \cdot 0.8\ H_2O$, is similar the composition given by DAWSON et al. (1956).

Therefore, a correlation between the structural sheet of schoepite, α-schoepite and dehydrated schoepite, similar to the approach of FINCH et al. (1998) is considered, and a theoretical structural sheet for the synthesized schoepite crystals is established (Fig.6.10). The reconstruction of the theoretical structural sheet of the synthetic dehydrated schoepite crystals, was accomplished by application of the chain stacking sequence method of MILLER et al. (1996) as shown in Figure 6.10.

6.2.2 Bond-valence calculation of polyhedron-chains of dehydrated schoepite

Having established a theoretical structural sheet topology (Chapter 6.2.1), it is possible to predict the morphology of the dehydrated schoepite crystals synthesized. Based on the bond-valence approach in Chapter (6.1), those polyhedron chains composed of $U^{6+}\phi_8$ and $U^{6+}\phi_7$ polyhedrons, having the lowest bond-valence deficiency will form the most stable edges terminating the structural sheet and will dominate the final morphology of the crystals (Fig. 6.11).

In Figure (6.11) the theoretical structural sheet and the results of the bond-valence deficiency calculations of different anions terminations are compared to the morphology of the crystals synthesized. The obtained results indicate that chains of polyhedrons parallel to the [100] and [130] directions have the lowest bond-valence deficiencies. These results are in agreement with the morphology of the dehydrated crystals synthesized (Fig. 6.11b), indicating that it is possible to determine the crystal morphology of sheet-like minerals by application of the bond-valence deficiency model while comparing the deficiencies of different polyhedron chains (edges) terminating the structural sheet.

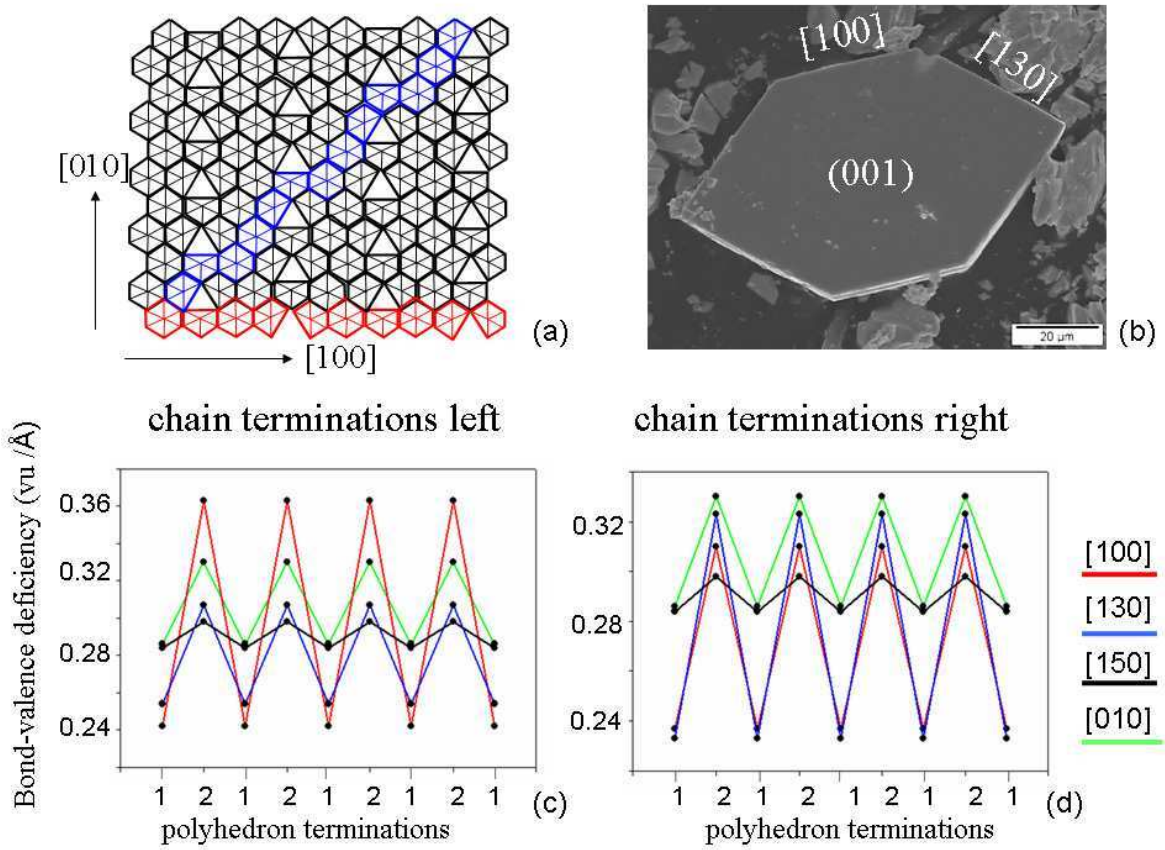

Fig.: 6.11 (a) Theoretical structural sheet of dehydrated schoepite. Blue: polyhedron chain running parallel to the [130] direction, red: polyhedron chain running parallel to the [100] direction. (b) SEM-image of dehydrated schoepite crystal synthesized. (c) and (d) Bond-valence deficiency diagrams of advancing polyhedron chains of different crystallographic orientation. According to the cluster-model (see text) only two terminations 1 and 2 need to be considered for each chain. The terminations parallel to the [100] and [130] direction having, the lowest bond-valence deficiency, dominate the sheet morphology of the crystals synthesized (b).

The diagrams (c) and (d) given in Figure (6.11), are simplifications of the bond-valence deficiency diagrams given in Chapter (6.1). Instead of calculating each individual polyhedral chain, only such polyhedron chains have been considered, which are terminated by polyhedron clusters. The results of both methods are comparable, but the later method has proven to be more efficient. Both methods are illustrated in Figures (6.13) and (6.14).

The comparison of both approaches shows that the polyhedron chains with the lowest bond-valence deficiencies can be detected. The advantage of calculating polyhedron chains, terminated by polyhedron clusters only, is the fewer number of different terminations to be calculated.

The bond-valence deficiencies of the different terminations have been calculated as described in Chapter 6.1, and are normalized to their respective unit-length. The average bond-valence for $^{[7]}U^{6+}$- O is 0.47 *vu* and 0.42 *vu* $^{[8]}U^{6+}$- O (FINCH et al.,1996; TAYLOR, 1971). The average O – H bond is 0.8 *vu* (BROWN, 1981). As an example the bond-valence deficiency of an oxygen atom having a $^{[7]}U$ – OH – $^{[8]}U^{6+}$ coordination is: 2 – (0.47 + 0.42 + 0.8) = 0.31 *vu* (Fig. 6.12).

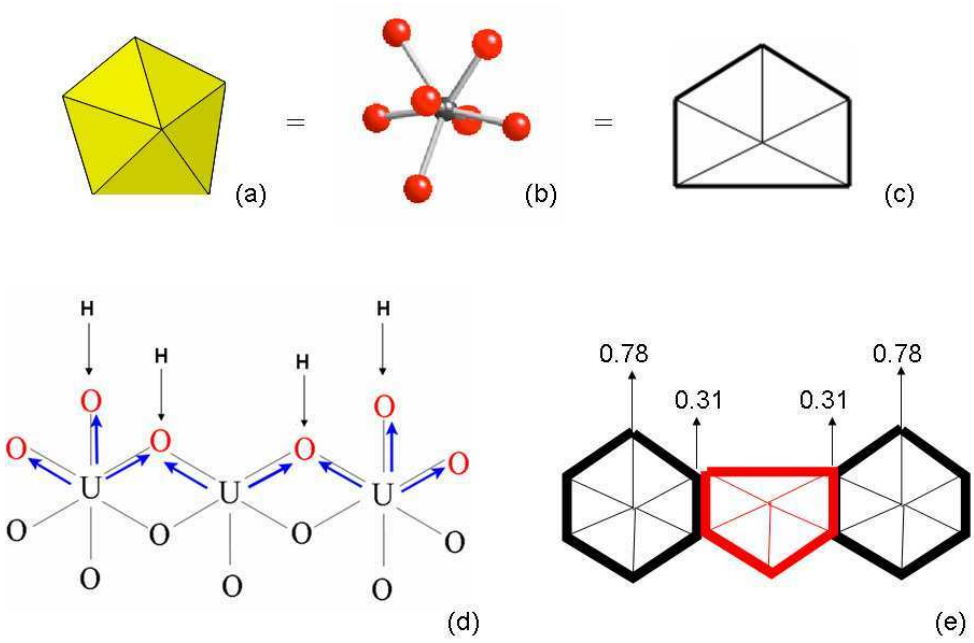

Fig.: 6.12 (a)-(c) Different representations of a $^{[7]}U^{6+}$-polyhedron. (a) Polyhedron representation (b) Ball-and-stick model, red: oxygen atoms, black: uranium arom. (c) Schematic representation used in the examples given for the structural unit of dehydrated schoepite. (d) Section of a polyhedron chain parallel to [100]. Oxygen atoms (red) terminating the polyhedron chain receive bonds (blue) form the bulk-uranium atoms and bonds from the attached H^+- ions. (e) Schematic representation of the polyhedron section (d). Given in numbers are the different bond-valence deficiencies of the oxygen atoms terminating the polyhedron chain.

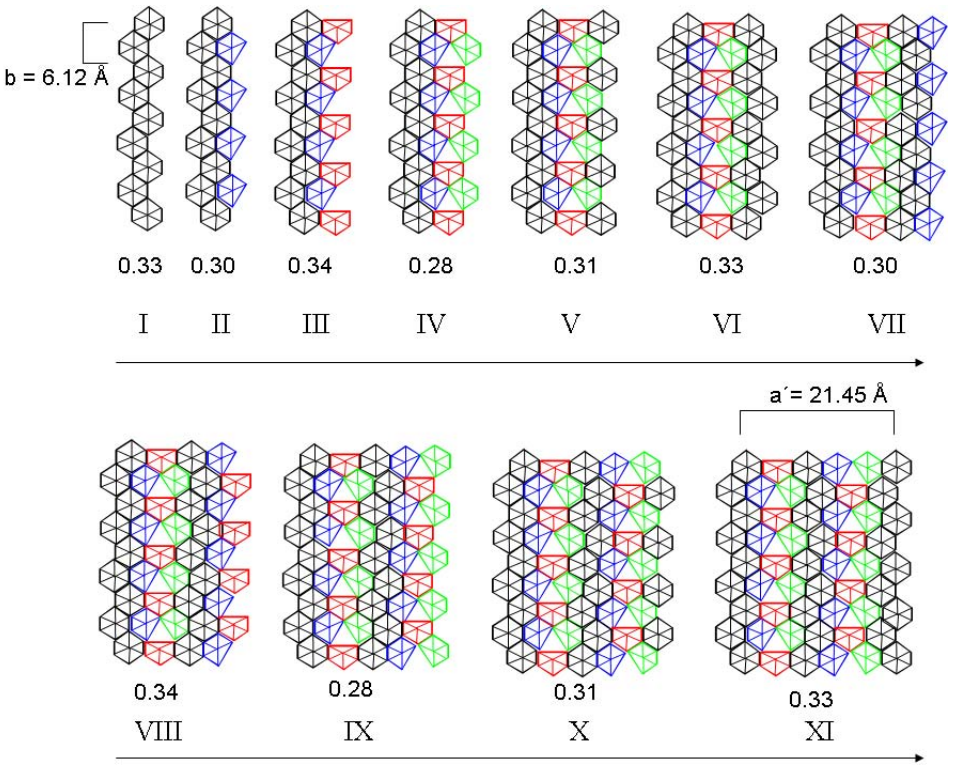

Fig.: 6.13 Schematic representation of an advancing polyhedron chain. The chain is oriented parallel to the [010] direction (b = 6,12 Å) and proceeds to advance in [100] direction (a`= 21.45 Å). The example given demonstrates how polyhedron chains can be calculated while attaching rows of single polyhedrons only. For each new termination the newly attached polyhedrons are marked in the same colour. The bond-valence deficiencies are stated below the images and are normalized to the lattice parameter b. The individual steps are labels I-XI. Starting with termination I the full translation parallel the [100] direction is reached at termination XI after 21.45 Å (a`). The terminations IV and IX having the lowest bond-valence deficiencies (0.28 *vu*/ Å).

Considering polyhedron clusters, instead of single polyhedrons, terminating a polyhedron chain is based on the work of BURNS et al. (1995), who classified the structure of borate minerals based on the topological character of fundamental building blocks (FBB). The general structure of borate minerals is based on $B\Phi_3$ and $B\Phi_4$ polyhedrons. These polyhedrons form finite clusters, chains, sheets and frameworks. BURNS et al. (1995) concluded that the polyhedrons can be combined to form finite clusters $[B_n\Phi_m]$, which can readily be recognized to occur as FBB´s in the structure of

borate minerals. The authors summarize: "*nature seems to produce structural diversity by using only small numbers of FBB´s and then polymerizing them in many different ways*."

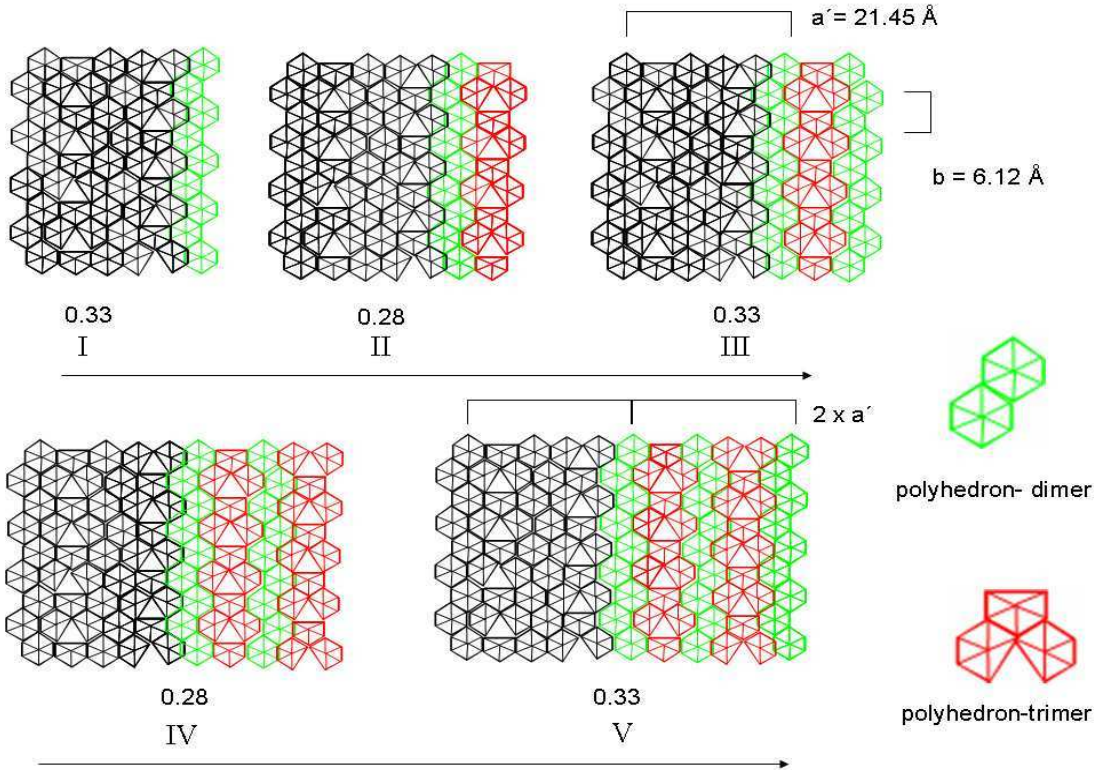

Fig.: 6.14 Advancing [010] termination. The number of terminations calculated is reduced, if the step advancement is considered to proceed due to the attachment of polyhedron clusters (see text). Only two different termination occur. Either the polyhedron chain is terminated by polyhedron-dimers (I, III) or polyhedron-trimers (II, IV). The later having the lowest bond-valence deficiency is equivalent to the terminations IV and XI in Figure 6.13.

Polyhedron clusters (FBB´s) can be identified in the theoretical structural sheet of dehydrated schoepite (Fig. 6.4 and 6.14). These fundamental building units are, a $U^{6+}\phi_8$ – dimmer and a $U^{6+}\phi_7$ – trimer. Only these two polymers are needed to construct the theoretical structural sheet of dehydrated schoepite.

An additional indication that polyhedron clusters have to be recognized, is there abundance as aqueous complexes in solutions (BAILEY et al., 2004; SUZUKI & BANFIELD, 1999). Depending on the pH of the solution different U^{6+}-complexes can be found in aqueous solutions.

As an example, the solubility of schoepite is at minimum around pH 6, at 25 C° and $P_{CO_2} = 10^{-3.5}$ (SUZUKI & BANFIELD, 1999). This is about the same pH range at which schoepite is expected to crystallize from a saturated solution. The most dominante aqueous species present at pH 5-6 (1mM ionic strength for 100 ppm U^{6+} and $P_{CO_2} = 10^{-3.5}$) is $(UO_2)_3OH^+_5$, a U^{6+}-trimer (SUZUKI & BANFIELD, 1999) and such U^{6+}-trimer clusters are very common in the structural sheet of schoepite (Fig. 6.4).

6.2.3 Dissolution features of dehydrated schoepite

In the previous Chapter (6.2.1) it has been outlined that polyhedron chains having a low bond-valence deficiency affect the morphology of dehydrated schoepite crystals.

The subsequent question that arises is, if the same polyhedron chains prove to be stable during leaching experiments. Due to the low solubility of the crystals synthesized the dissolution of the crystals could not have been observed *in situ.* Therefore, the leaching experiments have been carried out *ex situ* in sealed test tubes. In order to monitor the proceeding dissolution processes the samples have been scanned by an AFM-microscope (Dimension 3000), before and after the leaching experiments.

Each test tube contained 0.1g of the synthesized dehydrated schoepite sample and 1.5 ml solution (pH 6-7) of different composition (H_2O, KCl, $CaCl_2$ and $BaCl_2$). The concentration of the salts varied from 0.1 M to 1.0 M. The samples were recovered from the test tubes after time periods of 6, 12, 24 and 36 hours. Afterwards the residual was separated from the solution, washed and than dried at room temperature.

Finally the samples have been scanned by an AFM-microscope in air. The results of the experiments are compared in Table 6.1.

The solutions KCl, $CaCl_2$ and $BaCl_2$ have been chosen because they can be related to uranium-minerals, such as compreignacite $K_2[(UO_2)_3O_2(OH)_3]_2(H_2O)_7$, becquerelite $Ca[(UO_2)_3O_2(OH)_3]_2(H_2O)_8$, billietite $Ba[(UO_2)_3O_2(OH)_3]_2(H_2O)_4$ and protasite $Ba[(UO_2)_3O_3(OH)_2]_2(H_2O)_3$. All these minerals have a similar or equivalent structural-sheet topology (Fig.: 15. b), but vary in the composition of their interstitial-complexes. The pure H_2O-solution was chosen as a reference experiment.

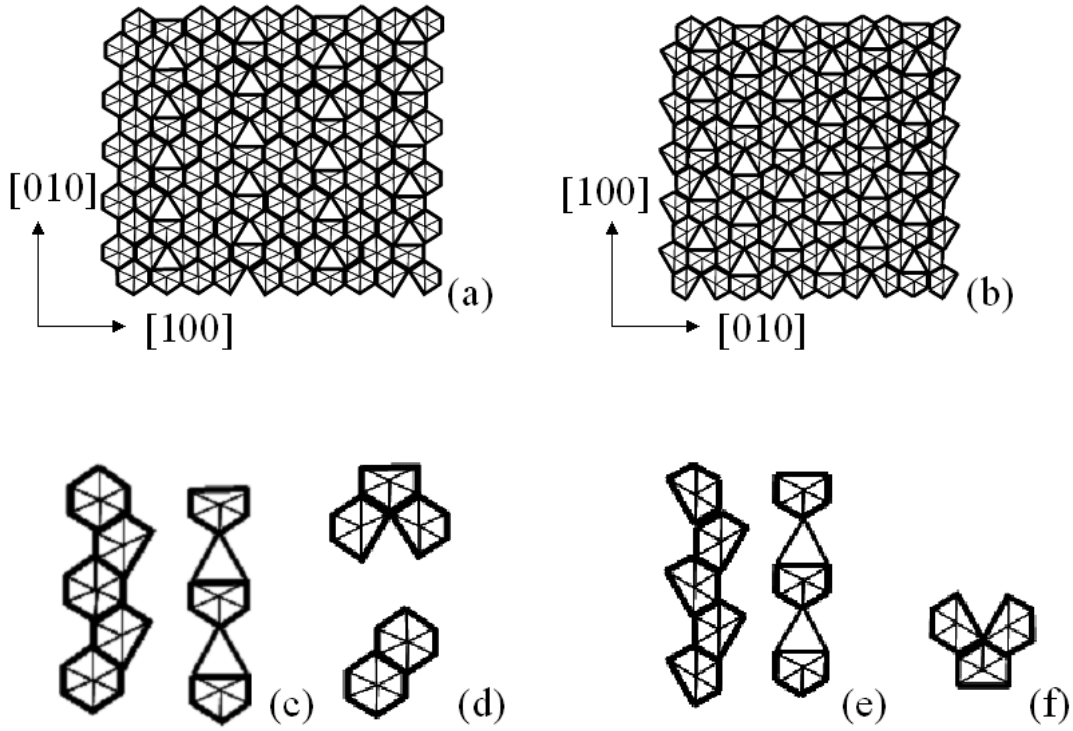

Fig.: 6.15 (a) Schematic representation of the theoretical structural sheet of dehydrated schoepite. (b) Schematic representation of the theoretical structural sheet of compreignacite, becquerelite and billietite (protasite). (c) Polyhedron chains (stacking sequence of anion chains) in the structural sheet of dehydrated schoepite. (d) FBB´s of the structural sheet of dehydrated schoepite. (e) Polyhedron chains (stacking sequence of anion chains) present in the structural sheets of compreignacite, becquerelite, billietite and protasite (BURNS, 1999). (d) FBB of the structural sheet of compreignacite, becquerelite, billietite and protasite.

Table 6.1

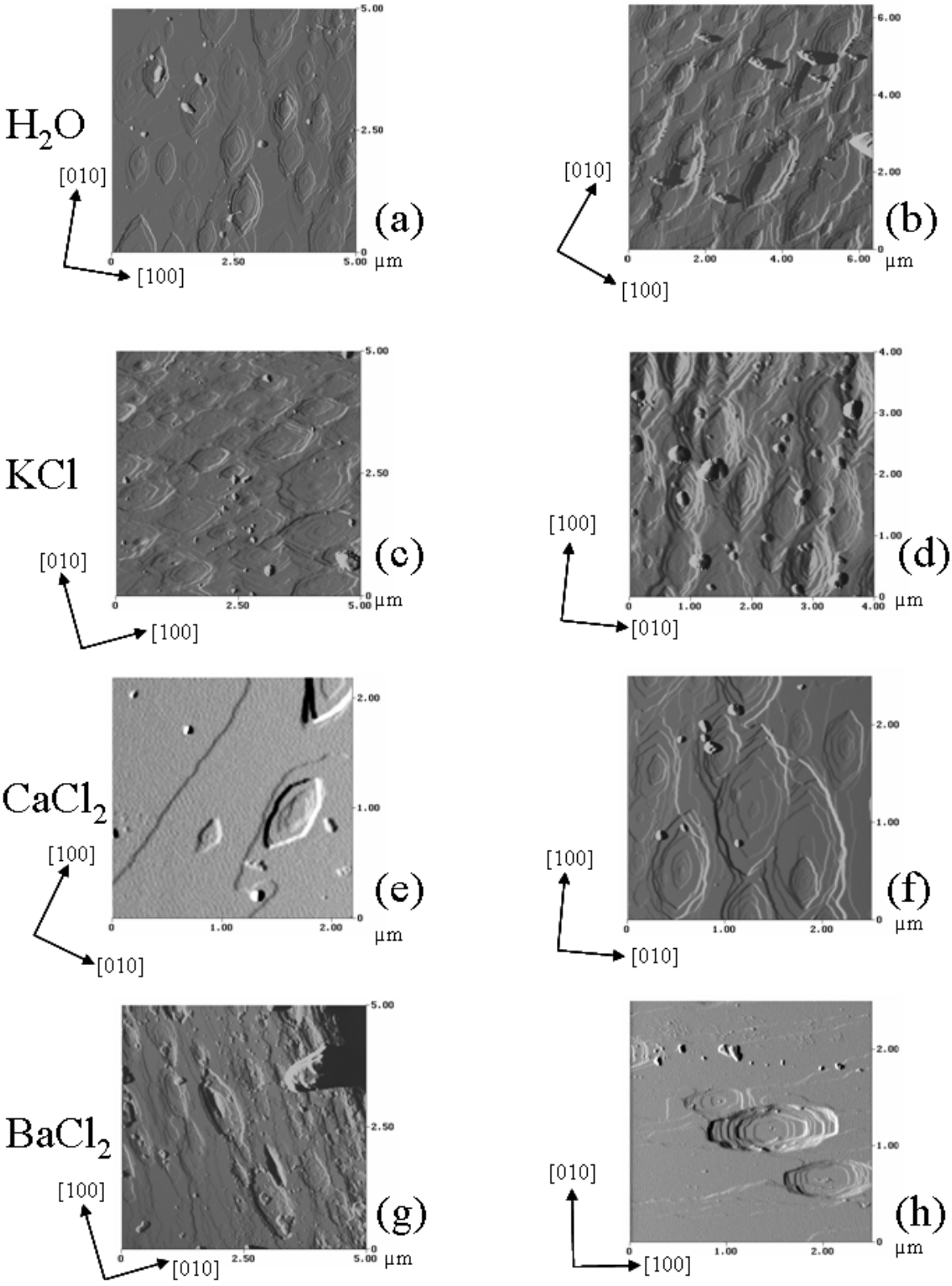

Previous page:

Tab.: 6.1 All images are deflection images of (001) crystal surfaces of dehydrated schoepite obtained with an AFM-microscope Dimension 3000. Shown are etch-pits formed during leaching experiments with different solutions. The orientations [100] and [010] have been obtained from the orientation of the crystals on the sample holder.

(a) and (b) Leaching experiment with H_2O. The edges are oriented parallel to the [010] and [130] directions. (a) after 3 hours, the [130] directions are dominante (b) after 24 hours. The depth of the etch-pits increased and more edges are oriented parallel to [010].

(c) and (d) Leaching experiment with KCl (1 M). The edges of the etch-pits are oriented parallel to the [010] and [130] directions. (a) after 6 hours (b) after 24 hours. The depth of the etch-pits increased during this time-periode.

(e) and (f) Leaching experiment with $CaCl_2$ (1 M). The edges of the etch-pits are oriented parallel to the [010] and [130] directions. (a) after 6 hours (b) after 36 hours. The depth of the etch-pits increased less compared to the former experiments (H_2O and KCl).

(g) and (h) Leaching experiment with $BaCl_2$ (1 M). The edges of the etch-pits are oriented parallel to the [010] and [100] directions. (a) after 3 hours (b) after 36 hours.

The results pictured in Table 6.1 can be explained by the different composition of the solutions chosen and as a result of the interaction of the ions present with the crystal surface. The results obtained are compared to the predictions made from the bond-valence deficiency calculations. The calculations given in Chapter 6.2.1 state that the most stable edges (polyhedron chains) of the structural-unit of dehydrated schoepite are oriented parallel to the directions [010] and [130].

As a preliminary prediction to our experiments, the edges of etch pits obtained during the leaching of the samples should be oriented parallel to polyhedron chains having a low bond-valence deficiency.

The AFM- deflection image (Tab.6.1 a, b), obtained after 3 and 24 hours of leaching with a pure H_2O-solution shows that the edges of the etch-pits obtained are oriented parallel to the [010] and [130] directions of the theoretical structural sheet of dehydrated schoepite. This result is in concordance with our predictions that at a neutral pH-range, and the absence of adsorbing ions, only those polyhedron chains with the lowest bond-valence deficiency, calculated from the structural-sheet only, are expected to be stable. The results obtained from the leaching experiments, in presence of foreign ions at pH 6-7, are also in concordance with our predictions, even to the extent that the shape of the edge-pits changes in the presence of Ba^{2+}-ions (Tab. 6.1 g, h, Fig. 6.16).

The leaching experiments with KCl, showed no major difference in the shape of the etch-pits compared to those etch-pit shapes obtained in the H_2O-reference experiments. In all the experiments undertaken, the edges of the etch-pits are dominated by the polyhedron chains [130] and [010]. Only a minor change in the relative relationship of these two directions was detected after the dehydrated schoepite samples have been treated with a 1.0 M KCl solutions for 24 hours.

The result of the KCl-leaching experiments can be explained by the low bond-valence distribution of K^+-ions adsorbing to the different possible polyhedron chains. The average bond-valence of K^+ is 0.126 *vu* (BROWN, 2002). This value is in good agreement with the bond-valences of K^+ calculated form the compreignacite-structure (BURNS, 1998). There the average K- O distance is given as $K\text{-}_{\Phi}$ = 2.85 Å, and the resulting bond-valence value is 0.136 *vu*. Comparing this value to the average bond-valence of a weak hydrogen-bond of 0.2 *vu* (BROWN, 2002), indicates that no major changes in the relationship between the bond-valence deficiencies of different polyhedron chains are to be expected.

The influence of K^+ ions, temporarily adsorbing to the polyhedron chains, is minor compared the possible formation of weak hydrogen bonds, and thus no major change in the shape of the etch-pits could be observed compared to the reference H_2O experiment.

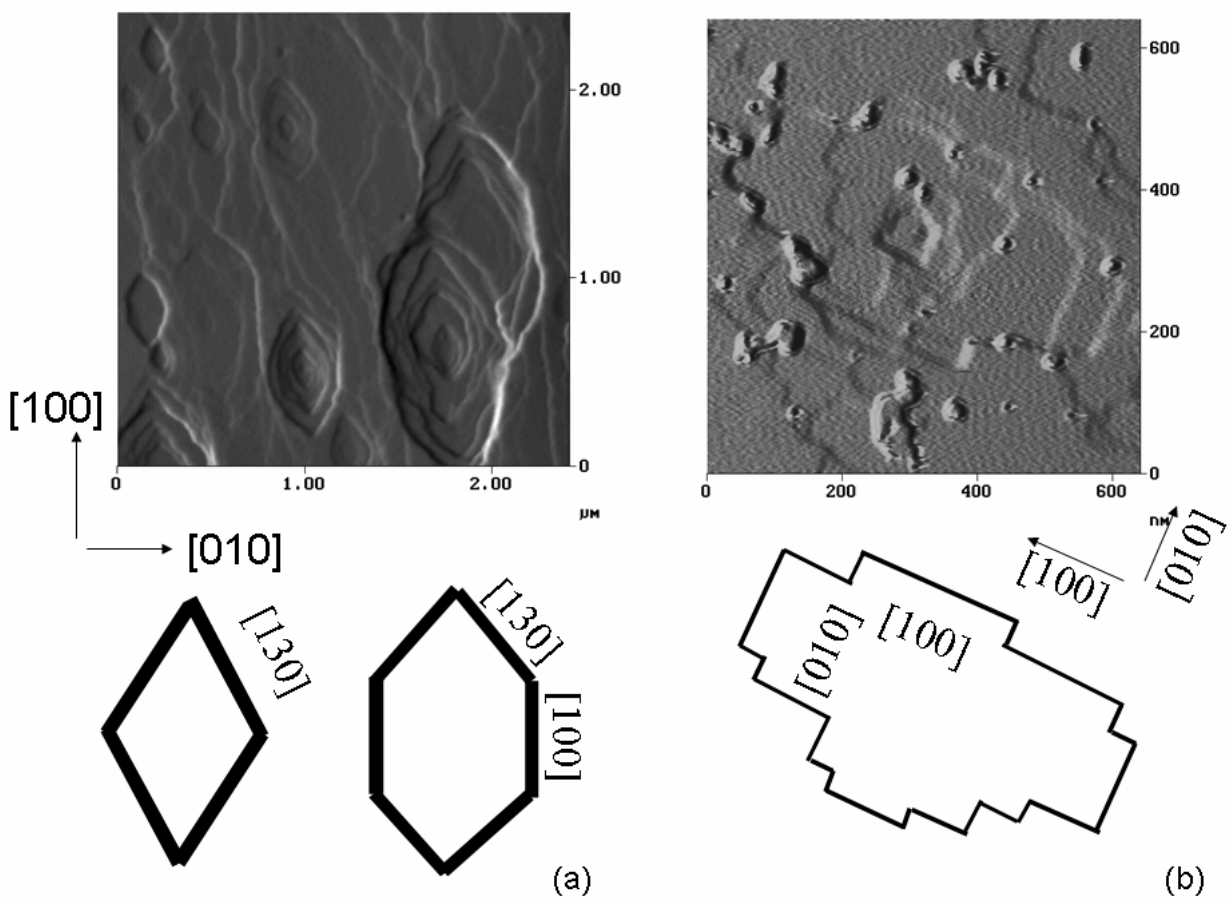

Fig.: 6.16 Differently shaped etch-pits on top of the (001) crystal surface of dehydrated schoepite. (a) The image and the drawings illustrate the shape of etch-pits formed during leaching experiments with a pure H_2O solution. (b) During the leaching with a 1 M $BaCl_2$-solution edges parallel to the [010] direction evolved.

In contrast the presence of divalent cations such as Ca^{2+} and Ba^{2+} should to some extent influence the shape of etch-pits formed. While such changes could well be observed in the Ba^{2+}-leaching experiments no differences occurred while the dehydrated schoepite samples where treated with Ca^{2+}-solutions. These results obtained (Tab. 6.1) seem to be

to some extent arbitrary to the results expected. The presence of higher charged ions in the solution should have an influence on the shape of etch-pits observed, but only the experiments in the presence of Ba^{2+} ions showed such changes (Tab. 6.1, Fig. 6.16).

The comparison of the average bond-valences given by BROWN (2002), Ba^{2+} = 0.195 *vu* and Ca^{2+} = 0.274 *vu* might be a first explanation of the different influences of these cations present. These different bond-valence values result from differences in the ideal coordination number of these two ions. But they can be counterbalanced when compared to the bond-valences calculated from the protasite, and becquerelite structures (PAGOAGA et al., 1987). The average bond-length of Ca – O in becquerelite is 2.51 Å, which is equivalent to 0.23 *vu*. The average bond-length Ba – O in protasite is 2.84 Å, equivalent to 0.223 *vu*. These results show that both ions Ba^{2+} and Ca^{2+} contribute a similar amount of bond-valences to their respective structural-units. Consequently the slight differences in the bond-valences contributed to the structural-unit cannot be responsible for the differences observed in etch-pit morphology.

The bond-length of Ba-O in billietite given by PAGOAGA et al. (1987), is not precise enough to be considered, as they only locate one Ba^{2+} in their structural analyses, concluding that their sample was not crystallized well enough. The average bond-length given is Ba - O is 3.03 Å which is equivalent to 0.1335 *vu*. For the detected coordination number of Ba (CN = 7), these values are too low, because the bond-valence sum is 7 x 0.1335 vu = 0.9345 *vu*, and significantly does not match the atomic valence of Ba^{2+}.

Neglecting the minor bond-valence differences of Ca^{2+} and Ba^{2+} as possible factors, structural factors might be responsible for the differently shaped etch-pits observed. A comparison of the structural units of becquerelite and billietite together with the distribution of the interstitial cations (Fig. 6.17 a, b), shows that the Ca^{2+} ions are oriented parallel to the [010] direction, while the Ba^{2+}-ions are oriented parallel to the [100] direction. These different orientations can be related to the theoretical structural sheet of dehydrated schoepite (Fig. 6.17 c,d). The structural sheets of becquerelite,

billietite and dehydrated schoepite can be compared by adjustment of the polyhedron chains. While the crystallographic orientations [010] and [100] for each individual structural-sheet remain unchanged, the polyhedron chains are aligned in parallel orientation (Fig. 6.17).

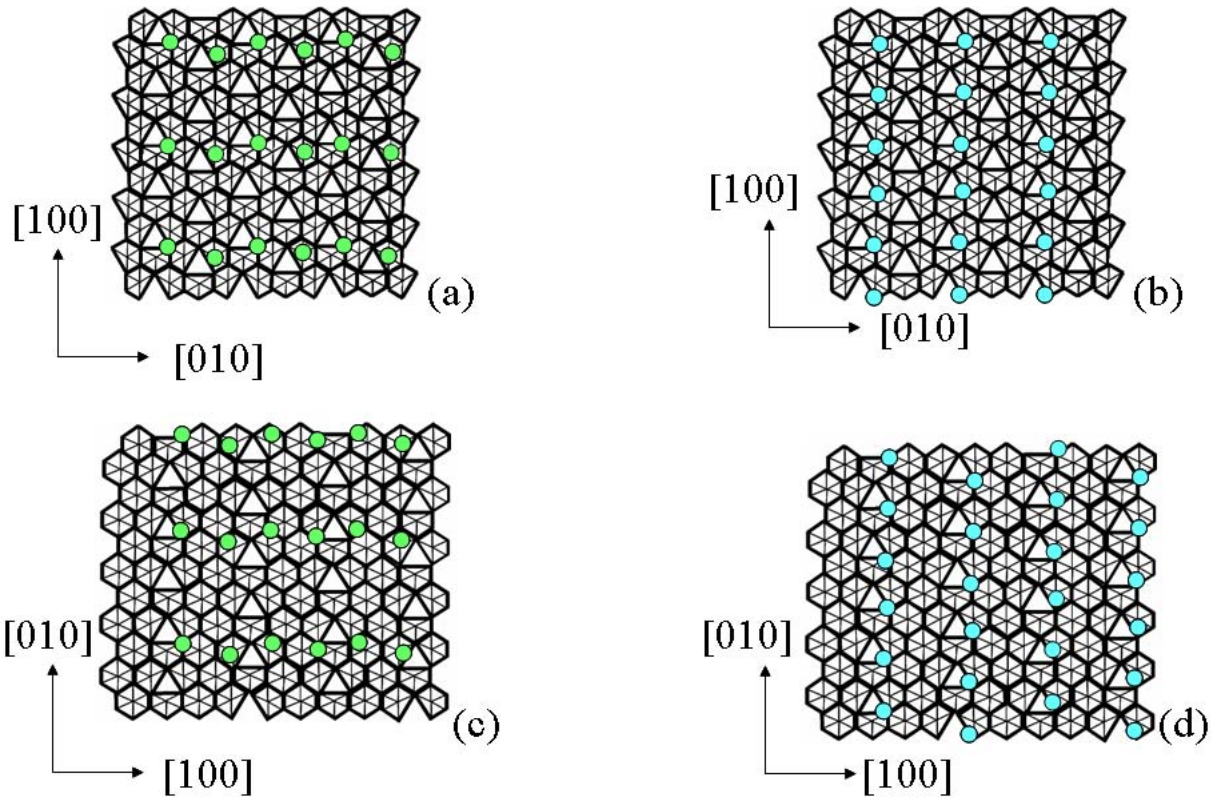

Fig.: 6.17 Comparison of the structural sheets of becquerellite, billietite and dehydrated schoepite. The polyhedron chains are oriented in the same direction, in order to compare the orientation of the structural-units of becquerellite and billietite to a similar oriented theoretical structural-unit of dehydrated schoepite. (a) Schematic representation of the structural sheet of becquerelite. The Ca-ions (green) are oriented parallel to the [010] direction. (b) Schematic representation of the structural sheet of billietite. The Ba-ions (blue) are oriented parallel to the [100] direction. (c) Schemetic representation of the structural sheet of dehydrated schoepite. The Ca-ions (green) are oriented parallel to the [100] direction. (d) Schematic representation of the structural sheet of dehydrated schoepite. The Ba-ions-ions (blue) are oriented parallel to the [010] direction.

Considering our leaching experiments of dehydrated schoepite in the presence of Ca- and Ba- bearing solutions we can deduce, that the Ca^{2+} - ions are predominately aligned parallel to the [100] direction of the theoretical structural sheet of dehydrated schoepite, while the Ba^{2+} ions are predominately oriented parallel to the [010] direction.

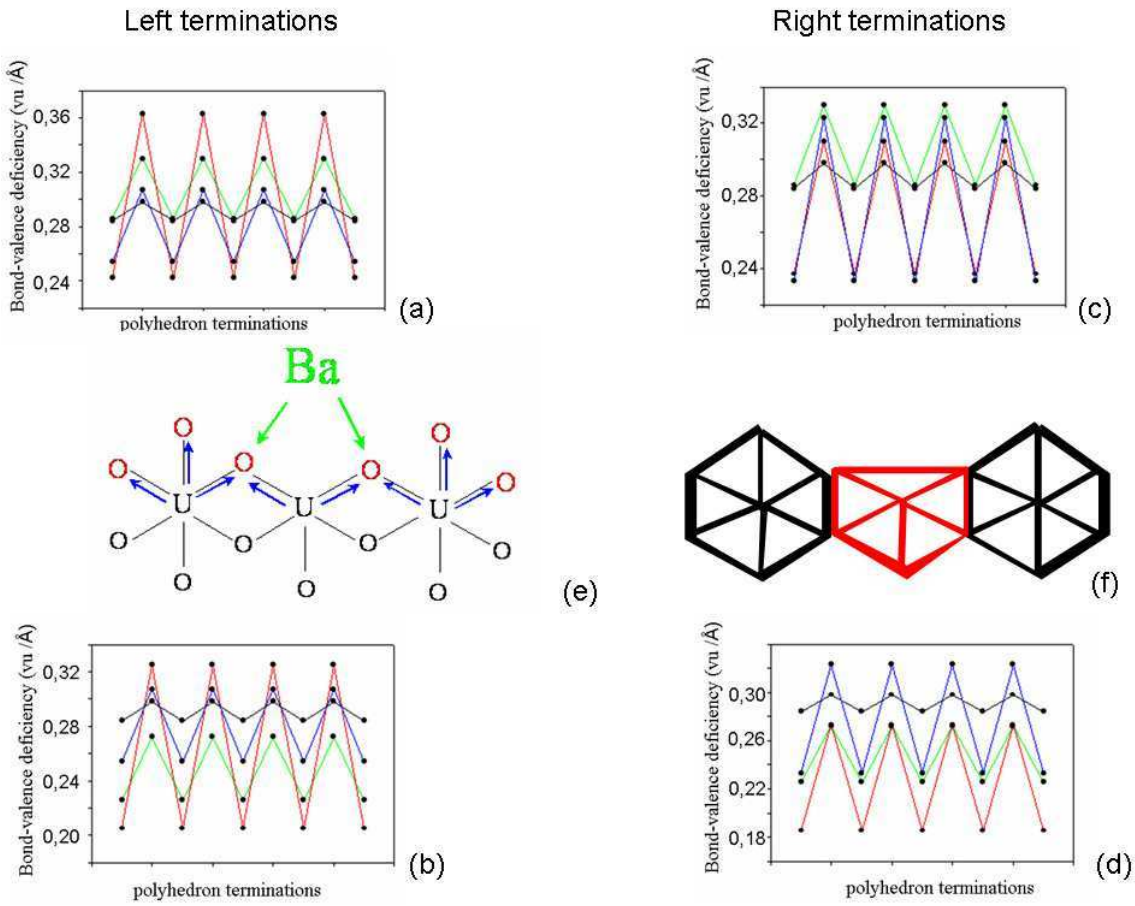

Fig.: 6.18 Comparison between the bond-valence deficiencies of different polyhedron chains in the structural sheet of dehydrated schoepite. (a) and (c) Deficiencies calculated for hydrated polyhedron chains. (b) and (d) Bond-valence deficiency diagrams after Ba-ions have selectively adsorbed to polyhedron chains parallel to the [001] and [010] directions. The diagrams show that due to the adsorption the bond-valence deficiencies of the polyhedron chains are lowered. Chains (edges) parallel to the [010] direction now have a lower bond-valence deficiency than polyhedron chains parallel to the [130] direction. (e) and (f) Possible attachment site of Ba-ions at a polyhedron chain parallel to the [010] direction.

This observation suggests that ions selectively adsorb to special positions relative to the structural sheet. Consequently, the ions can only add bond-valences to certain polyhedron chains, which in return lower their bond-valence deficiency more effectively. The Ca^{2+} ions are temporarily adsorbing to polyhedron chains parallel to the [100] direction of the structural sheet of dehydrated schoepite, and only contribute to an already low bond-valence deficiency. As a result no changes in the shape of etch-pits formed, compared to the reference experiment (pure H_2O- solution), are observed.

The Ba^{2+} ions predominately adsorb to polyhedron chains parallel to the [010] direction of the structural sheet of dehydrated schoepite. As a consequence the bond-valence deficiency of these polyhedron chains is lowered, and the etch-pit edges parallel to the [010] direction will be stabilised (Fig. 6.18).

6.3 Morphology changes due to interstitial cations

As a consequence of the results obtained in the previous chapter (6.2.3), the arrangement of interstitial complexes in minerals with identical structural units, may influence not only the shape of etch-pits observed, but may also influence the crystal morphology as a whole.

This can be well documented for becquerelite, $Ca(H_2O)_4[(UO_2)_3O_2(OH)_3]_2(H_2O)_4$, and billietite, $Ba(H_2O)_4[(UO_2)_3O_2(OH)_3]_2(H_2O)_3$. Figure 6.19. show the arrangements of the interstitial cations Ca^{2+} and Ba^{2+} in becquerelite and billietite, respectively. The interstitial Ca^{2+} atoms in becquerelite are arranged in rows parallel to [010], whereas the interstitial Ba^{2+} atoms in billietite are arranged in rows parallel to [100]. Evaluation of the bond-valence deficiencies of the structural units of becquerelite and billitite indicate, that the [100] and [110] are the most stable edges, whereas edges such as [010], [210], [130] and [310] are less stable (see Papers attached in Appendix V, SCHINDLER et al. 2004 a,b).

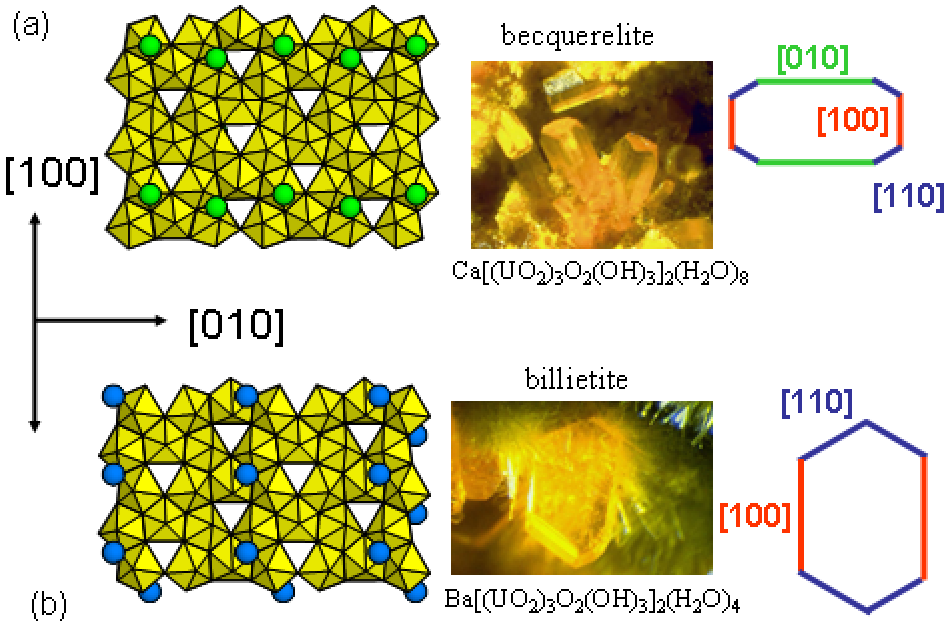

Fig.: 6.19 Left: structural sheets of becquerelite and billietite showing the different arrangements of interstitial cations. The Ca-ions (green) in becquerelite (a) are oriented parallel to the [010] direction. The Ba-ions (blue) in billietite (b) are oriented parallel to the [100] direction. Right: examples corresponding to the (001)-face morphology of becquerelite and billietite (image modified from SCHINDLER et al. 2004a).

Depending on the distributions of the interstitial cations the morphological importance of edge directions may be changed, giving rise to differently shaped crystals.

The edges [100] and [110] invariably occur on the (001) face of becquerelite and billietite alike and are therefore in good agreement with our predictions. Only becquerelite crystals are reported to be elongate parallel to [010], whereas billietite crystals can be elongate parallel to [100]. This readily implies that the occurrence of edges and their dominance on the final morphology is additionally controlled by the arrangement of the interstitial complexes (Fig. 6.19).

7. Application of the BVD-model to predict the morphology of polyhedral crystals (Internal factors)

The main reason for developing the BVD-model is to find a suitable method to predict crystal morphologies by combination of internal and external factors controlling the shape of polyhedral crystals. Internal factors such as the reticular density, lattice spacing (see Chapter 3) and face symmetry (this Chapter), will be incorporated into the BVD-model to describe a mineral surface by its bond-valence deficiency. Later, the bond-valence model is applied to external factors, such as ions present in a solution (Chapter 9). Finally, in Chapter 11 both factors (internal and external), having influence on the morphology of a crystal will be combined, because by then, both can be expressed via their respective bond-valences.

In the previous chapter it was demonstrated how the BVD-model can be applied to describe "two-dimensional" crystal surface features. A similar approach will be used in this Chapter to predict the morphology of "three-dimensional" polyhedral crystals. In Chapter (5) it is demonstrated how calculated BVDF-values can be applied to compare different crystal faces of a crystal having a simple cubic lattice type structure. In the example given, only faces with low (hkl)-indices have been compared. The application of the BVD-model, for the example given, obtained good results, but it must be stated that this approach will reach its limits when being applied to more complex crystal lattices or if faces with higher (hkl)-indices are compared. Therefore, additional internal factors, besides the number of dangling bonds emitted by the crystal surface, must be regarded to be involved in controlling the morphology of a crystal. Internal factors such as the reticular density and lattice density need to be considered when predicting the morphology of a polyhedral crystal. It has been demonstrated by BRAVAIS (1866), NIGGLI (1920) and DONNAY-HARKER (1937) that these factors have strong influences on the "equilibrium" or "abstract form" of crystals. Hence it is necessary to establish a correlation between the BVDF-values of a crystal surface and the internal structure of the crystal.

7.1 The BVD-model and reticular density

Incorporation of the reticular density model from BRAVAIS (1866) into the BVD-model is a first step to consider internal factors. Therefore the results obtained (Chapter 5) need to be reconsidered. In Fig.7.1 the BVDF-values of the (001)-faces, present in the three cubic Bravais-lattices types (Pm3m, Fm3m, Im3m), are compared.

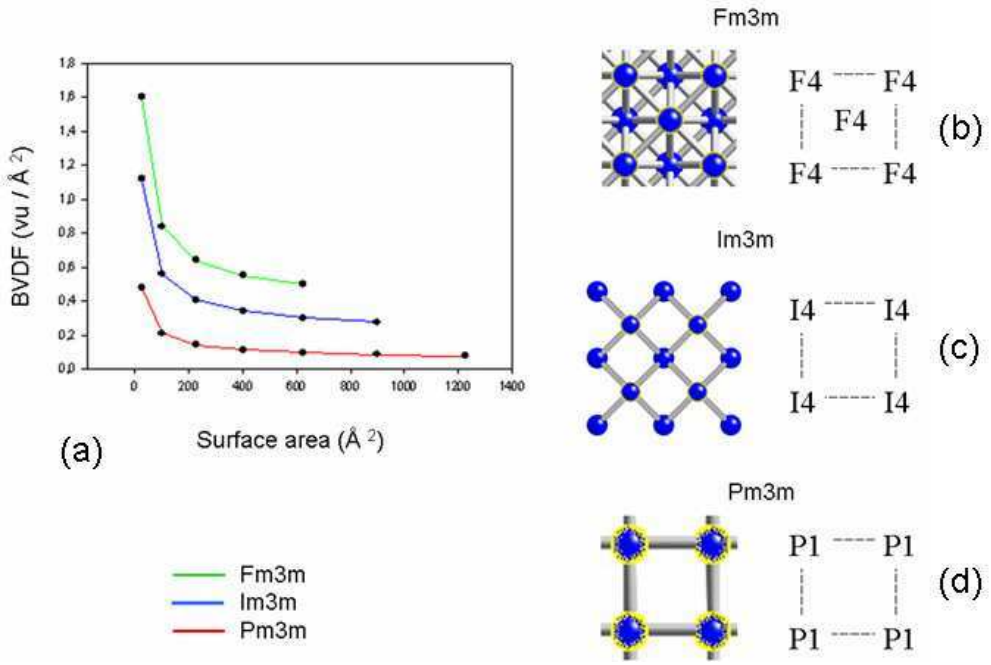

Fig.: 7.1 Comparison of the (001)-BVDF-values obtained in the Pm3m, Fm3m and Im3m Bravais-lattice type (a). All graphs in the diagram shown a negative gradient, tending towards a minimum (see text). Fig. (b-d) show the (001)-surfaces of the Pm3m, Fm3m, Im3m lattices corresponding to the starting point of the graphs at 25 Å² . The yellow circles show the atoms terminating these surfaces and the sketches indicate the number of dangling-bonds per surface atom.

The BVDF-values of each of the three faces compared in Figure (7.1), decreases as the size of the face increases. The slopes of the negative gradient of the graphs show that the BVDF-values tend towards a minimum. This minimum is characteristic for each face and is equal to the BVD-value of the corresponding two-dimensional unit-cell of

the face. This value will be called the "BVDU-value", referring to the bond-valence deficiency of an area of unit-cell dimension. Special attention has to be given to the number of lattice points present within the unit cell. The number of atoms or ions considered must be equivalent to the number of lattice points "*Z*" of the lattice-type. This approach is in concordance with the models of BRAVAIS (1866) and DONNAY-HARKER (1937) considering the reticular densities of the faces.
The reticular density (g^2) is calculated by considering the (hkl)-values of the face:

$$g^2 = h^2 + l^2 + k^2$$

The ranking so obtained for different (hkl)-values gives the order of morphological importance of these faces (Tab. 7.1).

hkl	g^2	hkl	g^2	hkl	g^2
(100)	1	(211)	6	(321)	14
(110)	2	(310)	10	(410)	17
(111)	3	(311)	11	(322)	17
(210)	5	(320)	13	(411)	18

Tab. 7.1 Given is the sequence of morphological importance for (hkl)-faces in the cubic primitive Bravais-lattice. Based on the increase of the reticular density value (g^2). Faces having a low g^2-value have a higher order of importance than faces with a high g^2-value.

Order of morphological importance of faces in the cubic primitive Bravais-lattice type:

(100) < (110) < (111) < (210) < (211) < (310) < (311) < (320) < (321) < (410)(322) < (411)

To obtain comparable values for different faces the number of lattice points in a unit-cell of a face (Z*) must be equalized to the number of lattice points "Z" of the Bravais-lattice type. The number of lattice points "Z" in the Fm3m-Bravais lattice is Z = 4. Calculating the number of lattice-points present in the unit-cells (Z*) for the (001),

(110) and (111)-faces (Fig. 7.2), yields, that only the unit-cell of the (111)-face has an equivalent number of lattice point (Z* = 4). The faces (001) and (110) only have Z* = 2. According to the approach of Bravais, the g^2-value of such faces must be doubled to receive comparable results. The values so obtained will give the right sequence of morphological importance of these faces. The Tables (7.2) and (7.3) show the results for the Fm3m- and Im3m-Bravais lattice.

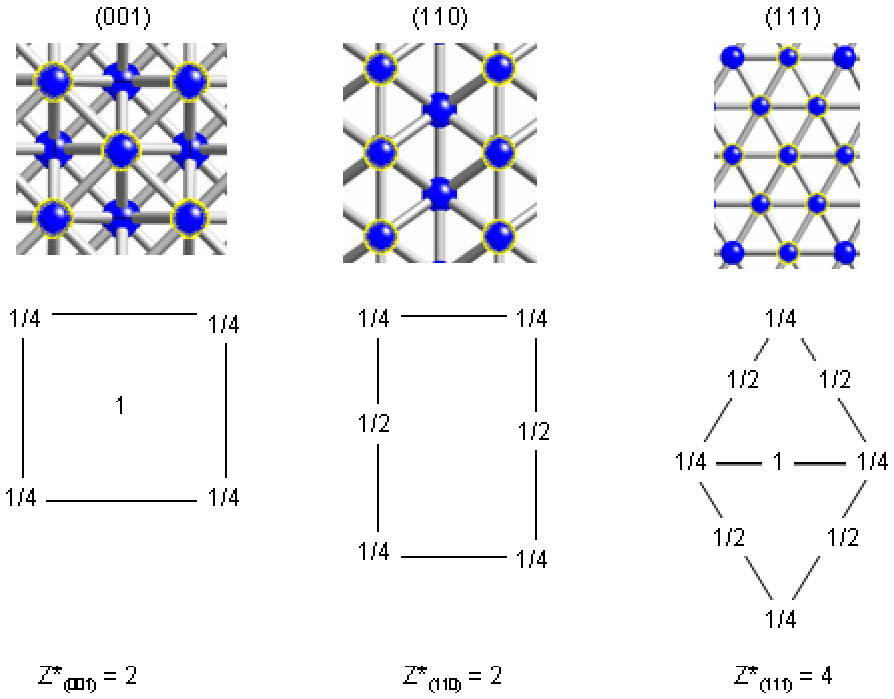

Fig.: 7.2 Given are the Z*-values for the (001), (110) and (111) lattice planes of a face-centered cubic lattice type. Top: atomistic graphic perpendicular to the lattice planes. Marked with yellow circles are the lattice points present at the surface. The diagrams below indicate the calculation of the number of lattice points (Z*) for the given unit-cells of the corresponding lattice planes (001), (110) and (111).

hkl	g^2	hkl	g^2	hkl	g^2
(200)	4	(422)	24	(640)	52
(220)	8	(442)	36	(642)	56
(111)	3	(620)	40	(331)	19
(420)	20	(311)	11	(511)	27

(111) < (100) < (110) < (311) < (331) < (420) < (422) < (511) < (442) < (620) < (640) < (642)

Tab.: 7.2 g^2-values calculated for the cubic face-centered lattice, normalized to Z = Z*. Given below is the ranking of the morphological importance of the different faces.

hkl	g^2	hkl	g^2	hkl	g^2
(200)	4	(211)	6	(640)	52
(110)	2	(442)	36	(321)	14
(222)	12	(310)	10	(411)	18
(420)	20	(622)	44	(332)	22

(110) < (100) < (211) < (310) < (111) < (321) < (411) < (420) < (332) < (442) < (622) < (640)

Tab.:7.3 g^2-values calculated for the cubic body-centered lattice, normalized to Z = Z*. Given below is the ranking of the morphological importance of the different faces.

Calculating the reticular density of lattice points is an integral part in the models of BRAVAIS and DONNAY-HARKER and can easily be recognized while calculating the BVDU-value of a crystal face. The factor applied to even the number of lattice points of the unit-cell of the crystal plane (Z*), to the number of lattice points of the crystal lattice (Z) will be called “RD-factor” (reticular density factor) and is listed in Table (7.4) for the Pm3m, Fm3m and Im3m cubic Bravais-lattices.

Face (hkl)	RD-factor Pm3m-Bravais lattice	RD-factor Fm3m-Bravais lattice	RD-factor Im3m-Bravais lattice
(100)	1	2	2
(110)	1	2	1
(111)	1	1	2
(210)	1	2	2
(211)	1	2	1
(221)	1	2	2
(311)	1	1	2
(331)	1	1	2

Tab.: 7.4 Comparison of the different RD-factors of the Pm3m, Fm3m and Im3m Bravais-lattices.

There appears to be one major problem if this method is applied directly to the BVD-model. In the models of BRAVAIS and DONNAY-HARKER the faces are compared considering their Miller-indices (hkl). The Miller-indices are used to describe the orientation of crystal planes within a three-dimensional lattice. In the BVD-model this terminology is applied in the same manner, namely to describe and distinguish between crystal-surfaces, oriented parallel to certain crystal planes. While calculating the BVDU-values of a crystal face we have to distinguish precisely between crystal planes and crystal faces.

In the calculations of BRAVAIS and DONNAY-HARKER the faces of a crystal are treated merely as crystal-planes, and these crystal-planes contain only lattice points having an identical environment. The two-dimensional unit-cells for such planes, for which the reticular density (g^2) is calculated, likewise contain only lattice points of identical environment (Fig. 7.3).

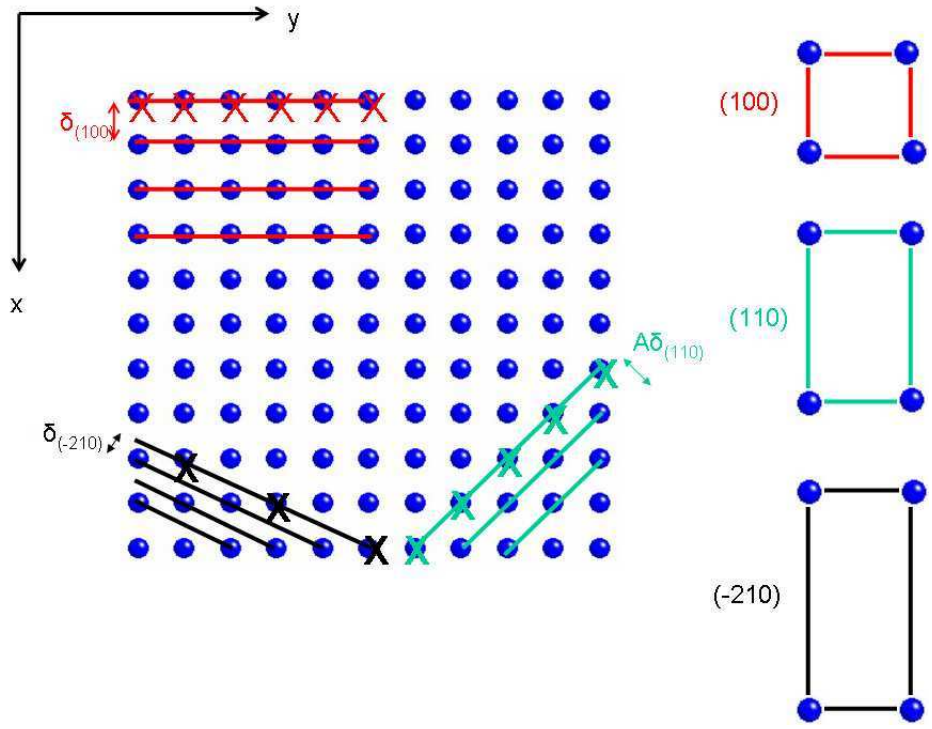

Fig.: 7.3 Given on the left is a (001)-lattice plane of a primitive cubic Bravais-lattice. The traces of the planes (100), (110) and (-210) are given in red, green and black respectively. Lattice points passed by these lattice planes are marked "X". Given on the right are the two-dimensional unit-cells of the corresponding lattice planes; given as polygons having lattice points at their corners.

Considering a crystal face from an atomistic point of view, gives some significant differences. The surface topology of many crystal faces is not a flat surface, rather they exhibit a stepped topography (Fig. 7.4). Consequently these surfaces contain "extra lattice points" not having an identical environment. Crystallographically these "extra lattice points" are still equivalent because they belong to an equivalent set of parallel planes (hkl), but from the atomistic approach of a crystal surface these "lattice points" are "non-equivalent", because in the atomistic approach applied in the BVD-model, the positions of "lattice points" are taken by atoms. As a consequence, these atoms can occupy geometrical equivalent positions, comparable to "lattice points", but as real atoms they share bonds with their neighbours, and the number of these bonds shared can diver, transferring "equivalent atoms" into non-equivalent" atoms (Fig. 7.5).

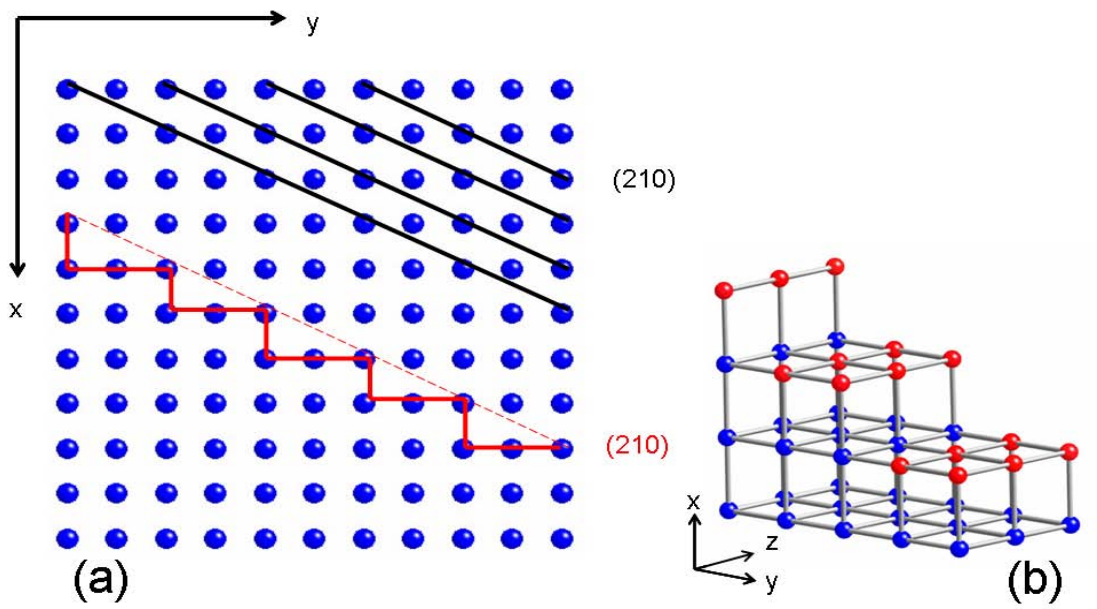

Fig.: 7.4 Comparison between a flat crystal lattice (210) marked black, and the stepped morphology of a (210) crystal surface (atomistic approach), oriented parallel to a (210) crystal plane, marked in red (a). The dashed red line indicates the (210) crystal lattice. The solid red line indicates the stepped (210) crystal surface, occupied by atoms. "Equal lattice points", (equal atoms) are positioned at the edges of terraces while additional "non-equivalent lattice points" (non-equivalent atoms), occupy the flat terraces of the stepped (210) crystal surface. Fig. (b) shows the stepped topology of the (210)-crystal lattice in a three-dimensional perspective (Pm3m-lattice type). Atoms exposed at the surface, contributing dangling bonds to the environment are marked as red balls. The "equivalent atoms" in the middle of the step have two dangling bonds, while the "non-equivalent atoms" in the middle of the terrace have only one danglingbond.

The "non-equivalent" lattice points (atoms) must be considered in the BVD-model, because these atoms also emit a certain number of dangling bonds to the environment and cannot be neglected, as they also contribute towards the surface energy of the face considered. Hence, the calculation of the reticular density of a unit-cell of unit-dimension for a given (hkl)-face must include both "equivalent" and "non-equivalent" atoms (lattice points).

In Figure (7.5) and Table (7.5) examples are given on how neglecting and including additional “non-equivalent” lattice points (atoms) influences BVDU-values calculated. The examples given are calculated for a primitive cubic lattice type(CN = 6, a_0 = 5 Å).

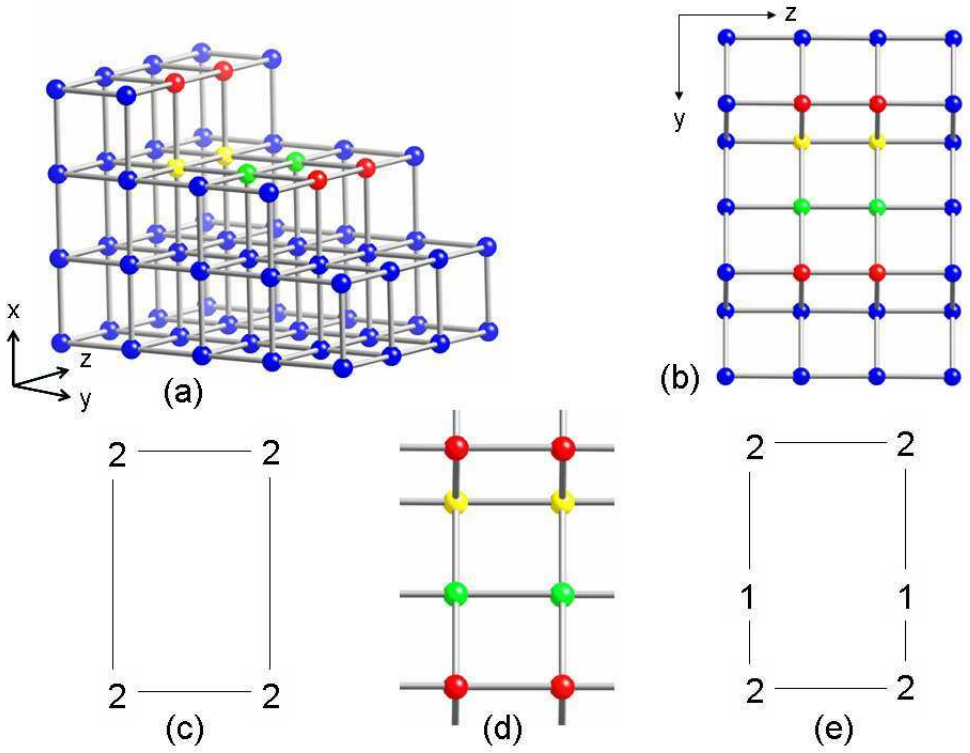

Fig. 7.5 (a) Three-dimensional perspective of the stepped (210) crystal surface of a primitive cubic Bravais-lattice. Marked in color are atoms exposed on the surface corresponding to the surface area of the (210) unit-cell. (b) View perpendicular to the (210) surface. Marked in red are atoms representing “equivalent lattice points”, marked green are atoms representing “non-equivalent lattice points”. Marked yellow are atoms not being “exposed” at the surface (at the bottom of the step, Fig .a), without contributing any dangling bonds to the environment, having a coordination number of CN=6. Fig. (d) detailed view of the (210) surface unit cell. Fig. (c). indicated by numbers are the numbers of dangling bonds (2), contributed to the environment by the “equal lattice points” (atoms) marked red (Fig.d). Fig. (e), similar to Fig (c), but in addition the number of dangling bonds emitted by the “non-equivalent lattice points” (atoms), are shown.

The morphology of the “abstract form” predicted, neglecting the “non-equivalent” atom positions would be misleading (Tab 7.5). Instead of resulting in a cube, the “abstract form” of a crystal having a Pm3m lattice type, would be terminated in our example, by crystal faces parallel to (331)-crystal planes. In contrast the calculation including “non-equivalent” atoms (Tab 7.5) results in an “abstract form” with the shape of a cube, because the (001)-faces are having the lowest BVDU-value.

(hkl)	Number of DB of “equivalent” atoms	BVDU of “equivalent” atoms	Number of “equivalent” and “non equivalent” atoms	BVDU of equivalent and “non equivalent” atoms
(100)	1	0,0400	1	0,0400
(110)	2	0,0566	2	0,0566
(111)	3	0,0693	3	0,0693
(210)	2	0,0358	3	0,0537
(211)	3	0,0490	4	0,0653
(221)	3	0,0200	10	0,0667
(311)	3	0,0181	10	0,0603
(331)	3	0,0138	14	0,0642

Tab.: 7.5 Comparison between the BVDU-values of atomic planes of unit-cell dimension considering only “equivalent” atom positions (“lattice points”) and the BVDU-values of crystal surfaces considering both, ”equivalent” and “non-equivalent atom positions.

Calculating the reticular density of a (hkl)-face, by application of the BVD-model, must therefore consider all atoms (lattice points) belonging to the same set of (hkl)-planes truncated by the crystal surface (hkl). As a further addition, the number of lattice points (Z and Z*) need to be reconsidered. Stated above: the number of lattice points (Z*) present in the two-dimensional unit cell of a (hkl)-face, must be equivalent to the number of lattice points (Z) of the corresponding crystal lattice. This rule must just as well be followed by the number of “non-equivalent lattice points” (atoms) present in the respective unit-cell.

Again we need to bear in mind that the term “lattice point” later must be substituted by the term atom or ion, when considering real crystal structures.

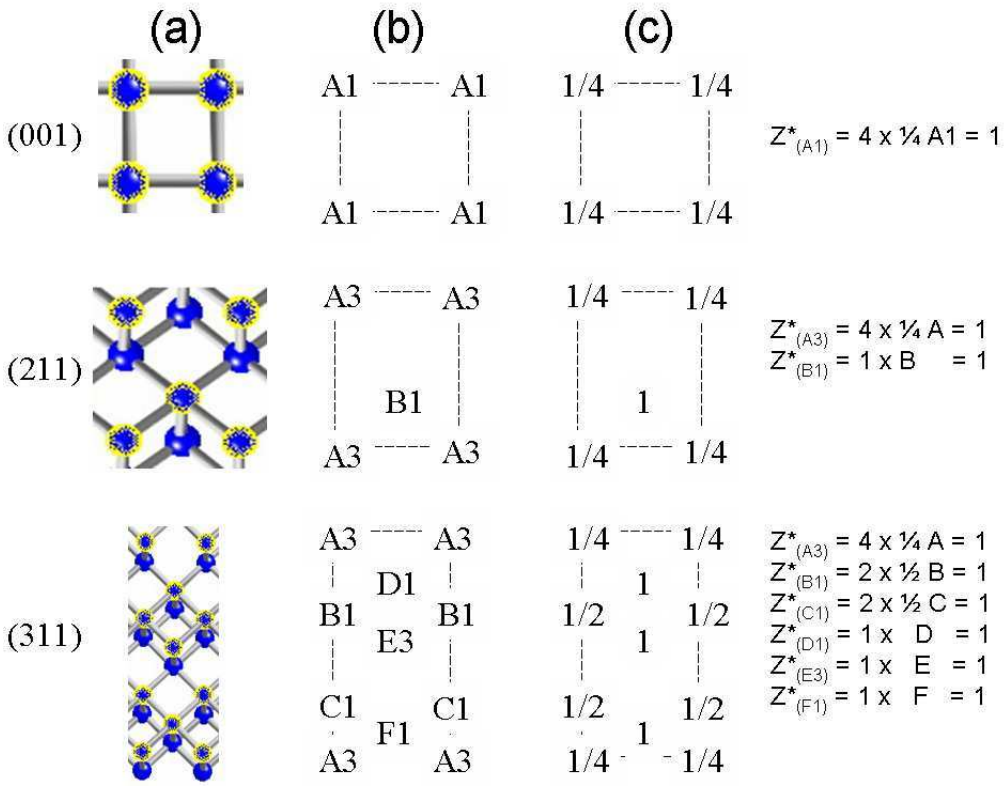

Fig.: 7.6 Column (a): Ball- and stick models of the crystal surfaces (001), (211) and (311) of a primitive cubic lattice type. Atoms exposed on the crystal surface are marked yellow. Column (b) Diagram quoting equal lattice points and the number of free dangling bonds of the representative atoms. “A” position of “equivalent atom positions”, B-F different “non-equivalent” atom positions. Column (c): Diagrams and equations giving the total number of lattice points (Z*) for the given face unit-cell. The equations and the diagram on the right show that for each “equivalent lattice point” and for each “non-equivalent lattice points” the number (Z*) is equal to the number of lattice points (Z) present in a primitive cubic Bravais-lattice.

Following the above mentioned amendments, the reticular density of unit-cell dimension, and the “abstract form” of a polyhedral crystal can be calculated. The results obtained by considering the reticular density only for the Pm3m, Fm3m and Im3m lattice type are given in Table 7.6. The examples calculated are corrected with the

RD-factor to account for the number of lattice points (Z), including both “equivalent” and “non-equivalent” atom positions. A graphic example of the morphological ranking of different faces for the face-centered cubic lattice type is plotted in Figure (7.7).

Pm3m Face (hkl)	DB	Surface area (Å²)	BVDU/Area (vu / Å²)	RD-factor	BVDU*/Area
(100)	1	25,00	0,0400	1	0,0400
(110)	2	35,35	0,0566	1	0,0566
(111)	3	43,29	0,0693	1	0,0693
(210)	3	55,90	0,0537	1	0,0537
(211)	4	61,23	0,0653	1	0,0653
(221)	10	149,99	0,0667	1	0,0667
(311)	10	165,82	0,0603	1	0,0603
(331)	14	217,94	0,0642	1	0,0642
Fm3m Face (hkl)	DB	Surface area (Å²)	BVDU/Area (vu / Å²)	RD-factor	BVDU*/Area
(100)	8	25,00	0,3200	2	0,6400
(110)	12	35,35	0,3394	2	0,6788
(111)	12	43,29	0,2771	1	0,2771
(210)	20	55,90	0,3578	2	0,7156
(211)	40	122,46	0,3266	2	0,6532
(221)	24	74,99	0,3200	2	0,6400
(311)	84	249,00	0,3373	1	0,3373
(331)	36	108,96	0,3304	1	0,3304
Im3m Face (hkl)	DB	Surface area (Å²)	BVDU/Area (vu / Å²)	RD-factor	BVDU*/Area
(100)	4	25,00	0,1600	2	0,3200
(110)	4	35,35	0,1131	1	0,1131
(111)	6	43,29	0,1386	2	0,2771
(210)	8	55,90	0,1431	2	0,2862
(211)	16	122,46	0,1306	1	0,1306
(221)	10	74,99	0,1333	2	0,2667
(311)	36	249,00	0,1446	2	0,2892
(331)	14	108,96	0,1285	2	0,2570

Tab.: 7.6 Given as BVDU* are the bond-valence deficiencies of different crystal faces of unit-cell dimension in the Pm3m, Fm3m and Im3m Bravais-lattice type structures. The asterix (*), implies that these bond-valence deficiency values calculated have been corrected by the RD-factor. The DB-value correlates to the total amount of dangling bonds of the atoms (“equivalent” and “non-equivalent”) terminating the respective crystal surfaces.

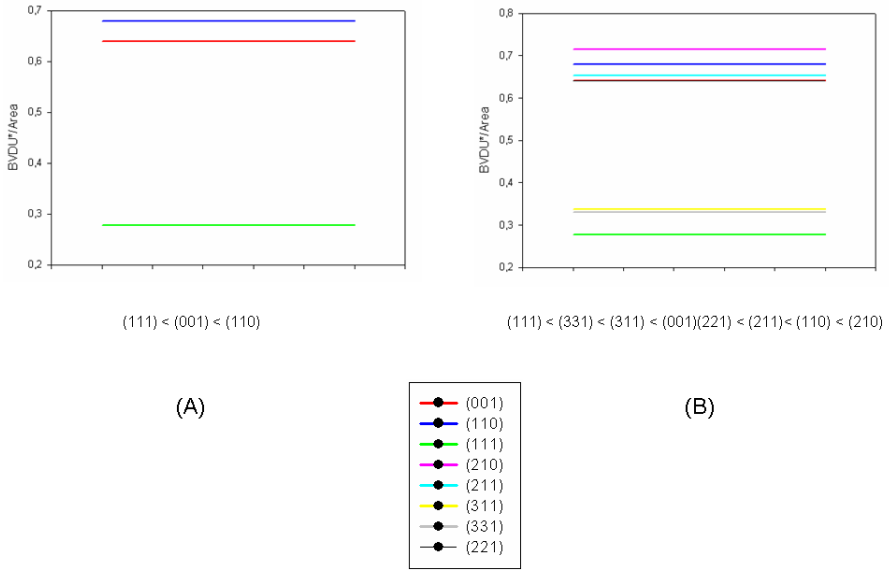

Fig.: 7.7 Image (A) shows the ranking of the morphological importance for the crystal faces parallel to (111), (001) and (110) for a face-centered cubic Bravais-lattice. In image (B) additional crystal faces having higher (hkl) values are added. Crystal faces having a low BVDU-value appear at the bottom of the images. In return, these faces should have a higher order of morphological importance.

The results of the diagram in Figure. (7.7 a) are similar to the ones expected by application of the Bravais-method. The ranking obtained is:

$$(111) < (001) < (110).$$

Problems occur when faces of higher indices are added (Fig.7.7b). The ranking of the morphological importance of the crystal faces is:

$$(111) < (331) < (311) < (001) < (110) < (210)$$

This ranking is totally inconsistent with the ranking obtained by application of the Bravais-model:

$$(111) < (001) < (110) < (311) < (331) < (210)$$

Even though it seems necessary to consider the reticular density of crystal planes while calculating the bond-valence deficiency of faces, the results obtained so far are disappointing. Therefore some additional amendments (Chapter 7.2) have to be considered, similar to the revisions made by DONNAY-HARKER (1937).

7.2 The BVD-model and lattice spacing

Lattice type is the basis for calculating the reticular density according to Bravais - empirical law. In lattice types, only symmetry elements with no translation, i.e. the center of symmetry, the symmetry plane, and the symmetry axes, are included. Consequently the geometry of the fourteen types of Bravais lattices and thirty-two crystal groups are the basis for calculating the reticular density (SUNAGAWA 2005). According to DONNAY-HARKER (1937) this approach can be extended to the 230 space groups when translational symmetry elements such as glide planes and screw axes are included in the calculations. Their results turned out to match the observed morphology of natural minerals much better than those obtained by application of the Bravais - empirical law only.

The considerations of DONNAY-HARKER (1937) to implement the influence of screw-axis and glide-planes to predict the morphology crystals, is similar to the considerations of NIGGLI (1920). In both approaches the density of the lattice spacing in a crystal structure is considered to be relevant when predicting the ranking of the morphological importance of crystal faces.

Any attempt to combine the bond-valence deficiency of crystal surfaces with internal factors controlling the morphology of a crystal has to recognize the influence of the lattice spacing. This may have been a reason why the combination of the BVD-model and the reticular density model failed in the first approach. Similar to the amendments made by DONNAY-HARKER (1937), only the combination between reticular density,

lattice spacing and the BVD-model will bring forward a suitable prediction of the "abstract form" of a crystal.

Before starting to introduce an additional factor into the BVD-model, the term "lattice plane" must be reconsidered in this context. In our theoretical approach to deduce a factor considering the density of crystal lattice planes, similar to the approach of NIGGLI (1920), it is applicable if we refer to the term lattice as a periodic sequence of points, which have an identical environment. Later this terminology will be applied in a more broader sense, in so far, as atoms will substitute for the lattice points, and thus we actually consider the density of atoms or the density of atomic layers within a crystal.

7.2.1 Calculation of the lattice spacing (LD-factor)

According to NIGGLI (1920), a high lattice spacing (low density of lattices planes) corresponds to a slower growth rate of the corresponding crystal faces. Hence the number of parallel crystal lattices (hkl) is a criterion by which the morphological importance of a face can be measured. Thus the number of crystal lattices of a given crystal plane will be implemented in the BVD-model as the "LD-factor" (lattice density factor). This LD-factor is introduced into our calculations as the second internal factor controlling the morphological importance of a crystal face.

Depending on the crystal structure there are two methods applicable to calculate the density of crystal lattices. One is a mathematical approach suitable for simple structures such as the primitive cubic lattice. The second method is a graphical approach suitable for more complex crystal structures and crystals containing different building units (ions, atoms).

7.2.1.1 Calculation of the lattice density of a homöopolar primitive cubic crystal lattice (mathematical approach)

Considered as homöopolar are crystals not bonded via ionic bonds (heteropolar).

First, the distance "$d_{[uvw]}$" between equivalent lattice points perpendicular to the crystal lattice must be calculated. This distance is given by the equation:

$$d_{[uvw]} = a_0 \bullet \sqrt{u^2 + v^2 + w^2} \qquad [7.1]$$

In the next step the d-spacing "$d_{(hkl)}$" of the lattice is calculated by the equation:

$$d_{(hkl)} = \frac{a_0}{\sqrt{h^2 + k^2 + l^2}} \qquad [7.2]$$

By combination of these two equations [eqn. 7.3] the number of parallel lattice planes present in a three-dimensional crystal lattice of unit-dimension can be calculated. The result obtained is the LD-factor and is the quotient between the distance of two equivalent lattice points given as $d_{[uvw]}$ and the d-spacing "$d_{(hkl)}$" of the related crystal planes:

$$LD = \frac{d_{[uvw]}}{d_{(hkl)}} \qquad [7.3]$$

As an example the LD-factor of the (001) and (211) crystal planes in the Pm3m-Bravais lattice are calculated:

Example 1 : Calculation of the LD-factor for the (001) lattice planes in a Pm3m-Bravais lattice, a_0 = 5 Å.

$$d_{(uvw)} = a_0 \bullet \sqrt{u^2 + v^2 + w^2} \qquad \rightarrow \qquad d_{(uvw)} = 5 \bullet \sqrt{0^2 + 0^2 + 1^2} = 5$$

$$d_{(hkl)} = \frac{a_0}{\sqrt{h^2 + k^2 + l^2}} \qquad \rightarrow \qquad d_{(hkl)} = \frac{5}{\sqrt{0^2 + 0^2 + 1^2}} = 5$$

$$LD = \frac{d_{(uvw)}}{d_{(hkl)}} \qquad \rightarrow \qquad LD = \frac{d_{(uvw)}}{d_{(hkl)}} = \frac{5}{5} = 1$$

Result of Example 1: The LD-factor is 1. The lattice plane (001) is repeated only once within unit-cell of the three-dimensional Pm3m-Bravais lattice.

Example 2: Calculation of the LD-factor for the (211) lattice planes in a Pm3m-Bravais lattice, a_0 = 5 Å.

$$d_{(uvw)} = 5 \bullet \sqrt{2^2 + 1^2 + 1^2} = 12.247$$

$$d_{(hkl)} = \frac{5}{\sqrt{2^2 + 1^2 + 1^2}} = 2.041$$

$$LD = \frac{d_{(uvw)}}{d_{(hkl)}} = \frac{12.247}{2.041} = 6.00$$

Result of Example 2: The LD-factor is 6. The lattice plane (211) is repeated 6-times until an “equivalent” position is reached in the three-dimensional Pm3m-Bravais lattice.

7.2.1.2 Calculation of the lattice density of a homöopolar primitive cubic crystal lattice (graphic approach)

First the positions of translation equivalent lattice points at the distance $d_{[uvw]}$ are marked in the crystal lattice. Then the lattice planes (hkl) corresponding to the two lattice points are drawn and the number of "lattice plane translations" between the two equivalent lattice points are calculated. Additional sets of parallel lattices are added if additional equivalent lattice points appear at distances $d_{(hkl)}$. The number of lattices present (number of translations) is equal to the LD-factor (Fig. 7.8). Both methods, the mathematical approach and graphic approach lead to the same results.

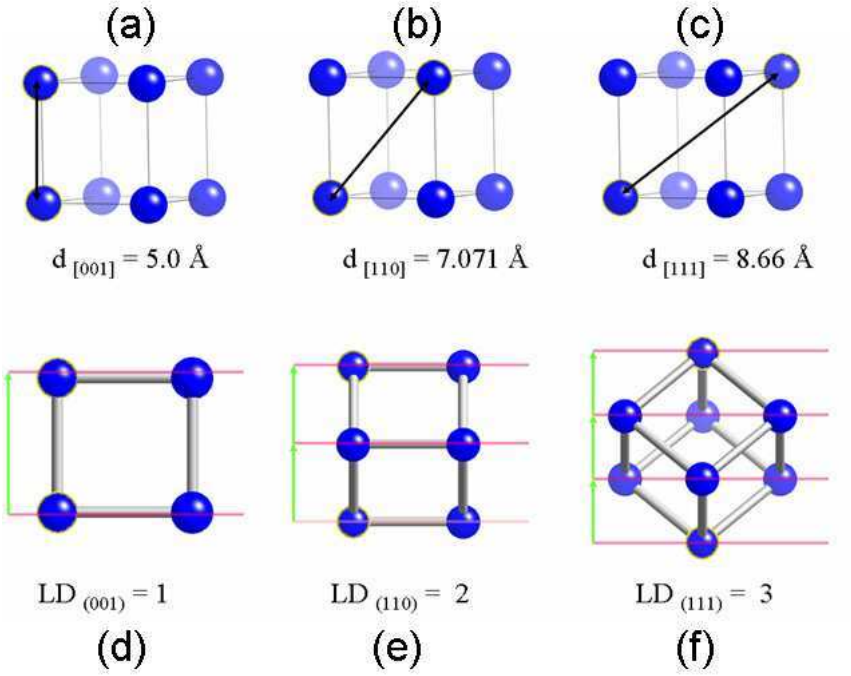

Fig.: 7.8 (a)-(c) Unit-cells of a Pm3m Bravais-lattice, a_0 = 5 Å . Equal lattice points at the translation distance $d_{[uvw]}$ are marked by black arrows. The corresponding distances $d_{[uvw]}$ are given below the images. Fig. (d)-(f) Crystal lattices parallel to (001), (110) and (111) are marked by red lines. Given by green arrows is the translational distance $d_{(hkl)}$ of these lattice planes. The number of green arrows represents the number of translations needed to return to an "equivalent" lattice plane. The number of arrows calculated is equivalent to the LD-factor of the corresponding lattices planes (stated below the image).

Later, as this approach will be applied to real crystals consisting of atoms rather than lattice points the term “lattice plane” must be substituted by the term “atomic layer” or “atomic lattice”. This is only a change in terminology, and the relevance of considering the density of “lattices” and therefore the LD-factor remains unchanged.

7.2.1.3 Calculation of the LD-factor for more complex crystal structures

The difference between the three cubic Bravais-lattices is their different number of lattice points Z. The additional lattice points in the Fm3m- or Im3m Bravais-lattice, compared to the Pm3m-Bravais lattice, occupy certain crystallographic sites. These “extra” lattice points not only influence the reticular density of certain crystal planes, they also are responsible for additional lattice planes within the crystal lattices (Fig. 7.9). The results for all three cubic Bravais-lattices are summarized in Table (7.7).

Face (hkl)	LD-Factor Pm3m-Bravais lattice	LD-Factor Fm3m-Bravais lattice	LD-Factor Im3m-Bravais lattice
(100)	1	2	2
(110)	2	4	2
(111)	3	3	6
(210)	5	10	10
(211)	6	12	6
(221)	9	18	12
(311)	11	11	22
(331)	19	19	38

Tab.: 7.7 Comparison of the different LD-factors of the three cubic Bravais-lattice types.

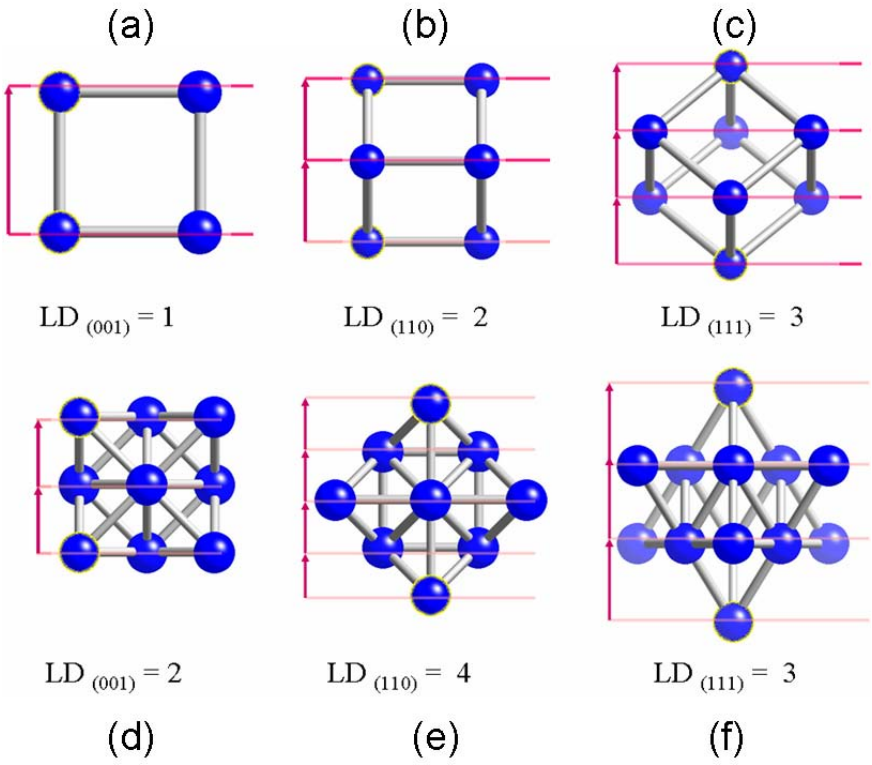

Fig.: 7.9 Ball and stick models of primitive cubic lattices (a) – (c) and face-centered lattices (d) – (f). This images illustrate the different number of LD-factors appearing for similar crystal planes in a primitive and face-centered cubic crystal lattice. The differences occur because of additional lattice points present in the face-centered lattice, compared to the primitive cubic lattice. The additional lattice points (face-centered lattice) introduce e.g. additional lattice planes in the example of the (001)-lattice plane (a) and (d) and (110)-lattice planes (b) and (e). This is due to the special position of ½ $d_{(hkl)}$ of these additional lattice points in the face-centered cubic lattice type. No changes in the LD-factor appear in the case of the (111)-lattice plane (c) and (f), as the additional lattice points (f) settle on the same lattice planes as the lattice points part of the (111)-lattice planes in the primitive cubic lattice type structure (c).

The graphical approach to calculate the number of crystal lattices proves to be most effective because the LD-factor can be derived directly from the crystal structure. This is especially useful in the case of crystals with different building units. As an example the LD-factors for different crystal faces of a crystal having a sodium-chloride structure will be calculated employing the graphical method (Fig. 7.10). The LD-factors for NaCl are to some extent different from the LD-factors of a face-centered cubic

Bravais-lattice, even though they have the same space group symmetry (Fm3m). The reason is the differences in the number of different building units. The lattice-points in the face-centered cubic Bravais-lattice are occupied by equivalent building units (lattice points). Comparable sides in a real crystal structure, for example in the sodium-chloride structure are occupied by different ions. This difference gives rise to additional atomic layers (lattice planes) in the sodium-chloride structure as the (111)-lattice planes (atomic layers) are now alternatively occupied by either cations or anions (Fig 7.10).

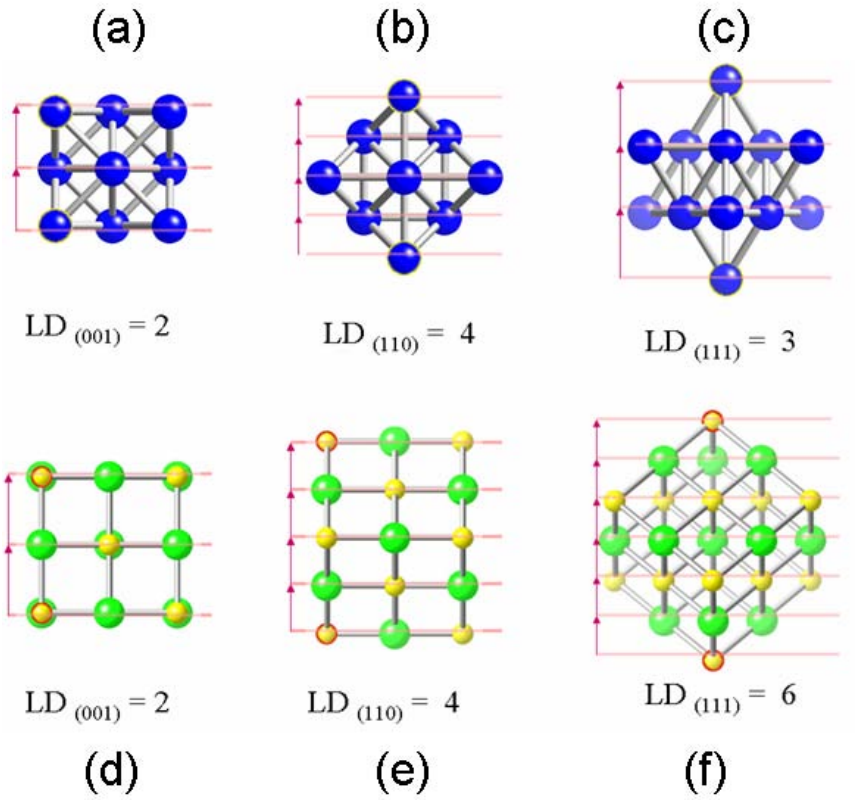

Fig.: 7.10 (a)-(c) Ball- and stick representation of a face-centered cubic Bravais-lattice type structure. (d)-(c) Ball- and stick representation of the NaCl-crystal structure. Sodium-ions are given in yellow, chlorine-ions are given in green. Comparing both structural representations shows that the number of "lattice planes" parallel to (111) is doubled in the NaCl-crystal structure. This is due to the alternation of atomic layers occupied only by either cations or anions in the NaCl-structure type, thus doubling the number of planes (atomic layers) compared to the number of "lattice planes" of a face-centered Bravais-lattice structure type.

After the introduction of internal factors into our calculations (RD- and LD-factors) we have to reconsider the results of our calculations. From this stage on it is obvious that the calculated bond-valence deficiency values such as (BVDU**) no longer refer to "real" bond-valence values (vu) for a given ion, but represent relative values by which different faces can be compared (Tab. 7.8).

As an example, the bond-valence (vu) of a Na^+ ion, being coordinated by six Cl^- ions in the halite-structure, is on average 0.166 (vu) for each individual Na – Cl bond. Therefore, as a first approach the bond-valence deficiency of a Na-ion exposed at the (001) crystal surface can be correlated to the number of dangling bonds times the bond-valence of a Na-Cl bond, which is 1 x 0.166 = 0.166 (vu). Consequently the bond-valence deficiency of a sodium-ion exposed at a (111)-surface is 3 x 0.166 ~ 0.5 (vu).

By multiplication of the number of dangling bonds per unit-cell dimension with the bond-valence deficiencies of each atom present at the surface the BVDU-value can be calculated (Tab. 7.8). In our example the unit-cell of the (001)-crystal lattice of halite will emit 4 dangling bonds. Normalized to the number of lattice-points (atoms) in the unit-cell there will be two dangling bonds for the sodium-ions and two for the chlorine-ions present. The BVDU-value is 4 x 0.166 vu = 0.664 vu. Considering the dimension of the unit-cells, the BVDU-value per A^2 can be deduced. This value needs to be corrected by the RD-factor and the LD-factor.

Considering the LD-factor in our calculations, the meaning of the BVDU-values will be changed. The LD-factor counts for the lattice density of crystal lattices in a mineral, and consequently has no direct correlation to bond-valences of bonds formed between two ions. In the broader sense, the LD-factor factorizes the influence of the lattice density (density of atomic layers) on the final crystal morphology. The "real" bond-valence values are now changed to become "apparent" bond-valence values, such as the BVDU**-value. These "apparent" bond-valence values can now be used to compare different crystal faces to each other, by considering internal crystal structure data linked to unsatisfied bonds present at the mineral surface.

	BVDU	Unit-cell dimension (A^2)	BVDU/(A^2)	RD-factor	BVDU*	LD-factor	BVDU**
(001)	0,664	31,69	0,0209	2	0,041	2	0,083
(110)	1,328	44,82	0,0296	2	0,059	4	0,237
(111)	1,992	54,90	0,0363	1	0,036	6	0,217
(210)	1,992	70,87	0,0281	2	0,056	10	0,562

Tab.: 7.8 Calculated bond-valence deficiencies of different crystal faces of halite. The bond-valence of each individual Na-Cl bond have been considered to be 0.166 vu on average. (Further explanation see text).

7.3 The BVD-model and the face symmetry of crystals

The major feature of crystalline minerals is their three-dimensional periodicity, which can be described by one of the 230 space groups. Having regard to the components in the mineral and the symmetry elements present, a crystal can be fully described.

The major factor controlling the crystal shape is the growth-velocity of its faces. This growth-velocity can be influenced by external factors, such as temperature, pressure and the concentration of solutes. Additionally the growth velocity of a crystal plane is controlled by the crystal surface itself. Building-units of a crystal (ions, atoms, molecules) present at the crystal surface form a so-called “matrix” which interacts with the external factors mentioned above. This “matrix” can be described as a combination between the topology of the crystal surface and the distribution of building units exposed on the crystal surface. The aspect of the matrix depends on internal factors such as the reticular density (Chapter 7.1), lattice spacing (7.2) and the symmetry elements of the crystal structure.

Crystallographic symmetry of a crystal lattice type has already played an important role in the investigations made so far. Symmetry was taken into account when the unit-cell dimension of a two-dimensional crystal lattice was determined in order to calculate the reticular density of a crystal plane. Translational symmetry elements have been considered while calculating the lattice spacing of crystal planes.

The influence of crystallographic symmetry for crystal surfaces is "visible" almost at any mineral surface, e.g. the shape of etch-pits can be used to determine the presence and kind of symmetry elements in a crystal. Further, crystallographic symmetry seems to be important for the advancement of growth layers on the crystal surface (ENCKEVORT & BENNEMA, 2004).

As a consequence, the face symmetry of a crystal surface must be implemented into the BVD-model as another internal factor controlling the habit of a polyhedral crystal. While crystals consist of a symmetric periodic three-dimensional network of building-units, new building units adding to the growing crystal, neglecting any possible defects must, among other criteria, fit to the overall crystal symmetry.

Atoms, ions or molecules adsorbing to a crystal surface having a low symmetry can more easily find a place to fit, as they will possess more degrees of freedom where to adsorb. Building units adsorbing to faces having a high symmetry must fit not only the requirements of their direct bonding partner, they must as well fit the requirements of their next neighbors.

An example is given in Fig. 7.11, illustrating the dependence of a chlorine-ion on the face-symmetry while adsorbing to the (001), and (111)-faces of a sodium-chloride crystal. This example shows how the crystal symmetry influences the crystal surface (matrix), defining only certain adsorption site for the chlorine-ion to attach.

The image in Fig. 7.11(e) illustrates that a chlorine-ion adsorbing to a (001) crystal surface of halite, can best be adsorbed directly above a sodium ion, forming one bond

only. This position is in concordance with the given (001)-face symmetry (m3m) and the adsorbing position is equivalent to a Wyckoff position having the highest side symmetry (4mm) possible for the given crystal lattice (Chapter 7.4). Additionally the chlorine-ion adsorbing to this position will be at equal distance from any further chlorine-ions adsorbing to this surface.

In the Figure 7.11(f), the chlorine ion adsorbing to the (111)-crystal lattice forms three bonds of equal length to the sodium-ions in the crystal lattice below. This position is again in concordance with the face symmetry and it is the only possible adsorption point possible to distribute three equally long bonds between the chlorine-ion and the sodium-ions present at the crystal surface.

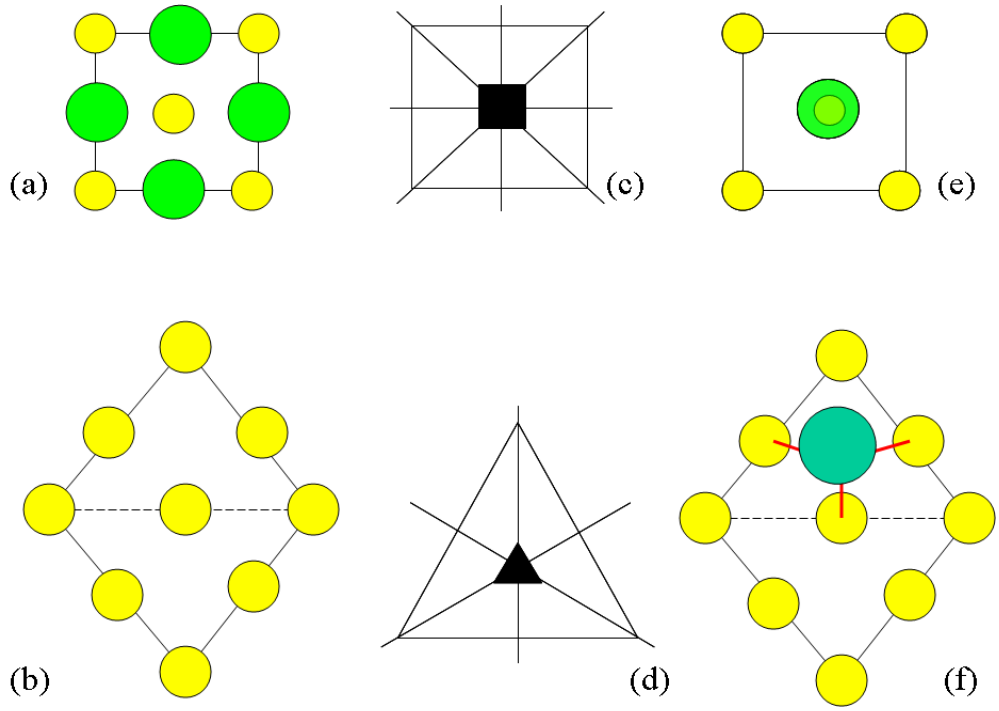

Fig.: 7.11 The figures (a) and (b) schematically illustrate the matrix of a (001) and a (111)-crystal plane of halite. The Sodium-ions are marked yellow, the chlorine-ions are marked green. Figures (c) and (d) give the face symmetry of the (001) and (111)-crystal lattices. The figures (e) and (f) show the adsorption positions of one additional chlorine-ion on the next adjacent layer parallel to the (001) and (111) crystal surface (matrix) illustrated.

Due to the number of bonds that will be formed, chlorine-ions most likely will adsorb to the (111)-crystal lattice and as a result will lower their own bond-valence deficiency more effectively than adsorbing to the (001)-crystal lattice. Consequently the growth rate of the (111)-crystal face has to be regarded higher than the growth rate of the (001)-crystal surface.

From this we can deduce:

The more complex the symmetry of a face the slower the periodicity of adsorption, lowering the growth rate of the crystal surface and giving the crystal-face a higher ranking of morphological importance.

Considering the effect of face symmetry, it is necessary to factorize this influence in our calculations. In the previous calculations it was stated that a low bond-valence deficiency accounts for a low reactivity and consequently this is a method to express a slow growth rate of a crystal surface. Considering face-symmetry as an additional factor to lower the growth rates of crystal faces this factor needs to be implemented in our calculations, and as this factor is directly related to the face symmetry of a crystal lattice it is called the "face symmetry factor" (FS). The FS-factor has to be considered as a division-factor in our calculations as a high face symmetry factor will lower the "bond-valence deficiency" of the crystal surface, giving the surface a higher ranking of morphological importance.

The application of a division-factor concerning the face symmetry of crystal surface seems to be to some extent arbitrary. Commonly, face symmetry is related to two-dimensional "flat" crystal lattices and is used to determine the corresponding two-dimensional space group. Though naturally, crystal surfaces are rarely flat and more frequently they are stepped three-dimensional bodies. Nevertheless, as described in Chapter 7.1, crystal surfaces can be treated as flat planes, similar to a crystal lattice in the BVD-model.

The differentiation between a crystal lattice and a crystal surface (Chapter 7.1) was necessary to implement the effect of “non-equivalent” atom positions on the bond-valence deficiency of a crystal surface. This discrimination is still fundamental, but has little effect on the face symmetry factor of a crystal surface. Comparing a stepped crystal surface (hkl) with a similar crystal lattice (hkl), shows that “equivalent lattice points” as well as “non-equivalent lattice” points, as well as the atoms terminating the crystal surface, obey the constraints given by the space group symmetry of the lattice (hkl) considered (Fig. 7.12). Consequently the face symmetry can be implemented into the BVD-model as the third internal factor controlling the morphology of the “abstract forms” of polyhedral crystals.

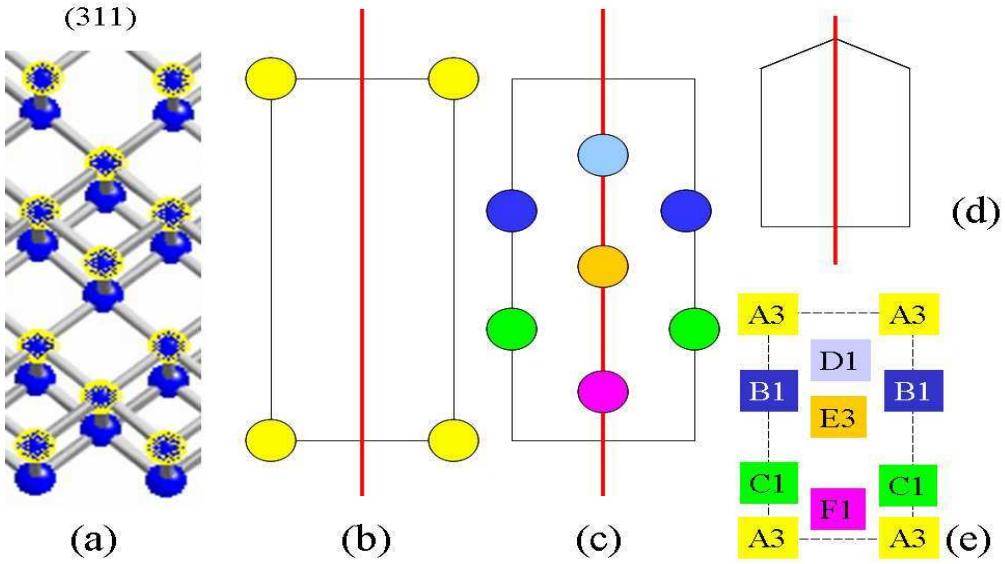

Fig.: 7.12 (a) Ball and stick model of the (311)-crystal surface of a primitive cubic lattice. Marked in yellow are the lattice points exposed to the surface. The images (b) and (c) demonstrate the influence of the face symmetry “m” (mirror plane). (b) The number of of “equal lattice points” (yellow) is doubled. (c) The different “non-equivalent lattice points” are doubled (dark blue and green), or reflected to themselves (light blue, orange and pink). (d) Face-symmetry is given graphically as (C_s). (e) Given by ciphers is the number of dangling bonds emitted by the different lattice points (A-F).

The face symmetry, also referred to as the "Eigensymmetry", is the full symmetry of a face, and can be derived from the symmetry elements perpendicular to that face. NIGGLI (1941) established a nomenclature for ten independent subgroups of face symmetries (Fig. 7.13), and found that only rotation-axis and mirror planes perpendicular to a face need to be considered to describe the full symmetry of a crystal lattice of a given crystal class.

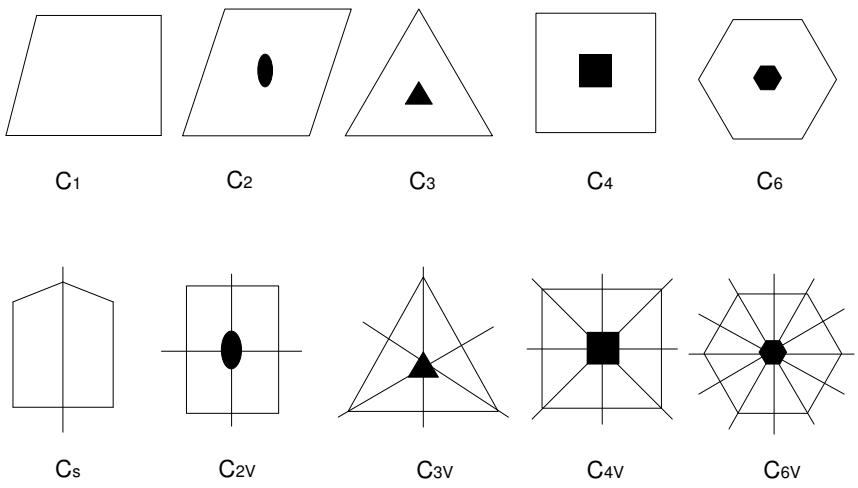

Fig.: 7.13 Illustrated are the ten different face symmetries considered by NIGGLI (1941). C_1 = assymetrisch, C_2 = digyrisch , C_3 = trigyrisch , C_4 = tetragyrisch , C_6 = hexagyrisch, C_s = monosymmetrisch , C_{2v} = disymmetrisch , C_{3v} = trisymmetrisch, C_{4v} = tetrasymmetrisch, and C_{6v} = hexasymmetrisch.

In order to deduce a symmetry factor for our calculations, NIGGLI´s approach from (1941), proved to be useful and therefore a derivation of his statements on the independent face-symmetry-groups needs to be summarized in more detail.

NIGGLI´s approach (1941):

The total symmetry of a crystal class can be addressed as a “full symmetry group”, which can be further subdivided into subgroups. These subgroups, in return, can be split up into “isometric subgroups” and “non-isometric subgroups”. “Isomorphic subgroups” include certain symmetry equivalent directions which are the so called “symmetry operators” of these directions.

If symmetry operations of a certain subgroup are coupled with some other symmetry operations, and therefore these symmetry operations do not correlate to a distinct direction within the full symmetry group, they are called “non-isomorphic subgroups”.

As an example NIGGLI (1941) states, that only the subgroups D_{6v}, C_{2v}, C_s and C_1 are “isomorphic subgroups” of the “full symmetry group” D_{6h} (Tab 7.9). If for example, the six-fold axis of the D_{6h} is running through a point, this point is also at the intersection of (3 + 3) mirror planes and the symmetry of this point is therefore C_{6v} (Fig. 7.14).

The distinction between “isomorphic” and “non-isomorphic subgroups” is of special interest, as only the symmetry operations of “isomorphic subgroups” perpendicular to a face are able to restore lattice point to their original position.

All subgroups of the crystallographic symmetry classes (crystal classes) may form crystallographic symmetry groups themselves. According to the symmetry operator of the “isomorphic subgroup”, the face-normal will be restored to its original position two,-three-, four-, six-, eight- or twelve-, in general ω-times.

The term ω is called the “Wertigkeit” of an element (direction, face normal, face, or point) possessing a certain symmetry constraint. In the end ω is equivalent to the symmetry operator, characteristic for that certain subgroup.

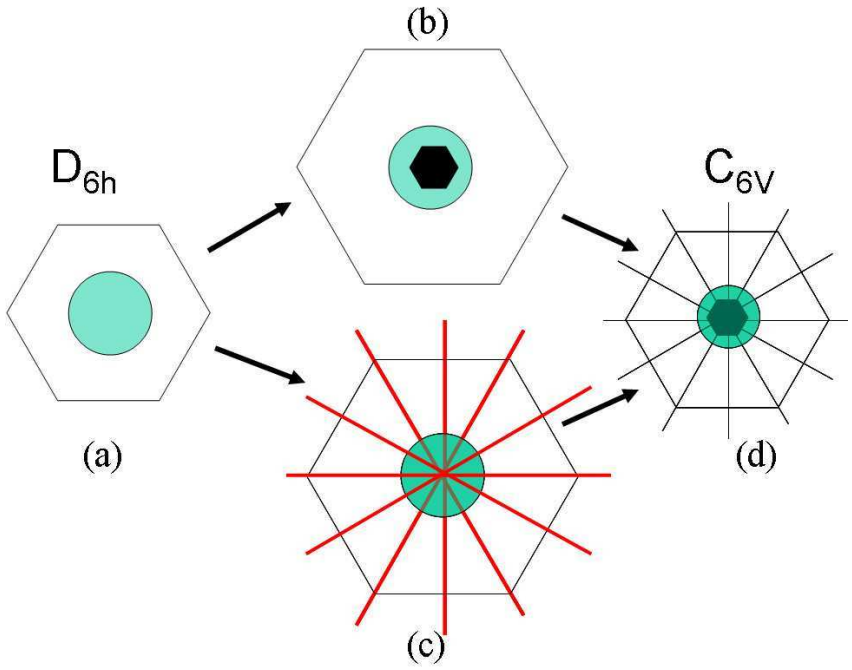

Fig.: 7.14 (a) Lattice point (green) having the full face symmetry of the crystal class D_{6h}. Through this lattice point a six-fold rotation axis can be drawn (b) and in addition 3+3 mirror planes intersect at this lattice points (c). Consequently the figures (b) and (c) are non-isomorphic subgroups from which the isomorphic subgroup C_{6V} (d) is derived. For further explanation see text.

Instead of referring to the symmetry parameters or "Eigensymmetry" of a face normal, one can equally address the dedicated face itself. The "Eigensymmetry" of a face is in general addressed as the face- or site symmetry. Hence, the symmetry of a face is determined by the symmetry operator perpendicular to this face. As isomorphic subgroups and therefore as the "Eigensymmetry" of a face, only such symmetry operators present as mirror planes and rotation axis can be considered (NIGGLI 1941). These are for all crystal classes next to C_1 (general position without symmetry operator) only the symmetries C_2 , C_3 , C_4 , C_6 , C_s , C_{2v} , C_{3v} , C_{4v} , and C_{6v}, receiving the "Wertigkeit" 1 ,2 ,3 ,4 ,6 , 8 and 12, respectively. At this point NIGGLI (1941) proposed the nomenclature by which the "Eigensymmtrien" of the isomorphic subgroups for a given crystal face can be distinguished (Fig.: 7.13).

In the BVD-model the term "Wertigkeit" (ω) of a crystal face is considered to be relevant to distinguishing between different site symmetries and is treated as a division factor in our calculations. This is the FS-factor referred to above. The purpose of this factor is to consider the different face symmetries present for different faces possible at a polyhedral crystal. This factor refers to the statement that faces with a high order of symmetry have a higher morphological importance than faces with a low order of symmetry. The value of the term ω (Wertigkeit), of each of the independent subgroups, stated in Table 7.9, can be transferred directly into the BVD-approach as it corresponds to the "Eigensymetrie" of the crystal face.

In addition to the term ω ("Wertigkeit") of a certain symmetry element, NIGGLI (1941) refers to another important factor called ξ ("Zähligkeit"). The term ξ describes the number of equivalent faces or points received if a certain symmetry element operates, and hence is an indicator for the multiplicity of certain faces, points or positions. For example, depending on the symmetry operator and the position of a face or lattice point in the Pm3m (O_h) space group, the multiplicity (ξ) of the faces can be 6, 8, 12, 24 or 48, respectively.

In their original use (NIGGLI, 1941), the face symmetry and the terms *Zähligkeit* and *Wertigkeit* have been employed to determine the "Formenzähligkeit" of a crystal, in such a sense, that it is possible to determine number of possible crystal faces (cube, octahedron, prism …) appearing on a polyhedral crystal.

The number of equivalent faces present can be calculated by the following equation:

$$\frac{\varsigma}{\omega} = \xi \qquad [7.4]$$

ς = "Zähligkeit" of the general position; ω = "Wertigkeit" of the independent subgroup; ξ = gives the number of equivalent faces of special forms.

This can be demonstrated for the crystal class D_{6h} (NIGGLI, 1941). The crystal class D_{6h} contains the independent subgroups C_{6v}, C_{2v}, C_s. According to Table 7.9, the ω-values of these subgroups are 12, 4 and 2 respectively. The value of "ς" of the general form is 24. By application of equation [7.4] the resulting number of faces of special forms is:

$C_{6v} = \frac{24}{12} = 2$ (special form: pinacoid)

$C_{2v} = \frac{24}{4} = 6$ (special form: hexagonal prism)

$C_s = \frac{24}{2} = 12$ (special form: hexagonal dipyramid or dihexagonal prism)

Within the crystal class D_{6h}, polyhedrons having 24-faces (general form), 12-, 6- or 2-faces (special forms), can be observed. The later faces (pinacoids) can only appear in combination with some other faces.

The term ς and ξ corresponding to the "Zähligkeit" of the general and special forms of crystal faces and can not be incorporated into the BVD-model, as these values describe the number of equivalent faces present for a given crystal polyhedron having a certain space group symmetry. Nevertheless, this information can be applied as an indicator to limit the number of faces to be considered and therefore indicating towards faces which should be considered as the first choice when starting BVD-calculations. Crystal faces of high symmetry should be considered prior to faces of low order of symmetry.

This chapter has shown that face-symmetry is one major internal factor that needs to be considered while calculating the "abstract forms" of crystals. But this derivation is only partly satisfactory as the impact of symmetry-factors to crystal morphology is even more profound as will be demonstrated in Chapter 7.4 regarding the influence of site symmetry factors in respect to the extension and growth of a crystal surface.

Table: 7.9 List of independent subgroups given for the 32 crystal classes (NIGGLI, 1941).

	"Zähligkeit" ς generell position	"Zähligkeit" ξ spezial position	Independend subgroups, „Wertigkeit" ω					
			ω=2	ω=3	ω=4	ω=6	ω=	ω=12
C_1	1	--	--	--	--	--	--	--
C_i	2	--	--	--	--	--	--	--
C_2	2	1	C_2 ξ= 1	--	--	--	--	--
C_S	2	1	C_S ξ= 1	--	--	--	--	--
C_{2h}	4	2	C_2 und C_S ξ = 2	--	--	--	--	--
D_2	4	2	C_S ξ= 2	--	--	--	--	--
C_{2V}	4	2, 1	C_S ξ= 2	--	C_{2V} ξ= 1	--	--	--
D_{2h}	8	4, 2	C_S ξ= 4	--	C_{2V} ξ= 2	--	--	--
C_3	3	1	--	C_3 ξ= 1	--	--	--	--
C_{3i}	6	2	--	C_3 ξ= 2	--	--	--	--
D_3	6	3, 2	C_2 ξ= 3	C_3 ξ= 2	--	--	--	--
C_{3V}	6	3, 1	C_S ξ= 3	--	--	C_{3V} ξ= 1	--	--
D_{3d}	12	6, 2	C_2 und C_S ξ = 6	--	--	C_{3V} ξ= 2	--	--
C_4	4	1	--	--	C_4 ξ= 1	--	--	--
S_4	4	2	C_2 ξ= 2	--	--	--	--	--
C_{4h}	8	4, 2	C_S ξ= 4	--	C_4 ξ= 2	--	--	--
D_4	8	4, 2	C_2 ξ= 4	--	C_4 ξ= 2	--	--	--

Continuation of Table.: 7.9

	"Zähligkeit"ς generell position	"Zähligkeit"ξ spezial position	Independend subgroups, „Wertigkeit" ω					
			ω=2	ω=3	ω=4	ω=6	ω=8	ω=12
C_{4V}	8	4, 1	C_S ξ= 4	--	--	--	C_{4V} ξ= 1	--
D_{2d}	8	4, 2	C_2 und C_s ξ= 4	--	C_{2V} ξ= 2	--	--	--
D_{4h}	16	8, 4, 2	C_S ξ= 8	--	C_{2V} ξ= 4	--	C_{4V} ξ= 2	--
C_6	6	1	--	--	--	C_6 ξ= 1	--	--
C_{3h}	6	3, 2	C_S ξ= 3	C_3 ξ= 2	--	--	--	--
C_{6h}	12	6, 2	C_S ξ= 6	--	--	C_6 ξ= 2	--	--
D_6	12	6, 2	C_2 ξ= 6	--	--	C_6 ξ= 2	--	--
C_{6V}	12	6, 1	C_S ξ= 6	--	--	--	--	C_{6V} ξ= 1
D_{3h}	12	6, 3, 2	C_S ξ= 6	--	C_{2V} ξ= 3	C_{3V} ξ= 2	--	--
D_{6h}	24	12, 6, 2	C_S ξ= 12	--	C_{2V} ξ= 6	--	--	C_{6V} ξ= 2
T	12	6, 4	C_2 ξ= 6	C_3 ξ= 4	--	--	--	--
T_h	24	12, 8, 6	C_S ξ= 12	C_3 ξ= 8	C_{2V} ξ= 6	--	--	--
O	24	12, 8, 6	C_S ξ= 12	C_3 ξ= 8	C_4 ξ= 6	--	--	--
T_d	24	12, 6, 4	C_S ξ= 12	--	C_{2V} ξ= 6	C_{3V} ξ= 4	--	--
O_h	48	24, 12, 8, 6	C_S ξ= 24	--	C_{2V} ξ= 12	C_{3V} ξ= 8	C_{4V} ξ= 6	--

7.4 Site symmetry of crystal surfaces

Even though this chapter deals with the last internal factor to be implemented into the BVD-model it also refers back to the principles introduced by Pauling (1929) about coordinated polyhedrons (Chapter 4).

Pauling´s first principle states, that for a coordinated polyhedron of anions formed around a cation, the cation-anion distance is determined by the radius sum of the ions, and additionally the coordination number of the central-cation is determined by the radius ratio of the ions. In his second rule Pauling states, that in a stable coordination structure the electric charge of each anion tends to compensate the strength of the electrostatic valence bonds reaching to it from the cation in the center of the polyhedron.

BROWN (2002) referred to these principles, correlating the kind of coordinated polyhedron to the symmetry of the bonded neighbours in the polyhedron. He deduced that Paulings rules, about the nature of a coordinated polyhedron, are best matched when the coordination polyhedron of anions around a central cation is one of high symmetry, which is able to lower the repulsion of the ligands to a minimum. Examples given by BROWN (2002) are, in the case of six coordination, the octahedron with the highest crystallographic site symmetry (m3m). For four coordination it is the tetrahedron with site symmetry ($\bar{4}$3m). Other high –symmetry arrangements are the 12-coordinated cubo-octahedron (m3m), the three-coordinated triangle (62m), and the eight-coordinated cube (m3m). Although the cube is the eight-coordinated environment with the highest symmetry, the square anti-prism (4mm) minimizes the repulsion between the ligands at the cost of lowering the symmetry. Other coordination numbers such as 5, 7, and 9 are encountered less frequently. Such coordination can only be accommodated by low-symmetry environments, in which the ligands cannot all be crystallographically equivalent (BROWN, 2002).

Based on these observations BROWN (2002) introduced his *Principle of maximum symmetry*:

> As *far as allowed by the chemical and geometric constraints, all atoms in a compound will be chemically and geometrically indistinguishable.*

Additionally BROWN (2002) extended this principle by two rules:

Rule 1 : In a given space group, all Wyckoff positions with the same multiplicity ,m_W, have site symmetry of the same order, m_S.
(m_w is the multiplicity of the Wyckoff position in the non-translational unit, m_s is the number of times the operation "S" transforms an atom into itself).

Rule 2 : The order of the site symmetry of any Wyckoff position is in inverse proportion to its multiplicity.

As an example BROWN (2002) refers to a cation occupying a special position having site symmetry m3m, for which m_S = 48. This ion would have 48 neighbours, if these neighbours would occupy general position, each having a multiplicity factor of 1. This high coordination number is impossible as only a few cations have coordination numbers higher than 12. Therefore, neighbours of a coordinated cation must occupy certain Wyckoff positions having a higher order of multiplicity. As an example, the neighbours of an octahedrally coordinated cation, having the site symmetry m3m, are required to have at least a site symmetry of the order 48/6 = 8. In this example 48 is the multiplicity factor of the general position (m_S), 6 equals the number of coordinated anions, and 8 is the multiplicity factor (m_W) of the Wyckoff position of the coordinated anions. As a result the six coordinating anions must be placed on the three four-fold axes, which pass through the cation, and their site symmetry must at least be equivalent to 4 mm (BROWN, 2002). The site symmetry of the ions may be higher, if they lie on a mirror plane not intersecting with the cation, but their symmetry cannot be lower (Fig. 7.15 a).

BROWN (2002) summarized his investigations on the relationship between a coordinated cation and the symmetry of his bonded ligands as:

The principle of maximum symmetry requires that the crystal structure adopted by a given compound be the most symmetric that can satisfy the chemical constraints. We therefore expect to find high-symmetry environments around atoms wherever possible, but such environments are subject to constraints such as the relationship between site symmetry and multiplicity and the constraints that each atom will inherit certain symmetries from its bonded neighbours.

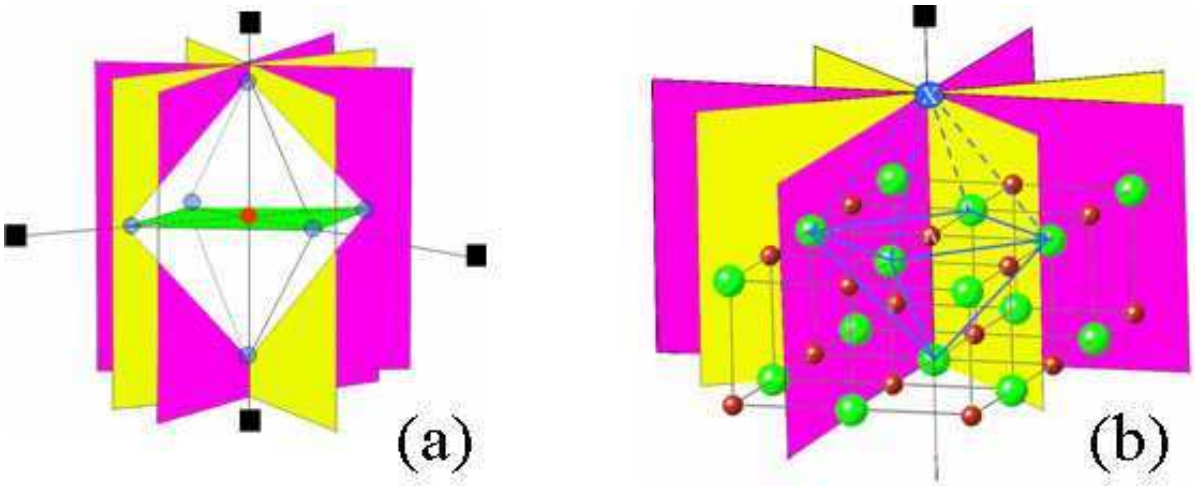

Fig.: 7.15 (a) Octahedral coordinated cation (red) with site symmetry m3m. Anions coordinating the cation are marked blue. Mirror-planes are marked green, yellow and pink. Four-fold rotation axes are indicated by a black square. The anions coordinating the central cation are placed along the four-fold axis and at the intersection of two mirror-planes. The site symmetry of the anions is 4mm. (b) NaCl-crystal structure. Cations are marked red, anions are green. Mirror-planes are yellow and pink and the four-fold axis is indicated by a black square. The coordination polyhedron around the central cation is given by blue lines. The anion (X), marked blue, adsorbing to the surface has a minimum site-symmetry of 4mm.

This approach can be applied to mineral surfaces in such a way, that the central cation of the coordinated polyhedron is considered to be part of the crystal lattice terminating a crystal surface (Fig. 7.15 b). In the BVD-mode such ions terminating a crystal surface

occupy special positions with a given Wyckoff symmetry. This is equivalent to the assumption of BROWN (2002) that cations in a coordinated polyhedron occupying a special position with a certain site symmetry.

Let us consider e.g. the crystal structure of a NaCl-crystal. Each ion Na^+ is octahedrally coordinated by six Cl^--ions, and vice versa. In return, ions terminating a crystal surface do not possess a full coordination sphere, a fact already considered for the calculation of the bond-valence deficiency of a given crystal surface. During growth this "incompleteness" is overcome due to the adsorption of new ions onto the crystal lattice, completing the coordinated polyhedron of the surface ions. According to BROWN (2002) the new ions adsorbing to the crystal lattice, filling the vacant positions of a coordinated polyhedron must have a minimum site symmetry of a given order (Fig. 7.15 b). The values of this symmetry factor are compatible with the 32 site symmetries of the three-dimensional point groups (Tab.: 7.10).

Depending on the face symmetry of a given crystal lattice (e.g.: 4mm, 3m or 2mm), the order of minimum site symmetry of an ion adsorbing to the crystal surface differs, and therefore needs to be considered. This factor, equivalent to the ω-factor in Chapter 7.3, is a measurement for the growth rate of a crystal planes parallel to its face normal, namely the "growth rate" mentioned in Chapter 3.1, implying that crystal faces, having a higher face symmetry will advance at a slower growth rate, compared to crystal faces having a lower order of face symmetry.

To simplify this approach, which in principle is based on the face symmetry of a crystal lattice terminating a crystal surface, it is applicable to reconsider the approach of NIGGLI (1941). He considered only 10 non-translational face symmetries to be of importance to describe the full symmetry of a crystal lattice (Chapter 7.3). By arranging these two-dimensional point groups in a similar fashion as the three-dimensional points groups (Tab. 7.11) the value of the ω-factor can be derived after having determined the face symmetry of the crystal surface.

Group order						
48	$\frac{4}{m}\bar{3}\frac{2}{m}$					
24	432	$\bar{4}3m$	$\frac{2}{m}\bar{3}$	$\frac{6}{m}\frac{2}{m}\frac{2}{m}$		
16	$\frac{4}{m}\frac{2}{m}\frac{2}{m}$					
12	23	622	$\bar{6}2m$	$6mm$	$\frac{6}{m}$	$\bar{3}\frac{2}{m}$
8	422	$\bar{4}2m$	$4mm$	$\frac{4}{m}$	$\frac{2}{m}\frac{2}{m}\frac{2}{m}$	
6	6	$\bar{6}$	32	$3m$	$\bar{3}$	
4	4	$\bar{4}$	222	$mm2$	$\frac{2}{m}$	
3	3					
2	2	m	$\bar{1}$			
1	1					

Tab.: 7.10 Table adopted from the International Tables for Crystallography (Vol. A). Given are the 32 three-dimensional point groups with their corresponding group order.

"Group order" (ω)-factor		
12	$6mm$	
8	$4mm$	
6	6	$3m$
4	4	$2mm$
3	3	
2	2	m
1	1	

Tab.: 7.11 Table adopted from the International Tables for crystallography (Vol. A). Given are the ten two-dimensional point groups after (NIGGLI 1941). From this table, the ω-factor (former Group order) can be deduced for each ion occupying a certain Wyckoff position.

The conformity of the ω-factors, either from the three-dimensional approach of BROWN (2002) and the "two-dimensional" approach of NIGGLI (1941), can be deduced by comparing the values of the site-symmetry given in Table 7.10 and 7.11.

Regarding the site-symmetry of an adsorbing ion to be relevant while considering the "growth rate" of a crystal plane parallel to its face normal, the influence of the "site-symmetry" on the extension of a crystal plane sideways needs to be considered as well. WULFF (1901) mentioned that the growth of a crystal has two aspects, one being the extension of a face sideways, the other aspect being its growth along the face normal (Chapter 3.1). A similar conclusion can be drawn considering the different attachment sites of an ion to the surface of a Kossel-crystal (Chapter 3.6). Kink-sites or stepped-edges of lattices offer more and better attachment sides than terraces. Consequently ions adsorbing to a crystal surface show the tendency to attach themselves more freely along the edges of a terrace instead of simply attaching themselves to the top of a terrace.

Therefore, reconsidering the approach of BROWN (2002), it must be stated that:

Ions attaching themselves to an edge of a terrace, must occupy a position of minimum site symmetry in relation to the ions of the edge of a crystal terrace.

Consequently an additional face-symmetry factor called Z-factor, considering the extension of a crystal lattice in two-dimensions, needs to be introduced into the BVD-model.

Let us consider a primitive crystal lattice with a 4 mm point-group symmetry (Fig.: 7.16). The Atoms occupy special positions having the full site symmetry 4mm. According to the principle of maximum symmetry, an ion (X) adsorbing to the lattice, extending it sideways, has to be placed on special positions of minimum site symmetry, and the "value" of this position gives the value of the Z-factor.

In our example the position taken by the ion is a Wyckoff position with the site symmetry (m) (Fig. 7.16). During further extension, by adding more ions to the lattice, the site symmetry of the ion (X) will increase until it is equally surrounded by neighbours receiving the full site-symmetry 4 mm.

The Z-factor derived from this approach is equivalent to the multiplicity factor of the Wyckoff position of minimum site symmetry, given in the Table 7.12, adapted from the International Tables for crystallography (Vol. A).

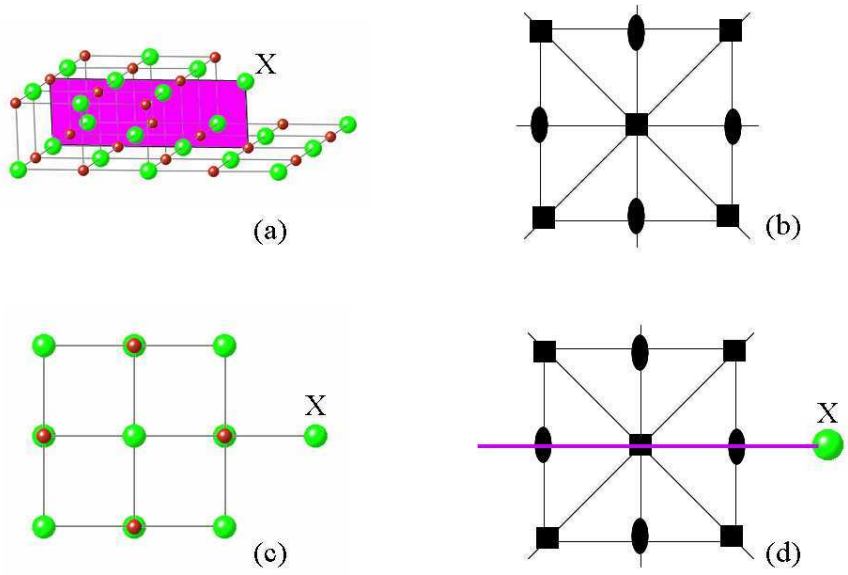

Fig.: 7.16 (a) NaCl-crystal structure type with face symmetry 4mm, cations are marked red, anions green. The mirror-plane is marked pink. (a) An anion (X) adsorbing to the edge of a crystal lattice has the minimum site symmetry m and must be placed onto the mirror plane. (b) Face-symmetry of the (001) crystal surface (c) Top view of the (001)-crystal plane with the anion (X) adsorbing to an edge. (d) Face symmetry of the (001)-crystal plane indicating that the anion (x) has a minimum site symmetry of m.

Z-factor			(ω)-factor
6	6*mm*		12
4	4*mm*		8
3	6	3*m*	6
2	4	2*mm*	4
1	3		3
1	2	*m*	2
1	1		1

Tab.: 7.12 Given in the middle are the ten two-dimensional point groups from NIGGLI (1941), and the corresponding values of the Z- and (ω)—factors (left and right).

Taking a look at the results obtained (Tab.7.12), differences can be noticed while comparing both symmetry factors (ω-factor and Z-factor). The ω-factors of a (001)-crystal plane, with the point-group symmetry 4mm is ω = 8, but the same crystal plane has a Z-factor of Z = 4. This difference is an indication for the two different "growth processes" already mentioned by WULFF (1901), "extension" and "growth". Consequently both values have to be treated differently while calculating the abstract form of a crystal by application of the BVD-model.

Both symmetry factors express the dependence of adsorbing ions on the face symmetry of a given crystal surface. Having introduced the ω-factors as a division factor, characterizing the growth rate of a crystal face in orthogonal direction, the Z-factor will be treated as a multiplication factor. This is to some extent a correction to the former ω-factor, considering the circumstance that a crystal surface having a high face symmetry may not advance as fast in an orthogonal direction, while at the same time a faster extension sideways is possible.

This might as well be related to growth processes observed on mineral surfaces. Depending on the environmental conditions, many minerals tend to complete an existing growth layer before an additional crystal layer on top of the former one is established.

Adding the symmetry factors (ω-factor and Z-factor) to our previous calculations, e.g. for a primitive cubic lattice, the final ranking of the crystal faces, considering all internal factors implemented into the BVD-model, is given in Table 7.13.

Face (hkl)	DB	Unit-cell (Å²)	BVDU (Å²)	RD	BVDU* (Å²)	LD	BVDU** (Å²)	ω	BVDU*** (Å²)	Z	ΔBVDU (Å²)
(100)	1	25,00	0,040	1	0,040	1	0,040	8	0,005	4	0,020
(110)	2	35,35	0,056	1	0,056	2	0,113	4	0,028	2	0,056
(111)	3	43,29	0,069	1	0,069	3	0,207	6	0,034	3	0,103
(210)	3	55,90	0,053	1	0,053	5	0,268	2	0,134	1	0,134
(211)	4	61,23	0,063	1	0,065	6	0,391	2	0,196	1	0,196
(221)	10	149,99	0,066	1	0,066	9	0,600	2	0,300	1	0,300
(311)	10	165,82	0,060	1	0,060	11	0,663	2	0,331	1	0,331
(331)	14	217,94	0,064	1	0,064	19	1,220	2	0,610	1	0,610

Tab.: 7.13 Complete set of calculation needed to describe the morphological ranking of crystal faces in a primitive cubic Bravais-lattice structure with a_0 = 5.0 Å. The BVDU-values marked with an asterix refer to different steps of refinement. BVDU* = RD-factor; BVDU** (RD- and LD-factor); BVDU*** (RD-, LD- and ω -factor); Δ BVDU = final result including RD-, LP-, ω - and Z-factors). All bond-valence deficiency values are given as valence-units (vu) and refer to a two-dimensional unit-cell of the corresponding crystal faces calculated from the number of dangling bonds (DB).

Comparing the ranking of the faces given in Table. 7.13 before and after the introduction of the face symmetry factors, no change in the ordering of morphological importance can be noticed. This does not imply that the symmetry factors can be neglected. It is only the consequence of the symmetry group chosen.

The primitive cubic lattice contains the full symmetry of the crystal class m3m (O_h), and the differences in the morphological ranking of the crystal faces are singled out by the influence of the RD- and LD-factors, only.

Morphological ranking ending with BVDU** / (Å²):

(100) < (110) < (111) < (210) < (211) < (221) < (311) < (331)

Morphological ranking ending with all symmetry factors:

(100) < (110) < (111) < (210) < (211) < (221) < (311) < (331)

The impact of the symmetry factors is emphasized by application to minerals crystallizing having a lower space group symmetry, for example the mineral pyrite with a space group symmetry Pa3, which is a subgroup of the crystal class m3m (Tab. 7.14).

Face (hkl)	DB	Unit-cell (Å²)	BVDU (Å²)	RD	BVDU* (Å²)	LD	BVDU** (Å²)	ω	BVDU*** (Å²)	Z	ΔBVDU (Å²)
(100)	2	29,34	0,07	2	0,14	2	0,27	1	0,27	1	0,27
(110)	4	41,50	0,10	2	0,19	4	0,77	1	0,77	1	0,77
(111)	12	50,83	0,24	1	0,24	3	0,71	3	0,24	1	0,24
(210)	2	65,62	0,03	2	0,06	10	0,61	1	0,61	1	0,61

Tab.: 7.14 Calculation of the Δ BVDU-values for different crystal faces appearing on pyrite crystals (Pa3). The BVD-value gives the amount of dangling-bonds (DB) calculated for the iron-ions, a_0 = 5,417 Å².

The example of pyrite (Pa3) given in Table (7.14) exemplifies the importance of the face symmetry factors (ω-factor and Z-factor). Considering only the RD- and LD-factors (BVDU **) the morphological ranking of the crystal faces is:

BVD-Model (with out symmetry factors): (100) < (210) < (111) < (110)

This ranking reflects the minor importance of the (110) crystal face. The high ranking of the (210) crystal face is close to the one expected, giving the (210)-crystal face on pyrite a higher order of morphological importance than the one compared to the (210)-crystal face in the super group of the Pm3m-crystal structure type.

However, this ranking does not correspond to the ordering given by DONNAY-HARKER (1937):

Donnay-Harker (1937): (111) < (100) < (210)< (110)

This discrepancy between the Donnay-Harker approach and the BVD-approach is solved, by considering the face-symmetry factors (ΔBVDU). The ranking of the morphological order of the crystal faces changes to:

BVD-Model (with symmetry factors): (111) < (100) < (210) < (110)

Concluding, it can be stated that by implementation of internal crystal structure factors, the BVD-model is capable of determining the "abstract form" of a polyhedral crystal, even to the extent that the influence of space group symmetries can be distinguished.

7.5 Application of the Wulff -plot to the BVD-model

While changing the equations of CURIE (1885), and correlating the capillary constants of crystal faces to the growth rates of these faces, WULFF (1901) was the first to apply this general concept and compared different crystal surface features as a function of their proportional effect on the central distance of crystal faces to the "Wulff-point" (Chapter 3). Therefore it seems applicable to write the Wulff-equation in a even more general term:

$$\frac{\gamma_1}{h_1} = \frac{\gamma_2}{h_2} = ...const. \qquad [7.5]$$

here γ_i describes the value of the surface attribute obtained and h_i corresponds to the face normal of the face F_i.

In terms of the BVD-model this general assumption (eqn. 7.5) proves to be useful, giving the opportunity to compare and calculate the influence of the bond-valence deficiencies of different faces on the final morphology of a polyhedron crystal. The equation therefore is transformed to:

$$\frac{\Delta vu_1}{h_1} = \frac{\Delta vu_2}{h_2}..... = const. \qquad [7.6]$$

Here the term $\Delta vu_{(i)}$, is the bond-valence deficiency of the face (F_i) of unit cell dimension.

If the bond-valence deficiency approach leads to reliable results while predicting the morphology of crystals, the substitution of the term $\gamma_{i,}$ in Eqn.7.6, by the term Δvu_i, should lead to Wulff-constructions, which are comparable to Wulff-constructions given in the literature. Such a comparison is given in Figure. 7.17. Here the Wulff-construction of a homöopolar Fm3m-lattice obtained by application of the methods of

Stranski-Kaischew (in LACMANN, 1974) is compared to the Wulff-constructions obtained by application of the BVD-model. The different polyhedrons shown in Figure 7.17 correspond to the successive steps in the BVD-calculation (Tab. 7.15).

The polyhedrons given in (Fig. 7.17), have been obtained by use of the *JCRYSTAL*-computer program, as this computer-software constructs crystal shapes depending on the relative length of the central distances of different crystal faces.

Face (hkl)	DB	Unit-cell (Å²)	BVDU (Å²)	RD	BVDU* (Å²)	LD	BVDU** (Å²)	ω	BVDU*** (Å²)	Z	ΔBVDU (Å²)
(100)	8	25,00	0,32	2	0,64	2	1,28	8	0,16	4	0,64
(110)	12	35,35	0,33	2	0,67	4	2,71	4	0,67	2	1,35
(111)	12	43,299	0,27	1	0,27	3	0,83	6	0,13	3	0,41

Tab.: 7.15 Bond-valence deficiency calculation of a homöopolar crystal having the space group symmetry Fm3m. The BVDU values calculated correspond to the number of dangling bonds (DB) and $a_0 = 5{,}0$ Å².

The different polyhedrons obtained in Figure (7.17) represent different possible "abstract forms" of a homöopolar crystal (Fm3m), considering the influence of the intermediate steps in the calculation (BVDU, BVDU*, …). The outset for the calculation is the number of dangling-bonds, as no real crystal is concerned and all bonds are considered to be equivalent. In the case of a real mineral, the number of dangling bonds must be multiplied by the bond-valence value of these bonds.

While Figure (7.17 a) represents an abstract form considering only the number of dangling-bonds per unit cell area, the image of Figure (7.17 e) is the final "abstract form", after having considered all internal factors, influencing the final morphology of the crystal. The figures (7.17 b-c) show the influence of the individual intermediate

factors (RD, LD, ω-factor and Z-factor). The difference between the final "abstract form" of the BVD-model and the "form" given by LACKMANN (1974), is due the fact that the faces (100) and (111) in his calculation are considered to be equivalent, both being faces with an similar φ-value. Consequently his "abstract form" is a cube-octahedron.

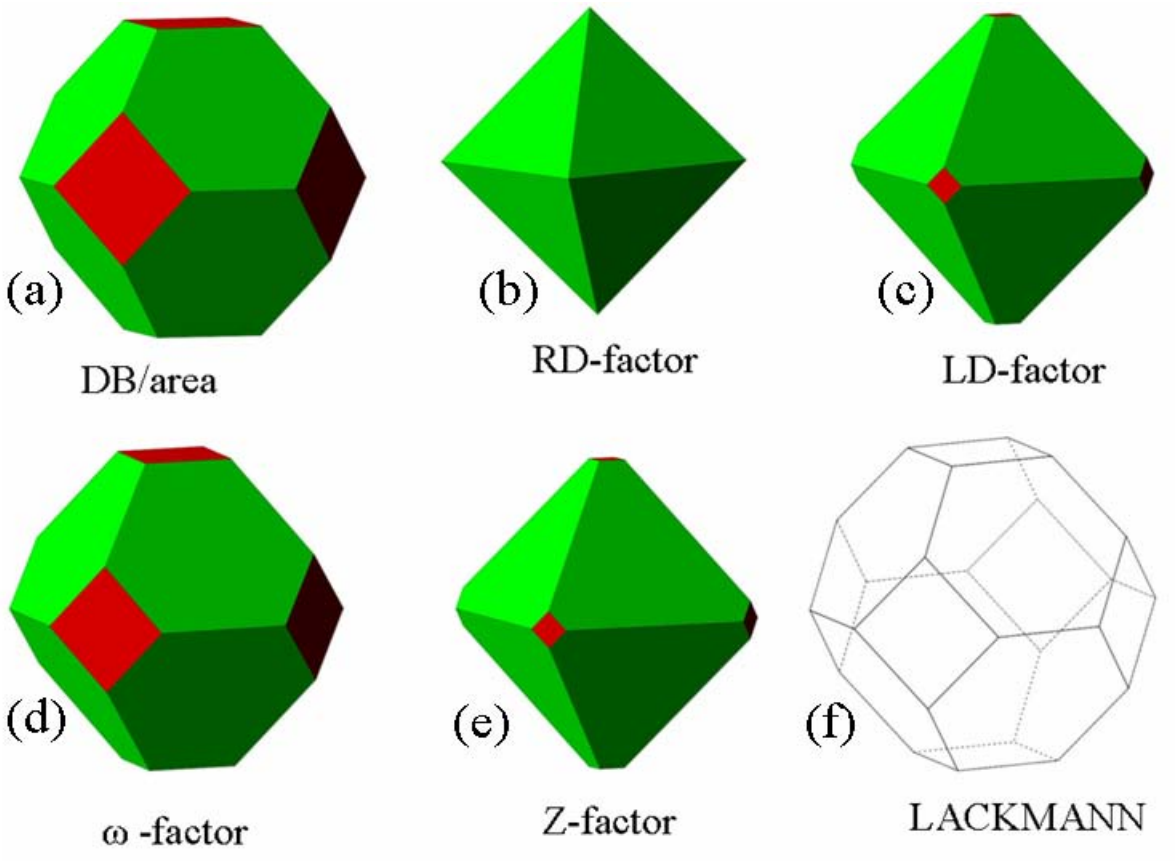

Fig.:7.17 The results of Tab. 7.15, for a homöopolar crystal (Fm3m), have been plotted as Wulff-constructions, using the computer software JCRYSTAL. Given is a sequence of polyhedral crystals forms obtained by application of the BVD-model (a-e, see text). Fig. (f) corresponds to an "abstract form" of a homöopolar crystal (Fm3m), calculated by the method of Stranski-Kaischew (LACKMANN, 1974).

8. Calculation of “abstract forms” of crystal structure types

The previous chapters have outlined the basic principles of the BVD-model. It has been demonstrated that internal factors such as reticular density, lattice density and crystal symmetry can be connected to the BVD-model. By comparing the bond-valence deficiencies of different crystal faces of a given mineral it is possible to predict an “ideal crystal morphology”. The forms so obtained, considering only internal factors taking control on the crystal morphology and are addresses as the “abstract forms” of the minerals. These theoretical crystal forms must be regarded as “matrix forms” of a crystal as they may be modified by external factors during the further growth process of the crystals (Chapter 11).

Minerals can systematically be grouped in different ways. The most prominent classification in mineralogy is the chemical classification. Due to their chemical composition inorganic minerals are divided into 12 different classes (I Elements; II Sulphides and Sulphosalts; III Halides; IV Oxides and Hydroxides; V Silicates, VI Borates, VII Phosphates, Arsenates and Vanadates; VIII Tungstates and Molybdates; IX Suphates; X Chromates; XI Carbonates; XII Nitrates and Iodates).

Another possible classification of minerals is the ordering by their structure types. This classification is more preferable for our concerns compared to the chemical classification, as for example more than 200 different minerals, including many halides, oxides, sulfides and others, crystallize having a NaCl-crystal structure type. These structure-types are characterized by their empirical formula and their space-group, which can be addressed as being expressions of the internal structures of the crystals.

In the following chapters some of the most prominent structure-types will be discussed and some exemplary mineral species will be described in detail. In some of the examples given, minor variations between the predicted “abstract form” and the most frequently observed morphologies of natural minerals might occur because natural

minerals almost never crystallize from pure solution and therefore morphological variations are due to external factors, for example the presence of foreign atoms, ions or molecules. Depending on the geological setting of the location, not only differences in the chemical composition of the solution occur, but also difference in the supersaturation, temperature and pressure will influence the morphology of natural samples. Nevertheless it can be observed that the most dominant "abstract forms" predicted by the BVD-model correspond very well with the most frequent habits of natural single crystals and the following chapters will give a general overview of different "abstract forms" applicable to various mineral structure-types.

Before the "abstract forms" are discussed in the following chapters, a short general introduction taken form literature is quoted for each structure type presented (KLOCKMANN, 1978; SCHRÖCK & WEINER, 1981, RÖSSLER, 1983, DANA´s NEW MINERALOGY, 1997).

8.1 Structure-Types of Elements (A – Type)

Depending on the bonding-type (metallic or covalent), several different structure types for native elements are possible. The most dominant are the Copper-Type (O_h^5 - Fm3m), the Iron-Type (α-Fe, O_h^9 - Im3m) and the α-Polonium-Type (O_h^1 - Pm3m) for metals and the Diamond-Type(O_h^7 - Fd3m), the Graphite-Type (D_{6h}^4 - $P6_3/mmc$) and the α-Sulfur-Type (D_{2h}^{24} - Fddd) for elements having covalent bonding.

Single polyhedral crystals of the elements e.g. gold, silver and copper are rare, although it is known that many of these single crystals have either an octahedral, cubic or dodecahedral habit.

Ignoring the influence of external factors to some extent, assuming “pure” solution with no foreign ions/atoms present, the most common crystal morphologies observed should be similar to the predicted “abstract forms” of the BVD-model.

Dealing with native elements we only need to consider one type of building unit (one sort of atom) and only one type of bond, either metallic or covalent. Additionally the bond-valences are distributed equally based on the coordination number of the atoms.

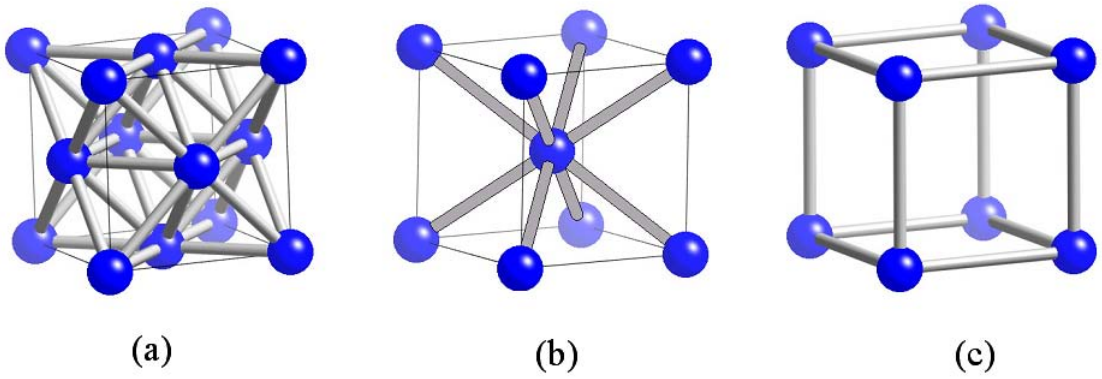

Fig.: 8.1 The figures illustrate the unit-cells of the three most common structure types of metals. (a) Copper-Type (O_h^5 - Fm3m). (b) Iron-Type (α-Fe, O_h^9 - Im3m). (c) α-Polonium-Type (O_h^1 - Pm3m).

8.1.1 Copper-Type (Fm3m)

Many of the native elements, predominantly metals, crystallize having a Copper-type structure (Fig.: 8.1a). The space group symmetry is (O_h^5 - Fm3m), Z = 4 and the coordinates of the atoms are 0 0 0, ½ ½ 0, ½ 0 ½ , 0 ½ ½ , giving rise to a face-centered cubic lattice, equivalent to the cubic closed-packing. The coordination number of the atoms is CN = 12 and the coordination polyhedron around the atom is a dodecahedron.

The morphological ranking of the crystal faces obtained by application of the BVD-model are given in Table (8.1). Note that this table is a general table for elements crystallizing in the copper-type structure (O_h^5 - Fm3m). The values given correspond therefore to a "theoretical native element". In order to receive the actual bond-valence deficiency of a crystal surface, the bond-valences of the bonds of the respective element and their lattice-spacing (a_0) have to substituted the corresponding values given in the Table (8.1). Graphic examples of the surfaces calculated are given in Appendix II.

Face (hkl)	DB	Unit-cell (Å²)	BVDU (Å²)	RD	BVDU* (Å²)	LD	BVDU** (Å²)	ω	BVDU*** (Å²)	Z	ΔBVDU (Å²)
(100)	8	25,00	0,32	2	0,64	2	1,28	8	0,16	4	0,64
(110)	12	35,36	0,34	2	0,68	4	2,72	4	0,68	2	1,36
(111)	12	43,30	0,28	1	0,28	3	0,83	6	0,14	3	0,42
(311)	56	165,83	0,34	1	0,34	11	3,71	2	1,86	1	1,86

Tab. 8.1: General calculation for an A-type crystal having a Copper-type crystal structure. The ΔBVDU-value given, corresponds to the bond-valence deficiencies of the respective faces after having considered the internal factors (RD = reticular density, LD = lattice density, ω = face symmetry and Z = site-symmetry). The values obtained have been calculated for a given number of dangling-bonds (DB), in this general example substituting the actual bond-valences.

The morphological ranking of the four most dominant faces, starting with the crystal faces having the lowest bond-valence deficiency (ΔBVDU) is:

$$(111) < (100) < (110) < (311)$$

According to the results obtained the most favorable “abstract form” predicted is a truncated octahedron (Fig. 8.2a). A change in the fluid composition (see later chapters) may promote a better development of some of the other faces. Generally, crystal surfaces having a low bond-valence deficiency will be more favored than faces having a higher bond-valence deficiency. Some possible combinations of the three dominant faces having low bond-valence deficiency are given in Fig 8 b-d. The examples given correspond to cases where the {111} surfaces are preferred (b), the development of {001} is substituted (c), or the bond-valence deficiency of the (110) crystal surface is lowered to the extend that it will start to become visible at the crystal (d). For a more detailed discussion of habit changes due to adsorption see Chapter 11.

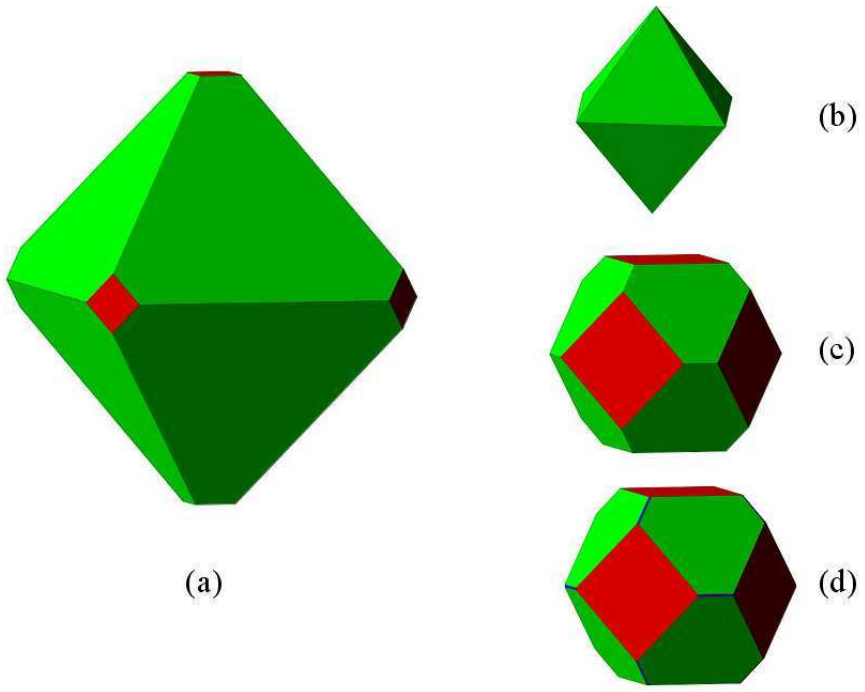

Fig.: 8.2 (a) “Abstract form” calculated from the ΔBVDU-values given in Table (8.1). The figures b-d show possible variations of this “theoretical form”, referring to different growth conditions (see text).

The predicted "abstract form" (Fig. 8.2a) is now correlated with the most frequent morphology of single crystals of copper, gold, silver and lead as given in *Dana´s New Mineralogy* (1997).

Copper (Cu)	:	octahedral and dodecahedral
Gold (Au)	:	cubic and dodecahedral
Silver (Ag)	:	cubic and octahedral
Lead (Pb)	:	rarely as octahedral, cubic and dodecahedral

A comparison of this list with the predicted morphological ranking, on favor for the octahedron and cube correlate well. No additional faces, except of the three crystal faces (111), (100) and (110) having the lowest bond-valence deficiencies, are dominant in natural samples. The preferences of one of these faces over the other, in contrast to the predicted "abstract form" might be due to differences in the external conditions during crystal growth (see Chapter 11).

8.1.2 Iron-Type (α-Fe, Im3m) and α-Polonium-Type (Pm3m)

Minerals crystallizing with the Iron-Type (α-Fe, O_h^9 - Im3m) and the α-Polonium-Type (O_h^1 - Pm3m) structure types are rare. Many of the elements more likely form bonds to other elements of the periodic table and do not appear as simple native elements, forming single crystals. The native elements such as Li, Na, Rb, Cs have an Iron-Type structure. Polonium as a short time living decay product within the uranium decay series, will never form single crystal species. The theoretical ranking of the morphological importance of the crystal faces are listed in Tab.8.2 and Tab 8.3. Graphic examples of the surfaces calculated are given in Appendix II.

The mineral wairauite (FeCo; Im3m, Z = 1) forms microscopic grains showing cubes and octahedrons. This morphology corresponds to the second and third ranked crystal faces predicted by the BVD-model (Tab. 8.2). The dodecahedral form predicted as the

most favorable by the BVDF-model, has not been observed so far. This may be explained by the fact that wairauite contains two different elements (Fe and Co) and therefore does not match exactly the composition for an A –type mineral having an Im3m-crystal structure type.

Face (hkl)	DB	Unit-cell (Å²)	BVDU (Å²)	RD	BVDU* (Å²)	LD	BVDU** (Å²)	ω	BVDU*** (Å²)	Z	ΔBVDU (Å²)
(100)	4	25,00	0,16	2	0,32	2	0,64	8	0,08	4	0,32
(110)	4	35,36	0,11	1	0,11	2	0,23	4	0,06	2	0,11
(111)	6	43,30	0,14	2	0,28	6	1,66	6	0,28	3	0,83
(210)	8	55,90	0,14	2	0,29	10	2,86	2	1,43	1	1,43
(211)	8	61,23	0,13	1	0,13	6	0,78	2	0,39	1	0,39

Tab.: 8.2 General bond-valence deficiency table of an A-type mineral, having an Im3m-crystal type structure and a_0 = 5,0 Å², calculated for a given number of dangling bonds (DB).

Face (hkl)	DB	Unit-cell (Å²)	BVDU (Å²)	RD	BVDU* (Å²)	LD	BVDU** (Å²)	ω	BVDU*** (Å²)	Z	ΔBVDU (Å²)
(100)	1	25,00	0,04	1	0,04	1	0,04	8	0,01	4	0,02
(110)	2	35,36	0,06	1	0,06	2	0,11	4	0,03	2	0,06
(111)	3	43,30	0,07	1	0,07	3	0,21	6	0,03	3	0,10
(210)	3	55,90	0,05	1	0,05	5	0,27	2	0,13	1	0,13
(211)	4	61,23	0,07	1	0,07	6	0,39	2	0,20	1	0,20

Tab. 8.3 General bond-valence deficiency table of an A-type mineral, having a Pm3m-crystal type structure and a_0 = 5,0 Å², calculated for a given number of dangling bonds (DB).

8.1.3 Diamond-Type (Fd3m)

The diamond-type structure has the space-group symmetry O_h^7 - Fd3m, Z = 8, a_0 = 3.567 (diamond). The coordinates of the atoms are (0 0 0), (0 ½ ½) , (½ ½ 0), (½ 0 ½) , (¼ ¾ ¼), (¾ ¼ ¼), (¼ ¼ ¾), (¾ ¾ ¾). The other four ¼ - positions are not occupied and the structure is not close-packed. Every C-atom has a coordination of CN = 4 and the coordination polyhedron is a tetrahedron (Fig.8.3a). Compared to the former A-type structures the bonding in diamond is covalent. Isotype to diamond are the elements Si, Ge and Sn (gray).

The morphological ranking of the diamond-structure is given for diamond itself, having a lattice constant of a_0 = 3.567, the bonds formed are equivalent and are considered to have a valence of 1,0 *vu* each, calculated from the atomic valence of the C-atom (4^+) and its tetrahedral coordination. The results obtained are given in Tab. 8.4. The unit-cell and the predicted "abstract forms" are shown in Fig. 8.3. Graphic examples of the surfaces calculated are given in Appendix II.

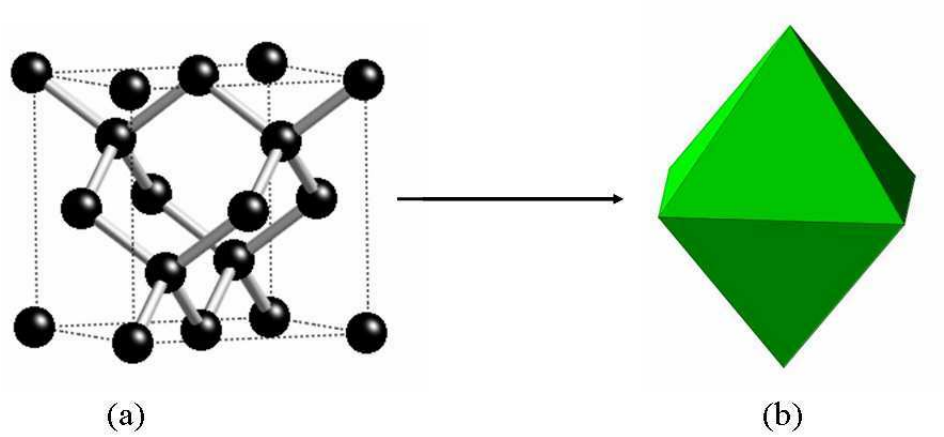

Fig.: 8.3 (a) Unit-cell of a diamond-crystal. (b) Predicted "abstract form" of diamond according to the values obtained from Tab. 8.3.

In Table (8.4) two different values for the (111) crystal surfaces are given. Both termination (111a) and (111b) are theoretically possible (Fig. 8.4), but only one of these terminations, (111a) having the lowest bond-valence deficiency, is the one expected to terminate octahedron shaped diamond crystals. The coordination-tetrahedrons are arranged in layers "a" and "b" (Fig. 8.4a). These layers are oriented in opposite direction and the vertices of the tetrahedrons, for example of layer-A meet, at almost the same level, the basis of the tetrahedrons of layer-B.

Face (hkl)	DB	Unit-cell (Å²)	BVDU (Å²)	RD	BVDU* (Å²)	LD	BVDU** (Å²)	ω	BVDU*** (Å²)	Z	ΔBVDU (Å²)
(100)	4	12,72	0,31	4	1,26	4	5,03	4	1,26	2	2,52
(110)	4	17,99	0,22	4	0,89	4	3,56	2	1,78	1	1,78
(111) a	4	22,04	0,18	2	0,36	3	1,09	6	0,18	3	0,54
(111) b	12	22,04	0,54	2	1,09	3	3,27	6	0,54	3	1,63
(210)	8	28,45	0,28	4	1,12	20	22,50	1	22,50	1	22,50

Tab.: 8.4 Bond-valence deficiency table of diamond, calculated for a given number of dangling bonds (DB) and a_0 = 3.56 Å². Two different surface terminations of the {111} crystal surfaces have to be considered (see text).

But instead of having two different (111) terminations (Fig 8.4c and d), only one termination of the {111}-crystal faces must be recognized and this is the termination parallel to (111a). This termination can be found in any direction crossing the diamond crystal perpendicular to the (111) crystal plane (Fig. 8.5). As a consequence, despite the fact that two different layers of coordination tetrahedron can be distinguished, no anisotropy-effect for the morphological ranking of the {111} faces must be considered, as is the case in the Sphalerite-structure type (Chapter 8.2.2).

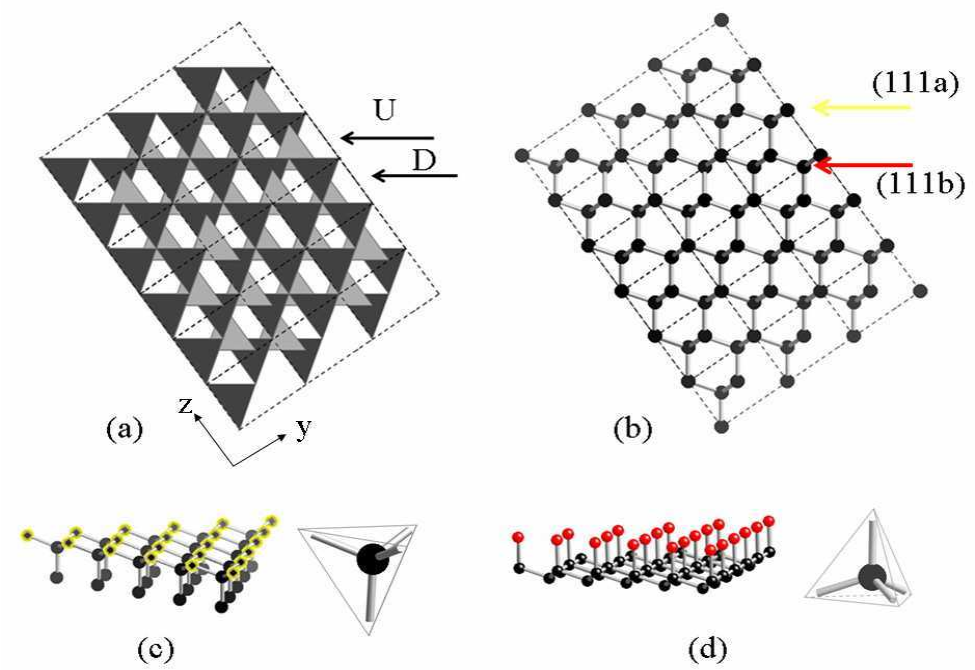

Fig.: 8.4 (a) Polyhedron model of diamond; view direction parallel to (111). Marked with arrows are planes of polyhedrons oriented in opposite directions (U = up,D = down). (b) Ball-and-stick model of diamond. The two possible (111) terminations are marked by arrows. (c) marked yellow are three-fold coordinated C-atoms, terminating the plane (111a). (d) marked red are the three-fold coordinated C-atoms terminating plane (111b).

Reconsidering Table 8.4, Fig. 8.4 and Fig. 8.5, additional conclusions about some major attributes of diamond minerals can be deduced. While the differences in the surface terminations (111a) and (111b) can be neglected in favor for the (111a)-termination, the anisotropies observed between the bond-valence deficiencies of these terminations correspond well to the perfect cleavage plane of diamond parallel to {111}. The C-atoms termination the (111b)-layer are coordinated only to one other C-atom of the bulk structure below, corresponding to another (111a)-layer. The “weak” bond of the C-atom terminating the (111b)-lattice plane, can easily be broken by mechanical forces, as a result diamond crystals can be cleaved along this plane. The crystal surfaces obtained have C-atoms in a three-fold coordination (111a), which correlate well with an other attribute of diamond, its Mohs scale value of H = 10.

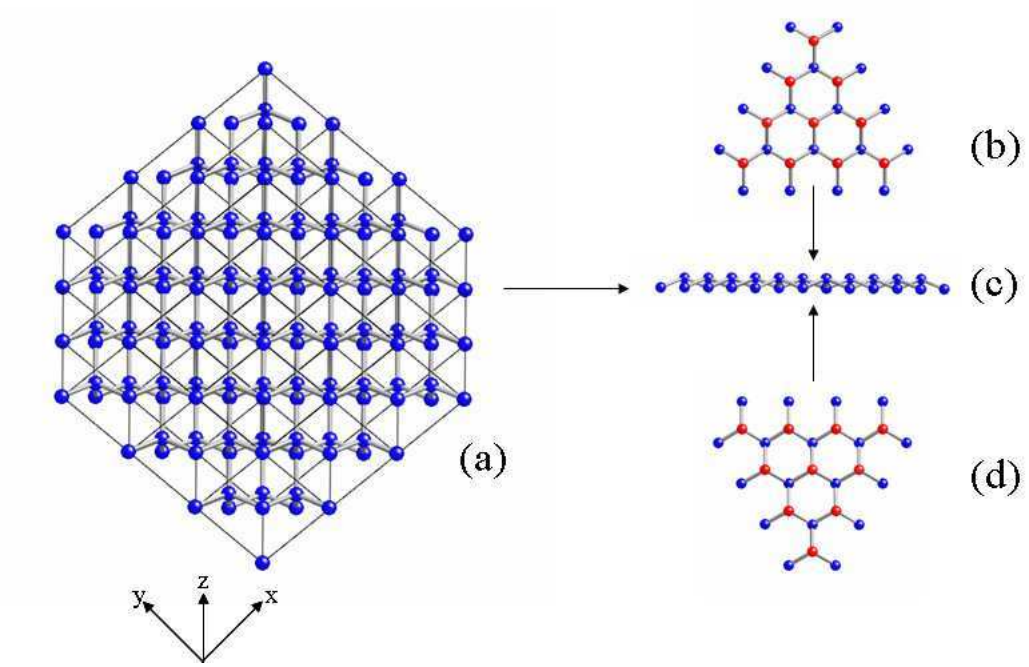

Fig.8.5 (a) Ball-and-stick model of diamond, view parallel to (111);C-atoms are marked blue. (b) single (111) layer of C-atoms. (b) and (d) top and bottom view of (111)-layer illustrating an equivalent surface topology of the {111}crystal planes, terminated by the (111a)-layer type.

8.2 AX-Structure Type

The AX-type structure is the most common mineral-structure. Many hundreds of natural minerals crystallize with either a NaCl-, CsCl, Sphalerite- (α-ZnS), Wurzite- (β-ZnS) or NiAs-type of crystal structure.

Similar to the previous chapter, the different components A and X occupy special positions, which when compared to crystal lattices are to be taken as equivalents to the positions of lattice–points of the respective the crystal-structure type. In addition, the presence of two different charged ions A and X will change some of the internal factors to be considered while others remain unchanged.

In both structure-types, A-structure and AX-structure type, crystals with the space group symmetry Fm3m are represented, for example the copper-structure type of the A-type minerals and the NaCl-structure of the AX-type minerals. While in the copper-structure the atoms can be placed to occupy all position similar to the position taken by lattice-points in a Fm3m Bravais lattice-type structure, the same positions are occupied by either cations or anions in the NaCl-structure. As either the cations or the anions can be placed to be a substitute for equivalent lattice points, the other ions (cations or anions) are located at half the distance between these special atomic positions. This arrangement will have no major influence on the face symmetry-factors to be considered, but it has an influence on the LD-factor (Chapter 7.2), as additional atomic layers must be considered in the NaCl-structure type compared to the copper-structure type.

The presence of two different ions also influences the coordination number of the coordination polyhedron around these ions. While the coordination number of a copper atom in the copper-structure is CN = [12] and the coordination polyhedron resembles a dodecahedron, the coordination number of the Na- and Cl- ions in the NaCl-structure type is CN = [6], and the coordination polyhedron is an octahedron.

8.2.1 NaCl-structure type (Fm3m)

The NaCl-structure type (Fig. 8.6), named after the most prominent mineral sodium chloride, has the space group symmetry O_h^5-Fm3m, Z = 4. The coordinates of the atoms are A^+ at (0 0 0), (0 ½ ½), (½ 0 ½), (½ ½ 0), and B^- at (0 0 ½), (0 ½ 0), (½ 0 0), (½ ½ ½). The coordination number of the ions is CN = 6 and the resulting coordination polyhedron around the ions is an octahedron.

There are more than 200 hundred minerals crystallizing having a NaCl- type structure type. Among these minerals are many halogenides, oxides, sulfides, selenides, tellurides and others. Some of the most common are: halite (NaCl), sylvite (KCl), chlorargyrite (AgCl), periclas (MgO), alabandin (MnS) and galena (PbS).

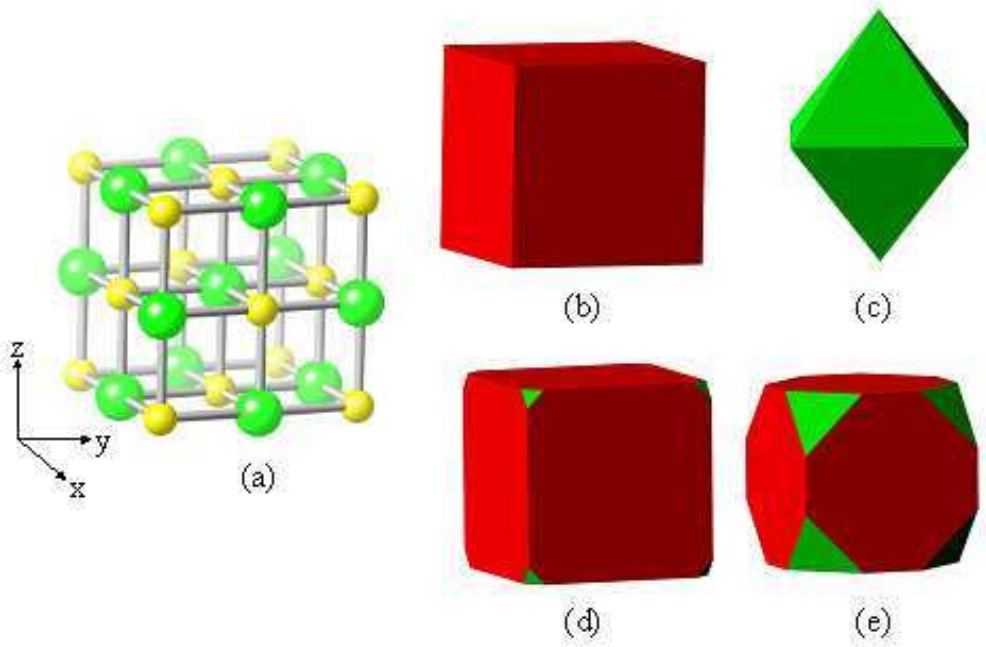

Fig.: 8.6 (a) Ball and stick model of the NaCl-crystal structure. Cations are represented by yellow balls, anions as green balls. (b) and (c) "abstract forms" of the two most dominant crystal faces of minerals having a NaCl-crystal structure (Table. 8.5). The truncated hexahedron (d) and the cubo-octahdron (e) are examples of some possible combinations of these most favorable crystal faces {001} and {111}.

The bond-valence deficiency calculated for a theoretical crystal having the NaCl-structure type and a theoretical lattice-spacing of a_0 = 5.0 Å^2 is given in Table (8.5). Examples of the natural minerals sodium chloride, considering its actual bond-valences and lattice-spacing are given in Appendix III and a graphical overview of some of the faces calculated is given in Appendix II.

Face (hkl)	DB	Unit-cell (Å²)	BVD U (Å²)	RD	BVDU * (Å²)	LD	BVDU** (Å²)	ω	BVDU*** (Å²)	Z	ΔBVDU (Å²)
(100)	4	25,00	0,16	2	0,32	2	0,64	8	0,08	4	0,32
(110)	8	35,36	0,23	2	0,45	4	1,81	4	0,45	2	0,90
(111)	12	43,30	0,28	1	0,28	6	1,66	6	0,28	3	0,84
(210)	12	55,90	0,21	2	0,43	10	4,29	2	2,15	1	2,15

Tab. 8.5 General calculation for a crystal having a NaCl-struture type with a theoretical lattice-spacing of a_0 = 5.0 Å^2. The ΔBVDU-value given, corresponds to the bond-valence deficiencies of the respective faces after having considered the internal factors (RD = reticular density, LD = lattice density, ω = face symmetry and Z = site-symmetry). The values obtained have been calculated for a given number of dangling-bonds (DB), substituting the actual bond-valences in this general example

Referring to Table (8.5), starting with the crystal surface having the lowest ΔBVDU-value, the morphological ranking calculated is:

$$(100) < (111) < (110) < (210)$$

According to the results obtained, the most favorable “abstract form” is the cube (Fig 8.6). Next are octahedral and dodecahedral faces. The cub-octahedron or cubes modified by octahedrons are possible combinations.

The listing of minerals given below demonstrates that the dominant habits of crystals, having a NaCl-structure type, are the cube and the octahedron. This is in good agreement with the BVD-predictions of Table 8.5.

The predicted “abstract forms” are correlated with the most frequent forms of single crystals of some exemplary minerals taken from *Dana´s New Mineralogy* (1997):

Villiaumite	(NaF) :	crystals rare; cubes sometimes modified by octahedron
Carobbiite	(KF) :	small cubes
Halite	(NaCl) :	usually cubes, rarely with {111}
Sylvite	(KCl) :	commonly in cubes or modified by octahedrons
Chlorargyrite	(AgCl) :	usually cubes, often modified by {111} and {011}
Bromargyrite	Ag(Br,Cl):	cubes, sometimes with {111}
Periklas	(MgO) :	rarely as octahedrons, cubes, or cubo-octahedrons
Bunsenite	(NiO) :	octahedral, sometimes modified by{110} or {011}
Monteponite	(CdO) :	octahedral
Wüstite	(FeO) :	octahedral
Galenite	(PbS) :	cubes and cubo-octahedral
Altaite	(PbTe) :	rare cubic crystals
Osbornite	(TiN) :	minute octahedral

Ranking the {111} crystal faces on the second position in the morphological ranking is a major difference compared to the rankings received by other models such as the Bravais empirical law, the methods of Donnay-Harker or Hartman-Perdok (Tab. 8.6). Only the models of Stranski and Kaischew give the {111}-faces, calculated for sodium chloride (STRANSKI 1932), a second ranking.

Sodium chloride (NaCl) is one of the most intensively investigated minerals. It crystallizes easily, its structure appears to be simple and its symmetry seems to be “perfect. Nevertheless, sodium chloride has proven to be a challenging mineral for morphology predictions.

Ranking of morphological importance	Bravais approach (P-lattice)	Bravais approach (F-lattice)	Donnay-Harker (1937)	Hartman (1953)	Stranski (1932)	BVD-model
I	(001)	(111)	(111)	(001)	(001)	(001)
II	(011)	(001)	(001)	(011)	(111)	(111)
III	(111)	(011)	(011)	(111)	(011)	(011)
IV	(012)	(133)	(012)	X	X	(012)

Tab.: 8.6 Comparison of the morphological ranking of crystals having a NaCl-structure type (explanations see text).

DONNAY & HARKER (1937) admit that by application of their model it is not possible to predict the "correct" morphological ranking of halite (Tab. 8.6). Their calculation would predict the octahedron to be the most favorable crystal shape of halite. Therefore they referred back to Bravais-empirical law, which at least stated the cube as the most stable form, but calculated as a P-lattice type structure (DONNAY & HARKER, 1937), instead of the "normal" Fm3m-lattice type structure of AX-compounds.

Hartman (1959), in his work about the "Gleichgewichtsformen einiger Ionenkristalle", states that as a consequence of the PBC-theory, the (111)-faces, ranked as K-faces should not be present, or at most they would blunt the corners of the cube. In contrast Stranski (1932) experimentally proved the presence of (111)-faces for sodium-chloride crystals and gave them the second place in the ranking of morphological importance, similar to the ranking obtained by application of the BVD-model.

Comparing the results from Table 8.5 (BVD-model), with the list given for natural minerals, it becomes obvious that the (111)-face plays an important role for the general habit of minerals crystallizing having a NaCl-crystal structure type.

The list further implies that the type of chemical bonding, which is another internal factor not incorporated in the BVD-model so far, may influence the favored habit of the crystals. Halides (ionic-bonding) tend to form cubes, sometimes modified by octahedrons, covalent bonded minerals such as the oxides tend to prefer the octahedral shape and sulfides such as galena, often appear as cube-octahedrons.

Another explanation might be different interaction mechanisms of the crystal surface with the surrounding solutions. The ionic-bonds in halite, having a bond valences of approximately 0.16 *vu* (BROWN, 2002), can readily match the average bond valences of water (~ 0.2 *vu*). Therefore, the overall bond-valence deficiency of the faces and the availability of ions on the surface, forming bonds to the solution have to be considered. Crystal faces having a higher bond-valence deficiency, such as the (111)-face interact more freely with the solute (water) and will be less stable than faces having a lower bond-valence deficiency such as the (001)-crystal surface. The calculated bond-valence deficiencies for sodium chloride are stated in Appendix II.

Galena, forming covalent bonds, having an average bond-valences of 0.33 *vu* (atomic valence/ coordination number), may not as freely interact with water (0.2 *vu*), giving rise to the appearance of crystal faces having a higher bond-valence deficiency as well. Further factors stabilizing crystal surfaces, such as foreign ions adsorbing to the surfaces are discussed in Chapter 11.

Recent computer simulations support the assumptions that the sort of bonding, ionic or covalent, may play an important role as an additional internal factor. BENNEMA et al. (2001) state that the most stable faces of crystals having a NaCl-type structure are the {100} and {111} faces. They quote that the appearance of {111} faces on silver halide crystals is promoted, if the dipole moment of the surface can be removed by reconstruction, or due to the interaction with a solvent.

A question still to be answered is: why does the method of Donnay-Harker fail to predict the {100}-crystal face of sodium chloride to be the one of highest morphological importance?

An answer can be deduced from the revision of the Donnay-Harker approach by HARTMAN & PERDOK (1956). Amongst other reasons Hartman-Perdok state, that the appearance of "pseudo-lattices", not considered by Donnay-Harker, lead to different estimations of the ranking of morphological importance of crystal faces.
Instead of treating either one of the charged {111}-crystal lattices of sodium chloride, as the structural lattice and the other as an additional "pseudo-lattice" (Fig. 7.10, Chapter 7.2), and consequently doubling the multiplication factors, Donnay-Harker did not consider these additional lattice -planes in their calculations. Thus the ranking they obtained is similar to the ranking of an A-type (Fm3m) structure, ranking the {111}-crystal faces as the ones of highest morphological importance.

Calculating the number of repeating lattices from a graphic representation (Chapter 7.2), seems to be trivial, but the importance of determining the number of parallel crystal-lattices present (LD-factor) is of vital importance, as this example demonstrates. The appearance of "pseudo-lattices, better referred to as "additional lattices", is one of the major differences to be observed while comparing space-group equivalent crystal structures, such as A-type, AX- or AX_2-type structures.

8.2.2 Sphalerite-structure type ($F\bar{4}3m$)

The sphalerite, or α-ZnS structure type (Fig.8.6) has the space group symmetry T_d^2-$F\bar{4}3m$ and Z = 4. The cations have the coordination (0 0 0), (½ ½ 0), (½ 0 ½), (0 ½ ½), and the anions (¼ ¾ ¼) , (¾ ¼ ¼), (¼ ¼ ¾), (¾ ¾ ¾). The structure is similar to the diamond structure, but the ZnS-tetrahedrons are polar oriented to the [111] direction. The favored growth forms are the tetrahedron or the rhomb-dodecahedron (Fig 8.6). Besides sphalerite, other minerals crystallizing having the sphalerite-sturture type are rare. The calculated bond-valence deficiencies of the crystal faces for sphalerite are given in Table. 8.6 and some graphic examples of crystal surfaces calculated are given in Appendix II.

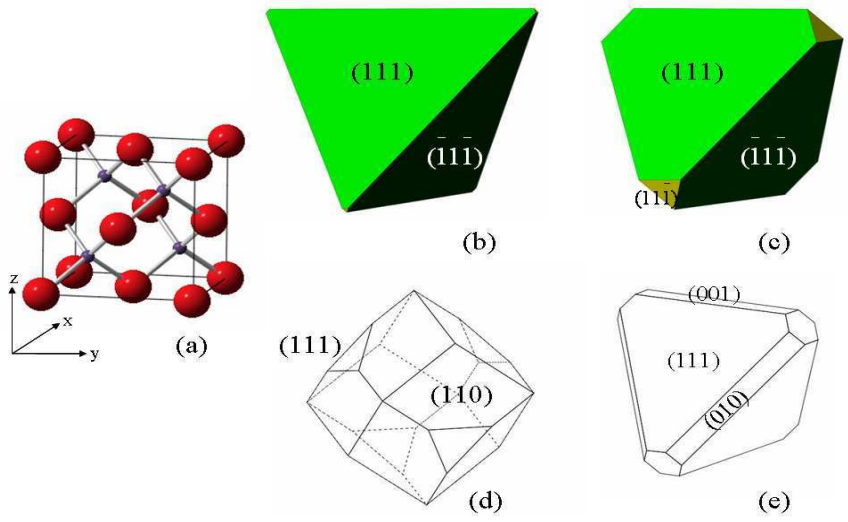

Fig. 8.6: (a) Ball-and-stick model a the sphalerite unit-cell. (b) The calculated abstract- form of sphalerite is a truncated tetrahedron. (c) Truncated tetrahedron calculated for a lower bond-valence deficiency of the {-1-1-1}-crystal faces. (d) truncated rhomb-dodecahedron and (e) truncated tetrahedron with (001)-crystal faces. (d) and (e) represent two different "growth forms" of sphalerite. Changes in the fluid composition may give rise to the appearance of crystal faces having higher bond-valence deficiencies (Chapter 11)

Face (hkl)	DB	Unit-cell (Å²)	BVDU (Å²)	RD	BVDU* (Å²)	LD	BVDU** (Å²)	ω	BVDU*** (Å²)	Z	ΔBVDU (Å²)
(100)	4	29,38	0,14	2	0,27	4	1,09	4	0,27	2	0,54
(110)	4	41,54	0,10	2	0,19	4	0,77	2	0,39	1	0,39
(111) a	4	50,89	0,08	1	0,08	3	0,24	6	0,04	3	0,12
(111) b	12	50,89	0,24	1	0,24	3	0,71	6	0,12	3	0,35

Tab.: 8.6 Bond-valence deficiency table of sphalerite. Two different {111}-terminations have to be considered (see text). The bond-valence deficiencies are calculated for the number of dangling bonds (DB) exposed at the surface and a_0 = 5,4 Å².

According to Table 8.6 the morphological ranking of the calculated surfaces of sphalerite stating with the surface having the lowest bond-valence deficiency is:

$$(111a) < (111b) < (110) < (100)$$

From these results obtained the most favorable abstract form is a truncated tetrahedron (Fig.:8.6), which correlates well with the most dominant habits of sphalerite observed in nature. A list of minerals crystallizing having a sphalerite-structure type, together with their favorite crystal habits, is given below (form *Dana´s New Mineralogy* , 1997):

Sphalerite (ZnS) : tetrahedral or dodecahedral
Metacinnabar (HgS) : rarely as small tetrahedral crystals
Tiemannite (HgSe) : tetrahedral crystals
Miersite (Ag,Cl)I : tetrahedral crystals
Marshite (CuI) : tetrahedral crystals

Two different, but "corrolate forms" of the {111}-terminations, the positive (111) and the negative (-1-1-1), are expected from the $F\bar{4}3m$ symmetry of this crystal structure. These terminations can be differentiated crystallographically by their geometric positioning (positive or negative), but differences in the physical or chemical behaviour are not detectable by such investigations. The application of the BVD model gives similar results, both terminations are detected as the terminations (111a) and (111b). In addition the differences in the physical and chemical behaviour are visualized by the different bond-valence deficiencies of these two terminations (Tab. 8.6). As a consequence of these results obtained, it can be proposed that the tetrahedral or truncated tetrahedral crystals are dominated by (111) crystals surfaces having a (111a) termination (Fig.: 8.7).

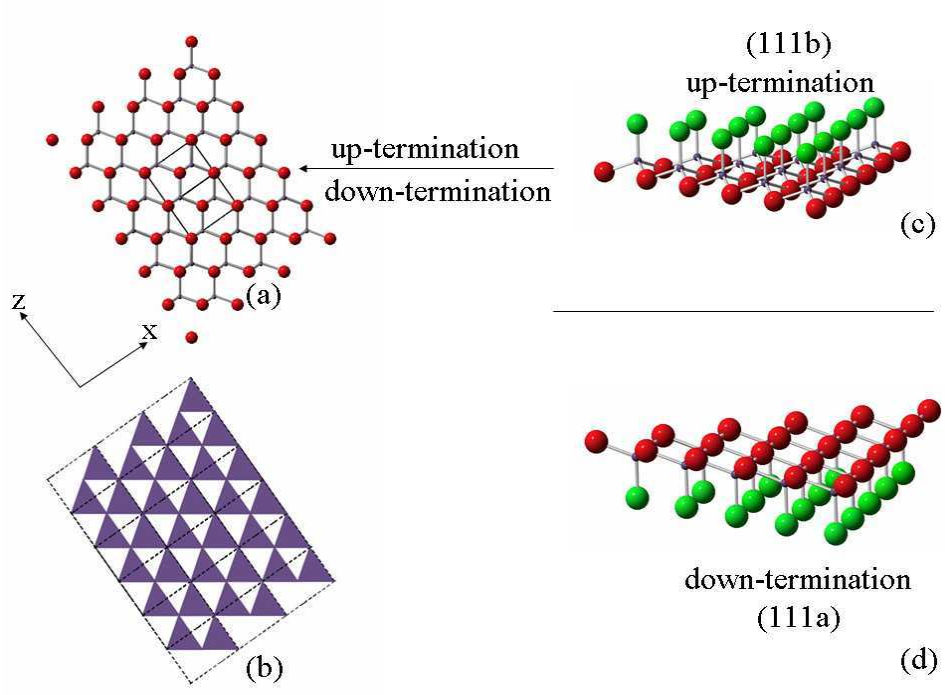

Fig.: 8.7 (a) Perspective ball-and-stick model of sphalerite parallel to the (111)-cyrstal lattice. Zn^{2+}-ions dark blue, S^{2-}-ions red. Marked by an arrow is a (111)-crystal lattice terminated by S^{2-}-ions. (b) Perspective model of sphalerite showing the polar oriented ZnS-tetrahedrons. (c) Ball-and-stick model of the (111b) termination. Marked in green are S^{2-} ions terminating this crystal surface. (d) Ball-and-stick model of the (111a) termination viewed from bottom up. The calculated bond-valence deficiencies for this crystal surface (Tab. 8.6) are calculated for the S^{2-} -ions marked red.

8.3 AX_2-Structure Type

Many minerals crystallize having an AX_2-structure type have a ionic bonding type. As a result the structures are determined by the relative size ratio of the cation and anion radius. In general the anions have a larger ionic radius than the cations, and consequently the coordination of the cations around the anions determines which AX_2-structure type will be present. Similar to the AX-structure type the coordination number of the ions can ranges between 8, 6 and 4, and the coordination number of the anion is always half of that of the cation. This relation-ship is reversed in the anti-fluoride structure A_2X.

Especially fluorides with large divalent cations and oxides with four-valent cations crystallize having a fluorite-structure type. The anti-fluoride-structure type is also common in oxides, sulfides and tellurides having alkali-metal cations.

Because there is a greater number of different AX_2-structure types, compared to the number of AX-structure types, only the most common AX_2-structures will be described in detail.

8.3.1 CaF_2 –structure type (Fm3m)

The fluorite structure type has the space group symmetry O_h^5 - Fm3m and Z = 4. The coordinates of the ions are Ca (0 0 0), (½ ½ 0), (½ 0 ½), (0 ½ ½), and F (¼ ¼ ¼), (¼ ¼ ¾), (¼ ¾ ¼), (¾ ¼ ¼), (¼ ¾ ¾), (¾ ¼ ¾), (¾ ¾ ¼), (¾ ¾ ¾). The Ca-ion is coordinated by 8 F-ions and the coordination polyhedron is a cube. The F-ions are coordinated by four Ca-ions and the coordination polyhedron of around the F-ions is a tetrahedron. The calculated bond-valence deficiencies of different fluorite-crystal faces are given in Tab.8.7 and the corresponding graphic examples are listed in Appendix II

Face (hkl)	DB	Unit-cell (Å²)	BVDU (Å²)	RD	BVDU* (Å²)	LD	BVDU** (Å²)	ω	BVDU*** (Å²)	Z	ΔBVDU (Å²)
(100)	8	29,81	0,27	2	0,54	4	2,15	8	0,27	4	1,07
(110)	8	42,15	0,19	2	0,38	4	1,52	4	0,38	2	0,76
(111) F	8	51,63	0,15	1	0,15	3	0,46	6	0,08	3	0,23
(111) Ca	16	51,63	0,31	1	0,31	3	0,93	6	0,15	3	0,46
(210)	16	66,66	0,24	2	0,48	10	4,80	2	2,40	1	2,40

Tab.: 8.7 Bond-valence deficiency table of fluorite. Two different terminations parallel to the (111)- crystal layer can be distinguished (details see text). The bond-valence deficiencies are calculated from the number of dangling bonds (DB) exposed at the crystal surfaces and a_0 = 5,46 Å².

The order or morphological importance obtained from Table 8.7, starting with the crystal face having the lowest bond-valence deficiency is:

$$(111\ F) < (111\ Ca) < (110) < (100) < (210)$$

Comparing the obtained ranking with the frequency of appearance of these faces on natural samples taken from *Dana´s New Mineraology*: *usually cubes {100}, less often octahedrons {111} and rarely {110} faces*; no match between the predicted abstract form and the occurrence in nature can be found. A graphical ranking of the calculated Abstract forms is given in Figure. (8.8).

This controversial observation is surprising but expected, for other undertakings concerning the prediction of the "abstract forms" of fluorite, have shown the same discrepancy. BRADISTILOV & STRANSKI (1941) have analyzed this "problem" in detail and concluded that the (100)-faces of fluorite have a high tendency to adsorb impurities. Consequently the growth rate of the (100)-faces is lowered, giving rise to a higher

morphological ranking observed in nature (see Chapter 11). BRADISTILOV & STRANSKI (1941) further argued that in addition a high degree of supersaturation will also lower the growth velocity of the cubic-faces.

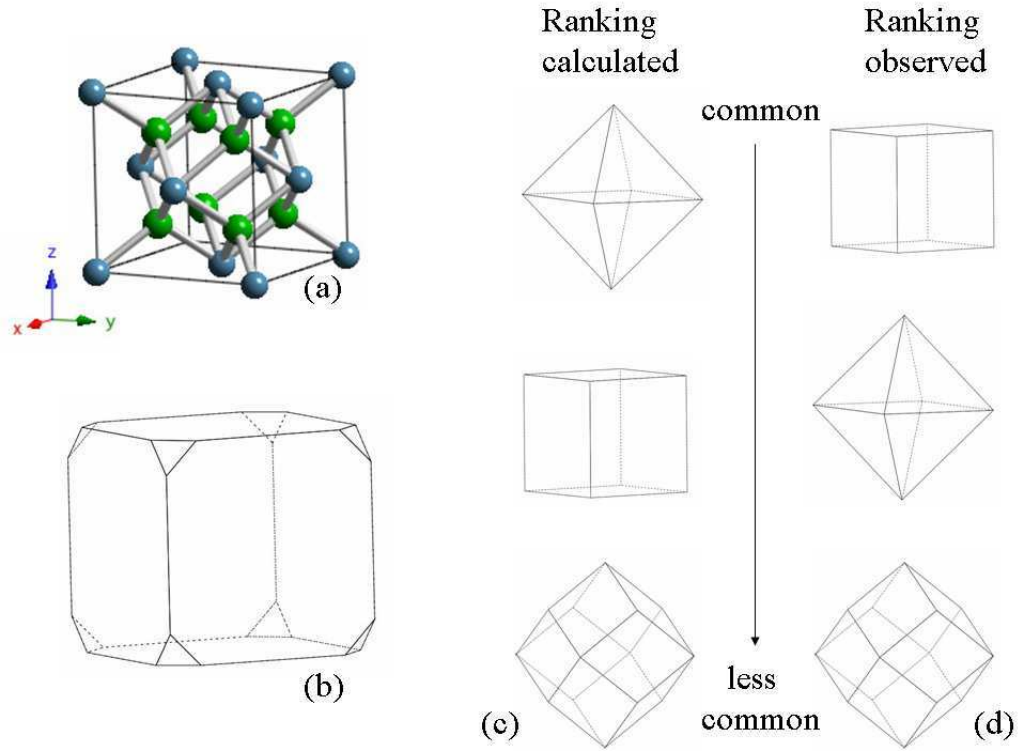

Fig.: 8.8 (a) Ball-and-stick model of the fluorite unit-cell. Ca-ions are given as blue balls, F-ions as green balls. (b) Common growth from of fluorite. In contrast to the predicted ranking of morphological importance the {001}-crystal faces are commonly observed in nature. (c) Morphological ranking calculated. (d) Morphological ranking observed in nature (*Dana´s New Mineraology,*1997).

As a result we can state that the (111)-faces are the most "stable" surfaces of the abstract forms, considering the internal crystal structure factors only. The influence of these factors on the final morphology can be outweighed by the influence of external factors such as impurities present in the solution. Therefore fluorite is a good example to demonstrate that both internal- and external factors must be combined to predict a reasonable crystal growth-morphology (see Chapter 11).

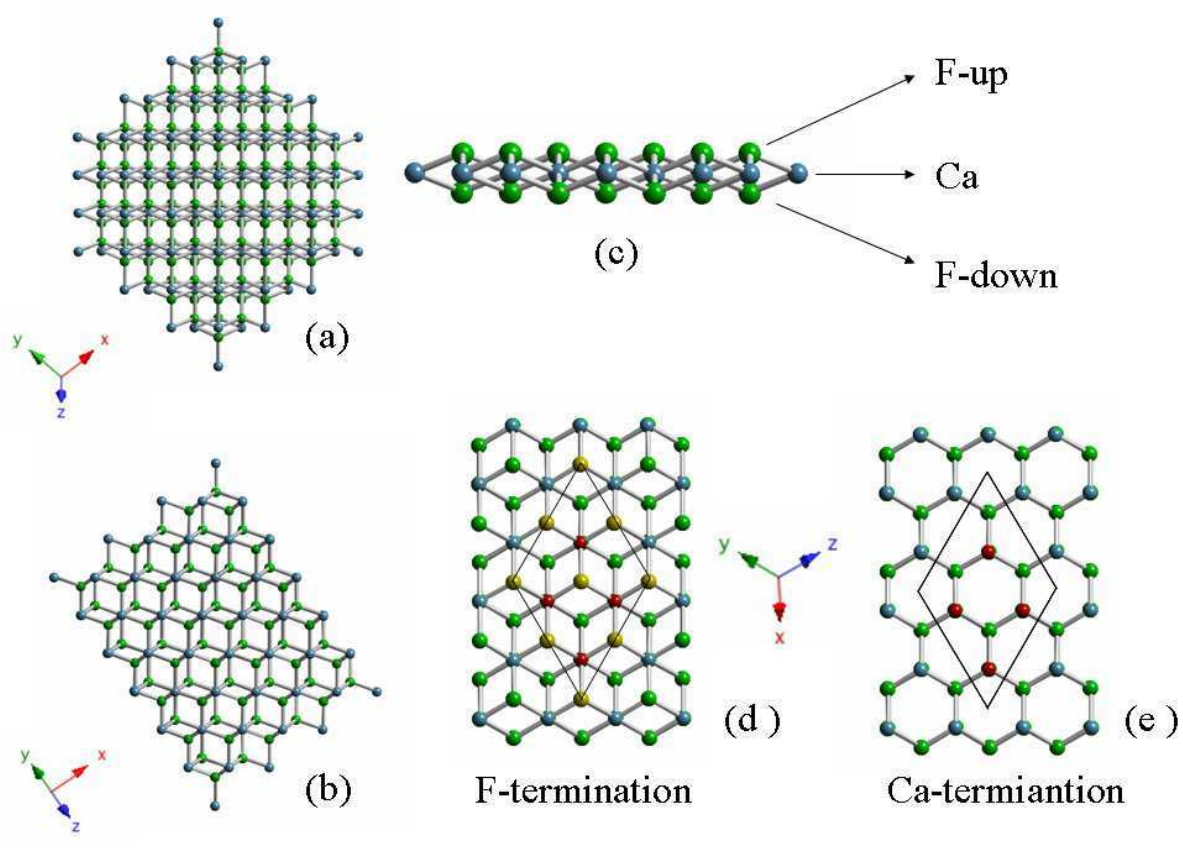

Fig.: 8.9 (a) and (b) perspective side views parallel to the (111) direction of a fluorite crystal. Ca-ions are marked blue, F-ions are marked green. (a) This perspective view shows that the Ca- and F- ions are arranged in "triple-layers". (b) The "triple-layers" are connected to each other only by one bond per ion, e.g. the Ca-ions of the F-Ca-F "triple layer" bond to four F-ions within the layers and only one F-ion in the adjacent layers above and below. (c) Single "triple-layer" parallel to the (111) crystal lattice. Both F-terminations have the same topology (d). (d) Topology of the (111)-F crystal lattice. Outlined by black lines is the shape of the (111) unit-cell. F-ions and Ca-ions terminating the crystal lattice are marked yellow (fluorine) and red (calcium). This termination has the lowest ΔBVDU-value of the (111)-terminations. (d) Ca-termination parallel to (111) crystal lattice. The surface is only terminated by Ca-ions (red) having a higher bond-valence deficiency compared to the F-terminations.

A detailed analysis of the (111)-crystal surface is given by Figure (8.9). There the crystal lattices (atomic layers) parallel to the (111)-crystal face are considered as a triple F-Ca-F-layer (Fig. 8.9c). Crossing this layer perpendicular to [111]-direction, yields up

to three possible terminations. Two of these (Fig. 8.9d) are terminated by F- and Ca-ions (F-termination), one layer (Fig. 8.9e) is terminated by Ca-ions only (Ca-termination). The respective bond-valence deficiencies are given in Table. (8.7). From the results obtained, it can be concluded that the most stable {111}-termination corresponds to the F-termination type. As an additional indication of the importance of this (111)-termination one can regard the almost perfect (111)-cleavage plane of fluorite. The cleavage plane separates the adjacent F-Ca-F triple-layers, and each of the cleavage planes is terminated by a F-termination.

These results obtained correlate well with results given in literature. As an example, PUCHIN et al. (2001) calculated the surface energies of CaF_2 (111), CaF_2 (110) and CaF_2 (100) surfaces using an *ab initio* Hartree-Fock method. According to their results the CaF_2 (111) surfaces have the lowest surface energies, followed by CaF_2 (110) and CaF_2 (100) surfaces. A similar calculation is given by TASKER (1979), considering the surface properties of uranium dioxide. He concluded that the lowest energy faces of a crystal having a fluorite structure type are the (111) surfaces followed by the (110) terminations. These results are comparable to the morphological ranking obtained by application of the BVD-model (Tab. 8.7).

8.3.2 Pyrite-structure type (Pa3)

The pyrite-structure type has the space group symmetry T_h^6 - Pa3 and Z = 4. The Fe-ions form a cubic-face centered lattice. Every Fe-ion is coordinated by 6 S-ions in octahedral coordination. The pyrite structure may be compared to the NaCl-structure type. Compared to NaCl the positions of the Na-ions are occupied by the Fe-ions and the positions of Cl-ions by S_2-dumbele-like pairs, parallel to the four cube diagonals.
All mirror-planes of the NaCl-structure type disappear and only the glide-planes parallel to (100) are restored. On the final morphology of the crystals these glide planes resemble in their appearance mirror-planes.

The calculated bond-valence deficiencies of pyrite are given in Table (8.8) and are calculated for the Fe-ions only. The corresponding graphical examples are listed in Appendix II. The crystal structure and some calculated "abstract forms" are shown in Figure 8.10.

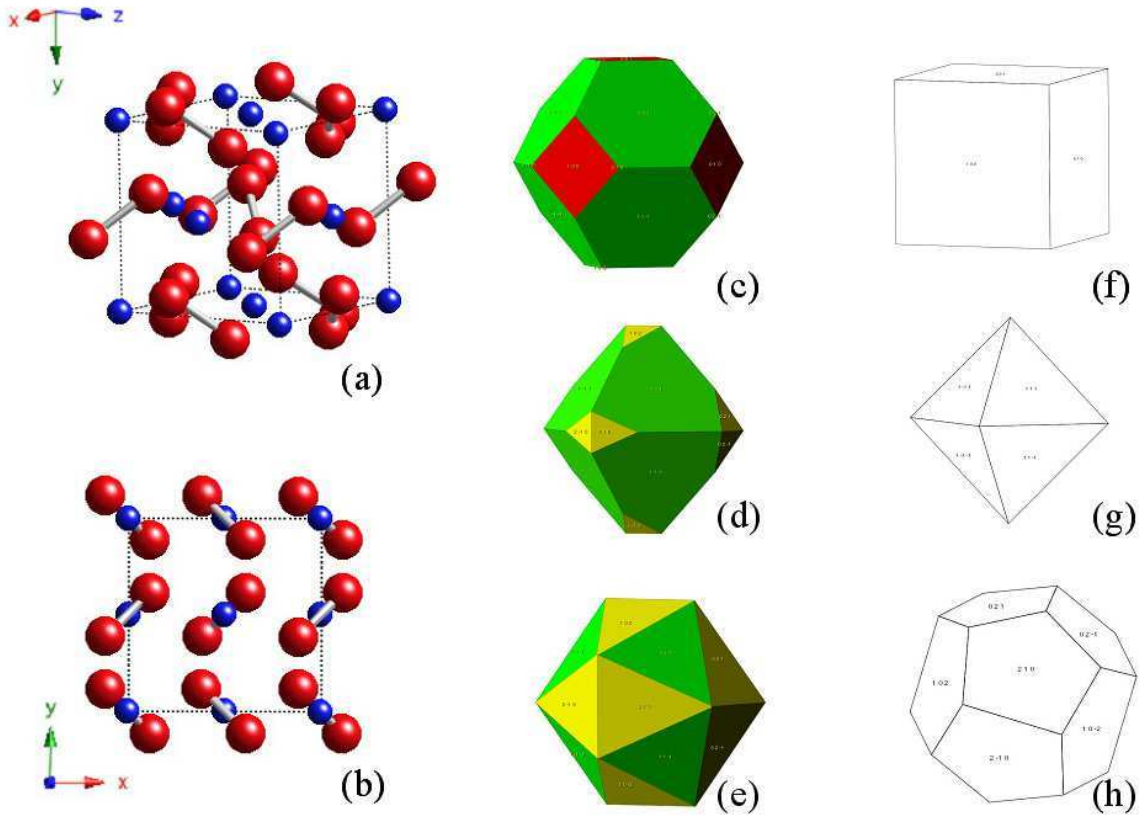

Fig.: 8.10 (a) and (b) Ball-and-stick models of pyrite. Fe-ions are given as blue spheres, S-ions as red spheres. (a) Perspective view of a pyrite unit-cell. The unit cell is outlined by dashed lines. (b) Perspective view along the z-axis. The orientation of S_2-dumbel-like pairs parallel to the cube diagonals is visualized. (c) Calculated "abstract form" of pyrite. (d) Calclated "abstract form" without the {001}-faces, showing the distribution of the {210}-faces. (e) Calculted "growth form" the bond-valence deficiencies of the {210}-faces is lowered. (f) - (h) Examples of pyrite morphology-types observed in nature.

Face (hkl)	DB	Unit-cell (Å²)	BVDU (Å²)	RD	BVDU* (Å²)	LD	BVDU** (Å²)	ω	BVDU*** (Å²)	Z	ΔBVDU (Å²)
(100)	2	29,34	0,07	2	0,14	2	0,27	1	0,27	1	0,27
(110)	4	41,50	0,10	2	0,19	4	0,77	1	0,77	1	0,77
(111)	12	50,83	0,24	1	0,24	3	0,71	3	0,24	1	0,24
(210	2	65,62	0,03	2	0,06	10	0,61	1	0,61	1	0,61

Tab.: 8.8 Bond-valence deficiency table of pyrite, a_0 = 5.41 Å². The BVD-values correspond to the number of dangling bonds (DB) of the respective Fe-ions terminating the crystal lattice.

The order or morphological importance obtained from Table (8.8), starting with the crystal face having the lowest bond-valence deficiency is:

(111) < (100) < (210) < (110)

The morphological ranking calculated for pyrite (Tab. 8.8), does well in matching the dominant morphologies of the minerals given in the list below and it coincides well with the results obtained by DONNAY & HARKER (1937).

Some minerals crystallizing having the space group symmetry Pa3 (*Dana´s New Mineraology,* 1997) are:

Vaesite	(NiS_2):	small octahedral and cubic crystals
Cattierite	(CoS_2):	cubic crystals
Villamaninite	(CuS_2):	cubic and octahedral crystals
Hauerite	(MnS_2):	octahedral crystals
Laurite	(RuS_s):	cubic, octahedral and pyritohedral
Dzarkenite	($FeSe_2$):	octahedral

8.4 A_mB_nX- Compounds

There is a vast number of compounds crystallizing having an A_mB_nX- composition, some of which include organic salts. Therefore we will restrict out investigations purely to inorganic minerals for which the components A and B are cations, and X is a non-metal, preliminary oxygen, sulfur or a halogen. As an example the spinel-structure type will be discussed in detail.

8.4.1 Spinel-structure type (Fd3m)

The spinel-structure type has the space group symmetry (O_h^7-Fd3m) and Z = 8. The general formula of minerals of the spinel-group is $A^{2+}B_2^{3+}O_4$. The oxygen atoms are arranged almost similar to a cubic-closed packed structure. The metal ions occupy the octahedral or tetrahedral vacancies. Consequently, within the general spinel-structure, 8-metal ions (A^{2+}) have an octahedral coordination, 16 (B^{3+}) -ions have tetrahedral coordination. In the "inverse spinel-structure", $B^{[4]}A^{[6]}B^{[6]}O_4$, 8 B-atoms have a tetrahedral coordination, and 8 A-atoms and 8 B-atoms have a octahedral coordination. Every oxygen-atom is part of one tetrahedron and 3 octahedrons (KLOCKMANN, 1978).

The calculated bond-valence deficiencies of different spinel-faces are given in Table 8.9, the corresponding graphical examples are listed in Appendix II. The crystal structure and some calculated "abstract forms" are shown in Figure (8.11).

Face (hkl)	BVD	Unit-cell (Å²)	BVDU (Å²)	RD	BVDU* (Å²)	LD	BVDU** (Å²)	ω	BVDU*** (Å²)	Z	ΔBVDU (Å²)
(100) O	20	65,36	0,31	2	0,61	4	2,45	4	0,61	2	1,22
(100 OT	28	65,34	0,43	2	0,86	4	3,43	4	0,86	2	1,71
(110 OT	28	92,40	0,30	2	0,61	4	2,42	2	1,21	1	1,21
(110) O	36	92,40	0,39	2	0,78	4	3,12	2	1,56	1	1,56
(111) O	28	113,16	0,25	1	0,25	6	1,48	6	0,25	3	0,74
(111) Ot	36	113,16	0,32	1	0,32	6	1,91	6	0,32	3	0,95

Tab.: 8.9 Bond-valence deficiency table of spinel calculated for dangling-bonds (DB) terminating the surfaces, a_0 = 8,08 Å². The letters O and T correspond to the coordination polyhedrons around the cations. The Mg-ions have a tetrahedral coordination, the Al-ions an octahedral coordination. Only such surfaces have been calculated which are terminated by a layer of polyhedrons. O indicating a layer of octahedrons, OT a mixed layer of octahedrons and tetrahedrons (further explanations see text.)

The order or morphological importance of the spinel-faces calculated (Table 8.9), starting with the crystal face having the lowest bond-valence deficiency is:

$$(111) < (110) \leq (100)$$

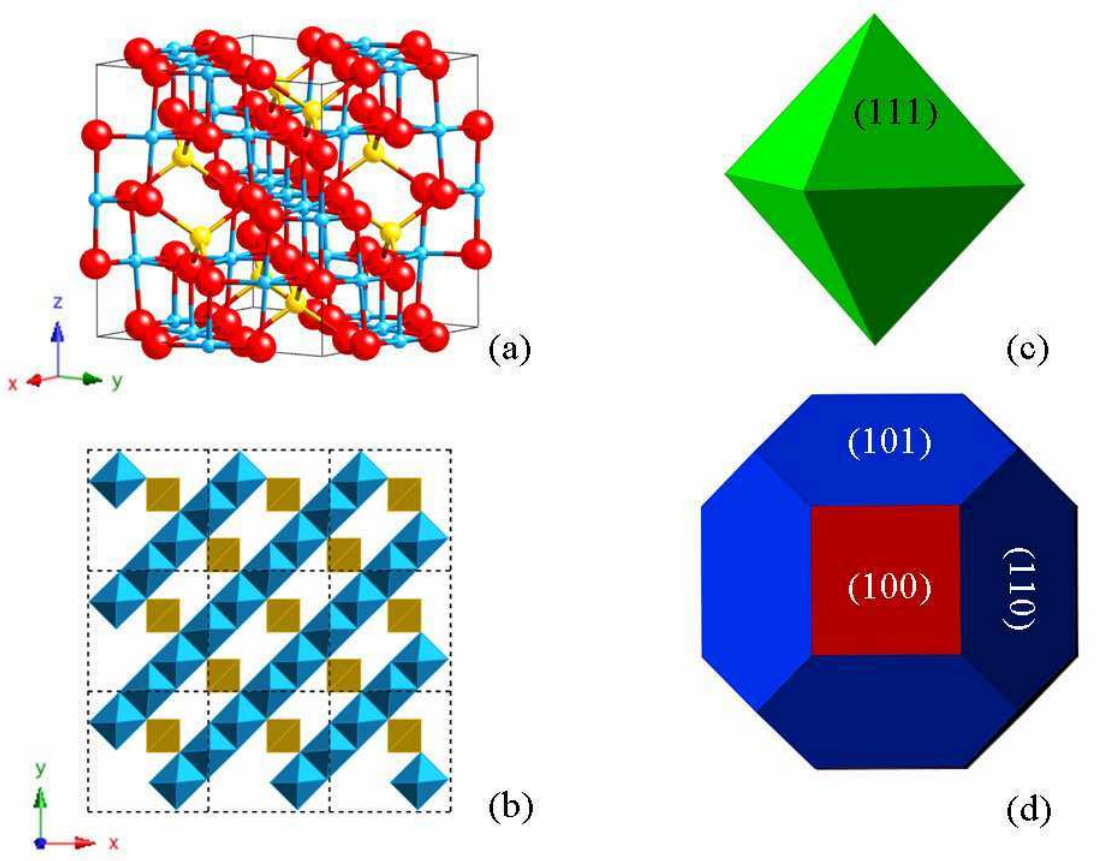

Fig.: 8.11 (a) Ball-and-stick model of spinel, perspective view. Yellow spheres: Mg-ions, blue-spheres: Al-ions, red-spheres: O-ions. (b) Polyhedral model of the (001) crystal surface of spinel, view along the c-axis, the unit-cells are marked by dashed lines. This figure shows the 2mm face-symmetry of the (001)-crystal layer. (c) The calculated "abstract form" of spinel is dominated by {111}-crystal faces (Tab. 8.9). (d) Calculated "abstract form" of spinel without the {111}-data sets. This "truncated" cubic form shows that the {100} and {110} faces are almost equally represented as faces of secondary morphological importance, which corresponds well to their less frequent appearance in nature (see list below).

This ranking obtained from Table (8.9), is in good agreement with the common crystal habits of spinel as well as with the morphologies of many crystals crystallizing having a spinel-type crystal structure.

Some examples, obtained from *Dana´s New Mineralogy* (1997), are:

Spinel	($MgAl_2O_4$):	usually octahedrons, rarely modified by {110} and {100}
Gahnite	($ZnAl_2O_4$):	octahedral crystals
Magnetite	($Fe^{2+}Fe_2^{3+}O_4$):	usually octahedral, sometimes dodecahedral
Franklinite	($ZnFe_2O_4$):	octahedrons, rarely modified by dodecahedrons
Chromite	($FeCr_2O_4$):	octahedral

Calculating surface topologies for more complex minerals such as minerals of the spinel-group with a general formula of $A^{2+}B_2^{3+}O_4$ have to be handled with more care compared to the more simple AX- or AX_2-crystal structures types. In the case of AX- and AX_2-structure types only two components A and X have to be considered, forming bonds of similar length. $A^{2+}B_2^{3+}O_4$ – structure types have three different components, with different coordination environments and different bond-length between the components A-O or B-O. Therefore the bond-lengths and thus the bond-valences of each individual bond have to be considered in more detail.

In the case of more complex, covalent bonded structures the coordination environment of the individual components is of higher importance, compared to e.g. ionic-bonded AX-compounds. The single ions of NaCl are not considered to form stable coordination polyhedrons in a solution, no stable $NaCl_6$-complexes expected to be present in the aqueous solution. Rather each of the ions is surrounded by a very unstable hydration spheres and Na^+ - and Cl^- -ions are considered to form bonds to each other at the beginning of nucleation. This process is to some extent different for components forming covalent bonds. Ions such as Si^{4+} and O^{2-} are considered to form bonds early during crystallization, forming anion-complexes such as $[SiO_4]^{4-}$. During crystallization such polyhedral complexes start to accumulate, building more complex structures (BURNS 1995, BROWN 2002).

Similar processes need to be considered in the case of $A^{2+}B_2^{3+}O_4$-components. If the bond-valence deficiencies of different crystal surfaces terminating a spinel-crystal are calculated, only such surfaces need to be taken into account, which consist of layers of polyhedrons (Fig. 8.12). In the given example (Table. 8.9), only surfaces terminated by Mg-tetrahedrons and/or Al-octahedrons are compared while calculating the "abstract form" of spinel.

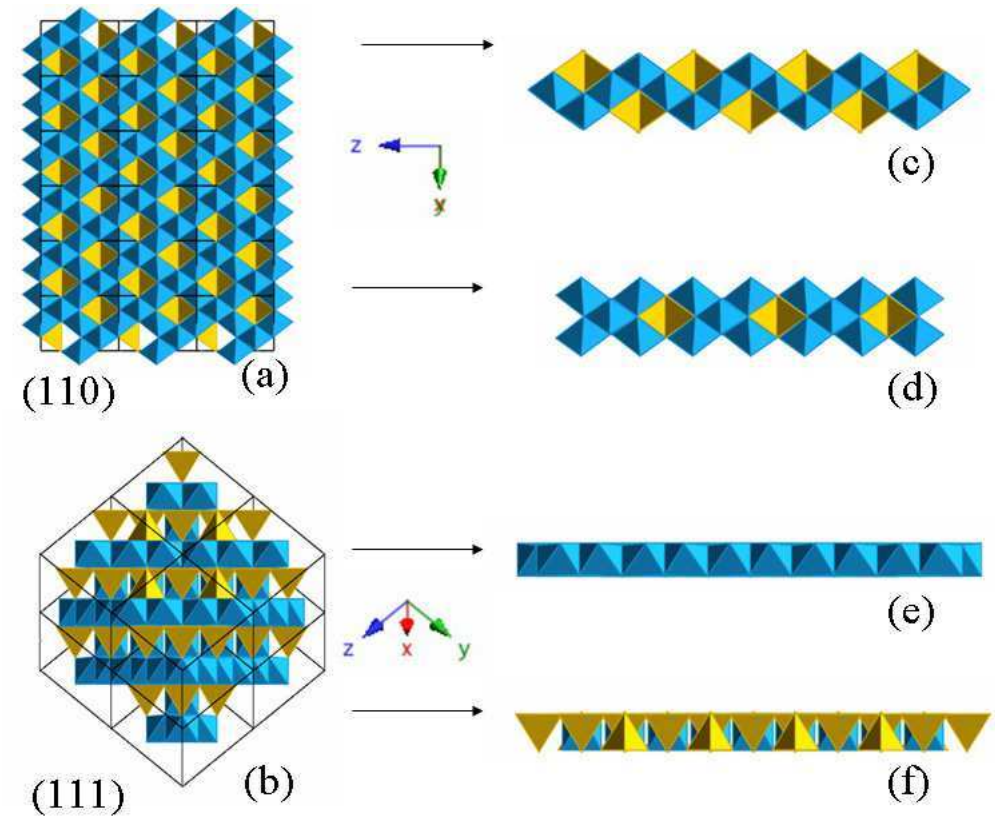

Fig.: 8.12 Polyhedron presentation of spinel. Al-octahedrons are blue, Mg-tetrahedrons are yellow. (a) Perspective view parallel to the (110)- face. (b) Perspective view parallel to the (111)-crystal surface. (c) and (d) Two different polyhedron-layers terminate the crystal lattices parallel to the (110). (c) Octahedral and tetrahedral termination of the (110)-lattice. (d) Octahedral termination of the (110)-lattice. (e) and (f) Two different polyhedron-layers terminate the crystal lattices parallel to the (111). (c) Octahedral termination of the (111)-lattice. (d) Octahedral and tetrahedral termination of the (111)-lattice.

8.4.1.1 Magnetite (An example)

Magnetite is a member of the spinel-group, but in contrast to normal spinels, magnetite crystallizes having an inverse spinel-structure type. “Normal spinels” with the general formula $A^{2+}B_2{}^{3+}O_4$ have divalent cations in the tetrahedral A-position and trivalent cations in the octahedral B-position. Inverse-spinels, such as magnetite (Fe_3O_4) have all divalent Fe^{2+} and half of the trivalent Fe^{3+} in the octahedral position and the other half of the trivalent Fe^{3+} occupy tetrahedral positions.

Face (hkl)	BVD	Unit-cell (Å²)	BVDU (Å²)	RD	BVDU* (Å²)	LD	BVDU** (Å²)	ω	BVDU*** (Å²)	Z	ΔBVDU (Å²)
(100) O	11,3	70,49	0,16	2	0,32	4	1,28	4	0,32	2	0,64
(100) OT	13,3	70,49	0,19	2	0,38	4	1,51	4	0,38	2	0,75
(110) OT	19,3	99,70	0,19	2	0,39	4	1,55	2	0,77	1	0,77
(110) O	13,6	99,70	0,14	2	0,27	4	1,09	2	0,55	1	0,55
(111) O	17,3	122,09	0,14	1	0,14	6	0,85	6	0,14	3	0,43
(111) Ot	15,5	122,09	0,13	1	0,13	6	0,76	6	0,13	3	0,38

Tab.: 8.10 Bond-valence deficiency table of magnetite. The bond-valence deficiencies (BVD) have been calculated for Fe^{3+} - O (1.88 Å) in tetrahedral coordination as 0.721 vu, and Fe^{2+}/Fe^{3+} in octahedral coordination as 0.406 vu (BARBIERI et al., 1994). The letters O and T correspond to the coordination polyhedrons around the cations. O indicates a layer of octahedrons, OT a mixed layer of octahedrons and tetrahedrons terminating the crystal surface. In contrast to the results obtained for the “normal Spinel” structure, the (111) crystal surfaces terminated by octahedrons and tetrahedrons has a lower bond-valence deficiency in the “inverse magnetite” structure and thus has a higher ranking of morphological importance.

This “inverse” arrangement of divalent and trivalent ions in the magnetite crystal structure has some influence on ranking of the morphological importance of surfaces terminating the crystals (Tab.: 8.10).

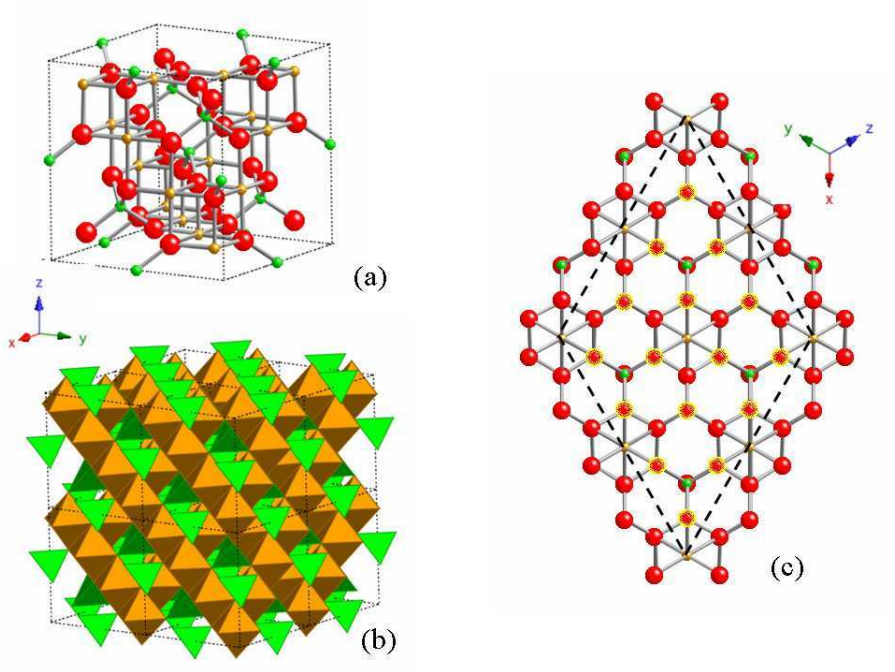

Fig.: 8.13 (a) Ball-and-stick model of the magnetite (unit-cell). Red balls: oxygen atoms, green balls: Fe atoms at tetrahedral position, brown balls: Fe atoms in octahedral position.(b) Polyhedron representation of magnetite. (c) Ball-and-stick model of a (111) crystal surface. The unit-cell is outlined by dashed lines. Oxygen atoms terminating the (111) crystal surface within the calculated area of unit-cell dimension are marked yellow.

From Table (8.10) we can deduce that the {111} crystal surfaces still dominate the crystal morphology of magnetite, which is in concordance with the morphological ranking obtained for the “normal”- spinel structure. The major difference to be noticed is, that the {111}- crystal surfaces with the lowest bond-valence deficiency now are those, which are terminated with Fe-ions in tetrahedral and octahedral coordination (Fig: 8.13). These results have been obtained by considering only such crystal surfaces, which are terminated by oxygen atoms assuming a polyhedral growth mechanism.

In technical applications mineral surfaces are treated by chemical or physical applications, giving rise to the possibility that other surface terminations will be stabilized than the ones calculated in the Table (8.10). The question that arises is, if such terminations can as well be predicted by the BVD-model. In order to test our model, different {111}-crystal surface of magnetite terminated by Fe-ions have been calculated (Fig. 8.14), and the results are compared to results obtained by BARBIERI et al. (1994) and LENNIE et al. (1996).

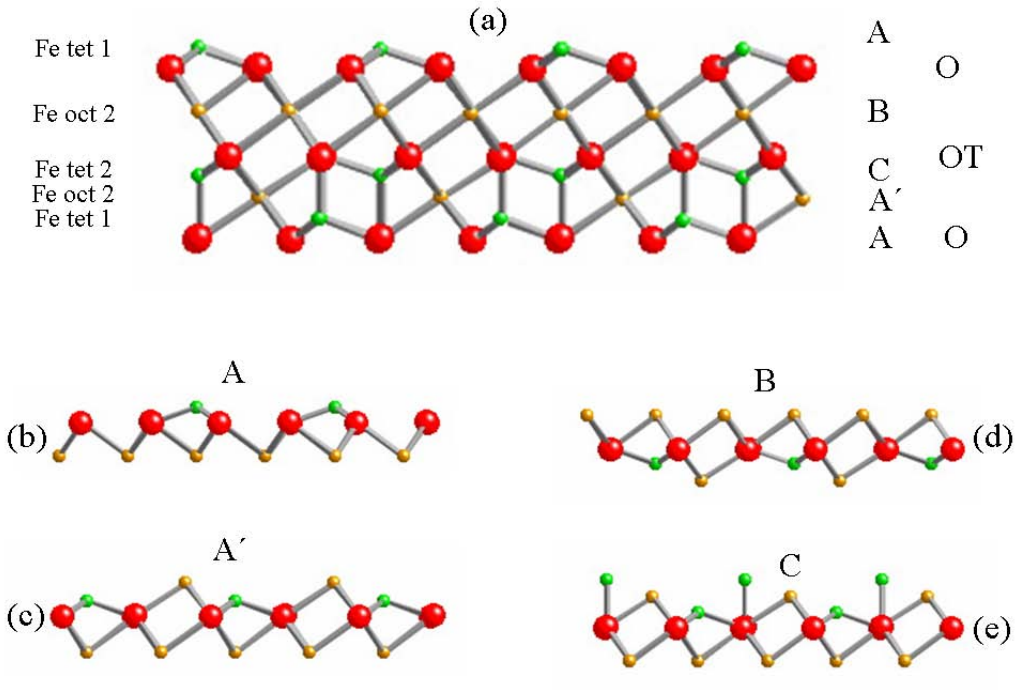

Fig.: 8.14 (a) Perspective view parallel to the (111) crystal planes of magnetite (ball –and stick model). The different Fe atom layers are labeled on the left. The corresponding Fe-terminations (A, A´, B and C) are labeled on the right together with the two different polyhedron layers O and OT. (b)-(e) Detailed ball-and-stick models of the different Fe-terminations (A, A´, B and C).

BARBIERI et al. (1994) determined the atomic structure of Fe_3O_4 (111) by means of dynamical low-energy electron diffraction (LEED). LENNIE et al. (1996), in addition applied a Scanning Tunneling Microscope (STM). In both of these investigations the magnetite crystal surfaces were treated by various methods, for example by argon-ion

bombardment and further annealing in O_2 (LENNIE et al., (1996). These investigations indicate the existence of two different iron-terminations called A and B, terminations which are identical with two out of four possible iron-terminations obtained by application of the bond-valence approach (Fig. 8.14).

If we compare the results obtained in Table (8.11) it is obvious that termination B (Fe_{oct2} – O), and C ($Fe_{tet\ 2}$ – $Fe_{oct\ 1}$- $Fe_{tet\ 1}$ - O), having high bond-valence deficiencies will less likely or not at all form stable (111) iron-terminated crystal surfaces. In contrast the terminations A and A´, having almost similar low bond-valence deficiencies, may equally be considered to terminate a (111)-crystal surface. The terminations A and A´ can be obtained by cleaving the bulk structure between $Fe_{tet\ 2}$ and $Fe_{oct\ 1}$ (Fig. 8.14) and thus behave like an up or down termination of the same (111) crystal surface. According to these bond-valence calculations, stepped (111) surfaces of magnetite are terminated most likely by either if the A-terminations (either A or A´) and the B-terminations.
These result are in concordance with the results given by BARBIERI et al. (1994) and LENNIE et al. (1996), for both studies indicate the A-terminations to be more stable than the B-terminations, which is in concordance with the ranking obtained in Table (8.11).

The difference of both studies, is the preference for either one of the two possible A terminations, and can be explained by differences in the substrates used or the surface preparation techniques (LENNIE et al. 1996). Furthermore the methods given by BARBIERI et al. (1994) and (LENNIE et al. 1996) to interpret their results and further lower the surface energy differ. BARBIERI et al. (1994) prefers surface relaxations processes to be relevant, as these processes, minimize both the number of dangling bonds and the electrostatic energy of the polar metal oxide surface. LENNIE et al. (1996) consider the occurrence of vacancies or the capping of Fe atoms by O atoms as a possible process to stabilize the surfaces.

Face (hkl)	BVD	Unit-cell (Å²)	BVDU (Å²)	RD	BVDU* (Å²)	LD	BVDU** (Å²)	ω	BVDU*** (Å²)	Z	ΔBVDU (Å²)
(111) A	12,0	122,09	0,099	1	0,099	3	0,297	6	0,049	3	0,148
(111) A´	11,6	122,09	0,095	1	0,095	3	0,285	6	0,048	3	0,143
(111) B	15,3	122,09	0,126	1	0,126	3	0,378	6	0,063	3	0,189
(111 C	17,5	122,09	0,144	1	0,144	3	0,432	6	0,072	3	0,216

Tab.: 8.11 Bond-valence deficiency table of magnetite (111) crystal surfaces terminated predominately by Fe-ions (Fig. 8.14). The bond-valence deficiencies (BVD) have been calculated for Fe^{3+} - O (1.88 Å) in tetrahedral coordination as 0.721 vu, and Fe^{2+}/Fe^{3+} in octahedral coordination as 0.406 vu (BARBIERI et al., 1994). The letters A, A´, B and C account for the different Fe-terminations (Fig. 8.14). The differences in the bond-valence deficiencies of the terminations A and A´ are minor, and the results obtained are not in favour of either termination. The A-termination preferred by BARBIERI et al. (1994), or the A´- termination preferred by LENNIE et al. (1996). But both terminations must be considered to be more stable than termination B and especially termination C.

Despite a little uncertainty which of the two possible A-terminations might be more favorable, after further annealing or relaxation, the given example demonstrates the capability of the bond-valence model to detect the most favorable (111)-iron termination to be either A or A´ instead of the terminations B or C.

9. Bond valences for liquids (External factors)

In the previous chapters the morphologies of crystals were predicted by considering the internal factors, such as reticular density, lattice spacing and symmetry, only. The crystal morphologies obtained correlated to ideal "abstract forms", neglecting the influence of external factors (temperature, pressure, pH and adsorption of foreign atoms, ions or molecules). While temperature and pressure have an influence on the bond-length of compounds, their influence on the crystal morphology can not be determined by the BVD-model, so far. However, external factors such as pH-changes, due to variations in the concentration of acids and bases present in the solution can be incorporated into the bond-valence model (Chapter 10). Each acid or base present in a solution can be given a certain bond-valence value, correlating to either its Lewis acid- or Lewis base- strength (BROWN, 1981). The same principle can be applied to any atom, ion or molecule adsorbing to a crystal surface. In general this has been outlined in Chapter 4 while discussing the bond-valence theory.

In the following chapters this principle will be discussed briefly, and it is shown that it is possible to assign bond-valences to the solute and the solvent of a solution in equal measure. A more detailed analysis is outlined by BROWN (2002).

By application of this approach we will be able to describe a solution via the bond-valence distributions of its compounds. Thus, having assigned bond-valences to each of these compounds in a solution, and having determined the bond-valences of a crystal surface (previous Chapters), we are able to consider the influence of these compounds on the morphology of polyhedral crystals via the application of the "valence matching principle" (Chapter 4.3).

9. 1 Bond-valences for "water"

In a first approach water is considered as a single molecule (Fig. 9.1). Its chemistry is determined by the basicity of the O-atom and the acidity of the H-atom. Together they permit the association of water molecules via hydrogen bonds (BROWN 1981). The chemistry of water is complex and depends mainly on the length of the O-H bond (Fig. 4.3). The length of the O-H bond can vary over a wide range depending on temperature and pressure as well as the bonding partner. BROWN (1976) found that bond valences of 0.8 *vu* for the internal O-H bonds and 0.2 *vu* for the weaker intermolecular hydrogen-bonds (H···), are the "normal" average bond valences found in water, considering a valence sum of 1.0 vu for the H- atom.

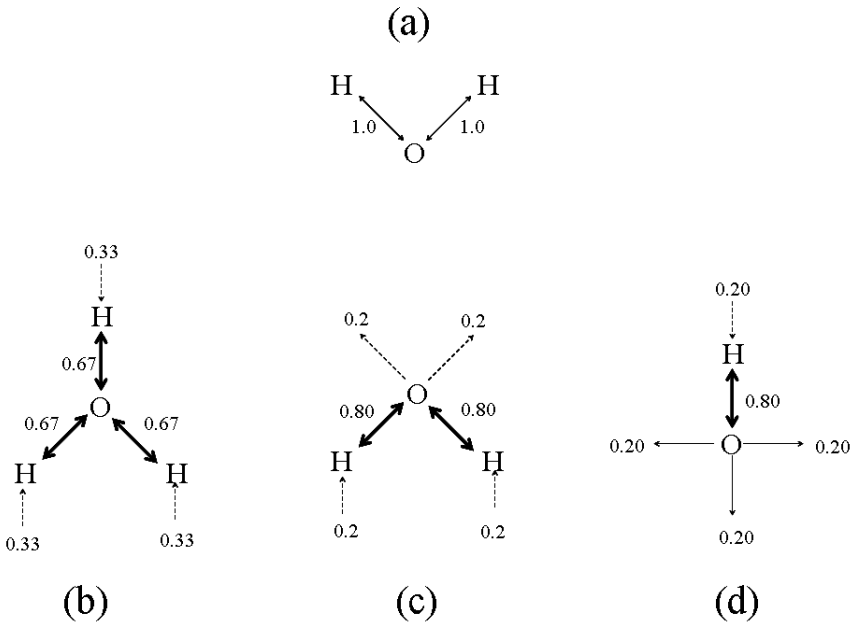

Fig.:9.1 Given are four different "water"-molecules. (a) Single H_2O-molecule showing the theoretical bond-valences of (O-H)-bonds. (b) Bond-valence distribution of an H_3O^+-molecule. (c) Average bond-valence distribution of H_2O-molecules as liquid water. (e) Bond-valence distribution of a OH^--molecule.

For the intermolecular bonds in liquid water, the H-atom is treated as a Lewis-acid, having an acid-strength of 0.2 *vu.* The O-atom can be addressed as a Lewis-base having a base-strength of 0.2 *vu*, respectively. This is assuming a coordination of CN = 4 for

the O-atom (BROWN, 1981). Therefore, water can be addressed as an acid-base network (Fig. 9.2), capable to react with other acid-base compounds present in the solution or with a mineral surfaces.

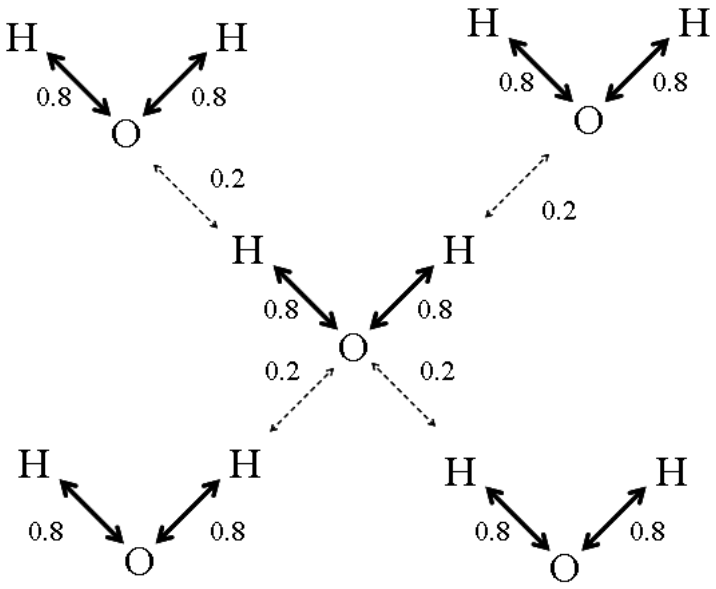

Fig.:9.2 Theoretical representation of the acid-base-network in water. The weak hydrogen bonds are considered to be labile and a high fluctuation of bonding partners is expected due to the fluid character of liquid water.

While the acid strength of the H-atom in water varies around 0,2 vu on the average, the base-strength of the O-atom can exhibit a wider variation of bond-vaelnces, depending e.g. on the number of H-atoms attached (Fig. 9.1). The base strength of the O-atom, e.g in the case of the OH^- anion, can range from 0.24 v*u* to 1.20 *vu* corresponding to its coordination-number which can range between 2 and 6 (BROWN, 1981).

According to this approach solids in a solution can react with water in many ways. Compounds for which the acid and base strengths are well matched and having strengths higher than 0.2 *vu* will, according to the valence-matching principle, tend to be “insoluble” since they form better bonds to each other than they do to surrounding water molecules (BROWN, 1981). Compounds matching the bonding strength of water will in contrast be more soluble.

As an example we can compare the solubility of galena with the solubility of sodium-chloride. The bonds formed between Pb^{2+} and S^{2-} in galena have an average bond-valence of 0.33 *vu.* Neither of the two ions will find a good match to surrounding water molecules, and this relates well to the low solubility of galena in water. In contrast the Na-Cl bonds of sodium-chloride have an average bond-valences of 0.16 *vu*. Therefore both ions will have a good match to the bond-valence of water (0.2 *vu*), and sodium-chloride is easily dissolved in water (Chapter 9.3).

9.2 Reactions of cations and anions with water

Any cation or anion present in liquid water will be surrounded by water molecules, and a coordinated hydration sphere will be formed. The number of coordinated water molecules around the cation or anion depends strongly on the bonding strengths of the ions. Additionally the bonding strength of the cations and anions will determine the stability of the hydrated complex formed.

The fluctuations of water molecules, attaching to or detaching form the hydration sphere around an ion, will be high if the bonds between the ion and the water molecules are weak. Sodium (Na^+), having an ideal coordination number of 6.4, and a bond-strength of 0.16 *vu* (BROWN, 2002) is expected to form a $Na(H_2O)_6^+$ complex. Since the Na-OH_2 bonds formed have a bond-valence of 0.16 *vu*, which is slightly lower than the bond valences of hydrogen bonds (0.2 *vu*), the complex is expected to be labile. The water molecules may as well be bound to the Na^+-cation, as well as to other water molecules, and as a consequence the water-molecules will attach and detach to the Na^+-ions in a short timescale.

The fluctuation of these bonds being attached or detached, compared to the fluctuations of the bonds between the water molecules themselves, might even be higher, for the bonds between the water molecules are slightly stronger than the bonds formed to the Na^+-ions.

Cations, as for example Cs^+, forming even weaker bonds of 0.109 vu (BROWN 2002), are expected to form very loose hydration-spheres. The bonds formed by Cs^+ are not strong enough to satisfy the anion bonding strength of water. The water molecules in contact with Cs^+-ions are forced to form weak hydrogen bonds to the Cs^+-ions, weaker compared to those they form to other water molecules.

Highly charged cations, e.g. Cr^{3+}, having an ideal coordination number of 6 and a bond-strength of 0.5 vu will form strong bonds to their hydration sphere (Fig. 9.3). The hydrogen bonds formed to the surrounding water molecules Cr-OH_2 (0.5 *vu*) will weaken the internal O-H bonds down to 0.75 vu. This is compensated by the H-atoms by the formation of higher hydrogen bonds (0.25 *vu*), leading to the establishment of a second hydration sphere (BROWN, 2002).

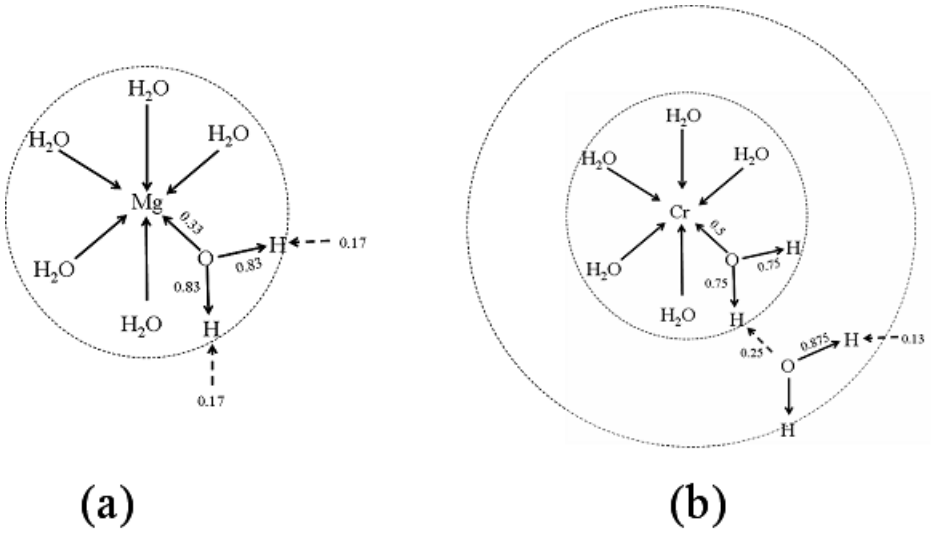

Fig.: 9.3 Depending on the bonding-strength of the central ion of a hydrated complex, more than one hydration sphere can be present. (a) Only one hydration-sphere around Mg^{2+} is formed. The hydrogen bonds of the first hydration sphere extending out, are not strong enough to sustain a permanent second hydration sphere. (b) The hydrogen-bonds emitted from the first hydration sphere around the central Cr^{3+}-cation, having bond-strength of 0.25 *vu,* form stronger bonds to the surrounding water molecules and consequently a second hydration-sphere can be established.

The ability of ions to form labile or stable hydration spheres was described by BROWN (2002) and referred to as the capability of these compounds to disorder the structure of bulk water. Ions having low bond-strength are considered as "structure breaking". Ions having a high bond-strength, and especially those which are able to form a second or third hydration sphere, are called "structure making". BROWN (2002) summarized these observations and found a correlation between the standard molar entropy of a solution as a function its bonding strength. These results are given in Figure. 9.4.

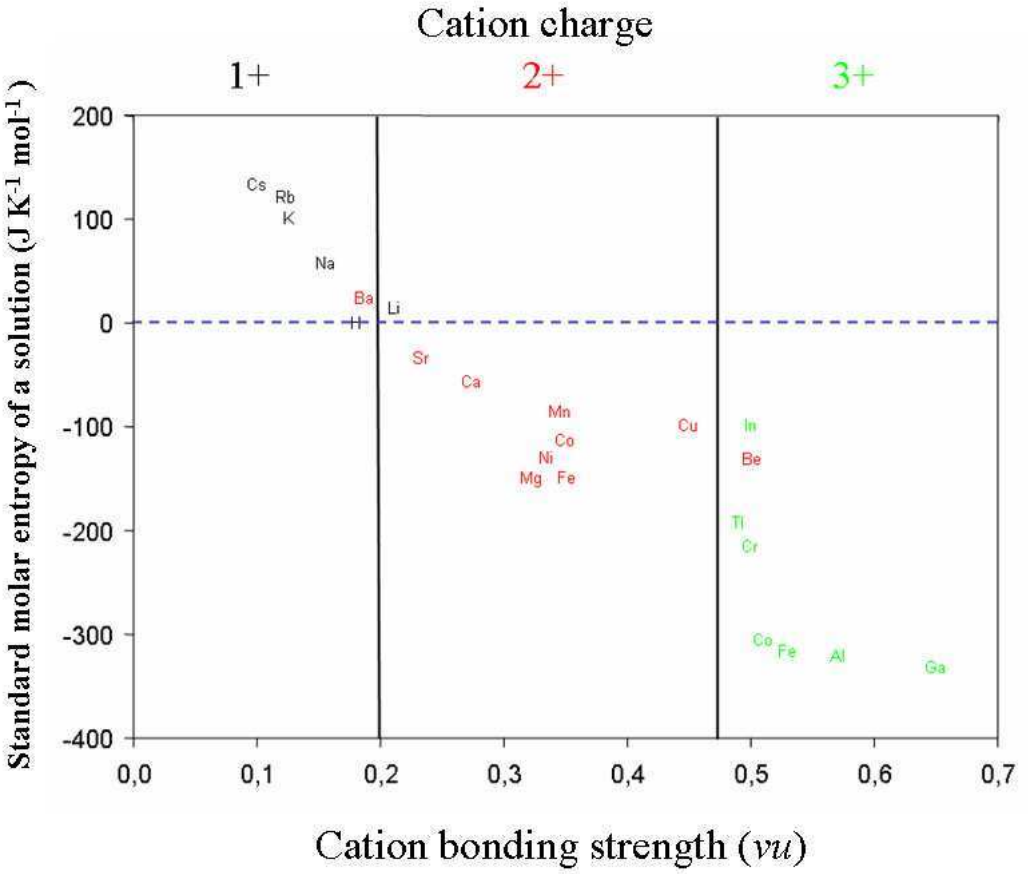

Fig.: 9.4 Correlation between the standard molar entropy of a solution (J K^{-1} mol^{-1}) and the cation bonding strength (*vu*). The values of the standard molar entropy are taken from BINNEWIES et *al.*(2000). The cation bond-strength corresponds to the ideal coordination number of the cation (Figure changed ; BROWN, 2002)

The ability of high charged ions to form more than one hydration-sphere can be related to a special ability of water molecules. This attribute is the capability of the O-atoms to form bonds having different bond-strength (Fig. 9.1) and was addressed by HAWTHORNE (1992, 1994, 1997) and SCHINDLER & HAWTHORNE (2001a), as the ability of water molecules to act as "bond-valence transformers" causing stronger bonds to be split into weaker bonds (Fig.: 9.5). In the example given in Figure. 9.3 the strong Cr^{3+}- O bond (0.5 *vu*) is transformed down to two weaker hydrogen bonds (0.25 *vu*). This transformation increased the strength of the hydrogen bonds, which in return can form stable bonds to water molecules out-side of the first hydration-sphere, giving rise to the establishment of a second hydration sphere.

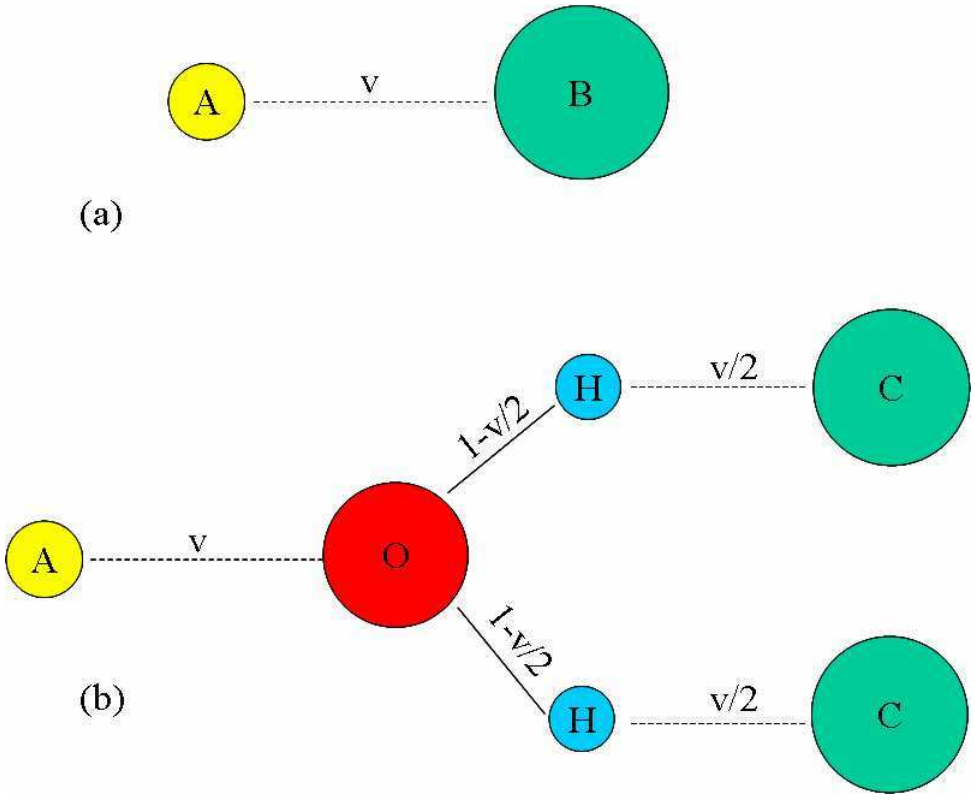

Fig.: 9.5 (a) Single bond of valence "*v*" between the cation A and the anion B. (b) Between the cation A and the anions C, the water molecule is acting as bond-valence transformer and splits the bond A-O into two weaker bonds *v/2* between H-C. The O-H bond in this example is reduced to the value 1- *v/2*. (Figure modified from, HAWTHORNE, 1992).

9.3 Bond-valences and the solubility of solids

By application of the bond-valence method BROWN (2002) describes, what happens when water interacts with a solid. This approach on how solids dissolve in water, is vital to the BVD-method as it is a first approach to describe the interaction between a solution and a solid in terms of bond-valences. These ideas have been the fundamental motivations to develop the BVD-model for crystal surfaces. Being able to describe both the mineral surface and the surrounding solution from the bond-valence perspective gives the possibility of establishing a new model to calculate the "abstract" as well as the "growth forms" of polyhedral crystals. Therefore the descriptions of BROWN (2002) about the "aqueous solubility" will be outlined in the following chapter for two examples. For more detail refer to BROWN (2002).

BROWN (2002):

> Dissolving a solid in water is a chemical reaction typically represented by:
>
> $$AB + (n+1)H_2O = A(H2O)_n^+ + HB + OH^-$$
>
> Depending on the relative bonding strength of A^+ and B^- several situations can be distinguished. The first occurs if the cation and anion are well matched and both have large bonding strengths, e.g Mg^{2+} and SiO_4^{4-} ($s_{Mg^{2+}} = s_{SiO_4^{4-}} = 0.33vu$).
>
> In this case there is no reaction with water, since the match between the two ions is better than the match between either of them individually and water. The solid is insoluble and, if the ions find themselves in solution together, they precipitate out as Mg_2SiO_4, the insoluble mineral forsterite. Such compounds have positive free energies of solution.

A second situation occurs when the two ions are well matched but have bonding strengths that are relatively small so that each ion is also well matched with water, e.g. Na^+ and Cl^- ($s_{Na^{2+}} = 0.16vu, s_{Cl^-} = 0.14vu$). In this case both the solution and the solid will be equally stable. The solid, in this case common salt, readily dissolves in water, but as readily recrystallizes when the water is removed. Its free energy of solution is close to zero.

These are only two examples, given by BROWN (2002), but they show how the bond-valence theory can be applied to link between a solid and a solution. The consequences and the possible applications for the BVD-model are outlined in the following chapters (10 and 11).

10. Bond valences at the boundary layer between solid and solution: Mineral surface reactions

In Chapter 8 the "abstract forms" of different crystal structure types have been outlined in detail and in Chapter 9 it has been demonstrated how the bond-valence approach can be applied to aqueous solutions. The focus of the following chapters is the boundary layer between a solid and a solution, the mineral surface itself. Some principal considerations about the acidity or basicity of mineral surfaces, their Zero-point of charge and net-proton charge are discussed briefly. A more detailed discussion is given in the papers attached in Appendix V (SCHINDLER et al. 2004 a, b).

10.1 The interaction of crystal surfaces with aqueous solutions

As noted above, the bond-valence sum incident at any cation or anion, forming a coordination polyhedron, must be as close as possible to its formal valence. In the bulk structure, the bond valences contributing to such a sum involve simple ions at the vertices of the associated coordination-polyhedron. With regard to a surface, we may identify two distinct situations:

(1) the surface of the crystal is adjacent to a vacuum;

(2) the surface of the crystal is adjacent to a liquid (or a gas).

In the first situation, the ions at the surface of a crystal by definition must have a coordination different from those in the bulk crystal, and these differences will exist over long time-scales. The surface structure responds to these differences by lengthening or shortening specific bonds; such differences in bond lengths (and bond angles) are commonly called the *relaxation* of the surface. As a result of these differences, the pattern of bond valences at and near the surface in a vacuum must differ

significantly from that in the bulk crystal, even to the extent that there may be a reorganization of the topology of the chemical bonds at the surface, termed *reconstruction.*

In the second situation, although the atoms at the surface must have a coordination different from that in the bulk crystal, the bond-valence requirements of these surface atoms are also partly met by neighboring atoms in the coexisting liquid (or gas). Hence surface relaxation will be much less than if the surface is exposed to a vacuum. Indeed, the atoms of the liquid will tend to arrange themselves such that relaxation at the surface of the solid is minimized, and one may well be able to consider local interactions among atoms as the average of what occurs at the surface over a longer time-scale. This discussion suggests that we may be able to use an "unrelaxed" surface model in which one treats bond valences of near-surface bonds as equal to the bond valences of the analogous bonds in the bulk structure.

10.2 Intrinsic acidity constants of anion terminations in oxide minerals

Consider a crystal in equilibrium with an aqueous solution. Depending on the pH of the solution, the surface is partly or fully hydrated, and aqueous species in the solution bond to anions or cations on the surface (chemisorption). The degree of hydration and type of chemisorption depend on the type of anion or cation on the surface and on the conditions in the coexisting solution. The degree of hydration can be predicted with the acidity constants of the different anion-terminations and the pH of the solution. Van Riemsdijk and co-workers (HIEMSTRA *et al.* 1996) developed a "multisite complexation model" (MUSIC), which can be used to predict anion acidities using a modified form of the following equation:

$$pKa = -A\,(\Sigma\, sj + V) \qquad [10.1]$$

where *pKa* is the intrinsic acidity constant [a constant valid for an uncharged surface (STUMM 1992)], *A* equals 19.8, *V* is the valence of the oxygen atom at the surface (–2), and $\Sigma\, sj$ is the bond-valence sum at the surface oxygen atom and is defined by

$$\Sigma\, s\, j = \{s_M + ms_H + n(1 - s_H)\} \qquad [10.2]$$

where s_M is the bond valence of the *M*–O bond, s_H is the bond valence of the H–O bond to the surface oxygen if the base is a hydroxyl group (assumed to be 0.80 *vu*), $(1- s_H)$ is the valence of weak hydrogen bonds from aqueous species to surface anions, and *m* and *n* are the numbers of stronger O–H and weaker O...H bonds, respectively.

HIEMSTRA *et al.* (1996) used fixed *M*–O bond-valences from unrelaxed bulk-structures to predict intrinsic acidity constants for surface groups. BICKMORE *et al.* (2003) used *ab initio* calculations for the average of *M*–O bond-valences of protonated and deprotonated relaxed surface-structures in 2:1 phyllosilicates; their average bond-valence values for Fe–O, Al–O and Si–O bonds are similar to the corresponding values used by HIEMSTRA *et al.* (1996). The key issue in the prediction of appropriate intrinsic acidity-constants is use of the correct *average coordination number of O* on the surface. Here, HIEMSTRA *et al.* (1996) used an average coordination of oxygen of [3] for the more compact surfaces of gibbsite and goethite, and an average coordination number of [4] for the more open surface of quartz.

10.2.1 Calculation of intrinsic acidity-constants for different U–O anion-terminations on edges of the basal face of uranyl-sheet minerals

For tetragonal, pentagonal and hexagonal bipyramidal uranyl polyhedrons, the characteristic equatorial U–φ bond-valences are 0.64, 0.54 and 0.45 *vu*, respectively (BURNS, 1999). However, individual equatorial $^{[a]}$U–φ bond-lengths vary over a larger range than the corresponding Al–O, Fe–O and Si–O bond-lengths (HIEMSTRA *et al.,* 1996). For example, the $^{[7]}$U–φ bond-lengths in schoepite, $[(UO_2)_8O_2(OH)_{12}](H_2O)_{12}$,

vary between 2.2 and 2.7 Å (FINCH *et al.* 1996), which correspond to bond valences of 0.73 *vu* and 0.27 *vu*, respectively. These high variations in individual bond-valences in uranyl-minerals may give rise to a range of intrinsic acidity-constants for one type of anion termination.

The type of anion termination on edges in uranyl-minerals is limited by the occurrence of [6]-, [7]- and [8]-coordinated $U6^+$: *e.g.*, [6]- and [8]-coordinated $U6^+$ never occur together, and always occur with [7]-coordinated $U6^+$. The type of anion termination can be indicated by the code $^{[a]}U–\varphi–n^{[b]}U$, where the φ is an unspecified anion that bonds to one U atom in [*a*] coordination and *n* x U atoms in [*b*] coordination. If we do not consider other oxyanions [*e.g.*, $(VO_4)^{3–}$, $(PO_4)^{3–}$, $(SiO_4)^{4–}$], the following combinations of anion terminations can occur on edges in uranyl-oxide sheet minerals:

$^{[8]}U–\varphi$, $^{[7]}U–\varphi$, $^{[6]}U–\varphi$,

$^{[8]}U–\varphi–^{[8]}U$, $^{[8]}U–\varphi–^{[7]}U$, $^{[7]}U–\varphi–^{[7]}U$, $^{[7]}U–\varphi–^{[6]}U$,

$^{[8]}U–\varphi–2^{[7]}U$, $^{7]}U–\varphi–2^{[7]}U$ $^{[6]}U–\varphi–2^{[7]}U$.

The wide variation in type of anion termination (Chapter 6) makes it difficult to determine an exact pHpzc for a uranyl-mineral. However, an exact pHpzc is required to scale the average coordination-number of the oxygen atoms on the edge surface .

As an example the intrinsic acidity-constants of anion terminations on the (001) face of schoepite will be calculated theoretically, and the results will be compared to titration experiments with dehydrated schoepite.

Schoepite, $[(UO_2)_8O_2(OH)_{12}](H_2O)_{12}$, has a prominent (001) basal face that dominates the morphology of its crystal habit (Fig 6.3). The corresponding uranyl-sheet contain $U6^+$ in [7]-coordination (Finch *et al.* 1996). There are three different types of equatorial anion-terminations on the (001) face:

$^{[7]}U–OH–2^{[7]}U$ $^{[7]}U–OH–^{[7]}U$ $^{[7]}U–O–2^{[7]}U$

In order to calculate the corresponding intrinsic *pKa* values for these terminations, we can use the overall characteristic bond-valence for $^{[7]}U–\varphi$ (0.54 *vu*), the average $^{[7]}U–\varphi$ bond-valence of the equatorial bonds in schoepite (0.47 *vu*), or the average $^{[7]}U–\varphi$ bond-valence for each of the three anion-terminations. Here, we use the average bond-valence of the equatorial bonds (0.47 *vu*) because this value is more appropriate than the characteristic $^{[7]}U–\varphi$ bond-valence, and it simplifies the calculation (relative to the use of individual average bond-valences). In many uranyl-hydroxy-hydrate minerals, the coordination number of equatorial O-atoms in the structural unit is close to [4]; oxygen bonds either to three U and one H, or to two U, one H and accepts one additional hydrogen bond. The acid–base reactions and the corresponding values of *pKa* (assuming $^{[4]}O$) are as follows:

$^{[7]}U–O–2^{[7]}U + H+ \leftrightarrow {}^{[7]}U–OH–2^{[7]}U$ $pKa = 7.7$ $[R_1]$

$^{[7]}U–O–^{[7]}U + H+ \leftrightarrow {}^{[7]}U–OH–^{[7]}U$ $pKa = 13.1$ $[R_2]$

$^{[7]}U–OH–^{[7]}U + H+ \leftrightarrow {}^{[7]}U–OH_2–^{[7]}U$ $pKa = 1.2$ $[R_3]$

The intrinsic *pKa* is calculated using the average bond-valence sum at O in the anion termination of the base (*i.e.*, for the termination on the left side of each equation).

In reaction [R_1], the oxygen atom in $^{[7]}$U–O–2$^{[7]}$U receives 3 x 0.47 *vu* (from the $^{[7]}$U atoms) + 0.20 *vu* (from a hydrogen bond) = 1.61 *vu*. This results in

$$pKa_{[1]} = -19.8(1.61 - 2) = 7.7 \qquad [R_1]$$

In reaction [R_2], the oxygen atom in $^{[7]}$U–O–$^{[7]}$U accepts 2 x 0.47 *vu* from $^{[7]}$U, and 2 x 0.20 *vu* from two additional hydrogen bonds; *i.e.*, its bond-valence sum is 1.34 *vu*, which corresponds to

$$pKa_{[2]} = -19.8\ (\ 1.43 - 2) = 13.1 \qquad [R_2]$$

In reaction [R_3], the oxygen atom in the $^{[7]}$U–OH–$^{[7]}$U termination receives 2 x 0.47 *vu* plus 0.80 *vu* from the O–H bond and 0.20 *vu* from an additional hydrogen bond; its bond-valence sum is 1.94 *vu*, which corresponds to

$$pKa_{[3]} = -19.8\ (\ 1.92 - 2) = 1.2 \qquad [R_3]$$

In order to compare calculated *pKa* values with observed values, one can determine the *pKa* values of the anion-terminations *via* titration of a fine suspension of schoepite with an NaOH solution. However, schoepite samples with a non-dehydrated surface are difficult to obtain from mineral samples or from synthesis. We decided therefore to use the structurally related phase dehydrated schoepite, which can be easily obtained by hydrothermal synthesis.

The titration experiments have been carried out using a fine suspension of 100 mg of dehydrated schoepite [$(UO_2)O_{0.2}(OH)_{1.6}$]. in 20 mL 0.1 and 1.0 mol L^{-1} NaCl solutions. These solutions then were titrated with 0.01 mol L^{-1} NaOH. Figure(10.1) shows the corresponding titration-curves with initial pH-values of 6.2 and 5.9, respectively.

The shift in the initial pH-values with change in concentration of the NaCl solution indicates adsorption of Na^+ cations at specific sites on the (001) face (Stumm 1992). This adsorption results in an overall positive charge of the surface, which must be balanced by deprotonation of the U–OH–2U terminations. In this way, the (001) face of dehydrated schoepite functions as a weak acid, which explains the slightly acidic pH at the beginning of the titration.

Because a NaCl solution is required to maintain a constant ionic medium, we modeled a curve for a titration in a 0.0 mol L^{-1} NaCl solution (Fig. 10.1). The initial pH of the dehydrated schoepite solution in the modeled curve is around 6.5, and the *pKa* value is around 7.0 ± 0.2. This *pKa* value corresponds to the acid–base reaction U–(OH)–2U ↔ U– O – 2U on the (001) face of dehydrated schoepite. [Note that in the anion-termination U–(OH)–2U of dehydrated schoepite, U occurs in [7]- and [8]-coordination. The [8]-coordination of U in dehydrated schoepite results from dehydration of schoepite and structural changes inside the uranyl sheet. The theoretical structural sheet of dehydrated schoepite is given in Chapter (6.2.1).

At the beginning and at the end of the titration, the (001) face of dehydrated schoepite most likely had the compositions $[(UO_2)O_{0.2+x}(OH)_{1.6-2x}]^{2x+}$ and $[(UO_2)O_2]^{2-}$, respectively. The calculations of the *pKa* value of schoepite and the experimentally determined *pKa* value of dehydrated schoepite are reasonably close, and suggest that the average coordination-number of [4] is an appropriate value in the case of the uranyl-oxide minerals schoepite and dehydrated schoepite.

For example, if one uses an average coordination-number of [3], the intrinsic *pKa* value of the acid–base reaction $^{[7]}U–O–2^{[7]}U + H+ \leftrightarrow {}^{[7]}U– OH–2^{[7]}U$ would be 11.7, significantly different from the observed value of 7.0 ± 0.2. The parameter A (-19.8) of the MUSIC model was fitted on the basis of experimental results on simple oxide minerals such as hematite, rutile and quartz. Hence, the equation in this form is not necessarily applicable to all uranyl-oxide minerals, and needs to be measured in the future on uranyl-oxide minerals. However, we will use this equation here in order to show how the intrinsic acidity constant is related to two other parameters that express

the strength of a base and an acid: Lewis basicity and Lewis acidity. For this purpose, we calculated intrinsic acidity-constants for all kinds of anion terminations using the above-listed average $^{[n]}U–\varphi$ bond-valences in uranyl-polyhedrons (Table 10.1).

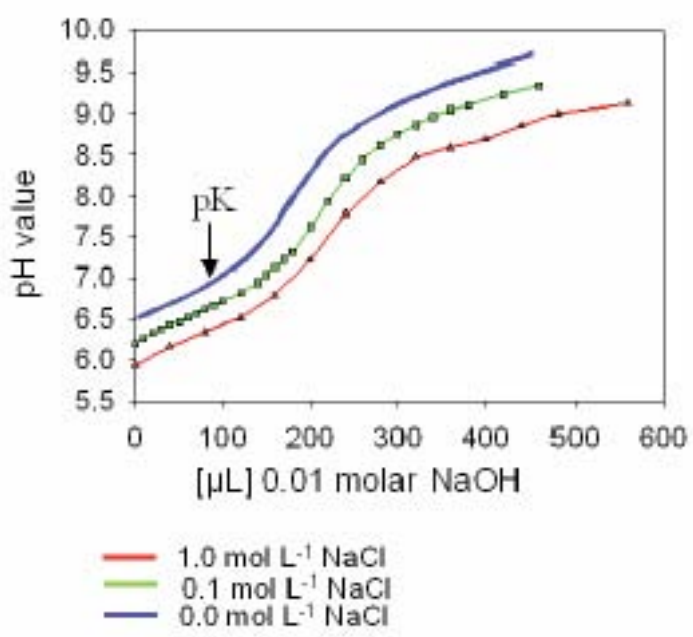

Fig.: 10.1 Titration curves with added 0.001 mol L-1 NaOH versus pH for a fine suspension of 100 mg of dehydrated schoepite in 20 mL 0.1 mol L-1 (green) and1 mol L-1 (red) NaCl solutions. Added is a modeled titration-curve (blue) in a hypothetical 0.0 mol L-1 solution (Figure. from SCHINDLER et al. (2004a), see Appendix V).

10.3 Lewis basicity and "acidity" of anion terminations

The intrinsic acidity-constant *pKa* is a measure of the strength of the acid in an acid–base equation:

> The higher the *pKa*, the weaker its acid strength or the stronger the base strength of the corresponding base.

Using the acid–base definition of LEWIS (1916), *pKa* expresses the ability of the base (Lewis base) to donate electrons to the acid (Lewis acid). HAWTHORNE (1997) and SCHINDLER & HAWTHORNE (2001a) defined the Lewis-base strength of a complex structural unit as the bond valence required by the (negatively charged) structural unit divided by the number of (weak) bonds accepted by the structural unit from the interstitial complex. Using this definition, we may calculate the Lewis-base strength (or Lewis-acid strength) of an anion termination by assuming again an average O-coordination number of [4].

For example:

> The Lewis base strength of the anion-termination $^{[7]}$U–OH is the required bond-valence [(2 – (0.54 + 0.80) = 0.66 *vu*] divided by the number of bonds accepted (two): 0.66 / 2 = 0.33 *vu*.
>
> For the anion termination $^{[a]}$U–OH_2, it is more useful to calculate its Lewis acidity because the constituent O-atom has an incident bond-valence sum greater than or equal to 2 *vu*.

The Lewis acidity of the $^{[a]}U–OH_2$ group is the characteristic bond-valence of each constituent hydrogen bond. Hence, the (H_2O) group transforms the bond-valence (*v vu*) of the $^{[a]}U–O$ bond into two weaker hydrogen bonds of bond-valence *v* /2 (Chapter 9.2). The Lewis acidity of the termination $^{[7]}U–OH_2$ is 0.54 / 2 = 0.27 *vu*. The Lewis acidities and Lewis basicities of all anion terminations are listed in Table 10.1 (end of this Chapter).

10.3.1 Lewis basicity and acidity constants

From Table 10.1 a correlation between the type of anion termination and its functionality as a Lewis acid or Lewis base can be derived and the different anion terminations can be merged together in groups.

Let us consider the anion terminations $^{[7]}U–OH$ and $^{[7]}U–O$ in the acid–base reactions [2] and [3] given in Table 10.1. The corresponding *pKa*2 and *pKa*3 values express the ability of the bases $^{[7]}U–OH$ and $^{[7]}U–O$ to donate electrons to the acid H^+. The Lewis basicities (0.33 and 0.49 *vu*) correspond to the *pKa*2 and *pKa*3 values of 5.1 and 17, respectively. For the general anion termination $^{[a]}U–OH_2$, with [*a*] = [8], [7] and [6], we assign a negative Lewis acidity and correlate it with the corresponding *pKa* values (-5, -6.7,- 8.7).

All the anion terminations listed in Table 10.1 can be subdivided into five groups correlating with either Lewis bases or Lewis acids:

(1) $^{[a]}U–OH_2$,

(2) $^{[a]}U–OH$,

(3) $^{[a]}U–O$,

(4) $^{[a]}U–OH–2^{[b]}U$

(5) $^{[a]}U–O–2^{[b]}U$.

For each group, there is a linear correlation between the Lewis basicity (acidity) and the corresponding *pKa* value (Fig. 10.2).
This correlation can be understood if we compare the corresponding equations for the acidity constant and the Lewis basicity:

$$pKa = -19.8\ [\Delta s - 0.20\ (4 - a(\text{U–O}) - b(\text{O–H}))] \qquad [10.3]$$

$$(LB) = \Delta s\ /\ [4 - a(\text{U–O}) - b(\text{O–H})] \qquad [10.4]$$

where Δs is the bond-valence deficiency of the O-atom at the anion termination without considering any accepted hydrogen bonds. The term $0.20\ [4 - a(\text{U–O}) - b(\text{O–H})]$ is the bond-valence contribution of weak hydrogen bonds, where a and b are the numbers of U–O and O–H bonds, respectively; (LB) is the Lewis basicity.
Writing $[4 - a(\text{U–O}) - b(\text{O–H})]$ as x and solving for pKa gives the following relation:

$$pKa = -19.8\ (\Delta s x - 0.2\ x) \qquad [10.5]$$

The parameter x is constant for one group of anion terminations, but varies from group to group (*e.g.*, from 1 in $^{[a]}\text{U–OH}_2$ to 3 in $^{[a]}\text{U–O}$ with a = 6, 7, 8). The correlation between Lewis basicity and *pKa* for all five groups of anion terminations is shown by the curved line in Figure 10.2.

Calculation of the intrinsic acidity-constant and the Lewis basicity of an anion termination requires the knowledge of the bond-valence deficiency at an oxygen atom. The average coordination-number of the oxygen atom at an anion termination scales the absolute values of the intrinsic acidity-constant and the Lewis basicity. The bond-valence deficiency at an oxygen atom is independent of the coordination number of the oxygen, and is a better parameter to characterize the basicity of an anion termination.

The bond-valence deficiency at an oxygen atom can be related to the free energy of the acid–base reactions [R_1], [R_2] or [R_3] (Chapter 10.2) as follows (Faure 1998):

$$\Delta_R G_{AT} = -2.303\ RT\ pKa \qquad [10.6]$$

where $\Delta_R G_{AT}$ is the free energy of the acid–base reaction at one anion-termination. Combination of equations (10.5) and (10.6) results in:

$$\Delta_R G_{AT} = -2.303\ RT\ [-19.8\ (\Delta sx - 0.20\ x)] \qquad [10.7]$$

Equations (10.5) and (10.7) indicate that the higher the bond-valence deficiency at an oxygen atom, the stronger the basicity of the anion termination, the stronger its affinity to hydrogen bonds or O–H bonds, and the more negative the free energy $\Delta_R G_{AT}$ of the corresponding acid–base reaction.

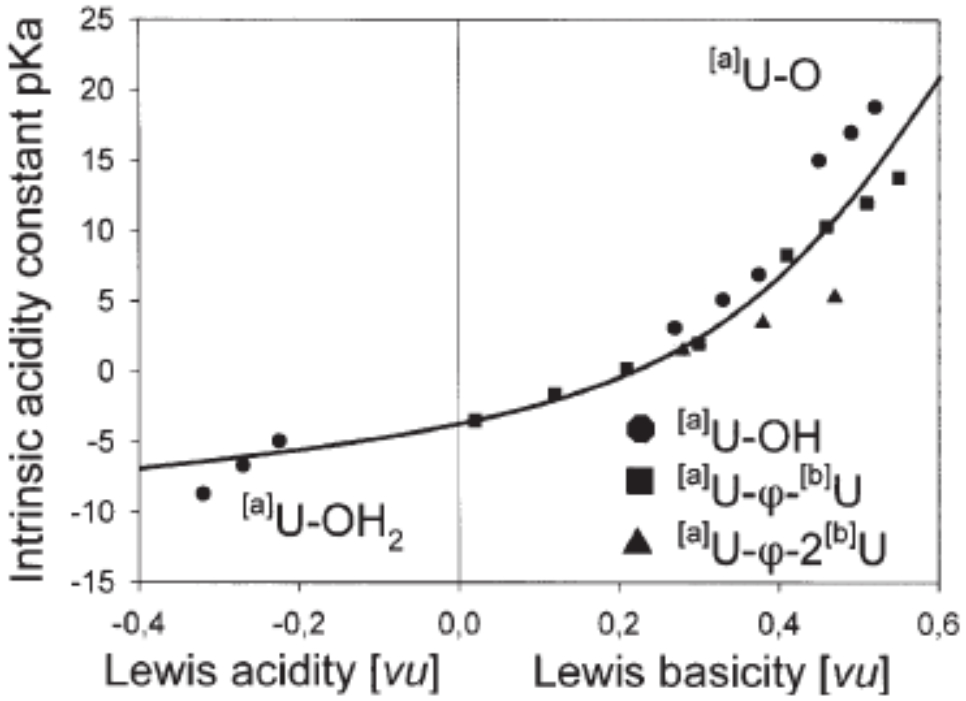

Fig.: 10.2 Lewis acidity and Lewis basicity *versus* intrinsic acidity constant, pK_a, of anion terminations on the edges of uranyl sheets (SCHINDLER et *al.*, 2004a, Appendix V).

10.3.2 Bond-valence deficiency, pKa, and free energy of a chain of polyhedrons (uranyl-sheet minerals)

The bond-valence deficiency of an edge may be defined as the sum of bond-valence deficiencies on anion terminations, normalized to its translation length. A chain of polyhedrons in the sheet ideally represents an edge on an F face, considering the PBC-theory termination. (Fig. 10.3). Each type of chain contains different types of anion terminations, and each type of anion termination corresponds to a specific *pKa*, Lewis basicity, and $\Delta_R G_{AT}$ value of a corresponding acid–base reaction.

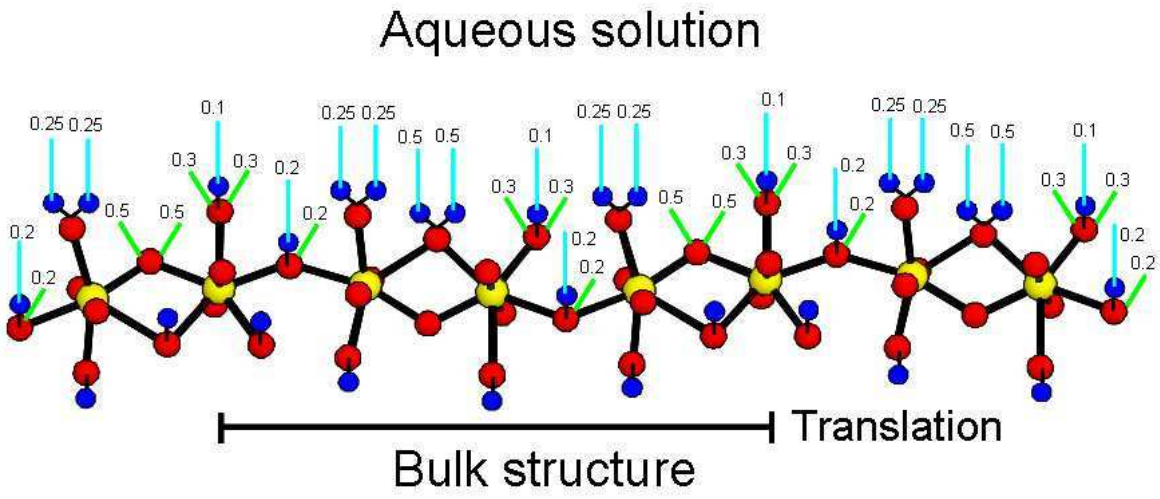

Fig.: 10.3 Ball-and-stick model of a possible protonated edge of uranyl-polyhedrons, parallel to the [010]-direction of the basal-sheet of schoepite. The outgoing bonds from the chain to the aqueous species in the solution are marked in blue lines. Incoming bonds, accepted by equatorial oxygen, are marked by green lines. The corresponding bond-valences (*vu*) are given as numbers besides the lines (modified from, SCHINDLER et *al.*, 2004a; see Appendix V).

Let us consider a chain of polyhedron of translation *a*, with *b* x $^{[7]}$U–O and *c* x $^{[7]}$U–O–$^{[7]}$U terminations. The *pKa* value of an acid–base reaction involving this chain of polyhedrons is designated ΔpK_{PC}, and depends on the numbers and types of different anion-terminations. The *pKa* value of an acid–base reaction involving any chain of polyhedrons may be written as ΣpKs, and may be defined as the sum of the *pKa* values of acid–base reactions at the corresponding anion-terminations per Å. For

the anion terminations considered ($^{[7]}$U–O and $^{[7]}$U–O–$^{[7]}$U) the following equation can be written:

$$\Sigma pK_{PC} = [b \text{ x } pKa\ (^{[7]}\text{U–O}) + c \text{ x } pKa\ (^{[7]}\text{U–O–}^{[7]}\text{U})] / a \qquad [10.8]$$

This equation can be rewritten as:

$$\Sigma pK_{PC} = [b \text{ x } \Delta s\ (^{[7]}\text{U–O}) + a \text{ x } \Delta s\ (^{[7]}\text{U–O–}^{[7]}\text{U})] / a \qquad [10.9]$$

The term [b x Δs ($^{[7]}$U–O) + a x Δs ($^{[7]}$U–O–$^{[7]}$U)] / a] is the O-atom bond-valence deficiency per Å for a chain of polyhedrons, considering the anion terminations ($^{[7]}$U–O and $^{[7]}$U–O–$^{[7]}$U). It correlates with the average value of *pKa* and the free energy of acid–base reactions along a chain, and indicates the affinity of the constituent O-atoms for hydrogen bonds or O–H bonds. The bond-valence deficiency per Å can be calculated from crystal-structure data. Further examples are given by SCHINDLER et *al.* (2004a), attached in Appendix V.

10.4 Further implications of the bond-valence approach to mineral surface reactions: pHpzc, net proton-charge, inner- and outer-sphere complexes

The pHpzc is also called the isoelectric point. STUMM (1992) defined the pHpzc as the point where the *total net surface-charge* is zero (this is the condition where particles do not move in an applied electric field). The total net surface-charge is the sum of:

(1) the permanent structural charge caused by isomorphic substitutions,
(2) the net proton-charge (*i.e.*, the charge due to the binding of protons or OH- anions),
(3) the charge of the inner-sphere complex,
(4) and the charge of the outer-sphere complex.

The distribution of surface charge can be idealized as an electric double- or triple-layer. In the case of a double layer, the first layer is the solid surface with a localized negative surface-charge, whereas the second layer is in contact with the first layer and is a solution containing dispersed ions of positive charge (the *Gouy–Chapman diffuse model*: STUMM, 1992).

This model cannot be applied to surfaces of high potential because the local concentrations of counter ions near the surface becomes too large. In the *Stern–mode* (STUMM, 1992), an additional compact layer of cations exists immediately adjacent to the mineral surface in order to balance the high charge of the surface. The ions in this layer are held tightly by "electrostatic forces" and are not free to move like the ions in the diffuse layer of the *Gouy–Chapman model*.

DZOMBAK & MOREL (1990) developed a surface-complexation model in which ions are attached by chemical bonding to the surface and not *via* "electrostatic effects", as assumed in the *Gouy–Chapman* and *Stern–Grahame models*. Therefore, cations of the inner-sphere complexes are treated in the surface-complexation model as part of the solid (STUMM 1992).

An inner-sphere complex and an outer-sphere complex occur if a cation or anion in the solution bonds directly or *via* (H_2O) groups to terminations on the surface. Hence, the presence of inner-sphere and outer-sphere complexes changes the net proton-charge of the surface. If the net proton-charge is zero, the total net surface-charge is not necessarily zero. However, charge and number of inner- and outer-sphere complexes depend on many factors, such as the size and number of specific sites for complexation on the surface, and on the charge, size and activities of cations and anions in solution. We can again simplify this problem if we factor surface, inner- and outer-sphere complexes and other aqueous species into three components:

(1) surface,
(2) chemisorbed species,
(3) and aqueous solution.

To be considered part of the surface, an atom has to conform to the space-group symmetry of the crystal, with the exception of H-atoms that strongly bond to O-atoms at the surface. Any other atom or group of atoms chemically bonded to the surface and *not* conforming to the space-group symmetry of the crystal will not be incorporated into the structure (to any significant degree), and although atoms chemically bonded to the surface, will have a short residence-time in this state. (For the impact of the face symmetry on e.g. the morphology of crystal polyhedron refer to Chapter 7).

In some chemical systems, such chemisorbed impurities can significantly modify habit development (Chapter 11), presumably depending on the residence lifetime of the species on the surface and the activity of that species in solution. In this way, we consider here only the change in interaction between an edge with different net proton-charges and the aqueous solution.

From a bond-valence perspective, the net proton-charge is the difference between the sums of the accepted and donated bond-valences between the termination on the surface and the species in aqueous solution. A termination that accepts bond valences is a *Lewis base*, and a termination that donates bond-valence is a *Lewis acid.* At zero net proton-charge, the strength and number of Lewis bases and Lewis acids are identical. The pH of a solution in which a surface has zero net proton-charge is called the point of zero net proton-charge, pHpzc (STUMM, 1992, p. 18). Depending on the intrinsic acidity-constant of the acid–base reaction, strong Lewis bases and acids occur only at low or high pH. Hence, weaker Lewis bases and acids occur mainly on a surface at the pHpzc. This approach emphasizes that at the pHpzc, the bond-valence transfer between Lewis bases and acids on the surface and the aqueous solution is at a minimum.

A surface may be positive, negative or neutral. The bond-valence deficiency at a face in this respect is therefore a measure of the bond valence required to achieve electron-neutrality at that face. If there is a low bond-valence deficiency at a face and the pH of the solution is identical to the pHpzc, there is a low interaction between the face and the

solution. This results in the formation of only a small number of activated sites, and hence the dissolution rate perpendicular to the face is small.

As a summary of this short excursion, we can define the pHpzc of a surface from a bond-valence perspective (not considering attached inner- or outer-sphere complexes):

At the pHpzc of a surface, there is a minimum in the number of highly charged terminations (i.e., strong Lewis acids and Lewis bases) on the surface, which results in low bond-valence transfer between surface acceptors and donors and the aqueous species.

A higher number of strong bonds between terminations and aqueous species enhances attachment and detachment of building units, and growth or dissolution rates should correlate with the type and number of activated sites, later defined by their respective bond-valence deficiency.

Tab.:10.1 Intrinsic acidity constants, Lewis acidities and Lewis basicities of equatorial anions terminating edges on uranyl-sheet minerals (SCHINDLER et al., 2004a, see Appendix).

Code	Acids and bases of the anion-termination $_{P}Ka_1$ $_{P}Ka_2$ $_{P}Ka_3$	$_{P}Ka_1$	$_{P}Ka_2$	$_{P}Ka_3$	Lewis acidity / Lewis basicity (*vu*)		
$^{8]}$U–φ	$^{[8]}$U–OH$_3$ ↔ $^{[8]}$U–OH$_2$ ↔ $^{[8]}$U–OH ↔ $^{[8]}$U–O	-5,0	6,9	18,8	0,225	0,375	0,52
$^{[7]}$U–φ	$^{[7]}$U–OH$_3$ ↔ $^{[7]}$U–OH$_2$ ↔ $^{[7]}$U–OH ↔ $^{[7]}$U–O	-6,7	5,1	17	0,27	0,33	0,49
$^{[6]}$U–φ	$^{[6]}$U–OH$_3$ ↔ $^{[6]}$U–OH$_2$ ↔ $^{[6]}$U–OH ↔ $^{[6]}$U–O	-8,7	3,1	15	0,32	0,27	0,45
$^{[8]}$U–φ–$^{[8]}$U	$^{[8]}$U–OH$_2$– $^{[8]}$U ↔ $^{[8]}$U–OH– $^{[8]}$U ↔ $^{[8]}$U–O– $^{[8]}$U	2,0	13,8		0,30	0,55	
$^{[8]}$U–φ–$^{[7]}$U	$^{[8]}$U–OH$_2$– $^{[7]}$U ↔ $^{[8]}$U–OH– $^{[7]}$U ↔ $^{[8]}$U–O– $^{[7]}$U	0,2	12		0,21	0,51	
$^{[7]}$U–φ–$^{[7]}$U	$^{[7]}$U–OH$_2$– $^{[7]}$U ↔ $^{[7]}$U–OH– $^{[7]}$U ↔ $^{[7]}$U–O– $^{[7]}$U	-1,6	10,3		0,12	0,46	
$^{[7]}$U–φ–$^{[6]}$U	$^{[7]}$U–OH$_2$– $^{[6]}$U ↔ $^{[7]}$U–OH– $^{[6]}$U ↔ $^{[7]}$U–O– $^{[6]}$U	-3,5	8,3		0,02	0,41	
$^{[8]}$U– φ –2$^{[7]}$U	$^{[8]}$U–OH– 2$^{[7]}$U ↔ $^{[8]}$U–O– 2$^{[7]}$U	5,3			0,47		
$^{[7]}$U– φ –2$^{[7]}$U	$^{[7]}$U–OH– 2$^{[7]}$U ↔ $^{[7]}$U–O– 2$^{[7]}$U	3,5			0,38		
$^{[6]}$U– φ –2$^{[7]}$	$^{[6]}$U–OH– $^{[7]}$U ↔ $^{[6]}$U–O– 2$^{[7]}$U	2,5			0,28		

11 Predicting the morphology of crystals

There are a number of external factors such as temperature, pressure and pH having influence on the morphology of a crystal specimen, but their influence to change the morphology of a crystal is in most cases minor compared to the influence of impurities on the crystal habit. Many minerals have not crystallized from a pure solution, but have been formed in the presence of one, two or more impurities and the results of such interactions are many fold, as one only needs to consider the variations in the crystal habits exposed by calcite crystals.

From this point of view it seems almost impossible to find an effective method to predict the morphology of a crystal. Even today, and only for the most simple systems, is it scarcely possible to calculate and consider the influence of all chemical and physical forces involved during the growth of crystal specimen. Still uncertainties persist, for in a solution having more than one solvent present, it may not be possible to determine which solvent adsorbs to the crystal surface and might lead to a different habit (BUCKLEY, 1951).

One suggestion to approach this problem is to separate the factors involved into an internal and external part. The internal part has been outlined in detail in the previous chapters, as the different internal factors from which “abstract forms” of a crystal can be calculated. As an example to specify external factors the bond-valence model was applied to solvents in Chapter 9.

The goal of the following chapters is two combine both aspects and predict the morphology of crystal by application of the bond-valence model.

11.1 Habit modification due to adsorption (A theoretical bond-valence approach)

In the introduction to this chapter it has been stated that adsorption of impurities is one of the most common processes to change the morphological appearance of a mineral. The question to be considered, is to which extent the BVD-model is able to describe changes in morphology due to the adsorption of impurities.

As described in previous chapters, the final morphology is a result of both internal (crystallographic) factors and external (fluid composition) factors. In Chapter 7 this was outlined in detail how internal factors (reticular density, lattice spacing and symmetry) influence the "structural" or "abstract form" of a crystal. It was shown that the internal factors can be incorporated in the BVD-model and different crystal faces can be compared in terms of the differences in their bond-valence deficiencies. Further, in Chapter 9 it is outlined how the bond-valence model can be applied to ions in aqueous solutions.

A combination of both approaches, connected by their bond-valence parameters, should lead to an applicable method to predict morphology changes induced by the adsorption of impurities. In a theoretical example we will discuss the influences of different ions adsorbing to different crystal surfaces. The crystal structure choosen is the NaCl-crystal type structure and the crystal faces of interest are (001), (110) and (111). The crystal consists of two theoretical components, A (the cation) and B an anion. The coordination number is CN = 6, a_0 = 5.0 Å and Z = 4.

In this theoretical example each bond is assigned a "theoretical" bond-valence of 0.5 vu, giving the "theoretical" ions an "atomic valence" of 3. In the first step the "structural form" of this crystal is predicted (Fig.: 11.1). This form will act as the matrix, which will interact with the different adsorbing ions. Changes in the bond-valence deficiencies due to adsorption will influence this matrix and an "abstract form" (actually a "growth form") for a certain state of adsorption will be obtained.

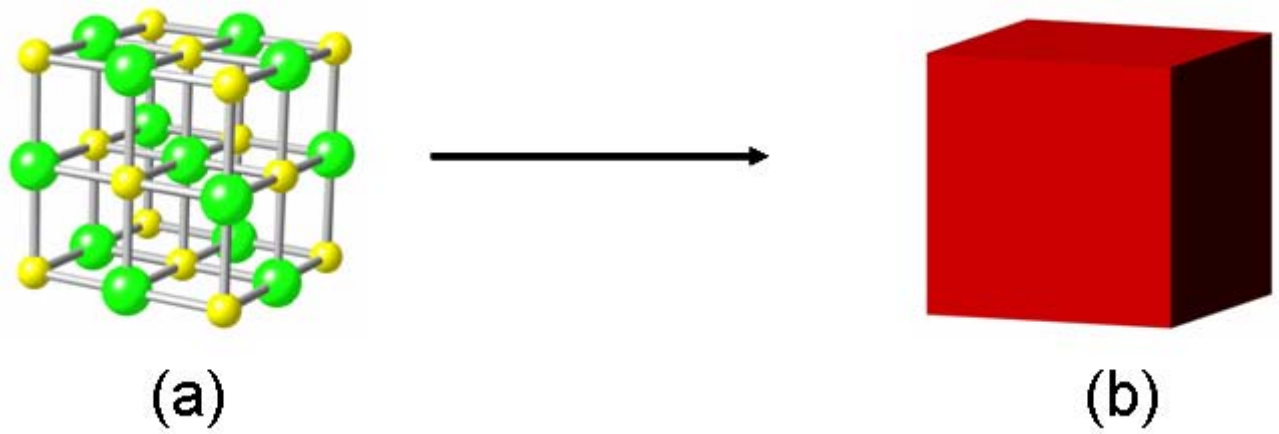

Fig.: 11.1 (a) Ball-and-stick representation of NaCl-crystal type structure. The cations (A) are represented by yellow balls, the anions (B) are represented by green balls. (b) general calculated "structural form" for the given crystal. The data set for the (100),(110) and (111) crystal faces can be taken from Fm3m-data set in Appendix III.

Having chosen an AX-crystal type, with a NaCl-structure, some special features of the faces have to be considered (Fig. 11.2 and 11.3). The (001) faces consists of an alternation of positively charges cations (A) and the negatively charged anions (B), representing a neutral surface in itself. Ions present in the solution therefore can only bond selectively to ions on the surface having an opposite charge. A similar consideration has to be taken into account for the (110) face. The (111) crystal faces consist of an alteration of positive or negative charged crystal lattices and therefore the surface holds only one sort of ion, either A (positive) or B (negative). Ions in the solution can only adsorb to this surface if they are negative (adsorption to A-layers) or positive (adsorption to B-layers).

Next the number of bonds emitted from the surfaces are different. Since ions in the (001)-face have 5 neighbors, only one bond of 0.5 vu can be donated to the surrounding solution. Ions on the (110)-crystal surface, only have 4 neighbors and can emit either two bonds (2 x 0.5 vu) or one stronger bond with a maximum valence of 1.0 vu.
The ions on the (111)-face are only bonded to three ions in the crystal and can emit three bonds (3 x 0.5 vu) to the ions in the solution. Two bonds having (2 x 0.75 vu) are as well possible as one bond with a maximum bond-valence of (1.5 vu).

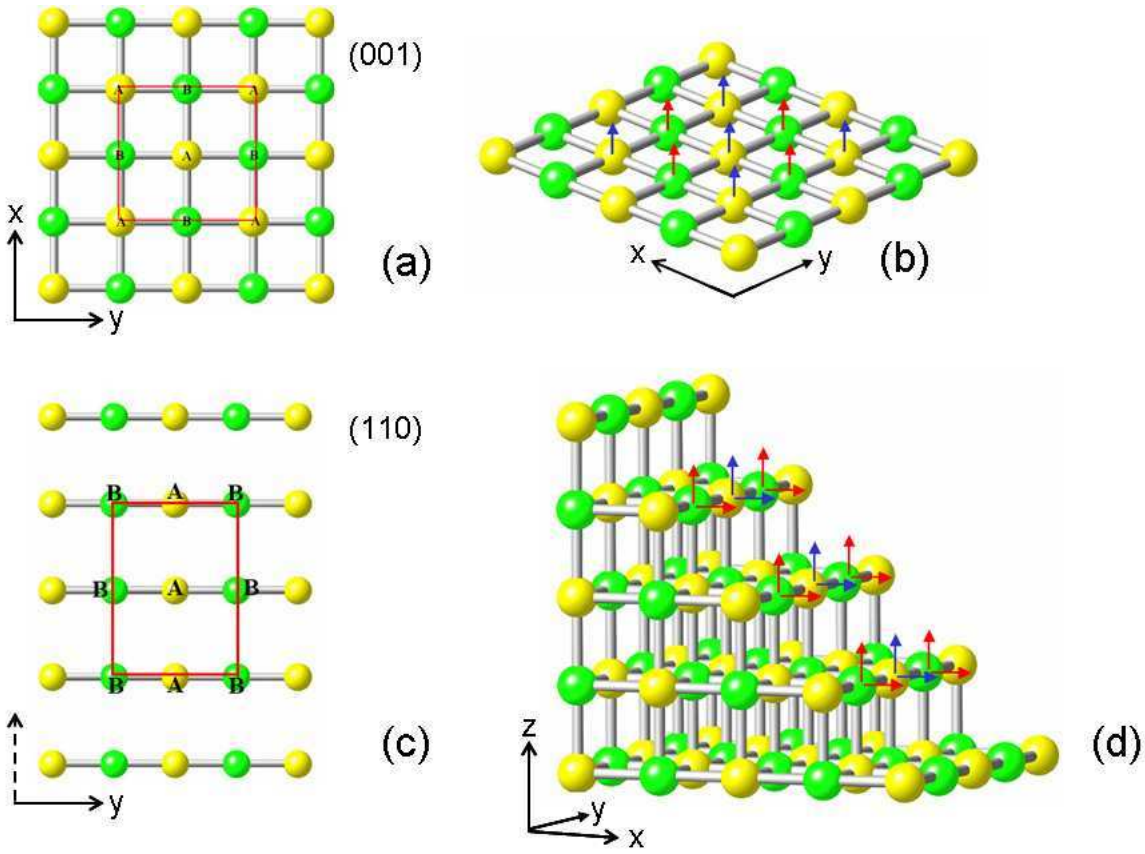

Fig.: 11.2 Shown are different views of a NaCl cyrstal structure. The cations "A" are given as yellow balls, the anions "B" as green balls. (a) Ball-and-stick model of a (001)-crystal lattice (Top view), showing the alteration of positive and negative charged ions. The contour of the corresponding unit-cell is marked red. (b) Side view of the (001) crystal lattice. The number of bonds (dangling bonds) emitted by the surface ions are marked with arrows (red = negative; blue = positive). (c) View perpendicular to a (110) crystal lattice. (d) Side view of a (110) crystal lattice. The number of bonds emitted by the ions present in the unit-cell are given by arrows. The actual number of bonds emitted by the surfaces of unit-cell dimension has to be corrected to the number of ions present in the unit-cell.

Having regard to the unit-cell dimension of the corresponding crystal faces, calculated differences in the number and sort of ions adsorbing to the surface, until all bonds are satisfied, must be considered. The (001) unit-cell can at maximum form 4 bonds, two of which are positive and two being negative. Therefore cations and anions as well are able to adsorb to the surface. Presumably the bond-valences of the bonds that formed match the bond-valences of the bonds emitted by the surface.

The (110)-unit cell can extend up to 8 bonds to the solvents in the solution, half of them being positive, the others negative. This is equivalent to two positive and two negative bonds (2 x 0.75), for each ion present on the surface forming only one bond. Similar to the (001)-face, cations and anions alike can be adsorbed to the (110)-crystal surface.

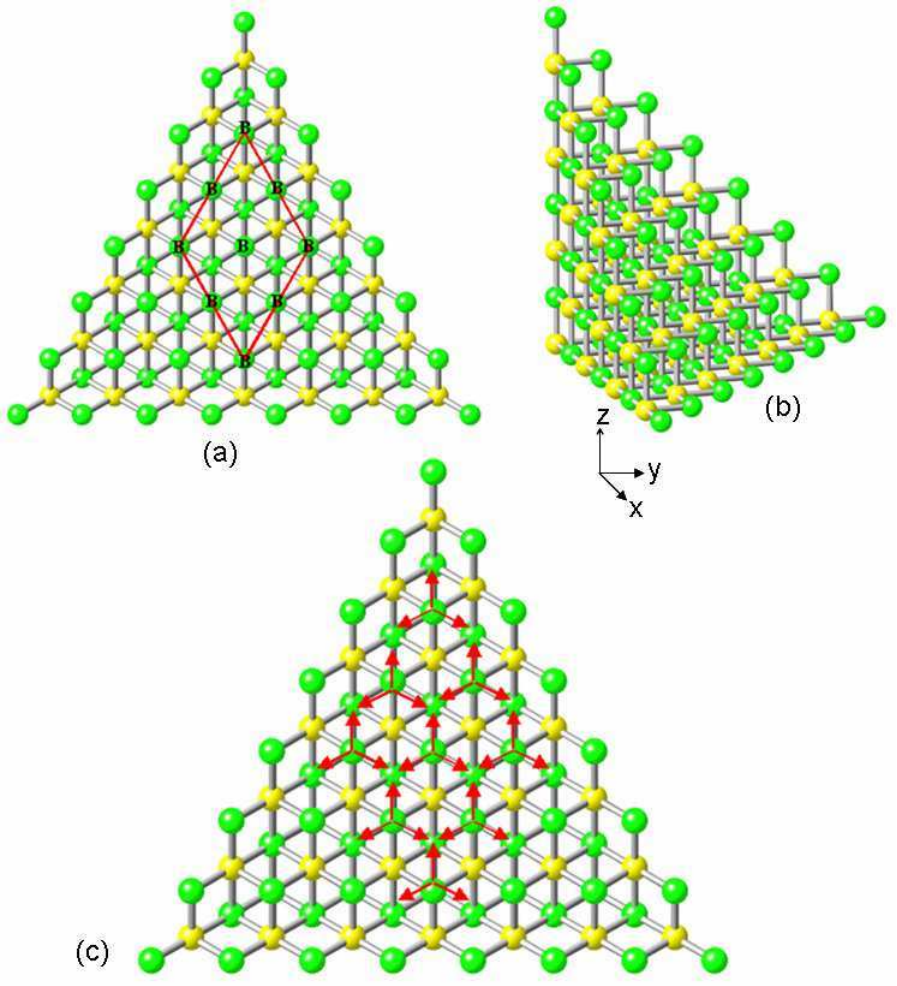

Fig.: 11.3 Ball-and-stick model of a (111) crystal lattice having a NaCl-crystal type structure. Cations "A" are given as yellow balls, the anions "B" as green balls. (a) Given is a (111)-crystal lattice terminated only by anions "B", the contour of the unit-cell is marked by red lines. (b) Side view of the (111)-crystal lattice showing the stepped topology of the surface. (c) Marked with red arrows are the dangling bonds emitted by the ions of the unit-cell given. The number of bonds calculated for the (111)-surface of unit-cell size has to be corrected to the number of the four ions present in the unit cell. The unit-cell will at maximum emit 4 x 3 = 12 bonds.

The unit-cell of the (111) surface, having Z = 4, can emit 12 bonds at maximum, three for each of the four ions present, and at minimum only 4 bonds can be emitted to the solvents in the solution. All bonds from the surface to the solution are charged equally , either positive or negative, and therefore the surface will only accept ions from the solution having an opposite charge.

Now we need to consider the ions (impurities) that will adsorb to the crystal faces. In nature the variations that will occur are numerous, as the ions can vary in their charge, the strength and number of the bonds they form (Fig. 11.4), their concentration and in the number of different sorts of ions or molecules present. As a consequence we have to be selective and only six case studies, covering a few of the possible variations will be given in detail.

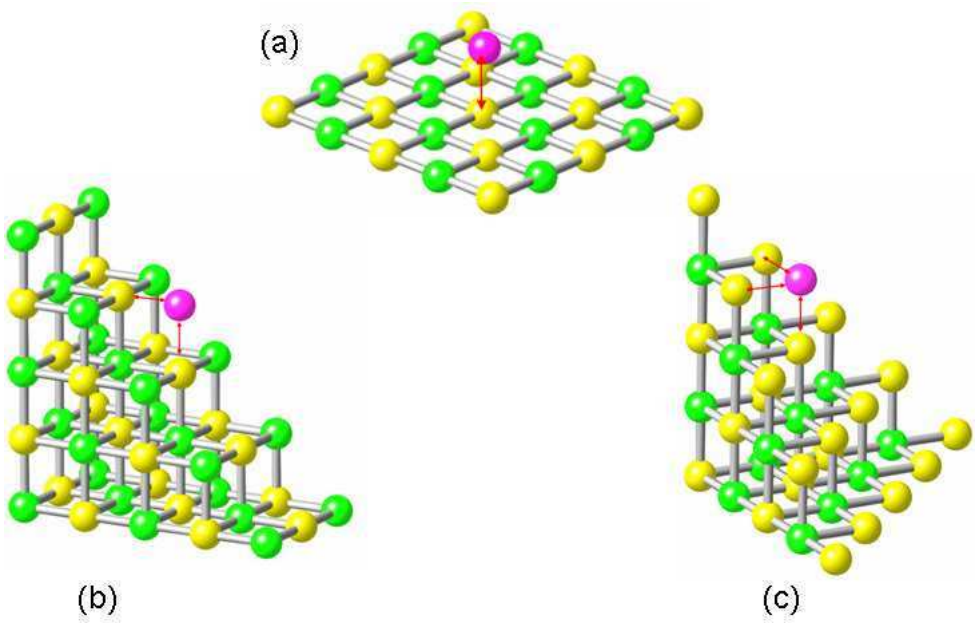

Fig.: 11.4 Ball-and stick representation of the topology of a (001), (110) and (111) crystal lattice having a NaCl-crystal type structure. Cations "A" are given as yellow balls, the anions "B" as green balls. In pink an anion attaching to these surfaces is shown. The number of bonds formed is marked with red arrows. (a) (001) crystal surface, the adsorbing anion attaches by forming one bond to a cation of the surface. (b) (110) crystal surface, an anion adsorbing to this crystal lattice can form up to two bonds to two different cations of the surface. (c) An anion absorbing to the (111) crystal lattice may form up to three bonds to three different cations of the surface.

Last we have to consider the adsorption of the impurities. The adsorption is assumed to be temporary. While adsorbed, the foreign ion, atom or molecule influences the growth of the corresponding surface, but the impurity is not considered to be incorporated into the crystal structure during the further growth of the crystal. Ions adsorbing to the surface will lower the bond-valence deficiency and therefore inhibit to some extent the growth process, giving rise to possible changes of the crystal morphology.
An increase in the concentration of the impurity is illustrated by increasing amounts of ions adsorbing to the surface, up to the extent that all bonds that are emitted by the crystal surface are connected to the ions adsorbing to the surface.

The examples considered are listed below as different case studies. In the first example (Case 1) the whole BVD-calculation will be given in detail (Tab.: 11.1), while for the other examples only the results and the predicted "growth forms" will be given. The calculations for the case-studies 2-6 are given in Appendix III.

Case 1.: Only one sort of ion, charged positive (or negative) present in the mother liquid will interact with the surface of the crystal (Fig.11.4), adsorbing only to ions of opposite charge. The valence value of the bonds to be formed to the crystal surfaces is 0.25 vu, being therefore lower than the bonds of the crystal (0.5 vu) itself. The number of bonds that can be formed by the ion is taken to be independent from its coordination number and can range in our examples from one bond to up to three bonds, each of which has a bond-valence of 0.25 vu.

In Table 11.1 the bond-valence deficiencies of the crystal faces (001),(110) and (111) of the theoretical crystal having a NaCl-crystal type structure,a_0 = 5.0 Å, CN = 6 and Z = 4 are given. The first data-set represents the calculation of the abstract form, regarding the internal factors, reticular density (RD), lattice density (LD), face symmetry (ω) and the site-symmetry (Z), only. The intermediate results of the bond-valence deficiency calculations are given as BVDU*,BVDU** and BVDU***. The final bond-valence deficiency including all internal factors is given as ΔBVDU.

The hexahedron shape of the calculated "abstract form" is given in Figure (11.1). Labeled I-IV are different adsorption steps, indicating an increasing amount of ions (1-4) adsorbed to the crystal lattice. In the case of the faces (001) and (110) no further adsorption is to be calculated after step II. All corresponding positions for a charged ion to adsorb are occupied. In the case of the charged (111) surface two more ions (III-IV) of opposite charge to the surface, may adsorb, and the bond-valence deficiency of this face is further lowered. The calculated "abstract forms", now to be addressed as "growth forms" are given in Fig. 11.5.

Face	BVD	Area (Å²)	BvD/ Å²	RD	BVD*	LD	BVD**	ω	BVD***	Z	ΔBVD
(001)	2	25,00	0,08	2	0,16	2	0,32	8	0,04	4	0,16
(110)	4	35,35	0,11	2	0,23	4	0,91	4	0,23	2	0,45
(111)	6	43,30	0,14	1	0,14	6	0,83	6	0,14	3	0,42
I.											
(001)	1,75	25,00	0,07	2	0,14	2	0,28	8	0,04	4	0,14
(110)	3,5	35,35	0,10	2	0,20	4	0,79	4	0,20	2	0,40
(111)	5,25	43,30	0,12	1	0,12	6	0,73	6	0,12	3	0,36
II.											
(001)	1,5	25,00	0,06	2	0,12	2	0,24	8	0,03	4	0,12
(110)	3	35,35	0,08	2	0,17	4	0,68	4	0,17	2	0,34
(111)	4,5	43,30	0,10	1	0,10	6	0,62	6	0,10	3	0,31
IIII.											
(001)	1,5	25,00	0,06	2	0,12	2	0,24	8	0,03	4	0,12
(110)	3	35,35	0,08	2	0,17	4	0,68	4	0,17	2	0,34
(111)	3,75	43,30	0,09	1	0,09	6	0,52	6	0,09	3	0,26
IV.											
(001)	1,5	25,00	0,06	2	0,12	2	0,24	8	0,03	4	0,12
(110)	3	35,35	0,08	2	0,17	4	0,68	4	0,17	2	0,34
(111)	3	43,30	0,07	1	0,07	6	0,42	6	0,07	3	0,21

Tab.: 11.1 Calculation of the bond-valence deficiencies for the (001), (110) and (111) crystal surfaces of case study 1 (explanations see text). The first data-set represents the calculated "abstract form". Labeled I-IV are the different adsorption steps. The bond-valence values (BVD) have been calculated by multiplication of the number of dangling bonds and the theoretical bond-valences (0.5 vu) for one single bond. (further explanation see text).

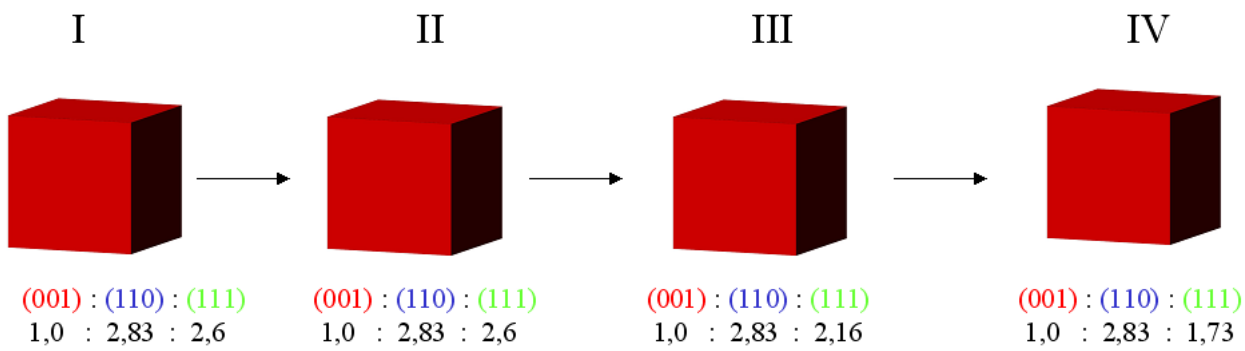

Fig.:11.5 Sequence of "growth forms" of a crystal having a NaCl.-type crystal structure. The labels I-IV correspond to the different amount of ions adsorbed to these surfaces in reference to the maximum number of ions adsorbed to the (111) crystal surface (see text). The surfaces (100), (110) and (111) are indicated by different colors (red, blue green) and the ratios of the bond-valence deficiencies are given in numbers below the images.

Figure (11.5) and Table (11.1) illustrate that due to the adsorption of ions to the crystal surfaces the bond-valence deficiencies of the faces is lowered. But the impact to the "growth form" is only minor. This is due to the low bond-valence contribution of the ion (0.25 vu/per bond) to the crystal surface. The bond-valence deficiency of the crystal faces (110) and especially (111) is lowered, as well as is the bond-valence deficiency of the (100) crystal surface. In this example the decrease in the bond-valence deficiency, corresponding to a slow-down of the relative growth rate of the crystal faces has no effect on the final shape of the "growth form". The decrease in the "growth rate" (bond-valence deficiency) of the (111) crystal face is not enough compared to the decrease of the "growth rate" of the (001) crystals lattice and has no visual effect on the final shape of the calculated "growth form". As a result we can state that the adsorption of only one sort of charged ion, contributing weak bonds to a crystal surfaces of a crystal having a NaCl-type crystal structure, does influence the relative growth rate of the crystal, but does not change the overall morphology of the abstract form" predicted for this crystal type.

Case 2.: Two sorts of ions are present in the solution. One being a cation, the other being an anion. The bond-valences of one bond formed by these ions to the crystal surfaces is 0.25 vu and the number of bonds that can be donated can vary between one and three. In this case all ions (cations and anions) present on the crystal surfaces can form bonds to the ions of opposite charge in the solution

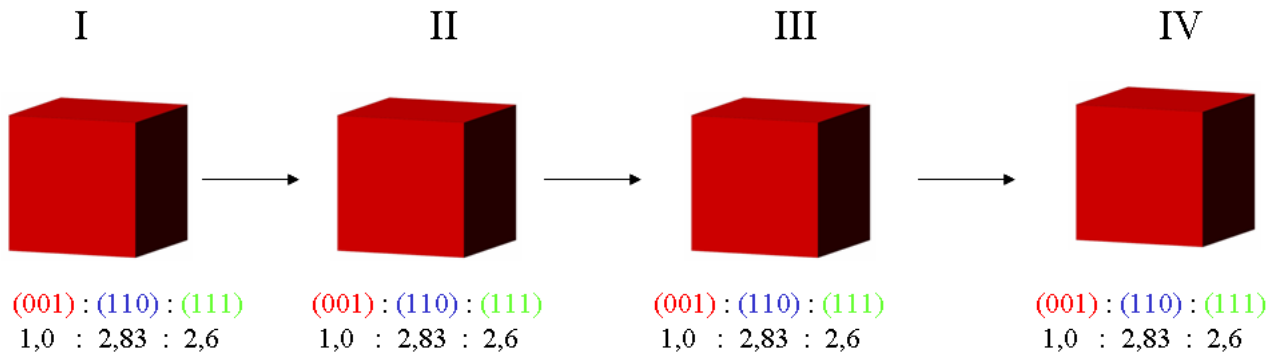

Fig.: 11.6 Sequence of "growth forms" of a crystal having a NaCl.-type crystal structure. The labels I-IV correspond to an increasing amount of ions adsorbed to these surfaces (see text). The surfaces (100), (110) and (111) are indicated by different colors (red, blue green) and the ratios of the bond-valence deficiencies are given in numbers below the images

In this example (Fig. 11.6) cations and anions present in the solution can adsorb to an maximum extent to the crystal surfaces. As a consequence the bond-valence deficiencies of the faces (100), (110) and (111) are lowered to a similar extent. The relative ratios of the bond-valence deficiencies of these faces, given in Fig. 11.6 does not change. As a result we can state that that the adsorption of cations and anions both contributing weak bonds to the crystal surfaces alike will not change the morphology of

the “growth forms” compared to the abstract form” predicted. Still a decrease in the relative growth rate can be observed (compare Tables given in Appendix III).

Case 3.: Similar to case 1, only one sort of charged ion present in the solution, either being charged positive or negative, will interact with the crystal surface. It may form one, two or three bonds to the crystal surface, but each of the bonds has a bond-valence value of 0.6 vu, therefore being stronger than the bonds formed by the crystal itself.

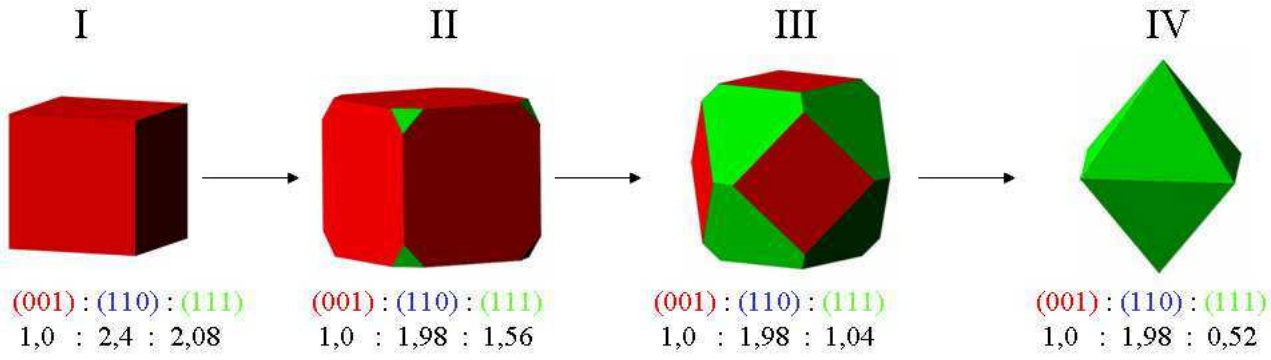

Fig.: 11.7 Sequence of “growth forms” of a crystal having a NaCl.-type crystal structure. The labels I-IV correspond to an increasing amount of ions adsorbed to these surfaces (see text). The surfaces (100), (110) and (111) are indicated by different colors (red, blue green) and the ratios of the bond-valence deficiencies are given in numbers below the images.

In this example illustrated in Fig. 11.7 the influence of ion adsorbing to the different crystal faces is evident, compared to the examples 1 and 2. The major difference is the different amount of bonds formed between the ion and the crystal surfaces. As the ion in the solution contributes at least a bond-valence of 0.6 *vu* to the ions of the surface, no bonds will be formed between the ions terminating the (100) surface and the ions of the solution, because the surface ions accept only bonds of 0.5 *vu*. The (110) crystal surface will accept bonds from ions of the solution, having an opposite charge. But, instead of

forming two bonds, as in the examples 1 and 2 only one bond of 0.6 *vu* is formed. This is due to the bond-valence deficiency of the ions termination the (110)-crystal surface. These ions, will at maximum accept a bond valence of 1.0 *vu*, as a result only one bond of a bond-strength of 0.6 *vu* can be accepted. A similar situation has to be taken into account for the charged (111) crystal surface. Instead of three bonds only two bonds can be formed between the surface and an ion of opposite charge in the solution.

The influence of ions contributing bonds of a higher bond-valence to the crystal surface can be clearly estimated from Figure. 11.7. As the "concentration"(amount of adsorbing ions) of these ions in the solution increases, their selective adsorption to the different crystal faces leads to a change in the habit of the crystal growing in such an environment.

Case 4.: In this case again two sorts of ions, a cation and an anion, are present in the solution. They may form up to three bonds to the crystal surface each of which has a bond-valence of 0.6 vu and therefore being stronger than the single bonds formed by the ions in the crystal themselves.

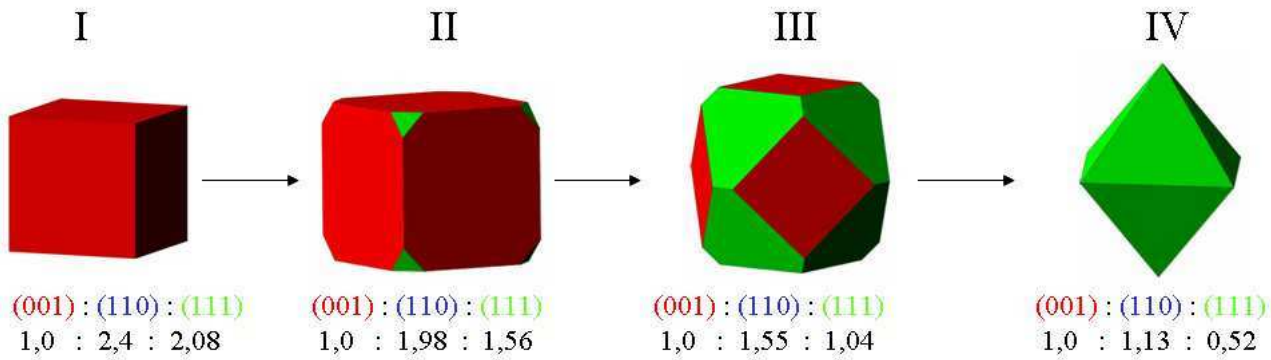

Fig.: 11.8 Sequence of "growth forms" of a crystal having a NaCl.-type crystal structure. The labels I-IV correspond to an increasing amount of ions adsorbed to these surfaces (see text). The surfaces (100), (110) and (111) are indicated by different colors (red, blue green) and the ratios of the bond-valence deficiencies are given in numbers below the images.

The sequence of "growth form" has not changed much compared to example 3. The amount of possible bonds formed is similar. Only the bond-valence deficiency of the (110)-cyrstal surface can be lowered further as now both sort of ions of the surface, cations and anions alike will form one bond to ions of opposite charge in the solution. Even the bond-valence can be lowered further (see ratios given in Figure 11.8, or the Table given in Appendix III), the influence is not strong enough to have an effect on the changing morphology of the "growth form" compared to the low growth rate exhibited by the (111) crystal surface.

Case 5.: This case resembles the adsorption of a highly charged ion, again either being positive or negative charged. The bonds donated by this ion to the crystal surface are much stronger, having a bond-valence of 0.9 vu. Again, up to three bonds will be assumed to be possible.

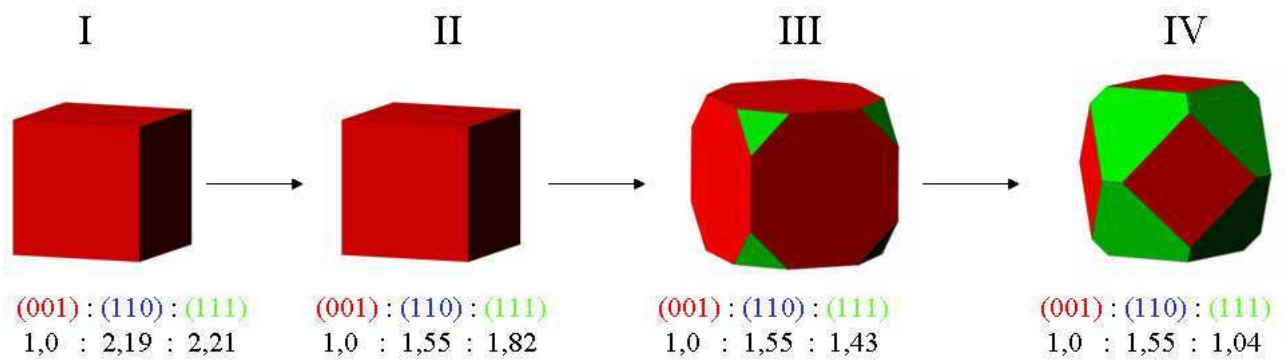

Fig.: 11.9 Sequence of "growth forms" of a crystal having a NaCl.-type crystal structure. The labels I-IV correspond to an increasing amount of ions adsorbed to these surfaces (see text). The surfaces (100), (110) and (111) are indicated by different colors (red, blue green) and the ratios of the bond-valence deficiencies are given in numbers below the images.

Increasing the bond-valence contribution of one sort of ion to the crystal surfaces still changes the morphology of the "growth forms" compared to the "abstract form", but the tendency to favor the (110) and (111) crystal lattice compared to the (100) as indicated in example 4 is not to be continued (see Appendix III). This is due to the strong bonds formed. Even though one individual bond having a bond-strength of 0.9 *vu* lowers the bond-valence deficiency to a much greater extent than one single bond having a bond-strength of 0.6 *vu*, the influence is compensated by the decreasing number of bonds that can be formed between the crystal surfaces and the ions in the solution. No bonds are formed between the ion and the (001) and crystal surfaces because there is no match between the maximum bond-strength of the individual ions of the surface and the bond-strength contributed by the ion of the solution. Only one bond for each ion of opposite charge is formed by the ions of the (110) and (111) crystal surface, as they can accept bond-valences of up to 1.0 *vu* (110) and 1.5 *vu* (111).

This example indicates clearly the influence of the internal crystal structure to the final morphology of the crystal. By increasing the strength of the bonds formed from ions in solution to the crystal surface, the decrease in the bond valence deficiency of the surface is limited by the number of bonds (and their respective bond valences) that can be accepted by the ions of the crystal surface.

This example further demonstrates the competition between the influence of internal factors and external factors. The internal factors are responsible of the surface topology of the different faces, controlling the number and strength of bonds that can be formed by the surface terminating ions, at the same time setting the limits to which extent the external factors (in this case a foreign ion) can interact with the different crystal surface.

Case 6.: This last example considers the adsorption of two differently charged ions (positive and negative). Similar to case 5, each of these ions can form up to three bonds each of which has a bond strength of 0.9 vu.

The growth sequence given in Figure 11.10, illustrates the influence of ions adsorbing to the crystal surface, changing the habit of the crystal exhibited during growth. The interaction between the surface ions and the ions in solution is similar to example 5, but the presence of positive and negative charged ions in the solution compensates for the selective adsorption onto the (111) crystal surface. Now the growth rate of the (110) crystal surface is lowered to a far greater extent, due to the acceptance of bonds from both sorts of ions present in the solution.

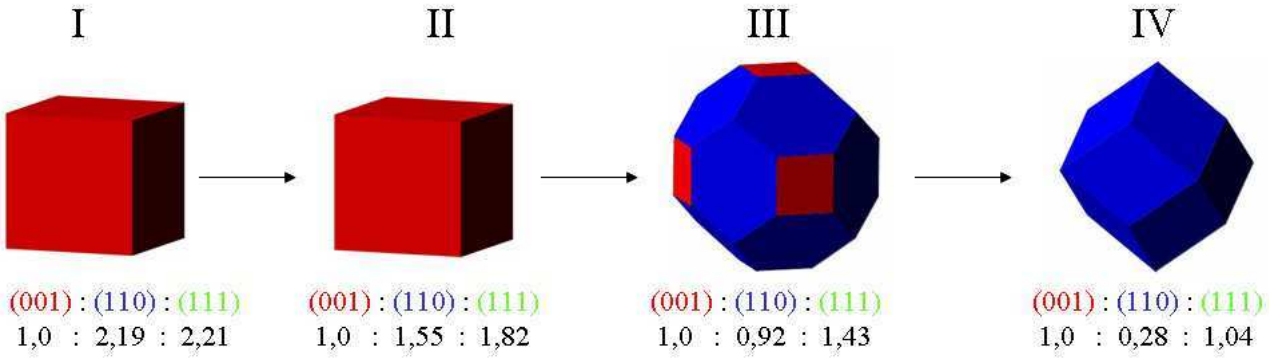

Fig.: 11.10 Sequence of "growth forms" of a crystal having a NaCl.-type crystal structure. The labels I-IV correspond to an increasing amount of ions adsorbed to these surfaces (see text). The surfaces (100), (110) and (111) are indicated by different colors (red, blue green) and the ratios of the bond-valence deficiencies are given in numbers below the images.

As a final remark to this chapter we can state, that in the examples given, it was shown that the BVD-model is capable not only to predict the "abstract forms" of crystal, but is also capable of being applied to account for the influence of external factors (ions/atoms or molecules) on the morphology of crystals. This result has been obtained by expressing the influence of internal factors and external factors via their respective bond-valence parameters. The combination of both contributions, the internal factors controlling the "matrix" of the crystal, and the external factors "shaping" this matrix , finally leads to a crystal growth model which is capable of considering both aspects present during crystal growth .

11.2 Habit changes of sylvite in the presence of Pb^{2+} ions (An example)

Similar to the investigation of magnetite (Chapter 8.4.1.1), the applicability of the BVD-model to predict habit changes, and thus the morphology of crystals during growth, in presence of foreign ions can be tested by comparing the obtained bond-valence data to experimental results given in literature.

Face	BVD	Area (Å²)	BvD/ Å²	RD	BVD*	LD	BVD**	ω	BVD***	Z	ΔBVD
(001)	0,7400	40,70	0,02	2	0,04	2	0,07	8	0,009	4	0,0364
(110)	1,3920	57,56	0,02	2	0,05	4	0,19	4	0,048	2	0,0967
(111)	2,0440	70,52	0,03	1	0,03	6	0,17	6	0,029	3	0,0870
I.											
(001)	0,572	40,70	0,01	2	0,03	2	0,06	8	0,007	4	0,0281
(110)	1,056	57,56	0,02	2	0,04	4	0,15	4	0,037	2	0,0734
(111)	1,54	70,52	0,02	1	0,02	6	0,13	6	0,022	3	0,0655
II.											
(001)	0,404	40,70	0,01	2	0,02	2	0,04	8	0,005	4	0,0199
(110)	0,72	57,56	0,01	2	0,03	4	0,10	4	0,025	2	0,0500
(111)	1,036	70,52	0,01	1	0,01	6	0,09	6	0,015	3	0,0441
III.											
(001)	0,404	40,70	0,01	2	0,02	2	0,04	8	0,005	4	0,0199
(110)	0,72	57,56	0,01	2	0,03	4	0,10	4	0,025	2	0,0500
(111)	0,532	70,52	0,01	1	0,01	6	0,05	6	0,008	3	0,0226
IV.											
(001)	0,404	40,70	0,01	2	0,02	2	0,04	8	0,005	4	0,0199
(110)	0,72	57,56	0,01	2	0,03	4	0,10	4	0,025	2	0,0500
(111)	0,028	70,52	0,00	1	0,00	6	0,00	6	0,00	3	0,0012

Tab.: 11.2 Bond-valence deficieny calculation of sylvite in the presence of Pb^{2+} impurities. The top lines represent the bond-valence deficiency values of the abstract form. Labeled I – IV are different adsorption stages. At stage I, one Pb^{2+} ions is adsorbed to all surfaces calculated. At stage II, two Pb^{2+} ions are adsorbed. At stage III and IV all possible adsorption positions are occupied for the (100) and (110) surface and additional Pb^{2+} are adsorbing only to the (111) crystal surfaces. Three Pb^{2+} ions at stage III and four

Pb^{2+} ions at stage IV, further decreasing the bond-valence deficiency of this respective crystal surface.

LIAN et al. (1990) investigated habit changes of growing KCl-crystals in aqueous solutions in the presence of Pb^{2+} impurities. The authors observed a change from the cubic to the cube-octahedral and finally to the octahedral from exhibited by the KCl-crystals, as the concentration of the Pb^{2+} ions in the solution was increased.

A similar *ab initio* experiment can be calculated by application of the Bond-valence deficiency model. Based on the ionic radius of K^+ and Cl^- reported by SHANNON (1979), the bonds valences of the K-Cl bond have been calculated as 0.163 *vu* for a K-Cl bond-length of 3.19 Å. According to these values a_0 value to calculate the surface area of unit size increase slightly to a_0 = 6.38 Å. The bond-valence value of the Pb^{2+} - Cl^- bonds, was taken to be 0.168 *vu*, assuming that the Pb^{2+} ions will be at similar equal distance apart from the Cl^- ions as the K^+ ions. The values so obtained are summarized in Table (11.2) and the development of the crystal faces is shown in Figure (11.11). The bond-valences calculated have been obtained by application of the "Bond-Valence calculator" provided on the internet-page: kristall.uni-mki.gwdg.de/softbv .

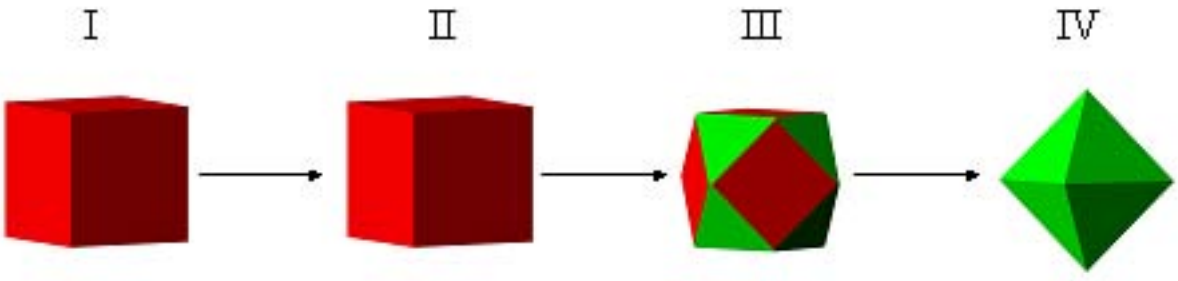

Fig.: Calculated development of different habits of sylvite crystals in the presence of increasing amounts Pb^{2+} impurities. The roman letters correspond to the different adsorption stages listed in Table 11.2.

The results obtained can be compared to the results stated by LIAN et al. (1990) and a similar habit change from a cube to an octahedral morphology can be noticed. Similar to the theory described in Chapter (11.1), only certain stages are monitored by the given bond-valence approach and are representative for the given bond-lengths. Different results will be obtained, if for example, the bond-length between the adsorbing Pb^{2+} ions and the Cl^- ions will be decreased and thus the bond-valence values will be increased. For this case it can be assumed that the growth rate of the {111}- crystal surfaces will be lowered and at the same time their morphological importance will be increased.

12 Concluding Remarks

The previous Chapters have outlined in detail the capability of the Bond-valence deficiency model (BVD-model) to be a useful method ready to be applied in Mineral Surface Science.

It was demonstrated that the contribution of internal and external factors, both having influence on the crystal morphology of a mineral, can be described by the relative bond-valence deficiencies of a crystal surfaces before and after a reaction between the crystal and a solution has occurred.

One of the major advantages of the BVD-model is its ease of use. Bond-valences can easily be assigned to atoms or ions, no matter if they are located in the crystal bulk structure, the crystal surface or the solution interacting with the mineral surface. Any changes in the crystal structure, at the crystal surface or the solution will change the respective bond-valence values, and these changes can be monitored by the changing bond-valence deficiencies calculated.

However, this approach cannot substitute for modern thermodynamic computer simulations, which are able to consider even minute changes in the potential energies of two or more interacting atoms. The BVD-model has proven to be applicable if such changes can be detected as variations in the lengths of bonds formed, as these changes will have an influence on the bond-valence values to be considered.

Therefore it seems practicable to consult the BVD-model as a method to be used prior to computer simulations, as the BVD-model can well distinguish and differentiate between the most common attributes of a crystal surface. In this sense the BVD-model can be applied as a first obstacle to be mastered before the decisions about more time and money consuming investigations is taken.

As more and more research is done to refine bond-valence values (Chapter 4.5), such as to incorporate the influences of the electronegativity of bonding partners, the effectiveness of the BVD-model to describe mineral surface reactions will increase. These advancements will definitely increase the accuracy of the bond-valence model, but the calculations necessary to describe mineral surface reactions are kept at the same manageable level, as all refinements will find their expression in values expressed in bond-valence values, readily to be incorporated into the Bond-valence deficiency model outlined in this script.

References

ADAMS, S. : Relationship between bond valence and bond softness of alkali halides and chalcogenides. Acta Cryst., B Vol. 57, pp. 278-287 ; (2001).

BAILEY, E.H, MOSSELMANS, J.F.W. & SCHOFIELD, P.F.; Uranyl acetate speciation in aqueous solutions – An XAS study between 25°C and 250°C. Geochim. Cosmochim. Acta, Vol. 68, No. 8. pp. 1711-1722; (2004).

BARBIERI, A., WEISS, W., HOVE M.A. van & SOMORJAI, G.A. : Magnetite Fe_3O_4 (111): surface structure by LEED crystallography and energetics. *Surface Science*, Vol. 302, pp. 259-279 ; (1994).

BENNEMA, P., & GILMER, G.H.: Kinetics of Crystal Growth. In" *Crystal Growth: An Introduction"*; P. Harman, ed., North-Holland, Amsterdam (1973).

BENNEMA, P. : Morphology of crystals determined by α factors, roughening temperature, F faces and connected nets. J. Phys. D: Appl. Phys., Vol 26, B1-B6. (1993).

BENNEMA, P; BÖGELS, G.; BOLLEN, D.; MÜSSIG, T. & MEEKES, H.: Crystal surfaces and crystal growth mechanisms: application to crystals having the NaCl structure and especially silver hailde crystals. Imaging Science Journal, Vol. 49, No. 1, pp. 1-32; (2001).

BICKMORE, B.R.; ROSSO, K.M., TADANIER, C.J., BYLASKA, E.J. & DOUD, D.: Bond-valence methods for pK_a prediction. II. Bond-vaelnce, electrostatic, molecular geometry and salvation effects. Geochimica et Cosmochimica Acta, Vol. 70, pp. 4057-4071; (2006).

BINNEWIES, M, JÄCKEL, M., WILLNER, H. & RAYNER-CANHAM, G.: Allgemeine und Anorganische Chemie. Spektrum Akademischer Verlag. (2004).

BOISTELLE, R. & ASTIER, J.P.: Crystallization mechanisms in solution. J. Crytsal Growth, Vol. 90, pp. 14-30; (1988).

BRADISTILOV, G. & STRANSKI, I.N.: Über die Gleichgewichtsform des Fluoritkristalls. Z.Krist., Vol. 103, pp. 1-29; (1941).

BRAVAIS, A.: *Études Crystallographiques*, Gauthier-Villars, Paris (1866).

BROWN, I.D. : On the geometry of O-H ··· O hydrogen bonds. Acta Cryst., A Vol. 32, pp. 24-31; (1976a).

BROWN, I.D.: The Bond-Valence method: An empirical approach to chemical structure and bonding. In "Structure and Bonding in Crystals". O´KEEFE & NAVROTSKY (eds.); (1981).

BROWN, I.D.: The chemical bond in inorganic chemistry. Oxford Press, (2002).

BROWN, I.D. & SHANNON, R.D. : Empirical bond-strength - bond-length curves for oxides. Acta Cryst., A Vol. 29, pp. 226-282; (1973).

BUCKLEY, H.E. : Crystal Growth. New York. John Wiley & Sons, (1951).

BURNS, P.C., GRICE, J.C. & HAWTHORNE, F.C.,: Borate minerals. I. Polyhedral clusters and fundamental building blocks. Can. Min., Vol. 33, pp. 1131-1151; (1995).

BURNS, P.C.: The crystal chemistry of uranium. In "Uranium". BURNS, P.C. & FINCH. R (eds.); Reviews in Mineralogy Vol. 38, (1999).

BURNS, P.C., FINCH, R.J., HAWTHORNE, F.C., MILLER , M. L. & EWING, R.C.: U^{6+} minerals and inorganic phases: a comparison and hierarchy of structures. Can. Min., Vol. 34, pp. 845-880; (1996).

BURNS, P.C.: The crystal chemistry of hexavalent uranium: polyhedron geometries, bond-valence parameters, and polymerization of polyhedra. *Can.Min.*, Vol. 35, pp. 1551-1570; (1997).

BURNS, P.C.: The structure of compreignacite, $K_2[(UO_2)_3O_2(OH)_3]_2(H_2O)_7$. *Can. Min.*, Vol. 36, pp. 1061-1067; (1998).

BURTON, W.K., CARBRERA, N. & FRANK, F.C.: The Growth of crystals and the Equilibrium structure of their surfaces. Phil. Trans. Roy. Soc., Vol. A 243; pp. 2399-358; (1955).

CURIE, P.: On the formation of crystals and on the capillary constants of their different faces. J. Chem. Edcn., Vol. 47, 1970, pp. 636-637 (translation of: Bull Soc. Franc. Min. Cryst., Vol. 8, pp. 145-150; (1885)

CURIE, P.: Über die Bildung der Krystalle und die Capilaritätsconstanten ihrer verschiedenen Flächen. Z. Krist. Vol. 12, pp. 651; (1887).

DANA`S NEW MINERALOGIE, 8th-edition: Editors: GAINES, R.V., SKINNER, H.C.W., FOORD, E.E, ROSENZWEIG A., KING, V.T. & DOWTY, E. Wiley & Sons, New York; (1997).

DAWSON, J.K., WAIT, E., ALCOCK, K. & CHILTON, D.R.: Some aspects of the system uranium trioxide – water. J. Chem. Soc. (London), pp. 3531 – 3540; (1956).

DONNAY, J.D.H. & HARKER, D. : A new law of crystal morphology extending the law of Bravais. Am. Min., Vol. 22, pp.446-467; (1937).

DZOMBAK, D.A. & MOREL, F.M.M.: Surface Complexation Medeling; Hydrous Ferric Oxide (J.Wiley and Sons ed. 1990): *In* STUMM, W.: *Chemistry of Solid-Water Interface*. John Wiley & Sons, New York, (pp. 428); (1992).

ENCKEVORT, W.J.P. van & BENNEMA, P. : Interlacing of growth steps on crystal surfaces as a consequence of crystallographic symmetry. Acta Cryst, Vol. A 60, pp. 532-541 ; (2004).

FAURE, G.: *Principles and Applications of Geochemistry* (2nd ed.) Prentice Hall, Upper Saddle River. New Jersey. (1998).

FINCH, R.J., COOPER, M.A., HAWTHORNE, F.C. & EWING, R.C.: The crystal structure of schoepite, [(UO2)8O2(OH)12](H2O)12. Can. Min., Vol. 34, pp. 1071-1088; (1996).

FINCH, R.J. & HAWTHORNE, F.C.: Structural relations among schoepite, metaschoepite and "dehydrated schoepite". Can. Min., Vol. 36, pp. 831 – 845; (1998).

GAUSS, C.F.: Principia Generalia Theoriae Figurae Fluidorum. Comment. Soc. Regiae Scient.Gottingensis Rec. 7 (1830). (Reprinted as: Grundlagen einer Theorie der Gestalt von Flussigkeiten im Zustand des Gleichgewichtes in Ostwald's Klassiker der Exakten Wissenschaften, Vol. 135, W. Engelmann, Leipzig, 1903.*Werke*, Vol. 5, pp.530; (1830).

GIBBS, J.W.: On the equilibrium of heterogenous substances. Trans. Con. Acad., Vol.3, pp. 343-542; (1878).

GIBBS, J.W.: The equilibrium of heterogeneous substances. Scientific Papers, (1906)

GIBBS, G.V., COX, D.F., ROSSO, K.M., KRIFEL, A., LIPPMAMM, T., BLAHA, P. & SCHWARZ, K. : Experimental and theoretical bond critical point properties for model electron denisty distributions for earth materials. *Phy. Chem. Minerals*, Vol. 32, 114-125, (2005).

HARTMAN, P.: Über die Gleichgewichtsform einiger Ionenkristalle. N. Jahrbuch f. Mineralogie, Monatshefte, pp. 73-84; (1959).

HARTMAN, P. & PERDOK, W.G. : On the realations between structure and morphology of crystals I. Acta. Cryst., Vol. 8, pp. 49-52 ; (1955a).

HARTMAN, P. & PERDOK, W.G. : On the realations between structure and morphology of crystals II. Acta. Cryst., Vol. 8, pp. 521-524 ; (1955b).

HARTMAN, P. & PERDOK, W.G. : On the realations between structure and morphology of crystals III. Acta. Cryst., Vol. 8, pp. 525-529 ; (1955c).

HARTMAN, P. & PERDOK, W.G. : An interpretation of the Law of Donnay and Harker. Am.Min., Vol. 41, pp. 449-459; (1956).

HAWTHORNE, F.C. : Structural hierarchy in $^{VI}M_x^{III}T_y\varphi_z$ minerals. Can. Min., Vol. 24, pp. 625-642; (1986).

HAWTHORNE, F.C. : Structural hierarchy in $M^{[6]}T^{[4]}$ ϕn minerals. Z. Krist., Vol. 192, pp.1-52; (1990).

HAWTHORNE, F.C. : Towards a structural classification of minerals: The $^{VI}M^{IV}T_2$ ϕ_n minerals. Am. Min., Vol. 70, pp. 455-473; (1985).

HAWTHORNE, F.C. : The role of OH and H_2O in oxide and oxysalt minerals. *Z. Krist*., Vol. 201, pp. 183-206; (1992).

HAWTHORNE, F.C. : Structural aspects of oxid and oxysalt crystals. *Acta Cryst*., B Vol. 50, pp. 481-510 ; (1994).

HAWTHORNE, F.C.: Structural aspects of oxide and oxysalt minerals. *In* Modular Aspects of Minerals (S. Merlino, ed.). Eur. Mineral. Union, Notes in Mineralogy, Vol. 1, pp. 373-429: (1997).

HIEMSTRA, T., VENEMA, P. & RIEMSDIJK, W.H. van : Intrinsic proton affinity of reactive surface groups of metal (hydro)oxides: The bond valence principle. *J. of colloid and interface science,* Vol. 184, pp. 680 – 692; (1996).

HONIGMANN, B.: Gleichgewichts. Und Wachstumsformen von Kristallen. Fortschritte der physik. Chemie. Vol. 4; (1958).

HUMAN, H.J., VAN DER ERDEN, J.P., JETTEN, L.A.M.J. & ODEKERKEN, J.G.M.: On the roughening transition of biphenyl: Transition of faceted to non-faceted growth of biphenyl for growth from different organic solvents and the melt. *J.Cryst. Growth*, Vol. 51, pp. 589-600; (1981).

KAISCHEW, R. & STRANSKI, I. N.: Zur kinetischen Ableitung der Keimbildungsgeschwindigkeit. Z. für physik. Chemie, B.26, pp. 317-326; (1934).

KAISCHEW, R.: Zur Theorie des Kristallwachstums. *Z. Für Physik A*; Vol. 102, No. 9-10; (1936).

KAISCHEW, R.: On the history of the creation of the molecular-kinetic theory of crystal growth. *J. Cryst. Growth.*, Vol. 51, pp. 643-650; (1981).

KIRFEL, A. & GIBBS, G.V. : Electron density distributions and bonded interactions for the fibrous zeolithes natrolite, mesolite and scolecite and related materials. *Phys. Chem. Minerals*, Vol. 27, pp. 270-284; (2000).

KLOCKMANN, F.: Lehrbuch der Mineralogie. 16. Edt., *Enke Stuttgart*; (1978).

KOSSEL, W. : Zur Theorie des Kristallwachstums. *Nachr. Ges. Wiss. Göttingen Math.-physik. Klasse*, pp. 135-143; (1927).

KOSSEL, W.: Über Krystallwachstum. *Die Naturwissenschaften*. Vol. 44, pp. 901-910; (1930).

KOSSEL, W. : Molecular formation as a question of atomic structure. Annalen der Physik, Vol. 49, pp. 229-362; (1916).

LASAGA, A.C.: Atomic treatment of mineral-water surface reactions. In "Mineral-Water Interface Geochemistry. HOCHELLA, M.F. and WHITE, A.F. (eds); Reviews in Mineralogy Vol. 23, (1990).

LACKMANN, R.: Die Gleichgewichtsform von Kristallen. N.Jb.Miner.Abh., Vol 122, pp. 36-89;(1974).

LAUE, M.v.: Der Wulffsche Satz für die Gleichgewichtsform von Kristallen. Z. Kristallogr. (A) 105; pp.124-133; (1943).

LENNIE, A.R., CONDON, N.G., LEIBSLE, F.M., MURRAY, P.W., THORNTON, G. & VAUGHAN, D.J. : Structures of Fe_3O_4 (111) surface observed by scanning tunnelling microscopy. *Phys. Rev.,* Vol. B 53, No. 15, pp. 10 244 – 10 253; (1996).

LEWIS, G.N.: The atom and the molecule. J.Am. Chem. Soc., Vol. 38; pp.762-786

LIAN, Li, TSUKAMOTO, K. & SUNAGAWA, I. : Impurity adsorption and habit changes in aqueous solution grown KCl crystals. *J. Cryst. Grwoth*, Vol. 99, pp.150-155. (1990).

LIEBAU, F. & WANG, X. : Stoichiometric valence *versus* structural valence: conclusions drawn from a study of the influence of polyhedron distortion on bond valence sum. Z. Krist., Vol. 220, pp. 589-591; (2005).

MILLER , M. L., FINCH, R. J., BURNS, P C; EWING, R C.: Description and classification of uranium oxide hydrate sheet topologies**.** J. Mater. Res., Vol. 11, pp. 3048-3056; (1996).

MOHRI, F. : A new relation between bond valence and bond distance. Acta Cryst., Vol. B56, pp. 626-638; (2000).

NIGGLI, P.: Beziehung zwischen Wachstumsformen und Struktur der Kristalle. Z. für anorganische und allgemeine Chemie, (1920).

NIGGLI, P.: Lehrbuch der Mineralogie und Kristallchemie. 3. Auflage, Teil 1. Berlin-Zehlendorf. Gebrüder Borntraeger. (1941).

PAULING, L.: The principles determining the structure of complex ionic crystals. J. Am. Chem. Soc., Vol. 69, pp. 542-554; (1929).

PAGOAGA, M.K, APPELMAN, D.E. & STEWART, J.M.: Crystal structures and chemistry of the uranyl oxide hydrates becquerelite, billietite and protasite. *Am. Min*., Vol. 72, pp. 1230-1238; (1987).

PARR, R.G. & PEARSON, R.G.: Absolute hardness: Companion parameter to absolute electronegativity. J. Am. Chem. Soc., Vol. 105, pp. 7512-7516; (1983).

PIANA, S., REYHANI, M. & GALE, J.D. : Simulating micrometre-scale crystal growth from solution. Nature, Vol. 438, No. 3 november, pp. 70-73; (2005).

PUCHIN, V.E., PUCHINA, A.V., HUISINGA, M. & REICHLING, M.: Theoretical modelling of steps on the CaF_2 (111) surface. *J. Phys.: Condens. Matter*, Vol. 13, pp. 2081-2094; (2001).

RÖSLER, H.J.: Lehrbuch der Mineralogie. 3. – Auflage. *VEB Verlag Leipzig*. (1984).

SCHINDLER, M. & HAWTHORNE, F.C.: A bond-valence approach to the structure, chemistry and paragenesis of hydroxy-hydrated oxysalt minerals. I. Theory. *Can. Min*., Vol. 39, pp. 1225-1242; (2001a).

SCHINDLER, M., MUTTER, A., HAWTHORNE, F.C. & PUTNIS, A. : Prediction of crystal morphology of complex uranyl-sheet minerals. I. Theory. *Can. Min*., Vol. 42, pp. 1629-1649; (2004a).

SCHINDLER, M., MUTTER, A., HAWTHORNE, F.C. & PUTNIS, A. : Prediction of crystal morphology of complex uranyl-sheet minerals. II. Observations. *Can. Min.,* Vol. 42, pp. 1651-1666; (2004b).

SCHROECKE, H. & WEINER, K.L.: Minerlogie. Gryter Verlag Berlin; (1981

SHANNON, R.D. & PREWITT, C.T.: Effective ionic radii in oxides and fluorides. Acta Cryst., Vol. B 25, pp. 925- 946; (1969).

SHANNON, R.D.: Bond strength considerations applied to cation coordination in mormal and high-pressure oxides. J. of solid state. Chem., Vol. 12, pp. 16-30; (1975).

SHANNON, R.D. : Revised effective ionic radii and systematic studies of interatomic distances in halides and chalcogenides. Acta Cryst., A Vol. 32, pp. 751 – 767; (1976).

SOHNKE, L.: Ueber Spaltungsflächen und natürliche Krystallflächen. Z. für Kristallogrpahie, Vol. 13, pp. 214-235; (1888).

STRANSKI, I.N. : Zur Theorie des Kristallwachstums. Z. Physik.Chemie, Vol. 136, pp. 259-278; (1928).

STRANSKI, I.N. : Beiträge zum Wachstum und Auflösen nichtpolarer Kristalle. Z. Physik. Chemie., B Vol. 11, pp. 342-349; (1931).

STRANSKI, I.N. :Wachstum und Auflösen der Kristalle vom NaCl-Typ. Z. Physik. Chemie. B Vol. 17, pp. 127-154; 1932).

STRANSKI, I.N. : Zur Definition der spezifischen freien Kanten- und Eckenenergie der Kristalle. Z. Krist., Vol. 105, pp. 287-290; (1943).

STRANSKI, I.N. : Eine Plauderei über Gleichgewichtsformen von Kristallen. J. Cryst. Growth, Vol, 13/14, pp. 3-8; (1972).

STRANSKI, I.N. & KAISCHEW, R. : Gleichgewichtsformen homöoplarer Kristalle. Z. Krist., Vol. 78, 373-385; (1935).

STRANSKI, I.N. & KRASTANOW, L. :Notiz zur Frage der Gleichgewichtsform homöopolarer Kristalle. Z.Krist., Vol. 83, pp. 155-156; (1932).

STUMM, W.: *Chemistry of Solid-Water Interface*. John Wiley & Sons, New York, (pp. 428); (1992).

SUNAGAWA, I. : Growth and morphology of crystals. Review Forma, Vol. 14, pp. 147-166; (1999).

SUNAGAWA, I. : Crystals. Growth, Morphology and Perfection.Cambridge Press. (2005).

SUZUKI, Y. & BANFIELD, J.F.: Geomicrbiology of uranium. . In "Uranium". BURNS, P.C. & FINCH. R (eds.); Reviews in Mineralogy Vol. 38, (1999).

TASKER, P.W.: The surface properties of uranium dioxide. *Surface Science*, Vol. 78, pp. 315-324; (1979).

TAYLOR, J.C.: The structure of the α form of uranyl hydroxide. Acta Cryst., B 27, pp. 1088-1091; (1971).

TOSCHEV, S.: Equilibrium forms. In" *Crystal Growth: An Introduction"*; P. Harman, ed., North-Holland, Amsterdam (1973).

VOLMER, M.: Versuche über Kristallwachstum und Auflösung. Z. für Physik, Vol. 35, No. 3; (1926).

WANG, X. & LIEBAU F. : Influence of lone-pair electrons of cations on bond-valence parameters. Z. Krist., Vol. 211, pp. 437-439; (1996).

WEYBERG, Z.: Studien über relative Wachsthumsgeschwindigkeiten der Krystallflächen. Z. Krist., Vol. 34, pp. 531-538; (1901).

WULFF, G. : Zur Frage der Geschwindigkeit des Wachstums und der Auflösung der Kristallflächen. Z. Krist., Vol. 34, pp. 449-530; (1901).

Appendix I

Graphical approach to calculate a Pm3m-lattice

Appendix I is an overview on how the bond-valence deficiency of a crystal surface can be determined. As an example crystal surfaces terminating a theoretical crystal with space-group symmetry O_h^1 (P 4/m $\bar{3}$ 2/m) have been chosen. For each individual surface (hkl) a ball-and-stick model is presented with atoms terminating a surface area of unit-cell dimension (Fig.A Ia). These atoms occupy the position of lattice-points. Marked in the same color are atoms at equivalent positions.

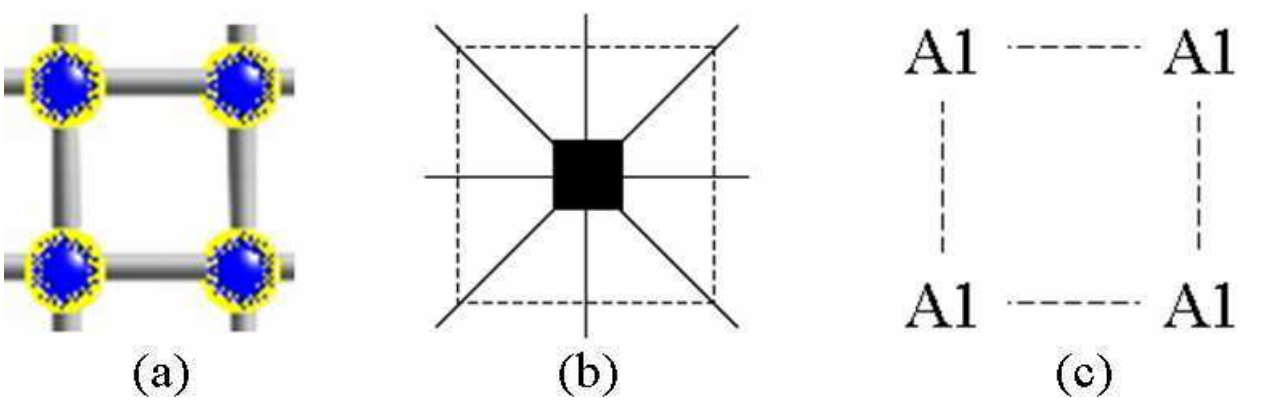

Fig.:A I (a) Ball-and stick model of a (001) crystal surface. (b) Schematic representation of the face symmetry of the crystal surface. (c) This graphic indicates the number of equivalent atoms and their respective number of dangling bonds (DB).

The next figure (Fig A.: I b) is a graphic representation of the corresponding face-symmetry. Rotation axis are indicated by their respective symbols, mirror-plane are indicated by solid lines, the unit-cell is outlined by dashed lines. The individual figures are labeled according to the nomenclature applied by NIGGLI (1941)

The third image (Fig.A I c) shows the number of atoms present at the crystal surface of unit-cell dimension (dashed lines). Equivalent atoms are labeled by the same letter and colour. The number following the letter states the amount of dangling bonds (DB).

Primitive cubic lattice-type (Pm3m)

(001)

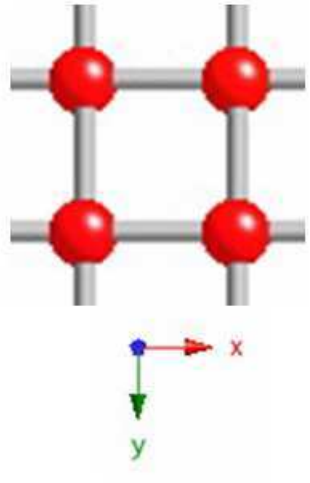

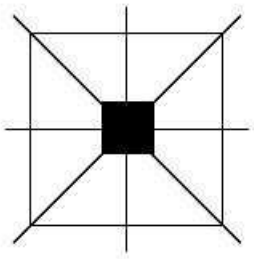

C4V

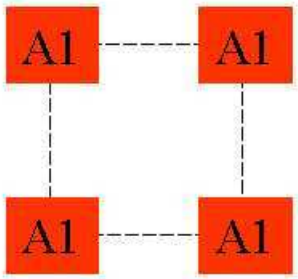

DB = 1

(110)

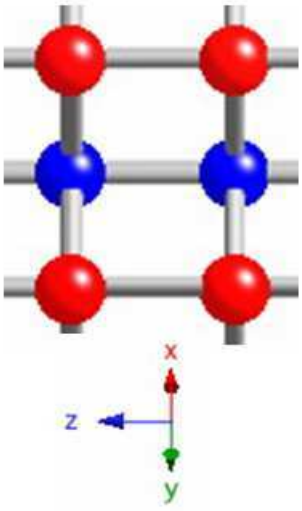

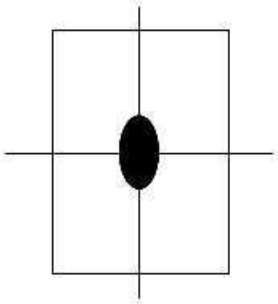

C2V

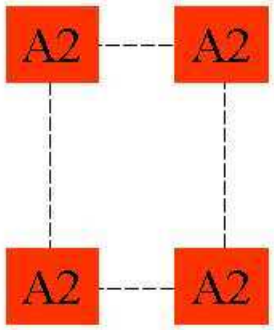

DB = 2

(111)

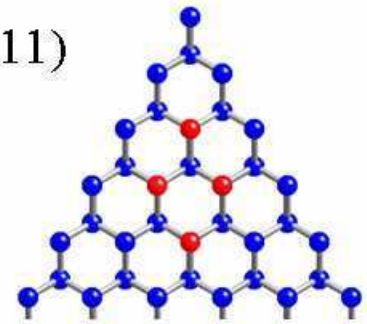

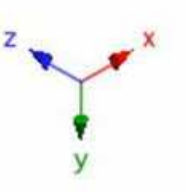

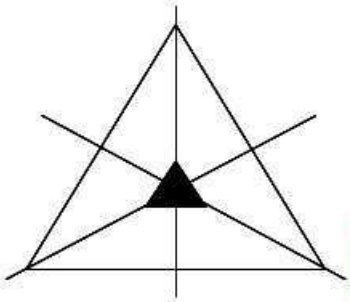

C3V

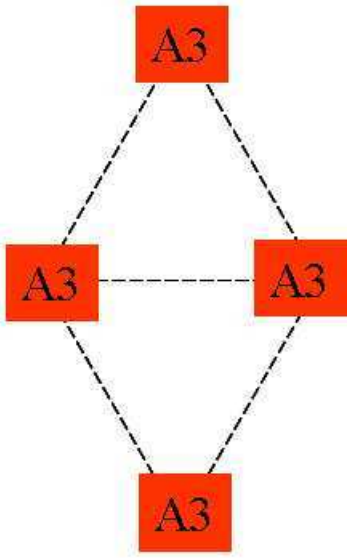

DB = 3

(210)

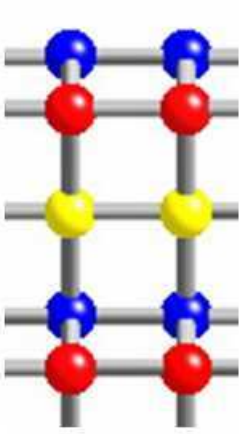

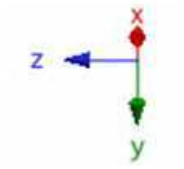

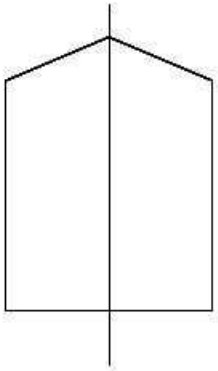

Cs

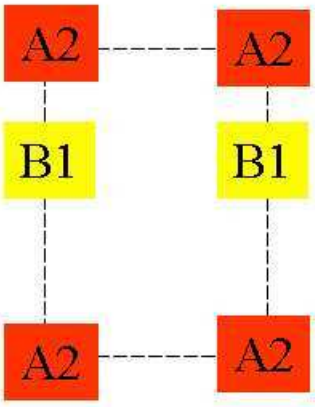

DB = 3

(211)

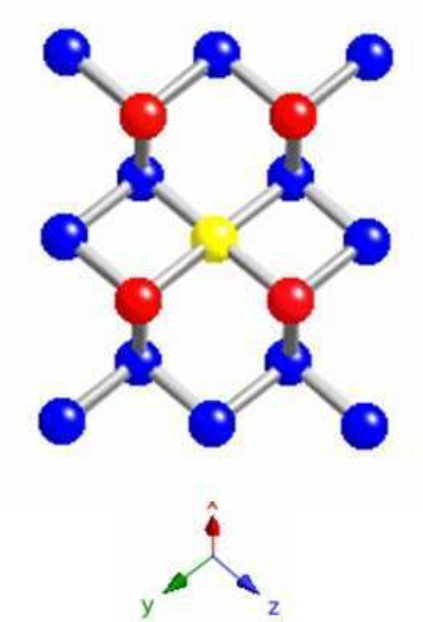

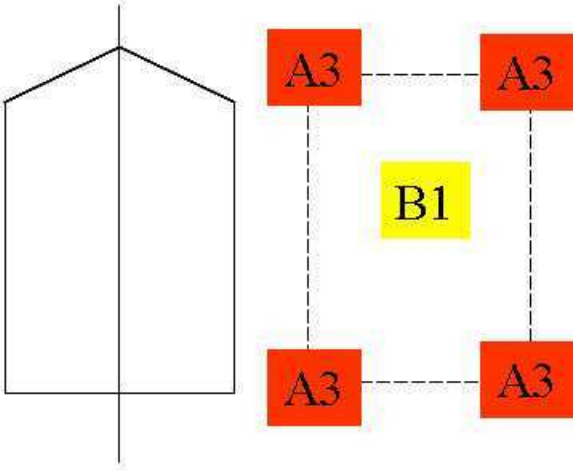

Cs DB = 4

(221)

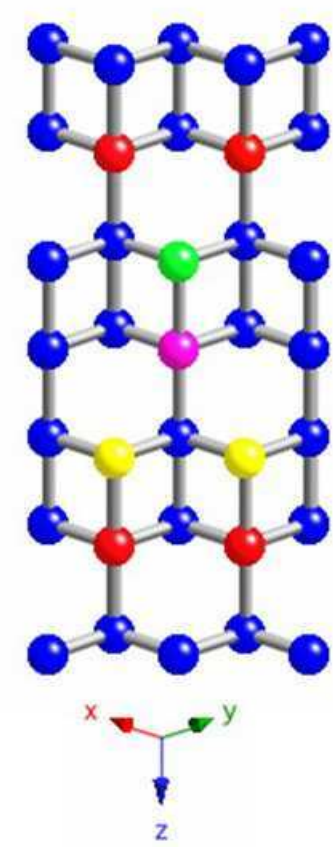

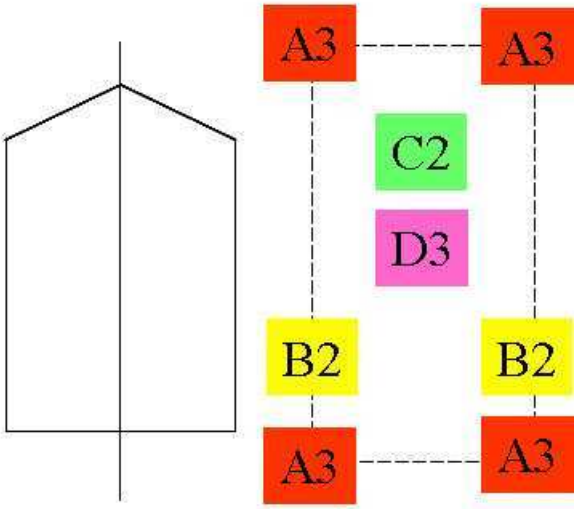

Cs DB = 10

(311)

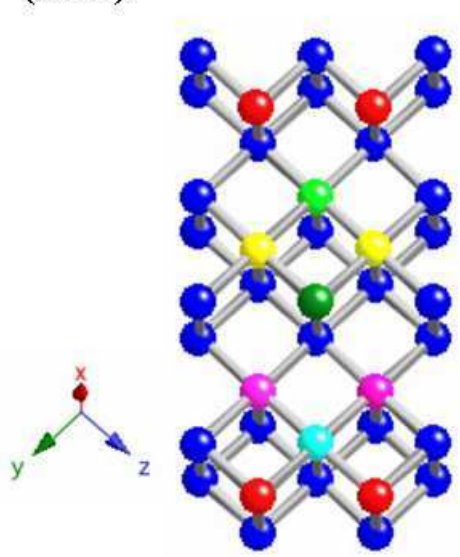

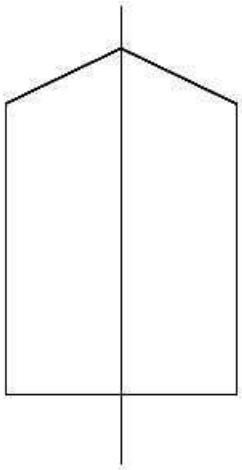

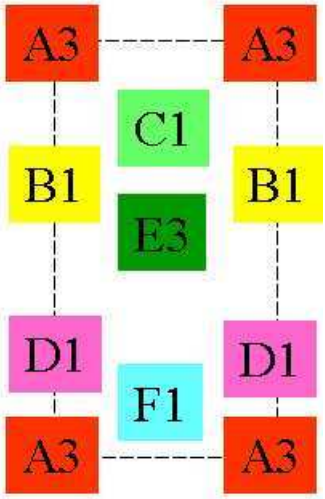

Cs

DB = 10

(331)

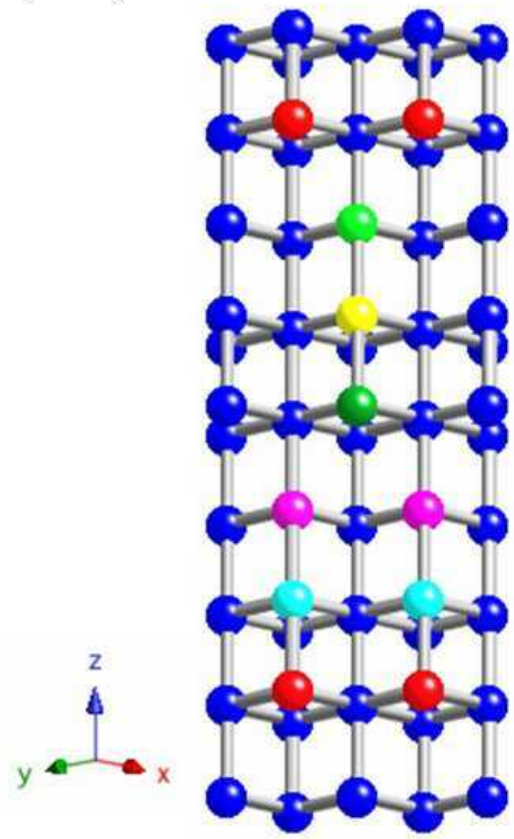

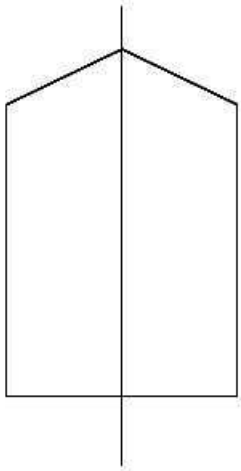

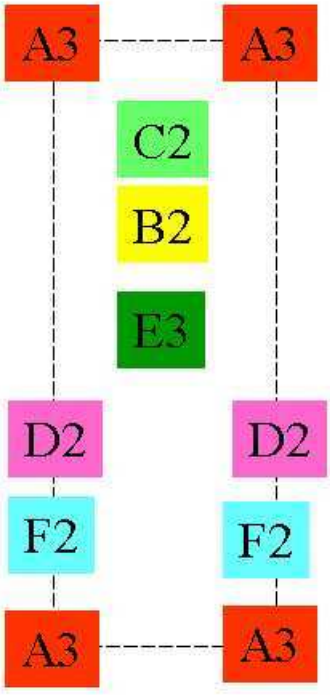

Cs

DB = 14

Appendix II

Graphical calculations of different mineral faces

Appendix II gives a graphical overview of the crystal surfaces described in Chapter 8. For all the surfaces described in this Appendix the calculated Tables are given in Appendix III.

Similar to Appendix I, a ball-and-stick model is presented fro each individual surface (hkl). Atoms terminating the surface and contributing "dangling bonds" to the environment are marked in different colours. Next, a graphic representation of the corresponding face-symmetry is given. Rotation axis are indicated by their respective symbols, mirror-planes are indicated by solid lines, the unit-cell is outlined by dashed lines, and the individual figures are labeled according to the nomenclature applied by NIGGLI (1941). The third image shows the different atoms terminating the surface. Equivalent atoms are labeled by the same letter and marked by the same colour. The number following the letter states the amount of dangling bonds (DB) emitted by these atoms.

In such cases where several terminations parallel to a given (hkl)-plane exist, but no differences in the bond-valence deficiency of the crystal surfaces occur (e.g. Fm3m-structure type parallel to the (001)-termination), only one surface is given as an example. In cases where several terminations parallel to a given (hkl)-plane exist, and differences in the bond-valence deficiencies of these terminations occur (e.g. spinel-structure type, parallel to the (111)-terminations), only the surfaces with the lowest bond-valence deficiencies are given.

Face Centered Cubic Lattice Type (Fm3m)

(001)

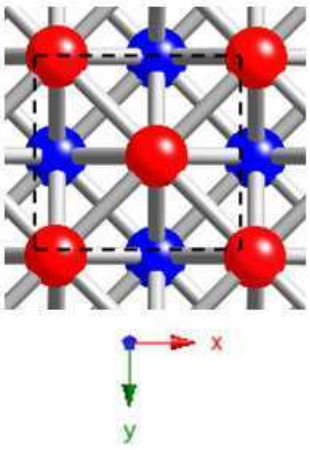

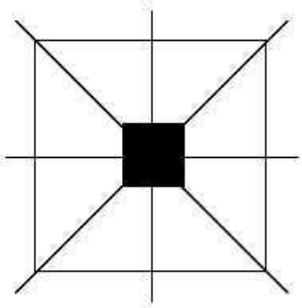

C4v

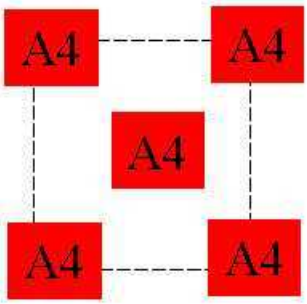

DB = 8

(110)

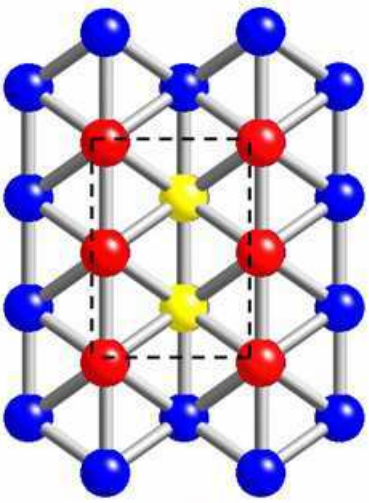

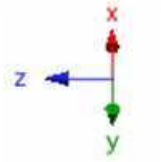

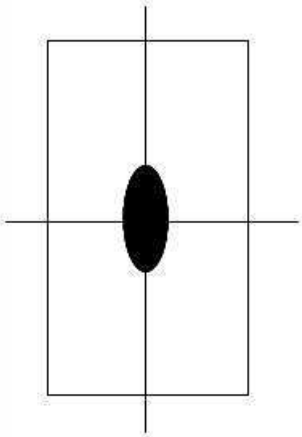

C2v

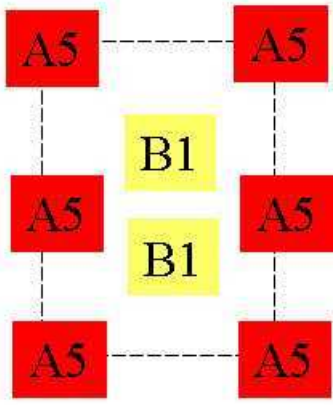

DB = 12

Face Centered Cubic Lattice Type (Fm3m)

(111)

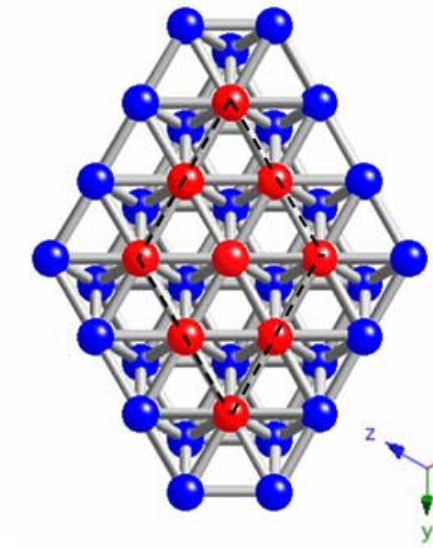

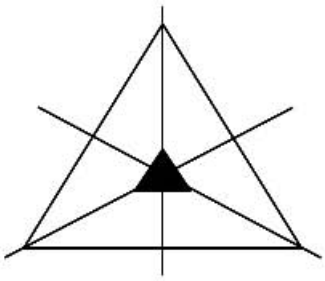

C3v

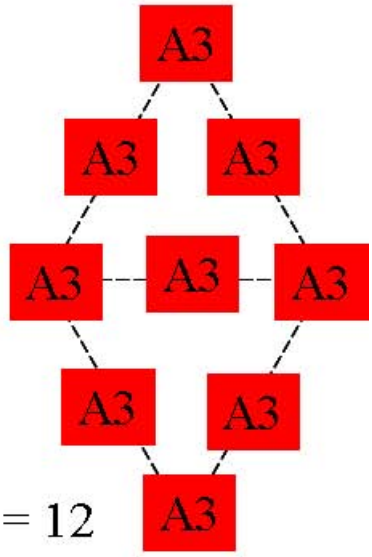

DB = 12

(311)

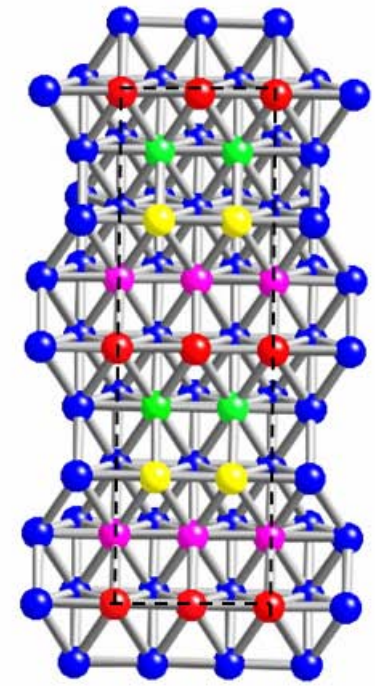

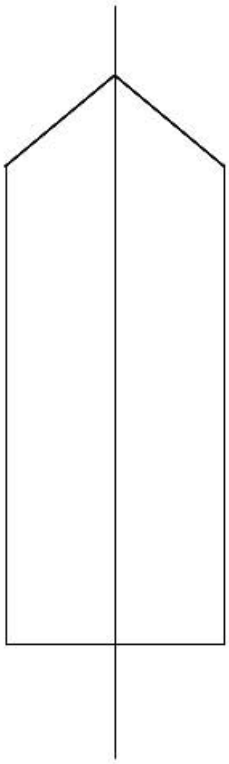

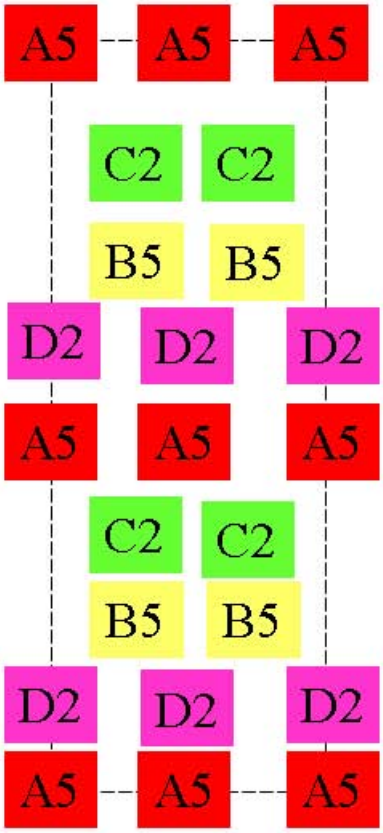

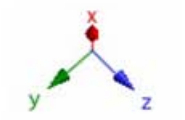

Cs

DB = 56

Body-Centered Cubic Lattice Type (Im3m)

(001)

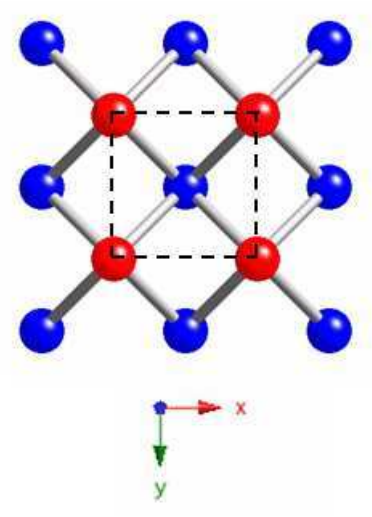

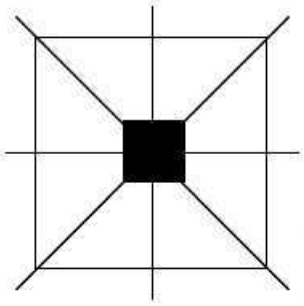

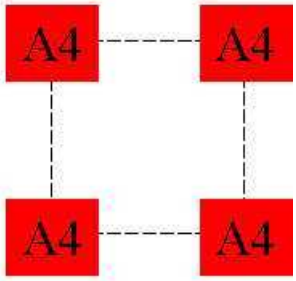

C4v

DB = 4

(110)

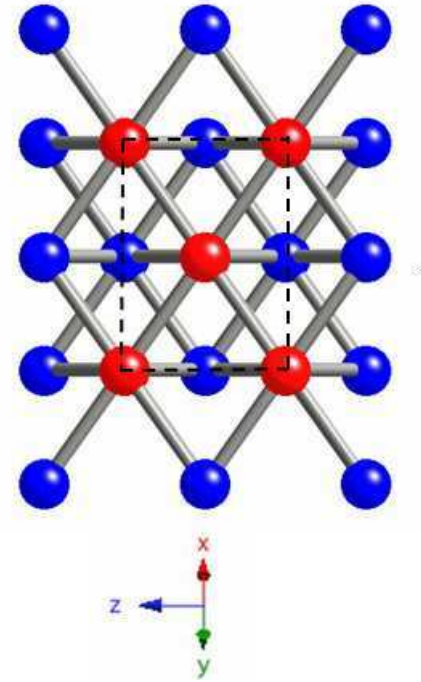

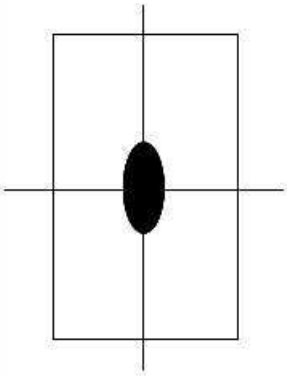

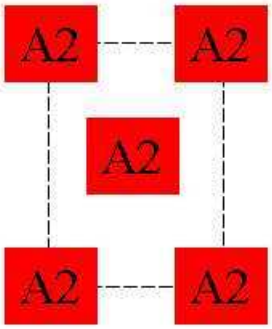

C2v

DB = 4

Body-Centered Cubic Lattice Type (Im3m)

(111)

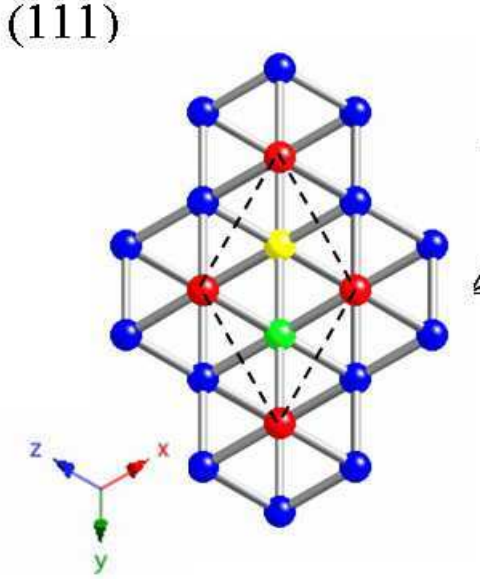

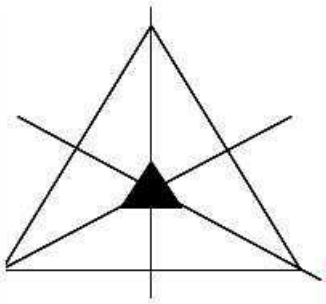

C3v

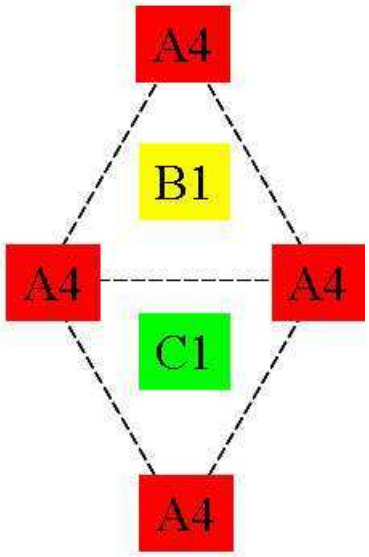

DB = 6

(211)

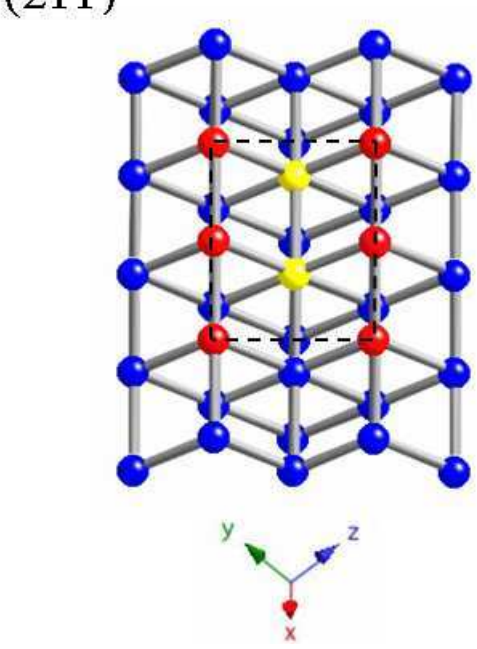

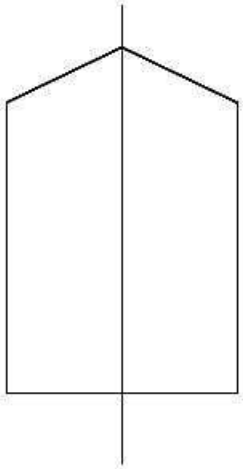

Cs

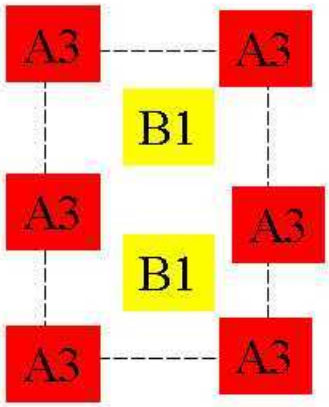

DB = 8

Diamond-Structure Type (Fd3m)

(001)

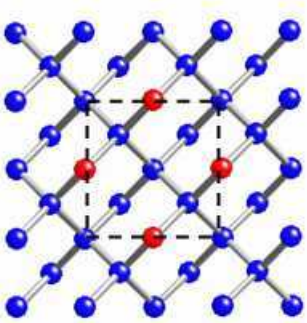

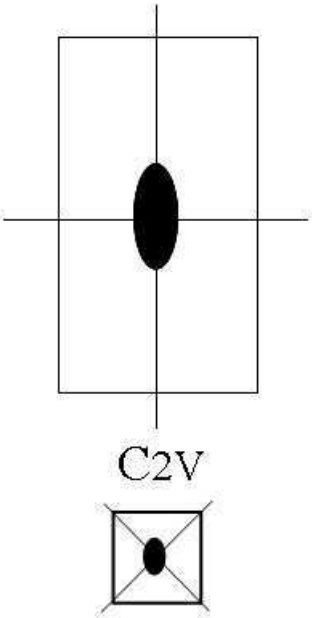

C2V

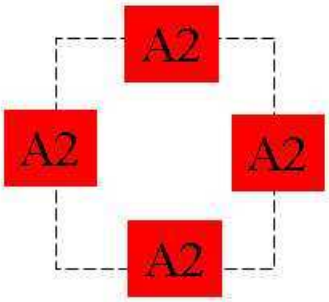

DB = 4

(110)

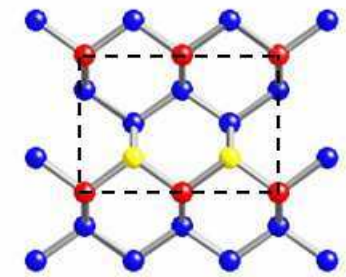

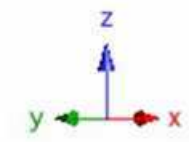

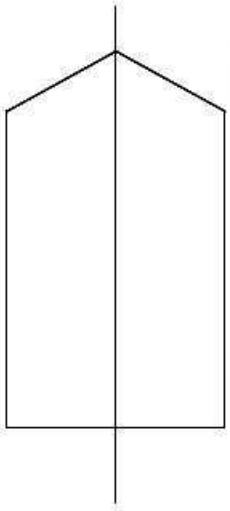

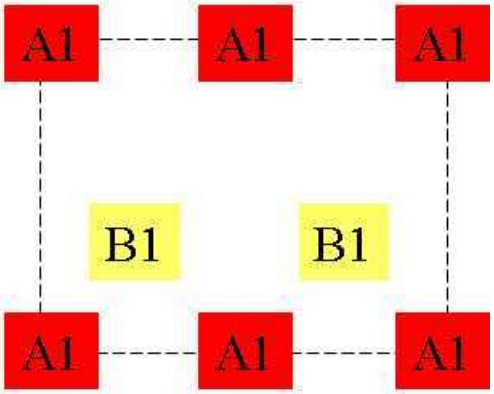

CS

DB = 4

Diamond-Structure Type (Fd3m)

(111)

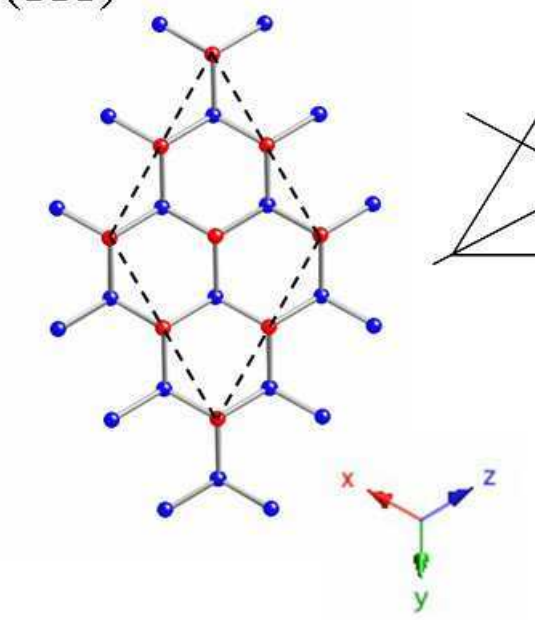

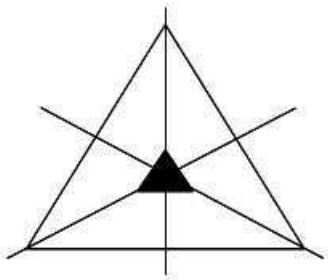

C3V

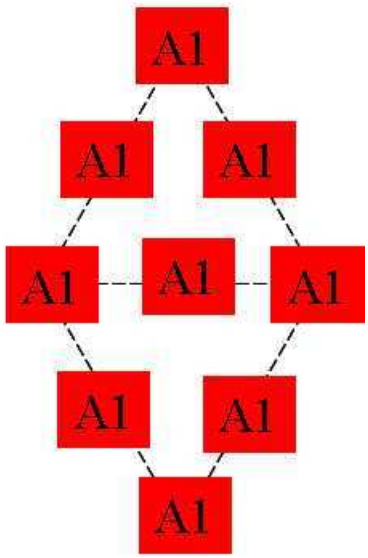

DB = 4

(210)

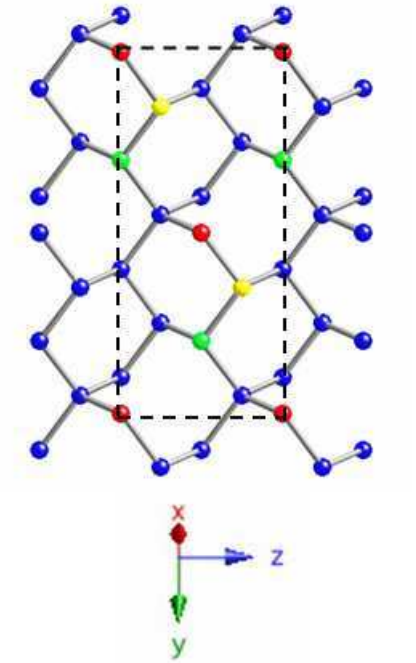

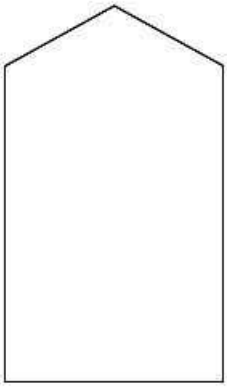

C1

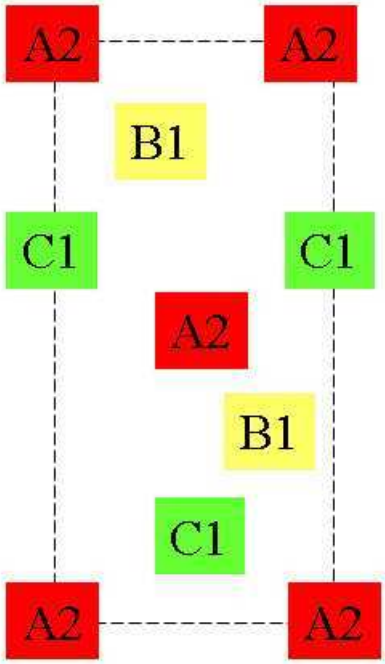

DB = 8

NaCl-Structure Type (Fm3m)

(001)

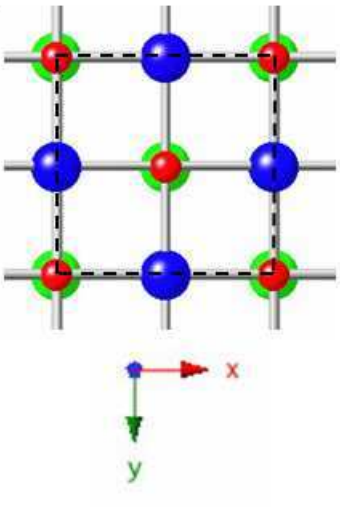

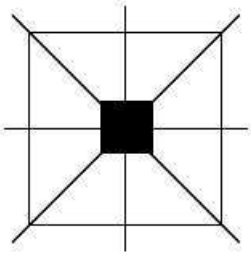

C4V

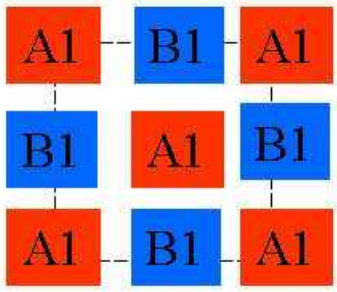

DB = 4

(110)

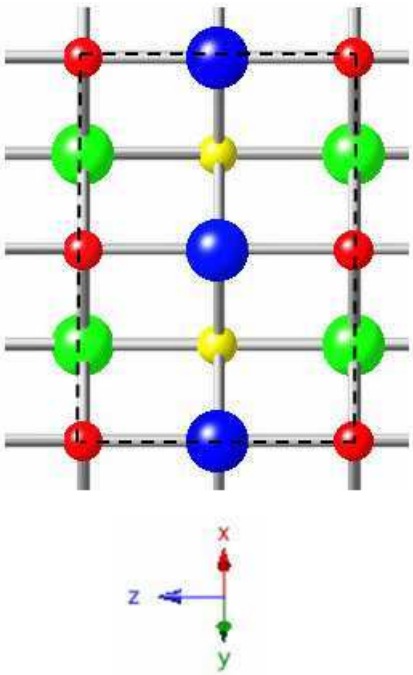

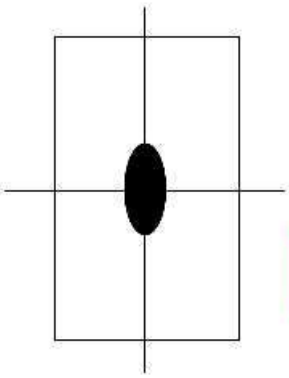

C2V

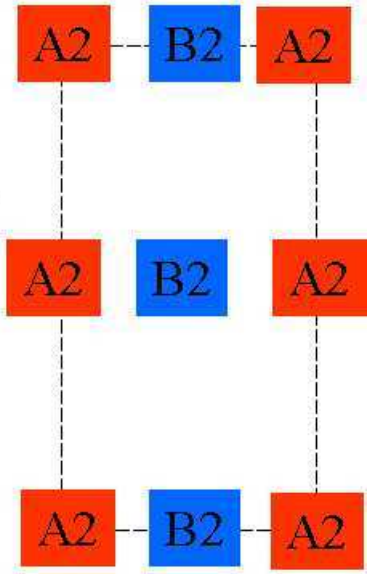

DB = 8

NaCl-Structure Type (Fm3m)

(111)

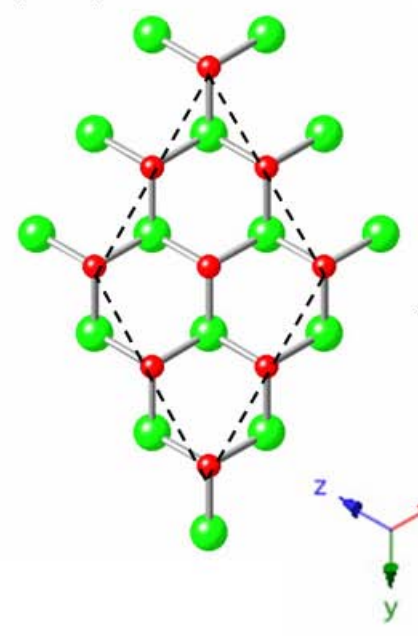

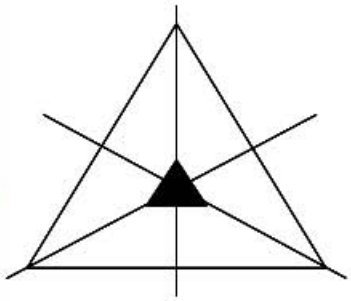

C3V

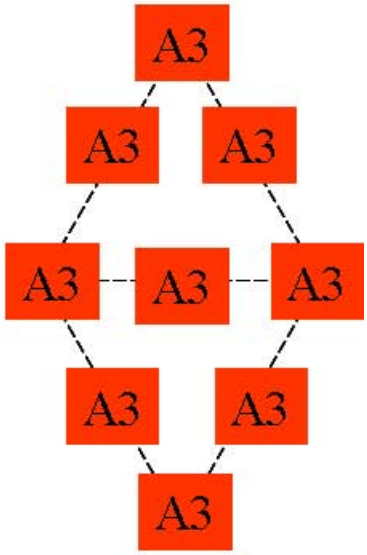

DB = 12

(210)

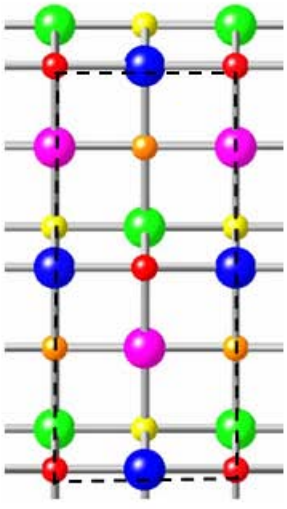

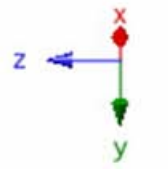

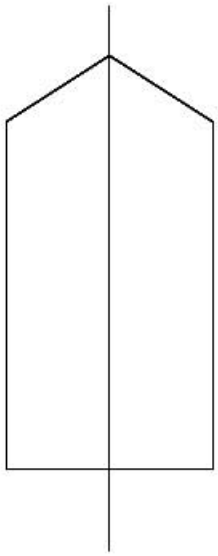

Cs

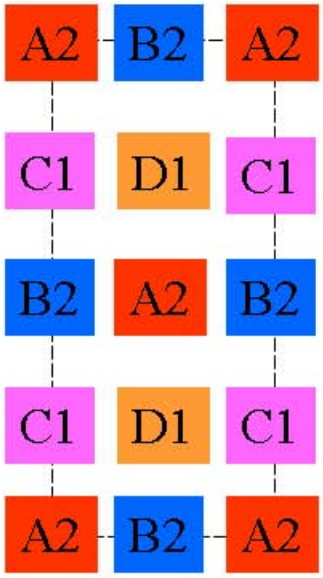

DB = 12

Sphalerite-Structure Type ($F\bar{4}3m$)

(001)

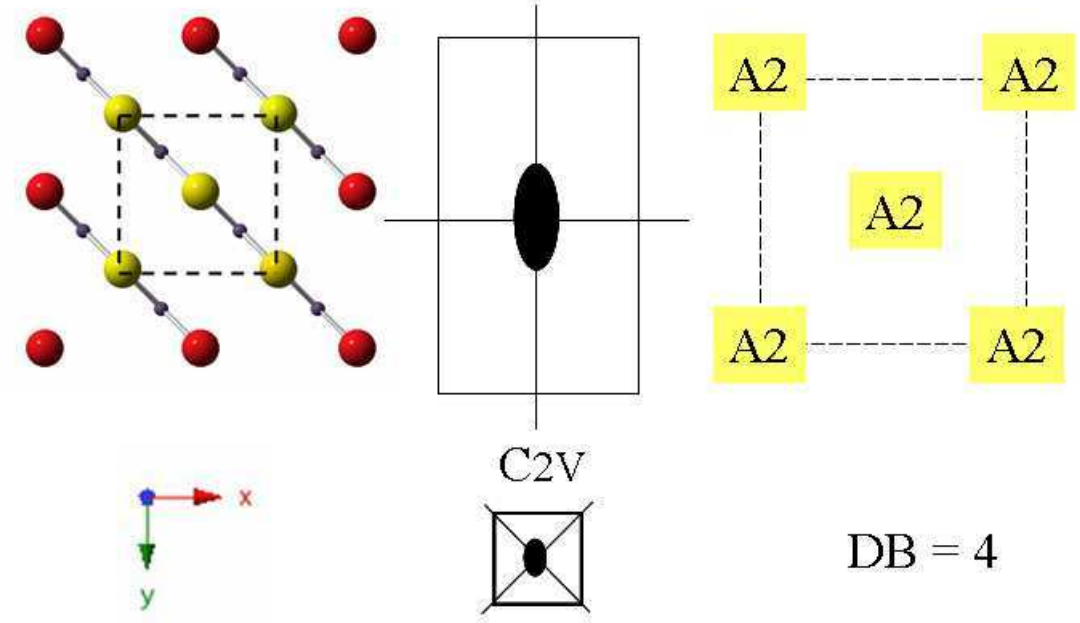

(110)

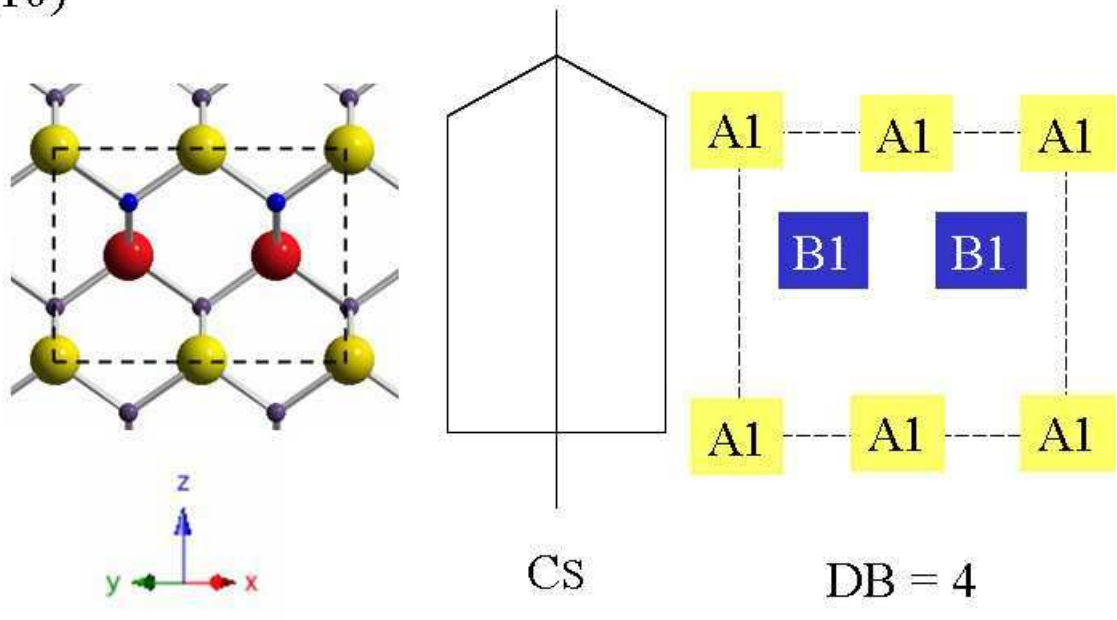

Sphalerite-Structure Type ($F\bar{4}3m$)

(111)

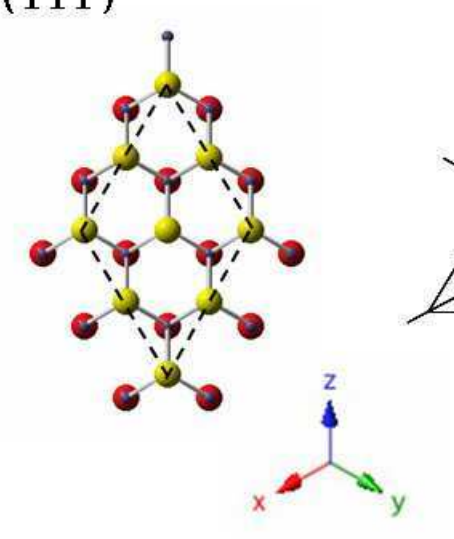

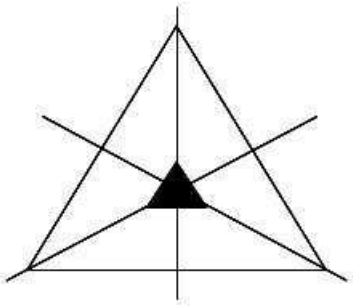

C3V

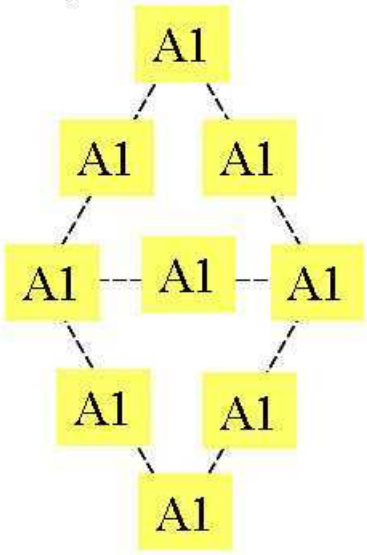

DB = 4

(311)

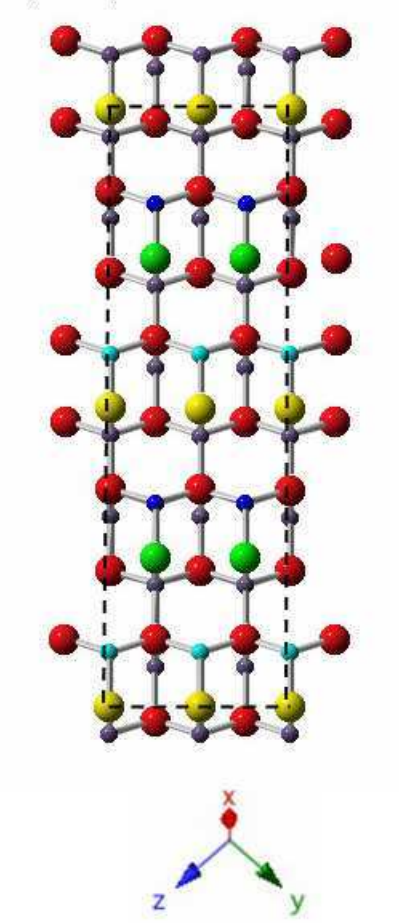

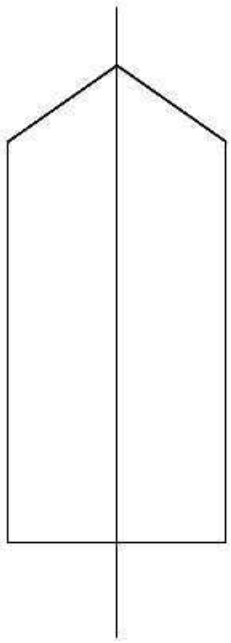

Cs

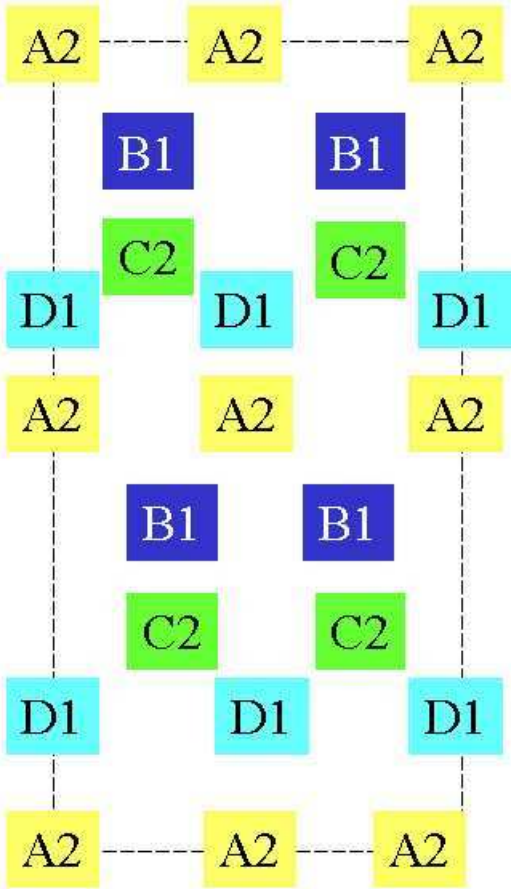

DB = 24

CaF_2-Structure Type (Fm3m)

(001)

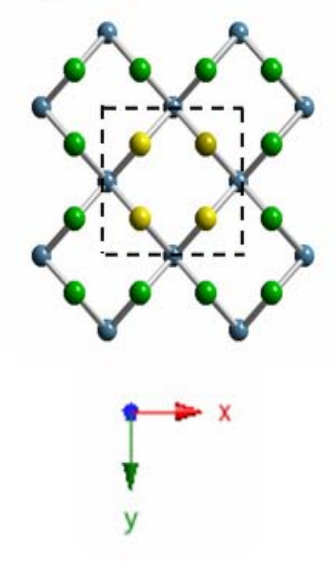

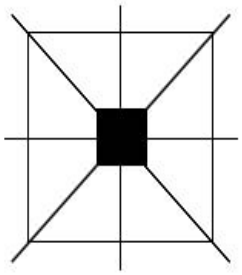

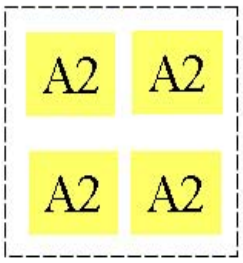

C4v

DB = 8

(110)

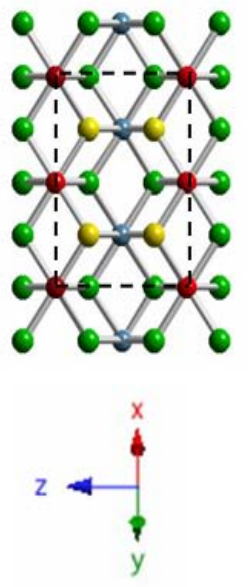

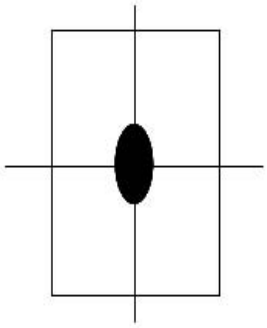

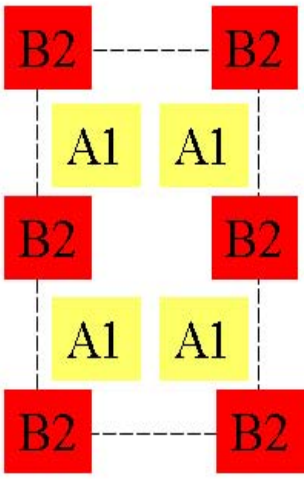

C2v

DB = 8

CaF_2-Structure Type (Fm3m)

(111)

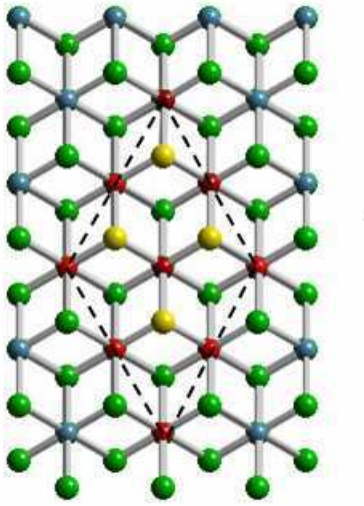

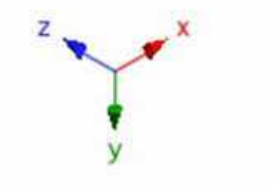

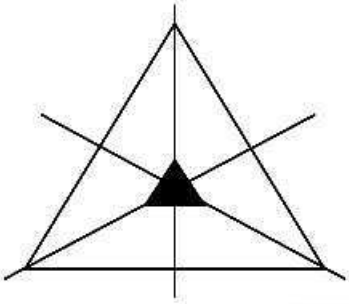

C3v

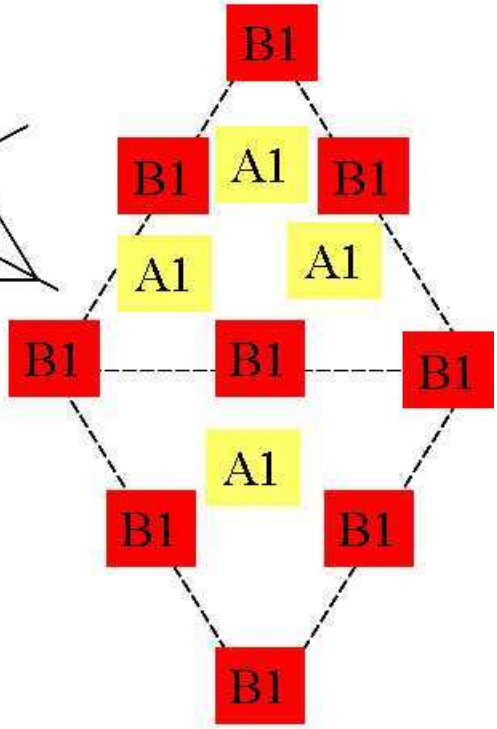

DB = 8

(210)

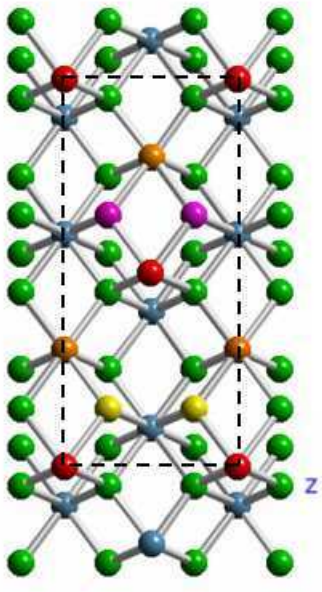

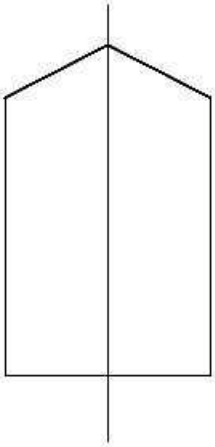

Cs

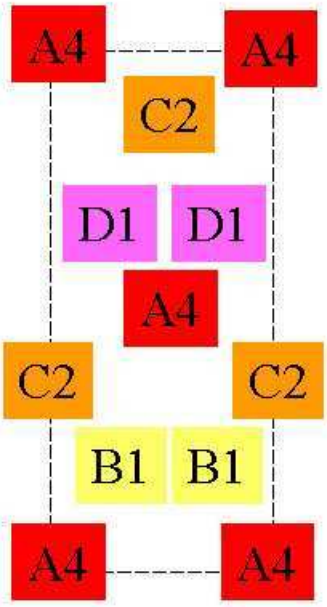

DB = 16

Pyrite Structure Type (Pa3)

(001)

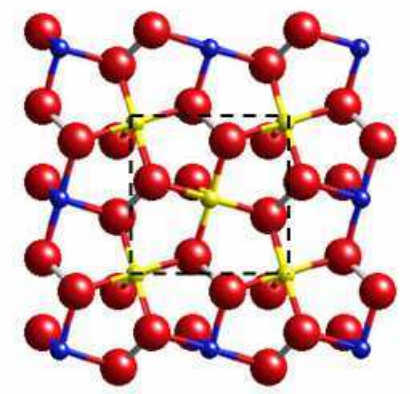

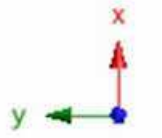

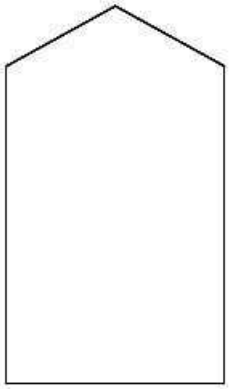

C1

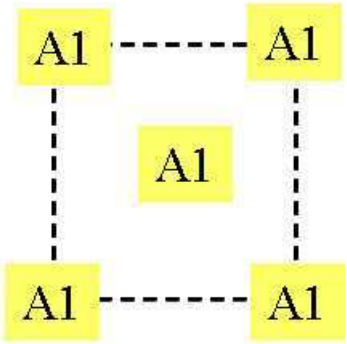

DB = 2

(110)

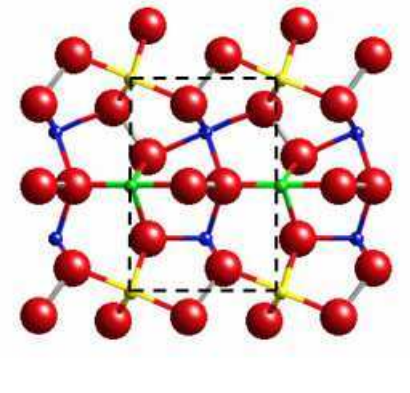

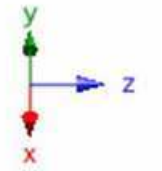

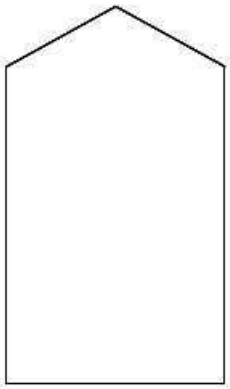

C1

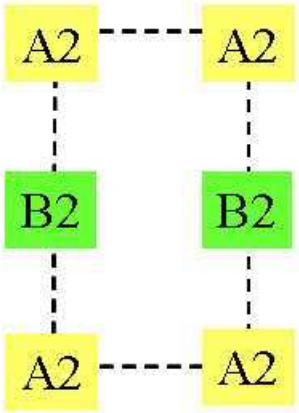

DB = 4

Pyrite Structure Type (Pa3)

(111)

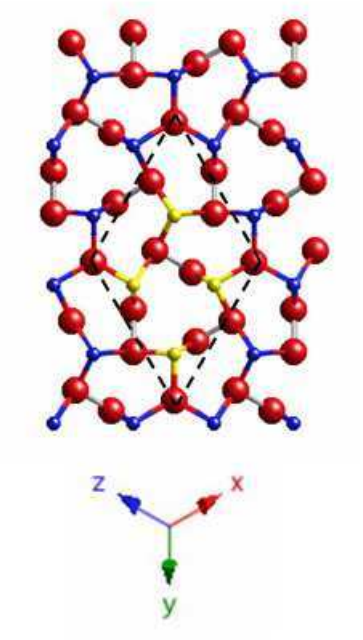

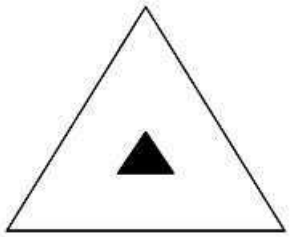

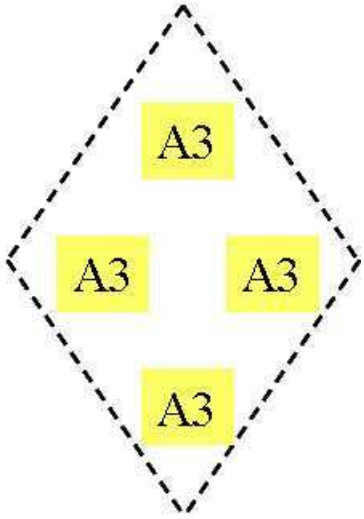

C3 DB = 12

(210)

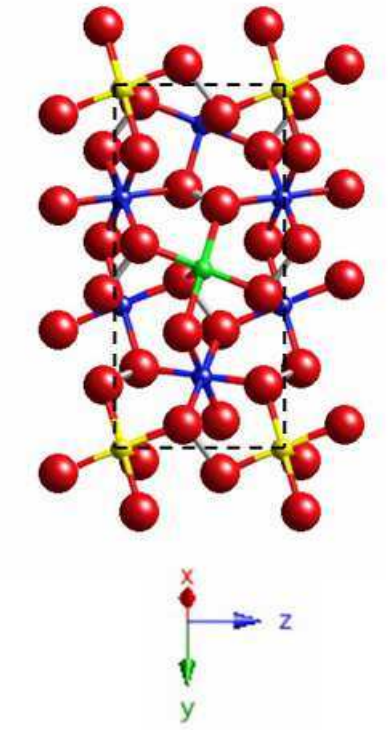

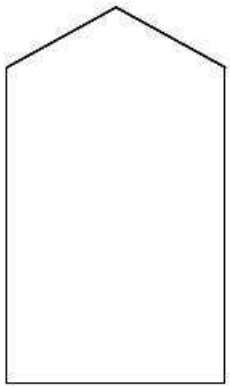

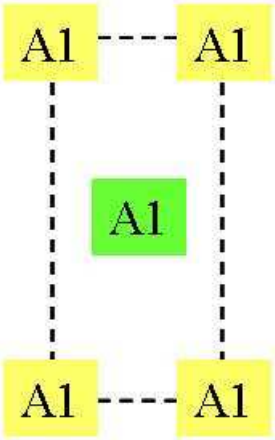

C1 DB = 2

Spinel Structure Type (Fd3m)

(001)

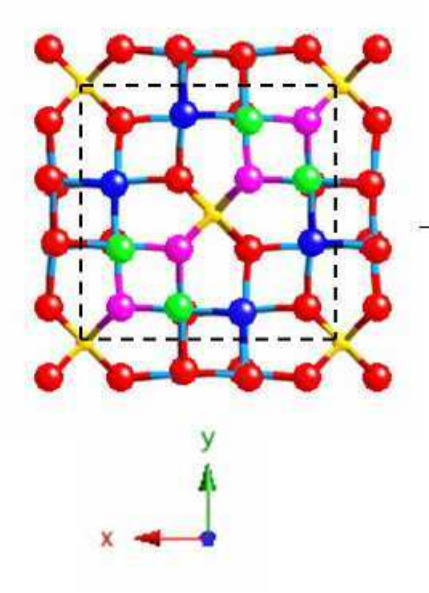

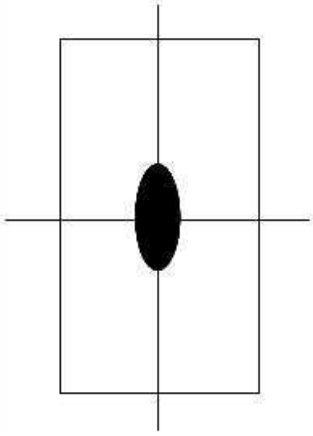

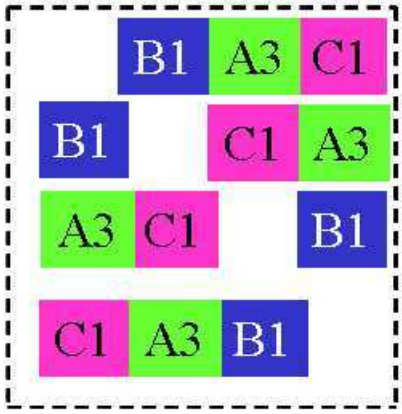

C2V

DB = 20

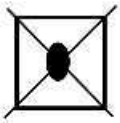

(110)

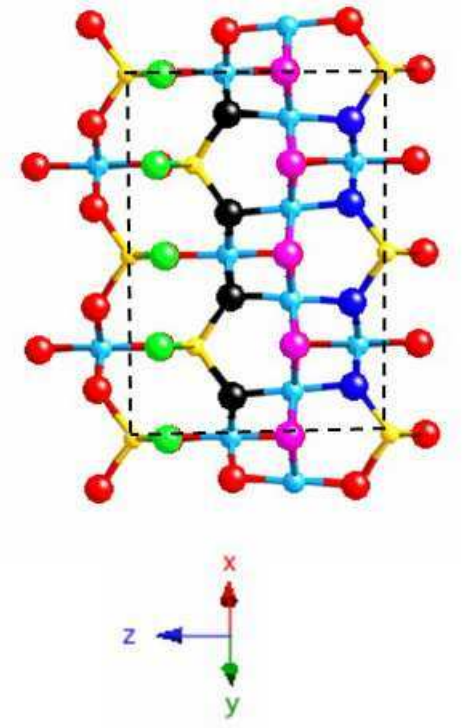

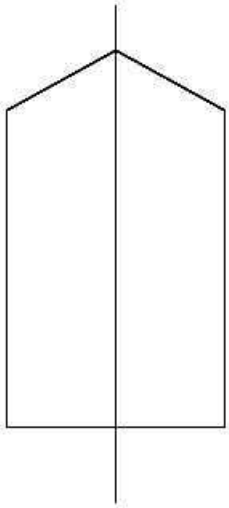

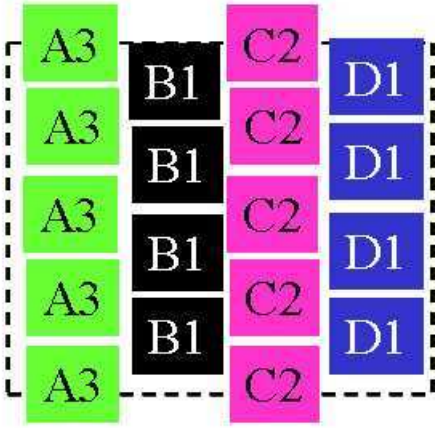

Cs

DB = 28

Spinel Structure Type (Fd3m)

(111)

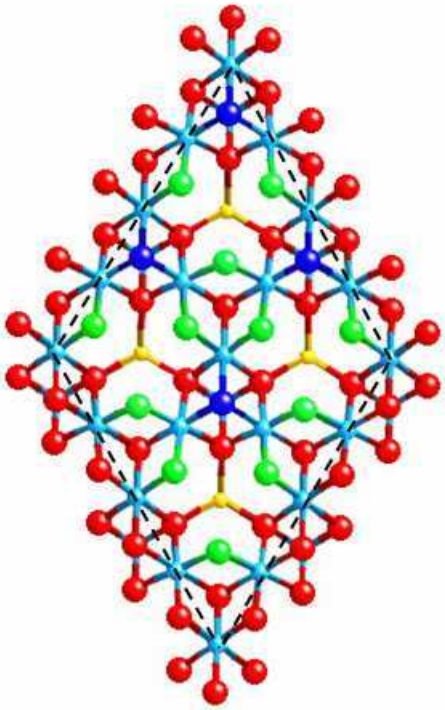

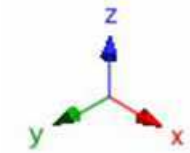

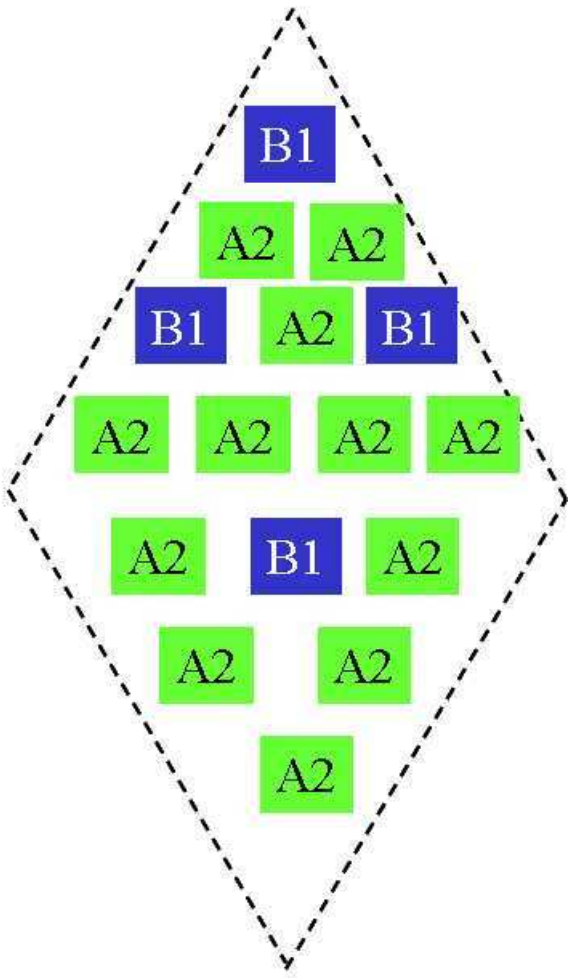

DB = 28

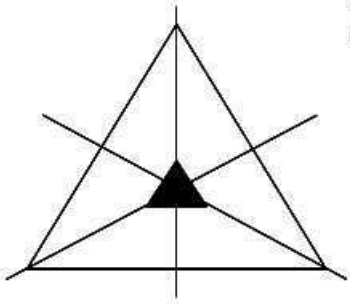

C3V

Appendix III

Bond-valence deficiency tables

This Appendix summarizes the calculated Bond-valence deficiency Tables of the graphic examples in Appendix I and II , additionally the Tables for the different "Case-studies" given in Chapter 11 are added at the end of this Appendix.

All surfaces of the graphical examples of Appendix II have been calculated for a given theoretical crystals having a_0 = 5,0 Å². The number of bond-emitted by atoms terminating the different surfaces of unit-dimension are given by the number of "dangling bonds" (DB).

Pm3m Structure Type

Face (hkl)	DB	Unit-cell (Å²)	BVDU (Å²)	RD	BVDU* (Å²)	LD	BVDU** (Å²)	ω	BVDU*** (Å²)	Z	ΔBVDU (Å²)
(100)	1	25,00	0,04	1	0,04	1	0,04	8	0,01	4	0,02
(110)	2	35,36	0,06	1	0,06	2	0,11	4	0,03	2	0,06
(111)	3	43,30	0,07	1	0,07	3	0,21	6	0,03	3	0,10
(210)	3	55,90	0,05	1	0,05	5	0,27	2	0,13	1	0,13
(211)	4	61,23	0,07	1	0,07	6	0,39	2	0,20	1	0,20
(221)	10	150,00	0,07	1	0,07	9	0,60	2	0,30	1	0,30
(311)	10	165,83	0,06	1	0,06	11	0,66	2	0,33	1	0,33
(331)	14	217,94	0,06	1	0,06	19	1,22	2	0,61	1	0,61

Fm3m Structure Type

Face (hkl)	DB	Unit-cell (Å²)	BVDU (Å²)	RD	BVDU* (Å²)	LD	BVDU** (Å²)	ω	BVDU*** (Å²)	Z	ΔBVDU (Å²)
(100)	8	25,00	0,32	2	0,64	2	1,28	8	0,16	4	0,64
(110)	12	35,36	0,34	2	0,68	4	2,72	4	0,68	2	1,36
(111)	12	43,30	0,28	1	0,28	3	0,83	6	0,14	3	0,42
(311)	56	165,83	0,34	1	0,34	11	3,71	2	1,86	1	1,86

Im3m Structure Type

Face (hkl)	DB	Unit-cell (Å²)	BVDU (Å²)	RD	BVDU* (Å²)	LD	BVDU** (Å²)	ω	BVDU*** (Å²)	Z	ΔBVDU (Å²)
(100)	4	25,00	0,16	2	0,32	2	0,64	8	0,08	4	0,32
(110)	4	35,36	0,11	1	0,11	2	0,23	4	0,06	2	0,11
(111)	6	43,30	0,14	2	0,28	6	1,66	6	0,28	3	0,83
(211)	8	61,23	0,13	1	0,13	6	0,78	2	0,39	1	0,39

Diamond Structure Type

Face (hkl)	DB	Unit-cell (Å²)	BVDU (Å²)	RD	BVDU* (Å²)	LD	BVDU** (Å²)	ω	BVDU*** (Å²)	Z	ΔBVDU (Å²)
(100)	4	25,00	0,16	4	0,64	4	2,56	4	0,64	2	1,28
(110)	4	35,36	0,11	4	0,45	4	1,81	2	0,91	1	0,91
(111)	4	43,30	0,09	2	0,18	3	0,55	6	0,09	3	0,28
(210)	8	55,90	0,14	4	0,57	20	11,45	1	11,45	1	11,45

NaCl Structure Type

Face (hkl)	DB	Unit-cell (Å²)	BVDU (Å²)	RD	BVDU* (Å²)	LD	BVDU** (Å²)	ω	BVDU*** (Å²)	Z	ΔBVDU (Å²)
(100)	4	25,00	0,16	2	0,32	2	0,64	8	0,08	4	0,32
(110)	8	35,36	0,23	2	0,45	4	1,81	4	0,45	2	0,91
(111)	12	43,30	0,28	1	0,28	6	1,66	6	0,28	3	0,83
(210)	12	55,90	0,21	2	0,43	10	4,29	2	2,15	1	2,15

Sphalerite Structure Type

Face (hkl)	DB	Unit-cell (Å²)	BVDU (Å²)	RD	BVDU* (Å²)	LD	BVDU** (Å²)	ω	BVDU*** (Å²)	Z	ΔBVDU (Å²)
(100)	4	25,00	0,16	2	0,32	4	1,28	4	0,32	2	0,64
(110)	4	35,36	0,11	2	0,23	4	0,91	2	0,45	1	0,45
(111)	4	43,30	0,09	1	0,09	3	0,28	6	0,05	3	0,14
(311)	24	165,83	0,14	1	0,14	11	1,59	2	0,80	1	0,80

Fluorite Structure Type

Face (hkl)	DB	Unit-cell (Å²)	BVDU (Å²)	RD	BVDU* (Å²)	LD	BVDU** (Å²)	ω	BVDU*** (Å²)	Z	ΔBVDU (Å²)
(100)	8	25,00	0,32	2	0,64	2	1,28	8	0,16	4	0,64
(110)	8	35,36	0,23	2	0,45	4	1,81	4	0,45	2	0,91
(111)	8	43,30	0,18	1	0,18	6	1,11	6	0,18	3	0,55
(210)	16	55,90	0,29	2	0,57	10	5,72	2	2,86	1	2,86

Pyrite Structure Type

Face (hkl)	DB	Unit-cell (Å²)	BVDU (Å²)	RD	BVDU* (Å²)	LD	BVDU** (Å²)	ω	BVDU*** (Å²)	Z	ΔBVDU (Å²)
(100)	2	25,00	0,08	2	0,16	2	0,32	1	0,32	1	0,32
(110)	4	35,36	0,11	2	0,23	4	0,91	1	0,91	1	0,91
(111)	12	43,30	0,28	1	0,28	3	0,83	3	0,28	1	0,28
(210)	2	55,90	0,04	2	0,07	10	0,72	1	0,72	1	0,72

Spinel Structure Type

Face (hkl)	DB	Unit-cell (Å²)	BVDU (Å²)	RD	BVDU* (Å²)	LD	BVDU** (Å²)	ω	BVDU*** (Å²)	Z	ΔBVDU (Å²)
(100)	20	25,00	0,80	4	3,20	4	12,80	4	3,20	2	6,40
(110)	28	35,36	0,79	4	3,17	4	12,67	2	6,34	1	6,34
(111)	28	43,30	0,65	2	1,29	6	7,76	6	1,29	3	3,88

Case 1 (Figure 11.5, pp. 211)

Face	BVDU	Area (Å²)	BVDU (Å²)	RD	BVDU* (Å²)	LD	BVDU** (Å²)	ω	BVDU*** (Å²)	Z	ΔBVDU (Å²)
(001)	2	25,00	0,08	2	0,16	2	0,32	8	0,04	4	0,16
(110)	4	35,35	0,11	2	0,23	4	0,91	4	0,23	2	0,45
(111)	6	43,30	0,14	1	0,14	6	0,83	6	0,14	3	0,42
I.											
(001)	1,75	25,00	0,07	2	0,14	2	0,28	8	0,04	4	0,14
(110)	3,5	35,35	0,10	2	0,20	4	0,79	4	0,20	2	0,40
(111)	5,25	43,30	0,12	1	0,12	6	0,73	6	0,12	3	0,36
II.											
(001)	1,5	25,00	0,06	2	0,12	2	0,24	8	0,03	4	0,12
(110)	3	35,35	0,08	2	0,17	4	0,68	4	0,17	2	0,34
(111)	4,5	43,30	0,10	1	0,10	6	0,62	6	0,10	3	0,31
IIII.											
(001)	1,5	25,00	0,06	2	0,12	2	0,24	8	0,03	4	0,12
(110)	3	35,35	0,08	2	0,17	4	0,68	4	0,17	2	0,34
(111)	3,75	43,30	0,09	1	0,09	6	0,52	6	0,09	3	0,26
IV.											
(001)	1,5	25,00	0,06	2	0,12	2	0,24	8	0,03	4	0,12
(110)	3	35,35	0,08	2	0,17	4	0,68	4	0,17	2	0,34
(111)	3	43,30	0,07	1	0,07	6	0,42	6	0,07	3	0,21

Case 2 (Figure 11.6, pp. 212)

Face	BVDU	Area (Å²)	BVDU (Å²)	RD	BVDU* (Å²)	LD	BVDU** (Å²)	ω	BVDU*** (Å²)	Z	ΔBVDU (Å²)
(001)	2	25,00	0,08	2	0,16	2	0,32	8	0,04	4	0,16
(110)	4	35,35	0,11	2	0,23	4	0,91	4	0,23	2	0,45
(111)	6	43,30	0,14	1	0,14	6	0,83	6	0,14	3	0,42
I.											
(001)	1,75	25,00	0,07	2	0,14	2	0,28	8	0,04	4	0,14
(110)	3,5	35,35	0,10	2	0,20	4	0,79	4	0,20	2	0,40
(111)	5,25	43,30	0,12	1	0,12	6	0,73	6	0,12	3	0,36
II.											
(001)	1,5	25,00	0,06	2	0,12	2	0,24	8	0,03	4	0,12
(110)	3	35,35	0,08	2	0,17	4	0,68	4	0,17	2	0,34
(111)	4,5	43,30	0,10	1	0,10	6	0,62	6	0,10	3	0,31
IIII.											
(001)	1,25	25,00	0,05	2	0,10	2	0,20	8	0,03	4	0,10
(110)	2,5	35,35	0,07	2	0,14	4	0,57	4	0,14	2	0,28
(111)	3,75	43,30	0,09	1	0,09	6	0,52	6	0,09	3	0,26
IV.											
(001)	1	25,00	0,04	2	0,08	2	0,16	8	0,02	4	0,08
(110)	2	35,35	0,06	2	0,11	4	0,45	4	0,11	2	0,23
(111)	3	43,30	0,07	1	0,07	6	0,42	6	0,07	3	0,21

Case 3 (Figure 11.7, pp. 213)

Face	BVDU	Area (Å²)	BVDU (Å²)	RD	BVDU* (Å²)	LD	BVDU** (Å²)	ω	BVDU*** (Å²)	Z	ΔBVDU (Å²)
(001)	2	25,00	0,08	2	0,16	2	0,32	8	0,04	4	0,16
(110)	4	35,35	0,11	2	0,23	4	0,91	4	0,23	2	0,45
(111)	6	43,30	0,14	1	0,14	6	0,83	6	0,14	3	0,42
I.											
(001)	2	25,00	0,08	2	0,16	2	0,32	8	0,04	4	0,16
(110)	3,4	35,35	0,10	2	0,19	4	0,77	4	0,19	2	0,38
(111)	4,8	43,30	0,11	1	0,11	6	0,67	6	0,11	3	0,33
II.											
(001)	2	25,00	0,08	2	0,16	2	0,32	8	0,04	4	0,16
(110)	2,8	35,35	0,08	2	0,16	4	0,63	4	0,16	2	0,32
(111)	3,6	43,30	0,08	1	0,08	6	0,50	6	0,08	3	0,25
IIII.											
(001)	2	25,00	0,08	2	0,16	2	0,32	8	0,04	4	0,16
(110)	2,8	35,35	0,08	2	0,16	4	0,63	4	0,16	2	0,32
(111)	2,4	43,30	0,06	1	0,06	6	0,33	6	0,06	3	0,17
IV.											
(001)	2	25,00	0,08	2	0,16	2	0,32	8	0,04	4	0,16
(110)	2,8	35,35	0,08	2	0,16	4	0,63	4	0,16	2	0,32
(111)	1,2	43,30	0,03	1	0,03	6	0,17	6	0,03	3	0,08

Case 4 (Figure 11.8, pp. 214)

Face	BVDU	Area (Å²)	BVDU (Å²)	RD	BVDU* (Å²)	LD	BVDU** (Å²)	ω	BVDU*** (Å²)	Z	ΔBVDU (Å²)
(001)	2	25,00	0,08	2	0,16	2	0,32	8	0,04	4	0,16
(110)	4	35,35	0,11	2	0,23	4	0,91	4	0,23	2	0,45
(111)	6	43,30	0,14	1	0,14	6	0,83	6	0,14	3	0,42
I.											
(001)	2	25,00	0,08	2	0,16	2	0,32	8	0,04	4	0,16
(110)	3,4	35,35	0,10	2	0,19	4	0,77	4	0,19	2	0,38
(111)	4,8	43,30	0,11	1	0,11	6	0,67	6	0,11	3	0,33
II.											
(001)	2	25,00	0,08	2	0,16	2	0,32	8	0,04	4	0,16
(110)	2,8	35,35	0,08	2	0,16	4	0,63	4	0,16	2	0,32
(111)	3,6	43,30	0,08	1	0,08	6	0,50	6	0,08	3	0,25
IIII.											
(001)	2	25,00	0,08	2	0,16	2	0,32	8	0,04	4	0,16
(110)	2,2	35,35	0,06	2	0,12	4	0,50	4	0,12	2	0,25
(111)	2,4	43,30	0,06	1	0,06	6	0,33	6	0,06	3	0,17
IV.											
(001)	2	25,00	0,08	2	0,16	2	0,32	8	0,04	4	0,16
(110)	1,6	35,35	0,05	2	0,09	4	0,36	4	0,09	2	0,18
(111)	1,2	43,30	0,03	1	0,03	6	0,1663	6	0,03	3	0,08

Case 5 (Figure 11.9, pp. 215)

Face	BVDU	Area (Å²)	BVDU (Å²)	RD	BVDU* (Å²)	LD	BVDU** (Å²)	ω	BVDU*** (Å²)	Z	ΔBVDU (Å²)
(001)	2	25,00	0,08	2	0,16	2	0,32	8	0,04	4	0,16
(110)	4	35,35	0,11	2	0,23	4	0,91	4	0,23	2	0,45
(111)	6	43,30	0,14	1	0,14	6	0,83	6	0,14	3	0,42
I.											
(001)	2	25,00	0,08	2	0,16	2	0,32	8	0,04	4	0,16
(110)	3,1	35,35	0,09	2	0,18	4	0,70	4	0,18	2	0,35
(111)	5,1	43,30	0,12	1	0,12	6	0,71	6	0,12	3	0,35
II.											
(001)	2	25,00	0,08	2	0,16	2	0,32	8	0,04	4	0,16
(110)	2,2	35,35	0,06	2	0,12	4	0,50	4	0,12	2	0,25
(111)	4,2	43,30	0,10	1	0,10	6	0,58	6	0,10	3	0,29
IIII.											
(001)	2	25,00	0,08	2	0,16	2	0,32	8	0,04	4	0,16
(110)	2,2	35,35	0,06	2	0,12	4	0,50	4	0,12	2	0,25
(111)	3,3	43,30	0,08	1	0,08	6	0,46	6	0,08	3	0,23
IV.											
(001)	2	25,00	0,08	2	0,16	2	0,32	8	0,04	4	0,16
(110)	2,2	35,35	0,06	2	0,12	4	0,50	4	0,12	2	0,25
(111)	2,4	43,30	0,06	1	0,06	6	0,33	6	0,06	3	0,17

Case 6 (Figure 11.10, pp. 217)

Face	BVDU	Area (Å²)	BVDU (Å²)	RD	BVDU* (Å²)	LD	BVDU** (Å²)	ω	BVDU*** (Å²)	Z	Face
(001)	2	25,00	0,08	2	0,16	2	0,32	8	0,04	4	0,16
(110)	4	35,35	0,11	2	0,23	4	0,91	4	0,23	2	0,45
(111)	6	43,30	0,14	1	0,14	6	0,83	6	0,14	3	0,42
I.											
(001)	2	25,00	0,08	2	0,16	2	0,32	8	0,04	4	0,16
(110)	3,1	35,35	0,09	2	0,18	4	0,70	4	0,18	2	0,35
x(111)	5,1	43,30	0,12	1	0,12	6	0,71	6	0,12	3	0,35

Appendix IV

Abbrevations for the Bond-valence deficiency model

BVD	: Bond-valence Deficiency
BVDF	: Bond-valence deficiency of a face.
BVDU	: Bond-valence deficiency of a crystal surface of unit-cell dimension
BVDU*	: BVDU-value corrected by RD-factor
BVDU**	: BVDU-value corrected by RD-factor and LD-factor
BVDU***	: BVDU-value corrected by RD-factor, Ld-factor and ω-factor
ΔBVDU	: BVDU-value corrected by RD-factor, Ld-factor, ω-factor and Z-factor
DB	: Dangling-bond
FS-factor	: Face symmetry factor.
ω-factor	: Symmetry factor considering the “Eigensymmetry” of the crystal face
LD-factor	: Lattice density factor
RD-factor	: Reticular density factor
Z-factor	: Symmetry factor considering the site symmetry of a crystal face

Appendix V

List of Presentations at Conferences (2001-2006) and papers published

MUTTER, A.; SCHINDLER, M. & PUTNIS, A.: AFM studies on U-minerals: Dissolution processes on the surface of minerals of the autunite-group. Berichte der Deutschen Mineralogischen Gesellschaft. European Journal Mineralogy Vol.14, pp.131; (2001)

SCHINDLER, M.; **MUTTER**, A. & PUTNIS, A.: AFM-studies on crystal growth and dissolution processes of uranyl-oxide minerals. 18th International Mineralogical Association Meeting. Glasgow, Scottland; (2002).

SCHINDLER, M; **MUTTER**, A. & PUTNIS, A.: AFM-examinations on the crystal growth of uranyl-oxide minerals on the surface of calcite. Goldschmidt Conference, Davos, Switzerland (2002).

MUTTER, A.; SCHINDLER, M & PUTNIS, A.: & PUTNIS, A.: AFM-examinations of dissolution and crystal growth processes on the (001) surface of schoepite. Goldschmidt Conference, Davos, Switzerland (2002)

SCHINDLER, M.; HAWTHORNE, F.C.; **MUTTER**, A; LÖNS, J. & PUTNIS, A. (2003): Prediction and observation of the crystal morphology of complex uranyl-sheet minerals. Beih. Z. Eur. Journ. Mineral., Vol. 15, pp. 171; (2003).

MUTTER, A.; SCHINDLER, M. & PUTNIS, A.: The bond-valence method – another perspective on crystal surface reactions. Gordschmidt Conference, Kopenhagen. (2004).

MUTTER, A.; . M. SCHINDLER, M. & PUTNIS, A.: Application of the bond-valence method to crystal growth and dissolution processes on crystal surfaces. 32nd International Geological Congress, Florence; (2004).

MUTTER, A. & PUTNIS, A.: The bond-valence method: An approach to crystal surface reactions. Beih. Z. Eur. Journ. Mineral., Vol. 16, pp. 96; (2004).

SCHINDLER, M.; **MUTTER**, A.; HAWTHORNE, F.C. & PUTNIS, A.: Prediction of crystal morphology of complex uranyl-sheet minerals. I Theory. Canadian Min., Vol. 42, Part 6., pp. 1629; (2004a); (Paper see below).

SCHINDLER, M.; **MUTTER**, A.; HAWTHORNE, F.C. & PUTNIS, A.: Prediction of crystal morphology of complex uranyl-sheet minerals. II Observations. Canadian Min., Vol. 42, Part 6., pp. 1651. (2004b). (Paper see below).

MUTTER, A. & PUTNIS, A.: The bond-vaelnce deficiency: An approach to describe crystal morphology changes. Beih. Z. Eur. Journ. Mineral., Vol. 17, pp. 96; (2005).

MUTTER, A.: Application of the Bond-vaelnce deficiency model. Beih. Z. Eur. Journ. Mineral., Vol. 18, pp. 98; (2006).

The Canadian Mineralogist
Vol. 42, pp. 1629-1649 (2004)

PREDICTION OF CRYSTAL MORPHOLOGY OF COMPLEX URANYL-SHEET MINERALS. I. THEORY

MICHAEL SCHINDLER[§] AND ANDREAS MUTTER

Institut für Mineralogie, Universität Münster, Corrensstr. 24, D-48149 Münster, Germany

FRANK C. HAWTHORNE

Department of Geological Sciences, University of Manitoba, Winnipeg, Manitoba R3T 2N2, Canada

ANDREW PUTNIS

Institut für Mineralogie, Universität Münster, Corrensstr. 24, D-48149 Münster, Germany

ABSTRACT

Edges on the basal face of uranyl-sheet minerals control dissolution and crystal-growth processes because of their higher interaction with the aqueous solution than the less reactive basal face. A basal face is parallel to the structural unit of a uranyl-sheet mineral and dominates its crystal morphology. Edges terminate a structural unit and define the morphology of the prominent basal face. Edges are parallel to linear periodic chains of polyhedra in the structural unit, at which anion terminations interact with a coexisting aqueous solution through acid–base reactions and acceptance of weaker bonds from cationic aqueous species. The bond-valence deficiency of an anion at an anion termination correlates with the intrinsic acidity constant, *pKa*, and the free energy, ΔG_{at}, of the corresponding protonation-type reaction. The degree of interaction of an edge with the coexisting aqueous solution can be described by the bond-valence deficiency per unit length of the anion terminations on the corresponding chain of polyhedra, *i.e.*, an edge at which each site is activated by interaction with aqueous species. The type and number of activated sites on an edge correlate with the bond-valence deficiency of the corresponding chain of polyhedra. Growth and dissolution at an edge are promoted by interaction between activated sites and aqueous solution. The interaction has its minimum at the point of zero-charge (pH_{pzc}) of the edge and at saturation with respect to the mineral, and increases with the difference between pH and pH_{pzc}, and with the degree of saturation. Edges containing a small number of activated sites are stable, grow and dissolve slowly, and invariably occur on the final morphology of the basal face. Edges containing an average number of activated sites are less stable, grow and dissolve faster, and will occur on the final morphology only if crystal growth occurs in solutions with a pH close to pH_{pzc}, and close to saturation with respect to the mineral. Edges with the highest number of activated sites have the lowest stability and may never occur on the final morphology. Interaction of an edge with the aqueous solution depends also on the shift between the layers and the arrangement of the interstitial complexes between the layers.

Keywords: uranyl minerals, morphology, surface structure, crystal growth, dissolution, bond valence.

SOMMAIRE

La bordure de la face parallèle à la base du feuillet des minéraux à uranyle régit la dissolution et les processus de croissance cristalline à cause de sa plus grande interaction avec la solution aqueuse que la face elle-même, moins réactive. Une telle face est parallèle aux unités structurales des feuillets contenant les groupes d'uranyle, et elle est déterminante du point de vue morphologique. Les bordures représentent la terminaison des unités structurales, et définissent la morphologie de la face de base, proéminente. Ces bordures sont parallèles aux chaînes linéaires périodiques de polyèdres de l'unité structurale, là où il y a interaction des terminaisons d'anions avec la solution aqueuse coexistante grâce à des réactions acide–base, et où des liaisons plus faibles provenant d'espèces aqueuses cationiques sont acceptées. Le déficit en valences de liaison d'un anion à la terminaison d'une chaîne d'anions dépend de la constante intrinsèque de l'acidité, *pKa*, et de l'énergie libre, ΔG_{at}, de la réaction correspondante de protonation. On peut décrire le degré d'interaction d'une bordure avec la solution aqueuse coexistante en évaluant le déficit en valences de liaison par unité de longueur des terminaisons des anions dans la chaîne de polyèdres correspondante, c'est-à-dire, une bordure à laquelle chaque site est rendu actif par interaction avec des espèces aqueuses. Le type et le nombre de sites ainsi

§ *Current address*: Department of Geological Sciences, University of Manitoba, Winnipeg, Manitoba R3T 2N2, Canada.
E-mail address: mschindl@lakeheadu.ca

activés à la bordure montre une corrélation avec le déficit en valences de liaison de la chaîne de polyèdres correspondante. La croissance et la dissolution à une telle bordure est accélérée par interactions entre sites activés et la solution aqueuse. L'interaction atteint son minimum au point de charge zéro (pH_{pzc}) de la bordure, et à saturation par rapport au minéral, et augmente avec la différence entre pH et pH_{pzc}, et avec le degré de sursaturation. Les bordures contenant un faible nombre de tels sites activés sont stables, croissent et se dissoudent lentement, et sont normalement développées dans l'expression morphologique finale de la face de base. Les bordures contenant un nombre moyen de tels sites activés sont moins stables, croissent et se dissoudent plus rapidement, et seront présentes dans l'expression morphologique finale de la face de base seulement si la croissance cristalline se déroule dans des solutions ayant un pH voisin de pH_{pzc}, et à des conditions voisines de la saturation par rapport au minéral. Les bordures ayant le nombre de sites activés le plus élevé auront une stabilité moindre, et pourraient bien ne pas être présentes dans l'expression morphologique finale. L'interaction d'une bordure avec la solution aqueuse dépend aussi du degré de déplacement entre les feuillets et de l'arrangement des complexes interstitiels entre les feuillets.

(Traduit par la Rédaction)

Mots-clés: minéraux d'uranyle, morphologie, structure de la surface, croissance cristalline, dissolution, valences de liaison.

Introduction

The morphology of a crystal, the geometry of an etch pit and the characteristics of two-dimensional growth islands on a crystal surface are presumably related to the structural arrangement of atoms in the crystal. This connection was explored by Hartman & Perdok (1955a, b, c), who developed the PBC (Periodic Bond-Chain) theory. The basic idea is as follows: when an atom or complex attaches to a growing surface of a crystal during crystallization, the probability of subsequent detachment is inversely proportional to the number of strong bonds between the atom or complex and the crystal surface. Thus, in PBC theory, the focus is on uninterrupted chains of strong bonds between building units, called PBCs, in which the strong bonds belong to the primary coordination of an atom or molecule. PBC chains that contain only strong bonds between atoms or molecules define the direction of major growth of a crystal, and PBC chains containing weaker bonds between atoms define directions of minor growth. PBC theory distinguishes three different types of faces: F (or flat) faces with two or more types of PBCs (periodic bond-chains) parallel to the face; S (or stepped) faces with one type of PBC parallel to the face, and K (or kinked) faces with no PBCs parallel to the face. In PBC theory, the morphology of a crystal is controlled by the occurrence of F faces. The prediction of morphology from the crystal structure involves (1) determination of PBCs, and (2) classification of (*hkl*) layers as F, S or K faces.

An alternative approach to the morphology of a crystal is to use molecular modeling (with either empirical or quantum-mechanical models) to calculate surface energies or step energies. The surface energy is the difference in energy between the bulk structure and the surface structure; thus, the lower the surface energy, the more stable the face. The step energy is the difference in energy between the surface and the corresponding step; thus, the lower the step energy, the more stable the step. Using such calculations, one can categorize different faces or steps, and calculate the energy of any face or step that might occur in a crystallization or dissolution process. These calculations work well as long as accurate interaction potentials are available for the constituent species. This is not usually the case for complex hydroxy-hydrated oxysalt minerals, which contain unusual coordination geometries and both (OH) and (H_2O) groups, *e.g.*, althupite, Al Th [(UO_2) {$(UO_2)_3$ $(PO_4)_2$ (OH) O}$_2$] $(OH)_3$ $(H_2O)_{15}$. This situation is unsatisfactory, as hydroxy-hydrated oxysalts constitute the bulk of the mineral kingdom and are by far the most important phases from an environmental perspective. Moreover, we know far less about the factors that control their atomic arrangements, chemical compositions, morphology, dissolution and stabilities than for the (usually) more simple rock-forming minerals. Here, we develop a more mechanistic approach to crystallization, dissolution and crystal morphology, and apply it to uranyl-sheet minerals. In addition, we measure the *pKa* value for dehydrated schoepite in order to compare it with the *pKa* value calculated with the MUSIC model of multisite complexation.

Surface Features on Basal Faces

Chemical reactions on the surfaces of uranyl-sheet minerals are an important issue, as they result in the release of $(UO_2)^{2+}$ to natural waters. Therefore, a detailed atomic-scale understanding of the surface chemistry of uranyl-sheet minerals is desirable. Uranyl-sheet minerals contain layers of polymerized uranyl-polyhedra with uranium in [6], [7] and [8]-coordination as tetragonal, pentagonal and hexagonal bipyramids, respectively. In these polyhedra, strong U–O uranyl bonds are not involved in linkage between uranyl polyhedra; they extend orthogonal to the sheet, whereas weaker equatorial U–φ bonds [φ = O^{2-}, $(OH)^-$, (H_2O)] link the polyhedra in the plane of the sheet (Fig. 1).

Periodic Bond-Chain theory (Hartman & Perdok 1955a, b, c) defines the basal face parallel to the sheets of uranyl polyhedra as an F face because the sheet contains more than one periodic bond-chain. If one considers polyhedra instead of bonds, a linear periodic bond-chain is part of a linear periodic chain of polyhe-

dra, which we will designate as a *polyhedron chain* or *chain*. A polyhedron chain that terminates a sheet contains ligands that bond either to U^{6+} cations or to U^{6+} cations *and* to species in the adjacent gas phase or aqueous solution. Any anion on a terminating chain, and the cations to which it is bonded, form a *termination*. The linearity of the chain of polyhedra requires that polyhedra should have a small number of U–φ terminations. In the case of uranyl minerals, we consider only those chains in which each polyhedron has no more than two terminations of the type $U-^{[1]}\varphi$. Figure 1 shows chains of polyhedra parallel to [100], [010], [120], [210] and [110] in the structural unit of schoepite, $[(UO_2)_8O_2(OH)_{12}](H_2O)_{12}$ (Finch *et al.* 1996).

The basal face of a uranyl-sheet mineral is the face parallel to the layers of uranyl polyhedra. Addition of one or more of these uranyl layers can form surface features such as *terraces* and *steps* on the basal face. The termination of one structural unit orthogonal to the basal face is called an *edge*. An array of coplanar edges defines a *step* or a *face* non-coplanar with the basal face. The edge and basal surfaces vary in reactivity owing to differences in the local stereochemistry of their constituent uranyl polyhedra. The reactivity of the basal surface is determined primarily by the reactivity of the apical atoms of oxygen of the uranyl group, $(UO_2)^{2+}$. These oxygen atoms receive an average of 1.6–1.7 valence units (*vu*) from the U–O bond, and hence they cannot be protonated (by H^+), as each O–H bond has an average bond-valence of 0.80 *vu*, and the aggregate incident bond-valence at the uranyl O-atom would be 1.6 + 0.8 = 2.4 *vu*, in conflict with the valence-sum rule (Brown 1981, Hawthorne 1994, 1997). Apical oxygen atoms of the uranyl group are therefore not involved directly in any acid–base reactions at the surface.

Equatorial oxygen atoms in the sheet of polyhedra commonly bond to two or three U^{6+}-atoms (Fig. 1). In contrast to the uranyl bonds, equatorial U–O bond-lengths vary over a larger range, with average bond-valences between 0.2 and 0.8 *vu*. Thus, equatorial O-atoms at basal and edge surfaces can participate in acid–base reactions through protonation and deprotonation. Hence, edge surfaces are much more reactive than basal surfaces because equatorial O-atoms on the edge surface almost always bond to fewer atoms of U^{6+} than O-atoms in the sheet, and hence must satisfy their

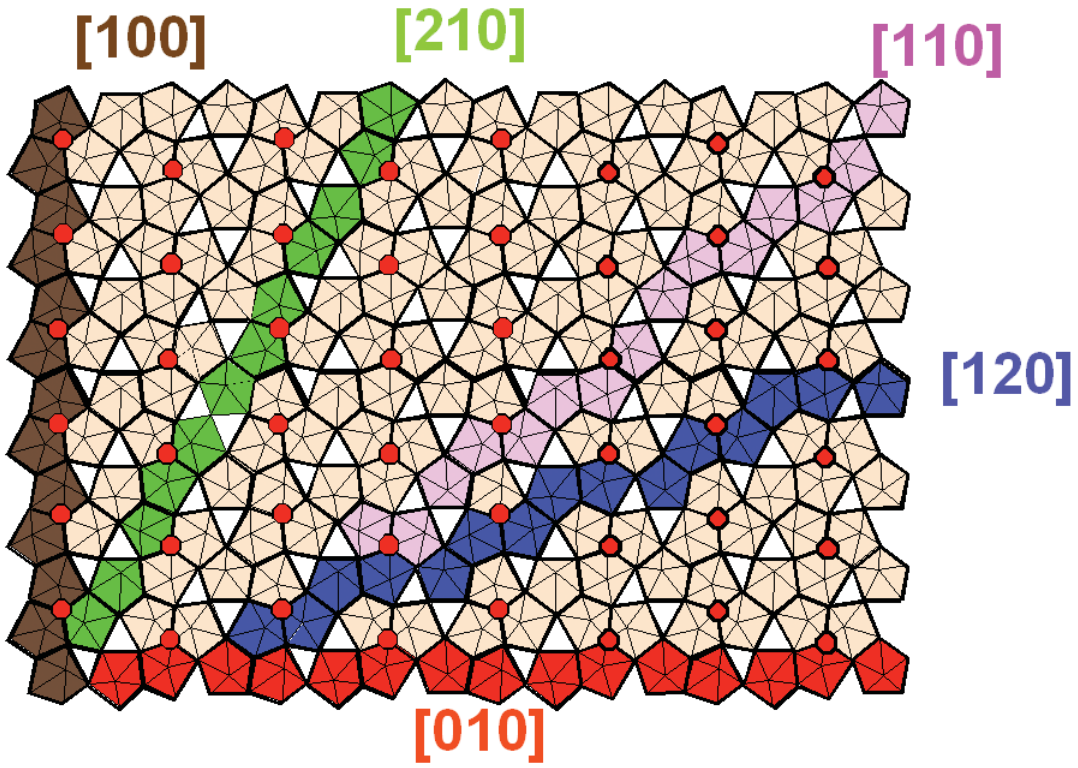

FIG. 1. Polyhedron representation of the uranyl-oxide hydroxy-hydrate sheet in schoepite, $[(UO_2)_8O_2(OH)_{12}](H_2O)_{12}$; chains of polyhedra parallel to [100], [010], [120], [110] and [210] are shown in brown, red, blue, pink and green, respectively; equatorial O^{2-} anions of the uranyl polyhedra are shown as red octagons, equatorial edges are shown as heavy black lines.

individual bond-valence requirements through a higher degree of protonation.

The reactivity of edges is an important factor in the dissolution of sheet minerals; for example, the dissolution of phyllosilicates is controlled by acid–base reactions on the corresponding edges (*e.g.*, Rufe & Hochella 1999). Thus in order to understand dissolution and growth processes for uranyl-sheet minerals, one requires details of the structures of their edges. Inspection of Figure 1 suggests the following question: which periodic bond-chains in uranyl sheets define the morphology of the corresponding F-faces? Application of PBC theory requires categorization of different types of bonds in these bond chains. Bonds between U^{6+} and O^{2-} or $(OH)^{-}$ can have similar strengths in all these chains, and therefore one must consider the distances to the central U^{6+} cations. PBC theory does not consider the type of equatorial ligands in the chain [O^{2-} or $(OH)^{-}$], the shift between the uranyl sheets, the arrangement of interstitial cations, the change in morphology with pH or the degree of supersaturation (see below). Here, we introduce an approach to crystal morphology that considers these issues, using characteristic bond-valence values between U^{6+} and its equatorial ligands. Furthermore, we will show that change in morphology with pH depends on the equilibrium constants of the anion terminations on the surface of uranyl-oxide minerals. For the surface structure of schoepite, $[(UO_2)_8O_2(OH)_{12}](H_2O)_{12}$, we calculate the bond-valence deficiencies for the various types of chains of polyhedra and use the equation of Hiemstra *et al.* (1996) to calculate the corresponding *pKa* values of the acid–base reactions on the anion terminations of the chains. In addition, we measure the *pKa* value of the anion terminations on the basal face of dehydrated schoepite by titration of a fine suspension of synthetic dehydrated schoepite, to compare with our calculated values.

Bond-Valence Theory

Quantitative bond-valence parameters were introduced by Brown & Shannon (1973), and Brown (1981) developed the first ideas on bond-valence theory. Hawthorne (1985, 1990, 1994) applied these ideas to complex oxysalt minerals and developed the idea of the structural unit with a characteristic Lewis basicity. Schindler & Hawthorne (2001a, b, c, 2004) and Schindler *et al.* (2000) extended these ideas and showed how extended bond-valence theory can be used to predict details of mineral composition and stability that are not accessible to other approaches. There has been some application of bond-valence ideas to mineral surfaces (*e.g.*, Barger *et al.* 1997a, b, c, Brown & Parks 2001), but this has focused on adsorption of "foreign" ions rather than on crystallization of the mineral itself.

Bond valence and the valence-sum rule

If interatomic distances are known, bond valences can be calculated from the following equations:

$$s = s_0\,[R / R_0\,]^N,\ s = [R / R_1]^n$$

or

$$s = \exp\,[(R / R_o) / B] \qquad (1)$$

where s is in valence units (*vu*), R is the observed bond-length, and R_0, N, R_1, n and B are constants (characteristic of cation–anion pairs) that are derived by fitting these equations to a large number of well-refined crystal structures such that the sum of the incident bond-valences at any atom be as close as possible to the formal valence of that atom (Brown & Shannon 1973, Brown & Altermatt 1985). In stable (observed) crystal structures, the *valence-sum rule* is obeyed: *the sum of the bond valences at each atom is approximately equal to the magnitude of the atomic valence*.

Characteristic bond-valence

Bond valences around a specific cation in a wide range of crystal structures lie within ~20% of the mean value, which is thus *characteristic* of that particular cation (Brown 1981). The characteristic bond-valences of cations correlate strongly with their *electronegativity*, a measure of the electrophilic strength (electron-accepting capacity) of the cation. The correlation with characteristic bond-valence indicates that the latter is a measure of the *Lewis-acid strength* of the cation (Brown 1981). The Lewis-base strength of an anion is similarly defined as the characteristic valence of the bonds formed by the anion. However, variations in bond valence around anions are much greater than around cations, and it is not useful to designate Lewis basicities for simple anions such as O^{2-}.

If we examine the $(CO_3)^{2-}$ group as an oxyanion, each O^{2-} receives 1.33 *vu* from the central C^{4+} cation and needs an additional 0.67 *vu* from other cations. In calcite, for example, the oxygen atoms of the $(CO_3)^{2-}$ group are [3]-coordinated, and hence need an additional two bonds if we consider the $(CO_3)^{2-}$ group as an oxyanion; the additional bond-valence needed is thus 0.33 *vu* for each of the oxygen atoms of the $(CO_3)^{2-}$ group. If this process is repeated for all (CO_3) groups in minerals, the mean value of the characteristic bond-valence obtained is 0.25 *vu* with only a small dispersion. In this way, we can define the *Lewis basicity* of an oxyanion (Brown 1981).

The valence-matching principle

The definitions of Lewis-acid and Lewis-base strengths lead to a specific criterion for chemical bond-

ing, the *valence-matching principle* (Brown 1981): *The most stable structures will form where the Lewis-acid strength of the cation closely matches the Lewis-base strength of the anion*. As a chemical bond contains two constituents, the properties of the constituents must match for a stable configuration to form.

Binary Structural Representation

One of the problems in dealing with mineral structures is the complexity of the atomic interactions; there are a large number of such interactions, and their spatial characteristics are important. However, we can simplify this problem in the following way: we factor a crystal structure into two components: the *structural unit* (an array of high-bond-valence polyhedra that is usually anionic in character) and the *interstitial complex* [an array of large low-valence cations, simple anions and (H_2O) groups that is usually cationic in character]. If we can calculate aggregate properties such as Lewis basicity and Lewis acidity, we can use the valence-matching principle to examine the interaction of the structural unit and the interstitial complex (Hawthorne 1985, 1986, 1990). Schindler & Hawthorne (2001a) described how to calculate Lewis basicity and Lewis acidity for a structural unit and an interstitial complex.

Interaction of a Surface with an Aqueous Solution: a Bond-Valence Approach

As noted above, the bond-valence sum incident at any cation or anion must be equal to its formal valence. In the bulk structure, the bond valences contributing to such a sum involve simple ions at the vertices of the associated coordination-polyhedra. With regard to a surface, we may identify two distinct situations: (1) the surface of the crystal is adjacent to a vacuum; (2) the surface of the crystal is adjacent to a liquid (or a gas). In the first situation, the ions at the surface of a crystal by definition must have coordinations different from those in the bulk crystal, and these differences will exist over long time-scales. The surface structure responds to these differences by lengthening or shortening specific bonds; such differences in bond lengths (and bond angles) are commonly called the *relaxation* of the surface. As a result of these differences, the pattern of bond valences at and near the surface in a vacuum must differ significantly from that in the bulk crystal, even to the extent that there may be a reorganization of the topology of the chemical bonds at the surface. In the second situation, although the atoms at the surface must have coordinations different from those in the bulk crystal, the bond-valence requirements of these surface atoms are also partly met by neighboring atoms in the coexisting liquid (or gas). Hence surface relaxation will be much less than where the surface is exposed to a vacuum. Indeed, the atoms of the liquid will tend to arrange themselves such that relaxation at the surface of the solid is minimized, and one may well be able to consider local interactions among atoms as the average of what occurs at the surface over a longer time-scale. This discussion suggests that we may be able to use an unrelaxed surface model in which one treats bond valences of near-surface bonds as equal to the bond valences of the analogous bonds in the bulk structure.

Intrinsic acidity constants of anion terminations in oxide minerals

Consider a crystal in equilibrium with an aqueous solution. Depending on the pH of the solution, the surface is partly or fully hydrated, and aqueous species in the solution bond to anions or cations on the surface (chemisorption). The degree of hydration and type of chemisorption depend on the type of anion or cation on the surface and on the conditions in the coexisting solution. The degree of hydration can be predicted with the acidity constants of the different anion-terminations and the pH of the solution. Van Riemsdijk and co-workers (Hiemstra *et al.* 1996) developed a "multisite complexation model" (MUSIC), which can be used to predict anion acidities using a modified form of the following equation:

$$pKa = -A\,(\Sigma s_j + V) \tag{2}$$

where pKa is the intrinsic acidity constant [a constant valid for an uncharged surface (Stumm 1992)], A equals 19.8, V is the valence of the oxygen atom at the surface (–2), and Σs_j is the bond-valence sum at the surface oxygen atom and is defined by

$$\Sigma s_j = \{s_M + ms_H + n(1 - s_H)\} \tag{3}$$

where s_M is the bond valence of the *M*–O bond, s_H is the bond valence of the H–O bond to the surface oxygen if the base is a hydroxyl group (assumed to be 0.80 *vu*), $(1 - s_H)$ is the valence of weak hydrogen bonds from aqueous species to surface anions, and m and n are the numbers of stronger O–H and weaker O…H bonds, respectively. Hiemstra *et al.* (1996) used fixed *M*–O bond-valences from unrelaxed bulk-structures to predict intrinsic acidity constants for surface groups. Bickmore *et al.* (2003) used *ab initio* calculations for the average of *M*–O bond-valences of protonated and deprotonated relaxed surface-structures in 2:1 phyllosilicates; their average bond-valence values for Fe–O, Al–O and Si–O bonds are similar to the corresponding values used by Hiemstra *et al.* (1996).

The key issue in the prediction of appropriate intrinsic acidity-constants is use of the correct *average coordination number of O* on the surface. Here, Hiemstra *et al.* (1996) used an average coordination of oxygen of [3] for the more compact surfaces of gibbsite and goethite, and an average coordination number of [4] for the more open surface of quartz. The resulting intrinsic acid-

ity-constants were used to calculate the point of zero-charge (pH_{pzc}, Stumm 1992) for gibbsite, goethite and quartz, and the results agree with experimental values.

Calculation of intrinsic acidity-constants for different U–O anion-terminations on edges of the basal face of uranyl-sheet minerals

The edges on uranyl sheets contain equatorial anions in a coordination different from that in the bulk structure. For tetragonal, pentagonal and hexagonal bipyramidal coordination, the characteristic equatorial U–φ bond-valences are 0.64, 0.54 and 0.45 *vu*, respectively (Burns 1999). However, individual equatorial $^{[a]}$U–φ bond-lengths vary over a larger range than the corresponding Al–O, Fe–O and Si–O bond-lengths. For example, the $^{[7]}$U–φ bond-lengths in schoepite, $[(UO_2)_8O_2(OH)_{12}](H_2O)_{12}$, vary between 2.2 and 2.7 Å (Finch *et al.* 1996), which correspond to bond valences of 0.73 and 0.27 *vu*, respectively. These high variations in individual bond-valences in uranyl minerals may give rise to a range of intrinsic acidity-constants for one type of anion termination.

The type of anion termination on edges in uranyl minerals is limited by the occurrence of [6]-, [7]- and [8]-coordinated U^{6+}: *e.g.*, [6]- and [8]-coordinated U^{6+} never occur together, and always occur with [7]-coordinated U^{6+}. The type of anion termination can be indicated by the code $^{[a]}$U–φ–$n^{[b]}$U, where the φ is an unspecified anion that bonds to one U atom in [*a*] coordination and $n \times$ U atoms in [*b*] coordination. If we do not consider other oxyanions [*e.g.*, $(VO_4)^{3-}$, $(PO_4)^{3-}$, $(SiO_4)^{4-}$], the following combinations of anion terminations can occur on edges in uranyl-oxide sheet minerals: $^{[8]}$U–φ, $^{[7]}$U–φ, $^{[6]}$U–φ, $^{[8]}$U–φ–$^{[8]}$U, $^{[8]}$U–φ–$^{[7]}$U, $^{[7]}$U–φ–$^{[7]}$U, $^{[7]}$U–φ–$^{[6]}$U, $^{[8]}$U–φ–2$^{[7]}$U, $^{[7]}$U–φ–2$^{[7]}$U and $^{[6]}$U–φ–2$^{[7]}$U. The wide variation in type of anion termination (even for one structure type) makes it difficult to determine an exact pH_{pzc} for a uranyl mineral. However, an exact pH_{pzc} is required to scale the average coordination-number of the oxygen atoms on the edge surface (see above).

An example: calculation of the intrinsic acidity-constants of anion terminations on the (001) face of schoepite

Schoepite, $[(UO_2)_8O_2(OH)_{12}](H_2O)_{12}$, has a prominent (001) basal face that dominates the morphology of its crystals. The corresponding uranyl-sheet contains U^{6+} in [7]-coordination (Finch *et al.* 1996). There are three different types of equatorial anion-terminations on the (001) face: $^{[7]}$U–OH–2$^{[7]}$U, $^{[7]}$U–OH–$^{[7]}$U and $^{[7]}$U–O–2$^{[7]}$U (Fig. 1). In order to calculate the corresponding intrinsic *pKa* values for these terminations, we can use the overall characteristic bond-valence for $^{[7]}$U–φ (0.54 *vu*), the average $^{[7]}$U–φ bond-valence of the equatorial bonds in schoepite (0.47 *vu*), or the average $^{[7]}$U–φ bond-valence for each of the three anion-terminations. Here, we use the average bond-valence of the equatorial bonds (0.47 *vu*) because this value is more appropriate than the characteristic $^{[7]}$U–φ bond-valence, and it simplifies the calculation (relative to the use of individual average bond-valences). In many uranyl-hydroxy-hydrate minerals, the coordination number of equatorial O-atoms in the structural unit is close to [4]; oxygen bonds either to three U and one H, or to two U, one H and accepts one additional hydrogen bond.

The acid–base reactions and the corresponding values of *pKa* (assuming $^{[4]}$O) are as follows:

$$^{[7]}\text{U–O–2}^{[7]}\text{U} + \text{H}^+ \leftrightarrow {}^{[7]}\text{U–OH–2}^{[7]}\text{U}, \quad pKa = 7.7 \qquad [1]$$

$$^{[7]}\text{U–O–}^{[7]}\text{U} + \text{H}^+ \leftrightarrow {}^{[7]}\text{U–OH–}^{[7]}\text{U}, \quad pKa = 13.1 \qquad [2]$$

$$^{[7]}\text{U–OH–}^{[7]}\text{U} + \text{H}^+ \leftrightarrow {}^{[7]}\text{U–OH}_2\text{–}^{[7]}\text{U}, \quad pKa = 1.2 \qquad [3]$$

The intrinsic *pKa* is calculated using the average bond-valence sum at O in the anion termination of the base (*i.e.*, for the termination on the left side of each equation). In reaction [1], the oxygen atom in $^{[7]}$U–O–2$^{[7]}$U receives 3×0.47 (from the $^{[7]}$U atoms) + 0.20 (from a hydrogen bond) = 1.61 *vu*. This results in a pKa_1 of $-19.8(1.61 - 2) = 7.7$. In reaction [2], the oxygen atom in $^{[7]}$U–O–$^{[7]}$U accepts 2×0.47 *vu* from $^{[7]}$U, and 2×0.20 *vu* from two additional hydrogen bonds; *i.e.*, its bond-valence sum is 1.34 *vu*, which corresponds to a pKa_2 of 13.1. In reaction [3], the oxygen atom in the $^{[7]}$U–OH–$^{[7]}$U termination receives 2×0.47 *vu* plus 0.80 *vu* from the O–H bond and 0.20 *vu* from an additional hydrogen bond; its bond-valence sum is 1.94 *vu*, which corresponds to a pKa_3 of 1.2.

In order to compare calculated *pKa* values with observed values, one can determine the *pKa* values of the anion-terminations *via* titration of a fine suspension of schoepite with an NaOH solution. However, schoepite samples with a non-dehydrated surface are difficult to obtain from mineral samples or from synthesis. We decided therefore to use the structurally related phase dehydrated schoepite, which can be easily obtained by hydrothermal synthesis.

Experimental procedure

Dehydrated schoepite, $[(UO_2)O_{0.2}(OH)_{1.6}]$, was synthesized under hydrothermal conditions at 120°C for 3 days with a molar ratio of 1:2.5 uranyl acetate and (H_2O). A fine suspension of 100 mg of dehydrated schoepite in 20 mL 0.1 and 1.0 mol L^{-1} NaCl solutions were titrated with 0.01 mol L^{-1} NaOH. Figure 2 shows the corresponding titration-curves with initial pH-values of 6.2 and 5.9, respectively. [Note that titration of the fine suspension of schoepite with a 0.01 mol L^{-1} HCl

solution produced an immediate drop in pH to 3–3.5.] The shift in the initial pH-values with change in concentration of the NaCl solution indicates adsorption of Na cations at specific sites on the (001) face (Stumm 1992). This adsorption results in an overall positive charge of the surface, which must be balanced by deprotonation of the U–OH–2U terminations. In this way, the (001) face of dehydrated schoepite functions as a weak acid, which explains the slightly acidic pH at the beginning of the titration. Because an NaCl solution is required to maintain a constant ionic medium, we modeled a curve for a titration in a 0.0 mol L^{-1} NaCl solution. The initial pH of the dehydrated schoepite solution in the modeled curve is around 6.5, and the *pKa* value is around 7.0 ± 0.2 (Fig. 2). This *pKa* value corresponds to the acid–base reaction U–(OH)–2U ↔ U–O–2U on the (001) face of dehydrated schoepite. [Note that in the anion-termination U–(OH)–2U of dehydrated schoepite, U occurs in [7]- and [8]-coordination. The [8]-coordination of U in dehydrated schoepite results from dehydration of schoepite and structural changes inside the uranyl sheet.] At the beginning and at the end of the titration, the (001) face of dehydrated schoepite most likely had the compositions $[(UO_2)O_{0.2+x}(OH)_{1.6-2x}]^{2x+}$ and $[(UO_2)O_2]^{2-}$, respectively.

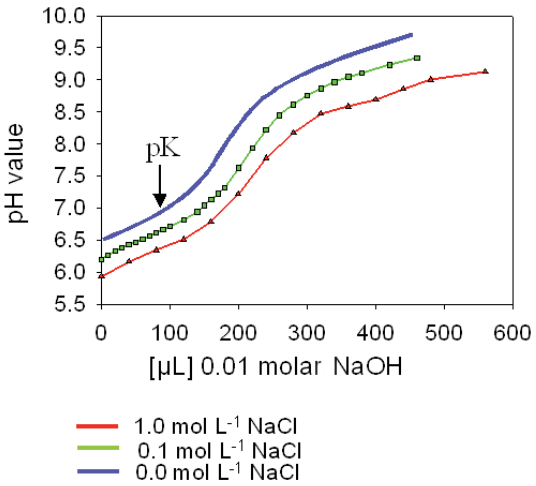

FIG. 2. Titration curves with added 0.01 mol L^{-1} NaOH *versus* pH for a fine suspension of 100 mg of dehydrated schoepite in 20 mL 0.1 mol L^{-1} (green) and 1 mol L^{-1} (red) NaCl solutions. A modeled titration-curve in a hypothetical 0.0 mol L^{-1} NaCl solution is indicated in blue (see text for details).

The calculations of the *pKa* value of schoepite and the experimentally determined *pKa* value of dehydrated schoepite are reasonably close, and suggest that the average coordination-number of [4] is an appropriate value in the case of the uranyl-oxide minerals schoepite and dehydrated schoepite. For example, if one uses an average coordination-number of [3], the intrinsic *pKa* value of the acid–base reaction $^{[7]}$U–O–2$^{[7]}$U + H^+ ↔ $^{[7]}$U–OH–2$^{[7]}$U would be 11.7, significantly different from the observed value of 7.0 ± 0.2.

The parameter 19.8 (equation 2) of the MUSIC model was fitted on the basis of experimental results on simple oxide minerals such as hematite, rutile and quartz. Hence, equation 2 in this form is not necessarily applicable to all uranyl oxide minerals, and needs to be measured in the future on uranyl oxide minerals. However, we will use this equation here in order to show how the intrinsic acidity constant is related to two other parameters that express the strength of a base and an acid: Lewis basicity and Lewis acidity. For this purpose, we calculated intrinsic acidity-constants for all kinds of anion terminations using the above-listed average $^{[n]}$U–φ bond-valences in uranyl polyhedra (Table 1).

TABLE 1. INTRINSIC ACIDITY CONSTANTS, LEWIS ACIDITIES AND LEWIS BASICITIES OF EQUATORIAL ANIONS TERMINATING EDGES ON URANYL-SHEET MINERALS

Code	Acids and bases of the anion-termination	pKa_1, pKa_2, pKa_3	Lewis acidity / Lewis basicity [*vu*]
$^{[8]}$U–φ,	$^{[8]}$U–OH_3 ↔ $^{[8]}$U–OH_2 ↔ $^{[8]}$U–OH ↔ $^{[8]}$U–O	–5, 6.9, 18.8	0.225 / 0.375, 0.52
$^{[7]}$U–φ	$^{[7]}$U–OH_3 ↔ $^{[7]}$U–OH_2 ↔ $^{[7]}$U–OH ↔ $^{[7]}$U–O	–6.7, 5.1, 17	0.27 / 0.33, 0.49
$^{[6]}$U–φ	$^{[6]}$U–OH_3 ↔ $^{[6]}$U–OH_2 ↔ $^{[6]}$U–OH ↔ $^{[6]}$U–O	–8.7, 3.1, 15	0.32 / 0.27, 0.45
$^{[8]}$U–φ–$^{[8]}$U	$^{[8]}$U–OH_2–$^{[8]}$U ↔ $^{[8]}$U–OH–$^{[8]}$U ↔ $^{[8]}$U–O–$^{[8]}$U	2, 13.8	0.30, 0.55
$^{[8]}$U–φ–$^{[7]}$U	$^{[8]}$U–OH_2–$^{[7]}$U ↔ $^{[8]}$U–OH–$^{[7]}$U ↔ $^{[8]}$U–O–$^{[7]}$U	0.2, 12	0.21, 0.51
$^{[7]}$U–φ–$^{[7]}$U	$^{[7]}$U–OH_2–$^{[7]}$U ↔ $^{[7]}$U–OH–$^{[7]}$U ↔ $^{[7]}$U–O–$^{[7]}$U	–1.6, 10.3	0.12, 0.46
$^{[7]}$U–φ–$^{[6]}$U	$^{[7]}$U–OH_2–$^{[6]}$U ↔ $^{[7]}$U–OH–$^{[6]}$U ↔ $^{[7]}$U–O–$^{[6]}$U	–3.5, 8.3	0.02, 0.41
$^{[8]}$U–φ–2$^{[7]}$U	$^{[8]}$U–OH–2$^{[7]}$U ↔ $^{[8]}$U–O –2$^{[7]}$U	5.3	0.47
$^{[7]}$U–φ–2$^{[7]}$U	$^{[7]}$U–OH –2$^{[7]}$U ↔ $^{[7]}$U–O –2$^{[7]}$U	3.5	0.38
$^{[6]}$U–φ–2$^{[7]}$U	$^{[6]}$U–OH –2$^{[7]}$U ↔ $^{[6]}$U–O –2$^{[7]}$U	2.5	0.28

Lewis basicity of anion terminations

The intrinsic acidity-constant *pKa* is a measure of the strength of the acid in an acid–base equation: the higher the *pKa*, the weaker its acid strength or the stronger the base strength of the corresponding base. Using the acid–base definition of Lewis (1916), *pKa* expresses the ability of the base (Lewis base) to donate electrons to the acid (Lewis acid).

Hawthorne (1997) and Schindler & Hawthorne (2001a) defined the Lewis-base strength of a complex structural unit as the bond valence required by the (negatively charged) structural unit divided by the number of (weak) bonds accepted by the structural unit from the interstitial complex. Using this definition, we may calculate the Lewis-base strength (or Lewis-acid strength) of an anion termination by assuming again an average O-coordination number of [4]. For example, the Lewis-base strength of the anion-termination $^{[7]}$U–OH is the required bond-valence [(2 – (0.54 + 0.80) = 0.66 *vu*] divided by the number of bonds accepted (two): 0.66 / 2 = 0.33 *vu*. For the anion termination $^{[a]}$U–OH_2, it is more useful to calculate its Lewis acidity because the constituent O-atom has an incident bond-valence sum greater than or equal to 2 *vu*. The Lewis acidity of the $^{[a]}$U–OH_2 group is the characteristic bond-valence of each constituent hydrogen bond. Hence, the (H_2O) group transforms the bond-valence (*v vu*) of the $^{[a]}$U–O bond into two weaker hydrogen bonds of bond-valence *v* /2 (Hawthorne 1992, 1994, 1997, Schindler & Hawthorne 2001a). For example, the Lewis acidity of the termination $^{[7]}$U–OH_2 is 0.54 / 2 = 0.27 *vu*. The Lewis acidities and Lewis basicities of all anion terminations are listed in Table 1.

Lewis basicity and acidity constants

Let us consider the anion terminations $^{[7]}$U–OH and $^{[7]}$U–O in the acid–base reactions [2] and [3]. The corresponding pKa_2 and pKa_3 values express the ability of the bases $^{[7]}$U–OH and $^{[7]}$U–O to donate electrons to the acid H^+. The Lewis basicities (0.33 and 0.49 *vu*) correspond to the pKa_2 and pKa_3 values of 5.1 and 17, respectively. For the anion termination $^{[a]}$U–OH_2, with [*a*] = [8], [7] and [6], we assign a negative Lewis acidity and correlate it with the corresponding *pKa* value. The anion terminations listed above can be subdivided into five groups: $^{[a]}$U–OH_2, $^{[a]}$U–OH, $^{[a]}$U–O, $^{[a]}$U–OH–2$^{[b]}$U and $^{[a]}$U–O–2$^{[b]}$U. For each group, there is a linear correlation between the Lewis basicity (acidity) and the corresponding *pKa* value (Fig. 3). This correlation can be understood if we compare the corresponding equations for the acidity constant and the Lewis basicity:

$$pKa = 19.8\ [\Delta s - 0.20(4 - a(\text{U–O}) - b(\text{O–H}))] \quad (4)$$

$$(LB) = \Delta s\ /\ [4 - a(\text{U–O}) - b(\text{O–H})] \quad (5)$$

where Δs is the bond-valence deficiency of the O-atom at the anion termination without considering any accepted hydrogen bonds; 0.20 [4 – *a*(U–O) – *b*(O–H)] is the bond-valence contribution of weak hydrogen bonds, where *a* and *b* are the numbers of U–O and O–H bonds, respectively; (*LB*) is the Lewis basicity. Writing [4 –

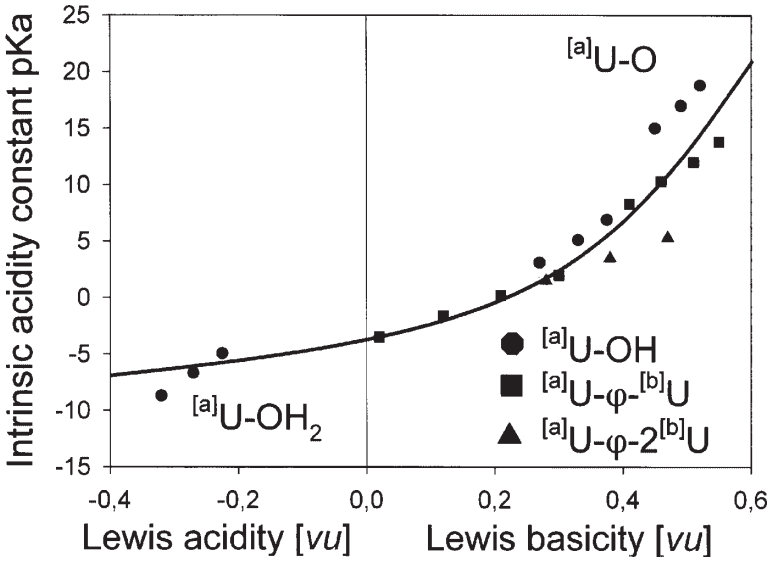

FIG. 3. Lewis basicity *versus* intrinsic acidity constant, *pKa*, of anion terminations on the edges of uranyl sheets (see text).

a(U–O) – b(O–H)] as x and solving for pKa gives the following relation:

$$pKa = 19.8\ (\Delta s.x - 0.2\ x) \quad (6).$$

The parameter x is constant for one group of anion terminations, but varies from group to group (*e.g.*, from 1 in $^{[a]}$U–OH_2 to 3 in $^{[a]}$U–O with a = 6, 7, 8). The correlation between Lewis basicity and pKa for all five groups of anion terminations is shown by the curved line in Figure 2.

Bond-valence deficiency at an anion termination

Calculation of the intrinsic acidity-constant and the Lewis basicity of an anion termination requires knowing the bond-valence deficiency at an oxygen atom [equations (3) and (4)]. The average coordination-number of the oxygen atom at an anion termination scales the absolute values of the intrinsic acidity-constant and the Lewis basicity. The bond-valence deficiency at an oxygen atom is independent of the coordination number of the oxygen, and is a better parameter to characterize the basicity of an anion termination. The bond-valence deficiency at an oxygen atom can be related to the free energy of the acid–base reactions [1], [2] or [3] as follows (Faure 1998):

$$\Delta_R G_{AT} = -2.303\ RT\ pKa \quad (7)$$

where $\Delta_R G_{AT}$ is the free energy of the acid–base reaction at one anion-termination. Combination of equations (3) and (7) results in

$$\Delta_R G_{AT} = -2.303\ RT\ 19.8\ (\Delta s - 0.20\ x) \quad (8).$$

Equations (3), (4) and (7) indicate that the higher the bond-valence deficiency at an oxygen atom, the stronger the basicity of the anion termination, the stronger its affinity to hydrogen bonds or O–H bonds, and the more negative the free energy $\Delta_R G_{AT}$ of the corresponding acid–base reaction.

Bond-valence deficiency, pKa, and free energy of a chain of polyhedra

The bond-valence deficiency of an edge may be defined as the sum of bond-valence deficiencies on anion terminations, normalized to its translation length. A chain of polyhedra in the sheet ideally represents an edge on an F face (Fig. 1). Each type of chain contains different types of anion terminations, and each type of anion termination corresponds to a specific pKa, Lewis basicity, and $\Delta_R G_{AT}$ value of a corresponding acid–base reaction. Let us consider a chain of polyhedra of translation a, with $b \times {}^{[7]}$U–O and $c \times {}^{[7]}$U–O–$^{[7]}$U terminations. The pKa value of an acid–base reaction involving this chain of polyhedra is designated ΔpK_{PC}, and depends on the numbers and types of different anion-terminations. The pKa value of an acid–base reaction involving a chain of polyhedra may be written as $\Sigma\Delta pK_{PC}$, and may be defined as the sum of the pKa values of acid–base reactions at the corresponding anion-terminations per Å.

$$\Sigma\Delta pK_{PC} = [b \times pKa\ (^{[7]}\text{U–O}) + c \times pKa\ (^{[7]}\text{U–O–}^{[7]}\text{U})] / a \quad (9).$$

Equation (9) can be rewritten as

$$\Sigma\Delta pK_{PC} = [b \times \Delta s\ (^{[7]}\text{U–O}) + a \times \Delta s\ (^{[7]}\text{U–O–}^{[7]}\text{U})] / a \quad (10)$$

The term $[b \times \Delta s\ (^{[7]}\text{U–O}) + a \times \Delta s\ (^{[7]}\text{U–O–}^{[7]}\text{U})] / a$ is the O-atom bond-valence deficiency per Å for a chain of polyhedra. It correlates with the average value of pKa and the free energy of acid–base reactions along a chain of polyhedra, and indicates the affinity of the constituent O-atoms for hydrogen bonds or O–H bonds. The bond-valence deficiency per Å can be calculated from crystal-structure data.

Dissolution rate and bond-valence deficiency

Sunagawa (1987) compared different crystal-growth parameters such as growth temperature, solute–solvent interaction, and roughness factor, α, with the corresponding medium of crystal growth, *e.g.*, melt, high-temperature solution, low-temperature solutions, chemical vapor-deposition and physical vapor-deposition. He showed that in low-temperature solutions, the solute–solvent interaction is the most important factor in controlling crystal growth and dissolution rates on surfaces and edges.

Uranyl-sheet minerals crystallize from low-temperature solutions, and the solute–solvent interaction at the edges of the basal faces should be the primary determinant of their stability. The solute–solvent interaction can be described *via* surface-controlled dissolution (Stumm 1992), which gives an understanding of how the dissolution kinetics of surfaces are controlled by protonation or by the presence of inner-sphere complexes. Protonation tends to increase dissolution rate because it leads to weaker bonds proximal to surface cations, and thus facilitates detachment of a surface group into solution. Surface-controlled dissolution is based on the idea that (1) attachment of reactants (H^+, OH^- or ligands) to surface atoms or groups of atoms is rapid, and (2) subsequent detachment of metal species from the surface into solution is slow (and thus rate-limiting). In the first sequence, the dissolution reaction is initiated by bonding to H^+, $(OH)^-$ and ligands that weaken and tend to break *M*–O–*M* bonds at the surface. This is schematically indicated in Figure 4 as a model of dissolution and growth of schoepite *via* detachment and attachment of clusters. The structure of a schoepite sheet is built from clusters

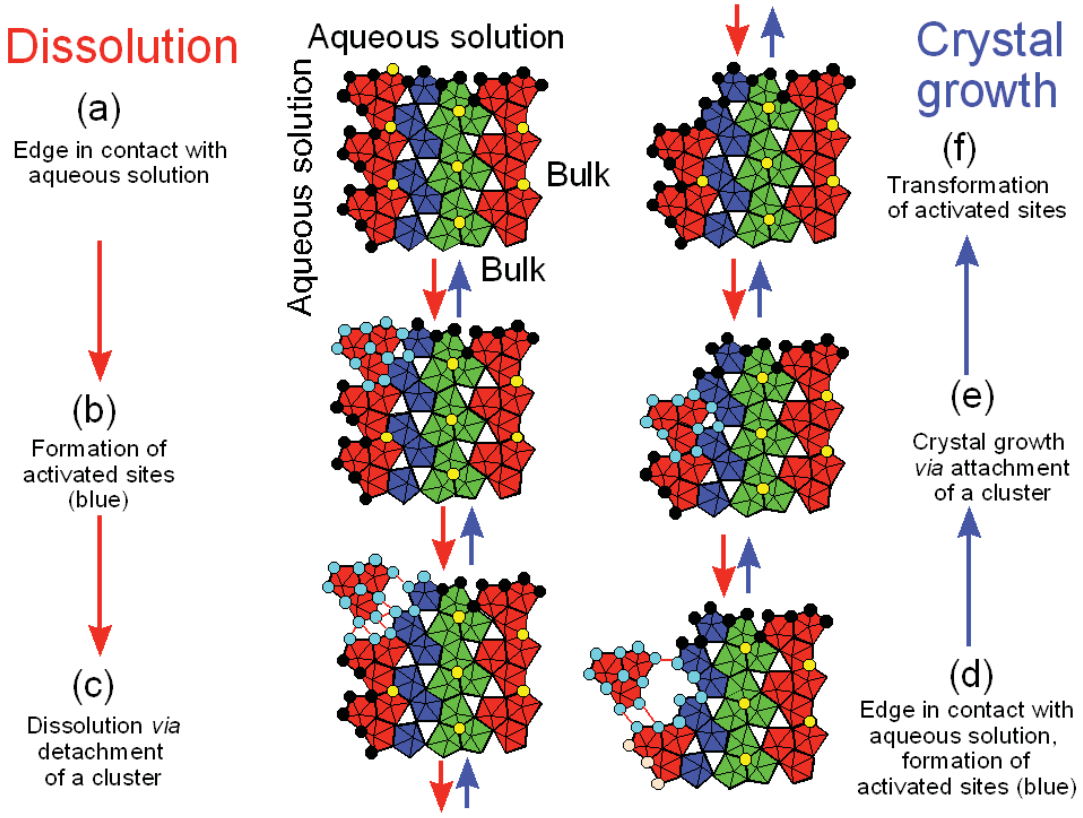

FIG. 4. (a) Schematic sketch of dissolution and growth processes at an edge of a sheet of schoepite. The sequence of dissolution is indicated with red arrows, and the sequence of crystal growth, by blue arrows. The sheet is built of clusters of three (red and green) and two (blue) pentagonal bipyramids that are structurally identical to the principal aqueous species $[(UO_2)_3(OH)_5(H_2O)_5]^+$ and $[(UO_2)_2(OH)_2(H_2O)_6]^{2+}$ in weak acidic solutions (*e.g.*, Moll *et al.* 2000); O^{2-} ligands in the sheet are indicated as yellow circles, and ligands that have interacted with the aqueous solutions are indicated in light blue; (a), (f): activated sites occur only at anion terminations, and activated sites in the layer are transformed to normal sites; (b), (e): formation of activated sites during the dissolution process *via* detachment of a cluster; ligands adjacent to potential detached clusters interact with the solution and are highlighted as light blue octagons; attachment of a cluster at a kink site occurs *via* release of one (H_2O) per common ligand between cluster and kink site; (c), (d): breaking (formation) of the U–φ–U bonds and detachment (or approach) of a cluster from (to) an activated kink-site on a layer of schoepite. Non-activated sites in contact with aqueous solution are indicated as black circles. Possible hydrogen bonds between uranyl clusters in solution and polyhedra at the kink sites are shown as solid pale-brown lines.

of three and two pentagonal bipyramids, which are structurally identical to the aqueous species $[(UO_2)_3(OH)_5(H_2O)_5]^+$ and $[(UO_2)_2(OH)_2(H_2O)_6]^{2+}$ (*e.g.*, Moll *et al.* 2000). These clusters involve edge-sharing pentagonal bipyramids, and link through common edges and corners (Fig. 4). Ligands on terminations interact with the aqueous solution *via* hydrogen bonding or acid–base reactions (Fig. 4a).

If dissolution occurs *via* detachment of clusters, the breaking of U–φ–U bonds occurs mainly at the linking O-atoms. This requires weakening of a number of U–φ bonds in the clusters through interaction between the ligands and the adjacent aqueous solution (Fig. 4b). As this weakening begins, the environment of a detaching cluster may be called an *activated site.* At an activated site, the interaction between aqueous solution and ligands provides the necessary weakening of the corresponding U–φ bonds, which finally break at the detachment of a cluster or a polyhedron (Fig. 4c). Thus an activated site involved in dissolution may be defined as follows: *An activated site involves the terminations around a polyhedron or a cluster of polyhedra where protonation or strong bonds between ligands and aqueous species results in weakening of U–φ bonds.*

If crystal growth occurs *via* attachment of clusters, the activated sites on the cluster and on the kink site of

the surface promote the attachment progress. Attachment produces one additional (H_2O) or (OH) group per common corner between cluster and kink site (Figs. 4d, e). Thus, an activated site involved in crystal growth may be defined as follows: *An activated site involves the terminations on a polyhedron or group of polyhedra where there are strong hydrogen bonds to a polyhedron or cluster of polyhedra in solution.*

The remaining common corners between cluster and former kink-site remain activated until the corresponding ligands do not require any additional bond-valence from bonds to aqueous species (Fig. 4f). Bonds between activated sites and aqueous species promote dissolution or crystal growth at an edge.

Bond-valence deficiency, kink sites, and O^{2-} ligands

The bond-valence deficiency of an edge increases with its number of kink sites, because an edge with a higher number of kink sites contains a higher ratio of stronger Lewis-bases (*e.g.*, $^{[7]}$U–φ) *versus* weaker Lewis-bases (*e.g.*, $^{[7]}$U–φ–$^{[7]}$U) (see *Calculation of bond-valence deficiency along chains of polyhedra* below). The bond-valence deficiency of an edge also increases with its number of O^{2-} ligands, because an edge with a higher number of O^{2-} ligands also has a higher ratio of stronger Lewis-bases ($^{[7]}$U–O and $^{[7]}$U–O–$^{[7]}$U) (*versus* weaker Lewis-bases, $^{[7]}$U–OH and $^{[7]}$U–OH–$^{[7]}$U). In contact with aqueous solution, the stronger Lewis-bases will either be protonated or form stronger bonds with the species in solution, which results in weakening of the corresponding U–φ bonds. Hence, edges with a higher number of kink sites or O^{2-} ligands contain a higher number of sites that can be activated during dissolution than edges with a lower number of kink sites or O^{2-} ligands.

A correlation between the growth rate of an edge and its bond-valence deficiency is not directly apparent because the edge and the cluster in solution are usually hydrated. However, a larger number of kink sites on an edge (*i.e.*, a high bond-valence deficiency) favors attachment of polyhedra because an attached polyhedron or cluster of polyhedra can share more common ligands with the corresponding polyhedra than it can on an edge with a lower number of kink sites. The negative charges of the O^{2-} ligands in a uranyl sheet closely balance the positive charge of the interstitial complex between the sheets. During crystal growth, these ligands occur on a hydrated edge, at which the ligands may be protonated differently than in the bulk structure. However, negative charges must also occur on an edge during crystal growth in order to balance the positive charge of either attached or incorporated interstitial cations. Hence, O^{2-} ligands in a bulk structure are potentially those ligands that are part of negative terminations on a protonated edge. A large number of negatively and positively charged terminations favors attachment of polyhedra or clusters of polyhedra on an edge (see below), because these terminations promote hydrogen bonding between polyhedra on an edge and the cluster in aqueous solution (*i.e.*, negatively charged terminations promote formation of activated sites during crystal growth).

The number and type of activated sites during crystal growth correlate [*via* the number of terminations (*i.e.*, the number of kink sites) and the number of negatively charged terminations] with the bond-valence deficiency of an edge in the bulk structure. The number of activated sites on an edge during dissolution or crystal growth correlates also with the difference between the pH of the solution and the pH_{pzc} of the edge (see below).

Activated sites and edges in schoepite and fourmarierite

In schoepite, $[(UO_2)_8O_2(OH)_{12}](H_2O)_{12}$, and fourmarierite, $Pb[(UO_2)_4O_3(OH)_4](H_2O)_4$, the layers have the same topology, but a different number of O and OH groups. Hence chains that terminate the [010] edge in both structures contain different numbers and types of ligands (Figs. 5a, b). At a specific pH, the [010] edge in fourmarierite must have a larger number of negatively charged terminations than the [010] edge in schoepite, because these terminations must charge-balance the incorporated or attached interstitial Pb^{2+} cations. However, at a different pH, the same chain on a [010] edge can have the same number and types of ligands in schoepite or fourmarierite. Figure 5c shows a possible model of hydration at such an edge, considering only the terminations along the edge. To activate terminations on the [010] edge of fourmarierite requires more protonation of ligands and more hydrogen bonding from the aqueous species to the ligands than on the [010] edge in schoepite. Thus the [010] edges in fourmarierite and schoepite contain different numbers and types of activated sites, even though they have identical ligands.

There are two different types of termination along the chain of polyhedra parallel to the [010] edge in schoepite and fourmarierite: U–φ and U–φ–U. Terminations of the same type have similar acid–base properties. Hence, one can assign identical hydration-models to each type of termination in schoepite and fourmarierite, *e.g.*, U–OH_2 and U–OH–U (along the chain parallel to the [010] edge). If one were to calculate the general stability of an edge based on identical models for each type of termination, one would similarly treat isostructural uranyl-sheets of different chemical composition. In other words, all equivalent edges in schoepite and fourmarierite would have similar relative stabilities. Consequently, the morphology of the (001) face should be identical on schoepite and fourmarierite crystals. However, this is not the case (see below), and therefore the different types and numbers of activated sites on edges in schoepite and fourmarierite cannot be neglected.

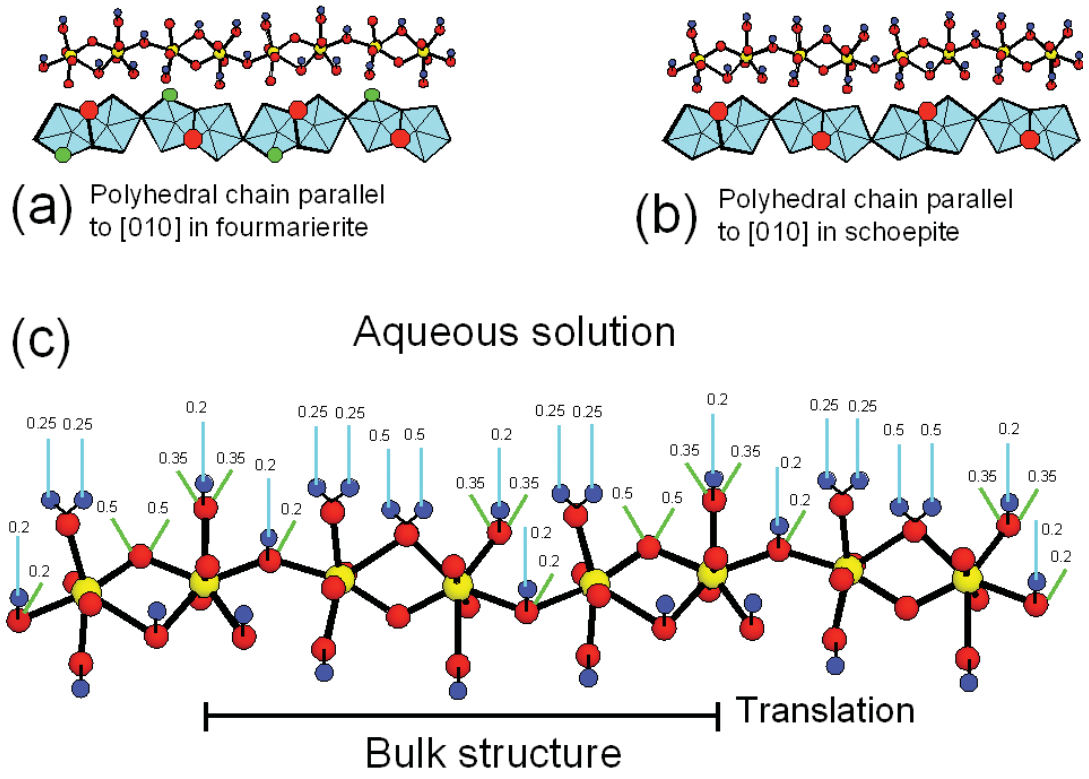

FIG. 5. (a), (b) Polyhedron and ball-and-stick representations of a chain of polyhedra parallel to [010] in fourmarierite and schoepite; in the ball-and-stick models, yellow, red and blue circles indicate U^{6+}, O^{2-} and H^{+}, respectively. In the polyhedron model, the positions of the O^{2-} equatorial ligands are indicated by green and red circles. (c) Ball-and-stick model of a possible activated edge parallel to [010]; outgoing bonds from terminations to aqueous species are indicated as blue lines, and incoming bonds accepted by the ligands of the terminations are indicated with green lines; the corresponding bond-valences (in *vu*) are given as numbers beside the lines.

pH_{pzc}, net proton-charge, inner- and outer-sphere complexes, and electric double- and triple-layers: a bond-valence perspective

The pH_{pzc} is also called the isoelectric point. Stumm (1992) defined pH_{pzc} as the point where the *total net surface-charge* is zero (this is the condition where particles do not move in an applied electric field). The total net surface-charge is the sum of (1) the permanent structural charge caused by isomorphic substitutions, (2) the net proton-charge (*i.e.*, the charge due to the binding of protons or OH-anions), (3) the charge of the inner-sphere complex, and (4) the charge of the outer-sphere complex.

The distribution of surface charge can be idealized as an electric double- or triple-layer. In the case of a double layer, the first layer is the solid surface with a localized negative surface-charge, whereas the second layer is in contact with the first layer and is a solution containing dispersed ions of positive charge (the *Gouy–Chapman diffuse model*: Stumm 1992). This model cannot be applied to surfaces of high potential because the local concentrations of counter ions near the surface becomes too large. In the Stern–Grahame triple-layer model, an additional compact layer of cations exists immediately adjacent to the mineral surface in order to balance the high charge of the surface. The ions in this layer are held tightly by "electrostatic forces" and are not free to move like the ions in the diffuse layer of the Gouy–Chapman model. Dzombak & Morel (1990) developed a surface-complexation model in which ions are attached by chemical bonding to the surface and not *via* "electrostatic effects", as assumed in the Gouy–Chapman and Stern–Grahame models. Therefore, cations of the inner-sphere complexes are treated in the surface-complexation model as part of the solid (Stumm 1992).

An inner-sphere complex and an outer-sphere complex occur if a cation or anion in the solution bonds directly or *via* (H_2O) groups to terminations on the

surface. Hence, the presence of inner-sphere and outer-sphere complexes changes the net proton-charge of the surface. If the net proton-charge is zero, the total net surface-charge is not necessarily zero. However, charge and number of inner- and outer-sphere complexes depend on many factors, such as the size and number of specific sites for complexation on the surface, and on the charge, size and activities of cations and anions in solution. We can again simplify this problem if we factor surface, inner- and outer-sphere complexes and other aqueous species into three components: (1) surface, (2) chemisorbed species, and (3) aqueous solution. To be considered part of the surface, an atom has to conform to the space-group symmetry of the crystal, with the exception of H atoms that strongly bond to O atoms at the surface. Any other atom or group of atoms chemically bonded to the surface and *not* conforming to the space-group symmetry of the crystal will not be incorporated into the structure (to any significant degree), and although chemically bonded to the surface, will have a short residence-time in this state. In some chemical systems, such chemisorbed impurities can significantly modify habit development, presumably depending on the residence lifetime of the species on the surface and the activity of that species in solution. In this way, we consider here only the change in interaction between an edge with different net proton-charges and the aqueous solution.

From a bond-valence perspective, the net proton-charge is the difference between the sums of the accepted and donated bond-valences between the termination on the surface and the species in aqueous solution. A termination that accepts bond valences is a *Lewis base*, and a termination that donates bond-valence is a *Lewis acid.* At zero net proton-charge, the strength and number of Lewis bases and Lewis acids are identical. The pH of a solution in which a surface has zero net proton-charge is called the point of zero net proton-charge, pH_{pzc} (Stumm 1992, p. 18). Depending on the intrinsic acidity-constant of the acid–base reaction, strong Lewis bases and acids occur only at low or high pH (see previous section). Hence, weaker Lewis bases and acids occur mainly on a surface at the pH_{pzc}. This approach emphasizes that at the pH_{pzc}, the bond-valence transfer between Lewis bases and acids on the surface and the aqueous solution is at a minimum.

An example: bond-valence transfer along a chain of polyhedra in schoepite and fourmarierite

Consider a chain of polyhedra parallel to the [010] edge in schoepite or fourmarierite (Fig. 5c). There are eight terminations ($4 \times$ [7]U–φ and $4 \times$ [7]U–φ–[7]U) per repeat length of the chain, and these interact with the aqueous solution. Figure 5c shows a hydration model for this chain, in which the incoming and outgoing bonds are shown in green and blue, respectively. In the repeat period of the chain, there are one U–O–U, one U–OH_2–U, two U–OH, two U–OH_2 and two U–OH–U terminations. In order to simplify the bond-valence calculations involving the incoming and outgoing bonds, we assign an average bond-valence of 0.50 *vu* to a [7]U–φ bond. An atom of oxygen of a [7]U–OH_2 group receives 0.50 *vu* from the [7]U–O bond and requires an additional 2×0.75 *vu* from the two O–H bonds in order to satisfy its bond-valence requirements. The two H-atoms require 0.25 *vu* from hydrogen bonds to an aqueous species in order to satisfy their own bond-valence requirements. Hence, any [7]U–OH_2 group donates two hydrogen bonds, each with a bond-valence of 0.25 *vu*, to the aqueous species.

An atom of oxygen of a [7]U–OH group receives 0.50 *vu* from the [7]U–O bond and requires an additional 1.50 *vu*. The O–H bond has a bond valence of 0.80 *vu*, and the oxygen atom thus requires an additional 0.70 *vu* from bonds from the aqueous species (Fig. 5c). In the same way, an atom of oxygen of an U–OH–U group receives 2×0.50 *vu* from two [7]U–O bonds and 0.80 *vu* from the hydrogen atom of the OH-group, and requires an additional 0.20 *vu* from a bond (or bonds) from an aqueous species. Hence, an atom of oxygen of a [7]U–O–[7]U group requires an additional 1.0 *vu* from bonds involving the aqueous species. The oxygen atom of a [7]U–OH_2–[7]U group accepts 2×0.50 *vu* from two [7]U–O bonds and requires an additional 2×0.50 *vu* from two O–H bonds; therefore, the [7]U–OH_2 group donates two hydrogen bonds with a bond-valence of 0.50 *vu*. The corresponding acid–base equilibria between the different Lewis bases and acids are listed in Table 1. The *pKa* values indicate that strong Lewis bases (such as [7]U–O–[7]U and [7]U–OH_2–[7]U) occur only at high and low pH, respectively. Thus the number of strong Lewis bases and acids on the [010] edge is very small in weak acidic, weak basic and neutral solutions.

We can now calculate aggregate bond-valences involving the outgoing and incoming bonds. There are $2 \times 0.20 + 4 \times 0.25 + 2 \times 0.20 + 2 \times 0.50 = 2.8$ *vu* donated from the terminations to the aqueous species, and there are $4 \times 0.35 + 2 \times 0.20 + 2 \times 0.50 = 2.80$ *vu* (Fig. 5) accepted from the terminations. The overall transfer of bond valence from or to the chain is thus $2.8 + 2.8 = 5.6$ *vu*. Because the accepted and donated bond-valences are equal, the chain is formally neutral. This is not surprising, as the number of the formally negatively charged terminations U–O–U (–1.0 *vu*) and U–OH (–0.50 *vu*) is equal to the number of formally positively charged terminations U–OH_2–U (+1.0 *vu*) and U–OH_2 (+0.5 *vu*), respectively.

If the pH of the solution is the same as the pH_{pzc}, there is not only an equal number of positively and negatively charged anion species, but there is also a minimum number of strong Lewis acids or bases such as U–O–U and U–OH_2–U at a given ionic strength of the solution. If the number of these terminations is infinitely small, the bond-valence transfer to or from the chain minimizes at 1.8 *vu*. If the pH differs from the pH_{pzc},

the Lewis acidities or basicities of the terminations vary sympathetically in both number and strength.

Consider an increase in the number of U–OH and U–OH_2 species. For four U–OH_2 and four U–OH–U terminations, there are $4 \times 0.20 + 8 \times 0.25 = 2.8$ *vu* donated by the terminations to the aqueous species, and there are $4 \times 0.20 = 0.80$ *vu* accepted by the terminations. The formal charge of this chain per repeat distance is $2.8 - 0.8 = 2^+$. For four U–OH terminations and four U–OH–U terminations, the terminations accept $8 \times 0.35 + 4 \times 0.20 = 3.6$ *vu* and donate $4 \times 0.2 + 4 \times 0.20 = 1.6$ *vu*; the *total* transfer of bond valence is $3.6 + 1.6 = 5.2$ *vu*, and the *net* transfer of bond valence is $1.6 - 3.6 = 2.0$ *vu*. These examples illustrate the fact that an increase in the number of U–OH or U–OH_2 terminations increases the total bond-valence transfer to and from the terminations, but not necessarily the net bond-valence transfer. The configuration of four U–OH_2 and four U–OH–U terminations results in a total bond-valence transfer of $2.8 + 0.80 = 3.6$ *vu*, which is equal to the minimum transfer at neutral charge: $1.8 + 1.8 = 3.6$ *vu*. The minimum total bond-valence transfer thus does not automatically occur at an edge with zero charge. However, an increase in the number of U–OH_2 terminations is normally the result of a decrease in pH, which also produces a higher ratio of U–OH_2–U to U–O–U terminations. A higher number of U–OH_2–U terminations increases the total bond-valence transfer, which will be higher than the minimum transfer at neutral charge.

From this discussion, we can define the pH_{pzc} of a surface from a bond-valence perspective (not considering inner- or outer-sphere complexes): *At the pH_{pzc} of a surface, there is a minimum in the number of highly charged terminations (i.e., strong Lewis acids and Lewis bases) on the surface, which results in low bond-valence transfer between surface acceptors and donors and the aqueous species.*

A higher number of strong bonds between terminations and aqueous species enhances attachment and detachment of polyhedra or groups of polyhedra, and growth or dissolution rates should correlate with the type and number of activated sites.

pH_{pzc}: faces

A surface may be positive, negative or neutral. The bond-valence deficiency at a face is a measure of the bond valence required to achieve electroneutrality at that face. If there is a low bond-valence deficiency at a face and the pH of the solution is identical to the pH_{pzc}, there is a low interaction between the face and the solution. This results in formation of only a small number of activated sites, and hence the dissolution rate perpendicular to the face is small.

Two examples: calculation of the pH_{pzc} of the (001) face of schoepite and dehydrated schoepite

Schoepite, $[(UO_2)_8O_2(OH)_{12}](H_2O)_{12}$, has a prominent basal (001) face that dominates the morphology of its crystals. The pH_{pzc} occurs where the average composition of the surface is equal to the composition of the structural unit, $[(UO_2)_8O_2(OH)_{12}]$. On the basis of the *pKa* values in equations [1] to [3], the $^{[7]}$U–φ–$^{[7]}$U termination occurs over a wide range of pH as $^{[7]}$U–OH–$^{[7]}$U, and is therefore not involved in acid–base reactions close to the pH_{pzc}. There are twelve $^{[7]}$U–φ–2$^{[7]}$U terminations in the asymmetric unit; two of them occur as $^{[7]}$U–O–2$^{[7]}$U, and ten of them as $^{[7]}$U–OH–2$^{[7]}$U. In order to have an average composition of the surface of $[(UO_2)_8O_2(OH)_{12}]$, there must be five times more $^{[7]}$U–OH–2$^{[7]}$U terminations than the $^{[7]}$U–O–2$^{[7]}$U termination. The pH_{pzc} can be calculated *via* the Henderson–Hasselbach equation (Atkins 1996) on the basis of the *pKa* value and the ratio of the terminations in the asymmetric unit:

$$pH_{pzc} = pH = pKa - \log [acid]/[base]$$
$$= 7.72 - \log [5]/[1] = 7.02 \quad (11).$$

In the case of dehydrated schoepite, the composition of the surface at pH_{pzc} must be identical to the composition of the structural unit, $[(UO_2)O_{0.2}(OH)_{1.6}]^0$. This is the case, as there are eight times more U–(OH)–2U terminations than U–O–2U terminations. On the basis of the experimentally determined pKa value of 7.0 (see above), the pH_{pzc} of dehydrated schoepite is therefore

$$ph_{pzc} = pH = pKa - \log [8]/[1]$$
$$= 7.0(2) - 0.9 = 6.1 \quad (12).$$

pH_{pzc}: edges

Because of the prominent basal faces in uranyl minerals, the formal charges at the different edges may contribute only a small amount to the overall surface-charge. However, the individual pH_{pzc} of an (activated) edge and the pH of the solution will control crystal growth and dissolution at this specific edge. Thus accurate prediction about the occurrence of edges can only be made if one knows their pH_{pzc}.

Example: calculation of the pH_{pzc} for edges on the (001) face of schoepite

The following anion-terminations occur on the edges of the (001) face of schoepite: $^{[7]}$U–O, $^{[7]}$U–OH, $^{[7]}$U–OH_2, $^{[7]}$U–O–$^{[7]}$U, $^{[7]}$U–OH–$^{[7]}$U, $^{[7]}$U–O–2$^{[7]}$U and $^{[7]}$U–OH–2$^{[7]}$U. The $^{[7]}$U–O, $^{[7]}$U–OH, $^{[7]}$U–O–$^{[7]}$U and $^{[7]}$U–O–2$^{[7]}$U terminations have formal negative charges of ~1.5, 0.5, 1 and 0.50, respectively. They all have a bond-valence deficiency and interact with the solution by accepting bond-valence *via* protonation or hydrogen

bonding. The $^{[7]}U–OH_2$, $^{[7]}U–OH_2–^{[7]}U$ and $^{[7]}U–OH–2^{[7]}U$ terminations have formal positive charges of ~0.5, 1 and 0.5, and interact with the solution by donating hydrogen bonds to aqueous species. The $^{[7]}U–OH–^{[7]}U$ anion-termination has a formal charge of zero and may both accept and donate one hydrogen bond. The charge on an edge is zero if there is an equal number of $^{[7]}U–OH_2$ and $^{[7]}U–OH$ terminations, $^{[7]}U–OH_2–^{[7]}U$ and $^{[7]}U–O–^{[7]}U$ terminations, and $^{[7]}U–O–2^{7]}U$ and $^{[7]}U–OH–2^{[7]}U$ terminations. Because $^{[7]}U–\varphi$ and $^{[7]}U–\varphi–^{[7]}U$ are the dominant terminations on the edges of schoepite, the pH_{pzc} of the edges is defined primarily by the following acid–base reactions:

$$^{[7]}U–O–^{[7]}U + H^+ \leftrightarrow {}^{[7]}U–OH–^{[7]}U, \quad pKa = 13.07 \qquad [5]$$

$$^{[7]}U–OH–^{[7]}U + H^+ \leftrightarrow {}^{[7]}U–OH_2–^{[7]}U, \quad pKa = 1.2 \qquad [6]$$

$$^{[7]}U–OH + H^+ \leftrightarrow {}^{[7]}U–OH_2, \quad pKa = 6.53 \qquad [7]$$

There are equal numbers of $^{[7]}U–OH_2–^{[7]}U$ and $^{[7]}U–O–^{[7]}U$ terminations at pH = (13.07 + 1.2) / 2 = 7.135, and an equal number of $^{[7]}U–OH$ and $^{[7]}U–OH_2$ terminations at pH = 6.534. Thus, every edge on the (001) face of schoepite has its pH_{pzc} at ~6.5 < pH < ~7.1. If the pH of the solution is in this range, there is the lowest interaction between the activated sites on an edge and the species in aqueous solution. [Note that as indicated above, the MUSIC equation in this form might not fit *all* uranyl-oxide minerals, and the calculated values of *pKa* should be seen as approximations rather than exact values.] This example shows that the pH_{pzc} of an edge cannot be used to predict its occurrence on a basal face. However, pH_{pzc} enables us to predict the *change* in morphology with a change in pH from the range in pH_{pzc} of the edges.

Change in morphology with change in pH

The change in morphology with change in pH depends strongly on the degree of supersaturation in the aqueous fluid. At high supersaturation, a large number of aqueous species will simultaneously attach to the surface, resulting in rough surfaces with fast growth-rates. In this case, the number and type of protonated anion-terminations will not be relevant for a slow-growth process in which the attachment of aqueous species produce smooth surfaces with a low number of kink sites. Hence, the following discussion on the effect of pH on the morphology is restricted to solutions at low supersaturation.

Figure 6 shows how the occurrence of an edge may vary with change in pH. Let us consider the edge with the lowest bond-valence deficiency of all possible edges. If the edge interacts with a solution of pH close to its pH_{pzc}, there is a weak interaction between the anion terminations and the aqueous species. The corresponding edge would contain only a small number of activated sites (see above), the dissolution or crystallization rate would be small, and the edge would survive on the final morphology of the basal face. If the pH of the solution differs from the pH_{pzc} by an amount ΔpH, there is a greater interaction between the terminations and the aqueous species. The number of activated sites increases with increasing ΔpH. However, the corresponding edge would still occur on the final morphology of the basal face, and depending on the bond-valence deficiency of the other edges, it might even dominate the morphology of the basal face (Fig. 6).

The explanation of this phenomenon can be found if we consider next an edge with an average bond-valence deficiency (*i.e.*, this edge has a higher bond-valence deficiency than the edge considered previously). At a pH close to its pH_{pzc} value, its anion terminations would interact slightly more with the solution than those of the previously considered edge. The resulting activated edge would therefore contain a higher number of activated sites than the previous activated edge. However, if the interaction between the second edge and a solution with a pH = pH_{pzc} of the second edge is still small, the corresponding dissolution or crystallization rates would be similar to the rates of dissolution or crystallization of the previous edge, and the edge would occur on the final basal face. The occurrence of those edges is therefore strongly controlled by the relation between dissolution or crystallization kinetics and ΔpH.

If ΔpH increases dramatically, the already higher number of activated sites will increase even more, and the morphology will change (Fig. 6). In this case, the higher rates of dissolution or crystallization (in comparison to the previous edge) presumably result in disappearance of the edge during growth or dissolution. Hence at higher ΔpH, the final morphology of a basal face is defined by the edges with the lowest bond-valence deficiency.

Finally, let us consider an edge with the highest bond-valence deficiency. The interaction of its terminations with an aqueous solution of a specific ΔpH will be the highest of all previous edges; *i.e.*, there is a high probability that the corresponding rates of dissolution or crystallization may be so high that the edge will disappear during these processes. Under normal circumstances, edges with the highest bond-valence deficiency should therefore never occur on the final morphology of the basal faces.

Similar considerations apply to the supersaturation parameter, β. At equilibrium, the saturation of a solution is unity ($\beta = 1$), and there is a minimum in the interaction between activated sites and species in aqueous solution. Where supersaturation increases or decreases by $\Delta\beta$, the interaction between aqueous solution and edge increases. Hence at high $\Delta\beta$, one would expect edges with the lowest bond-valence deficiency, whereas

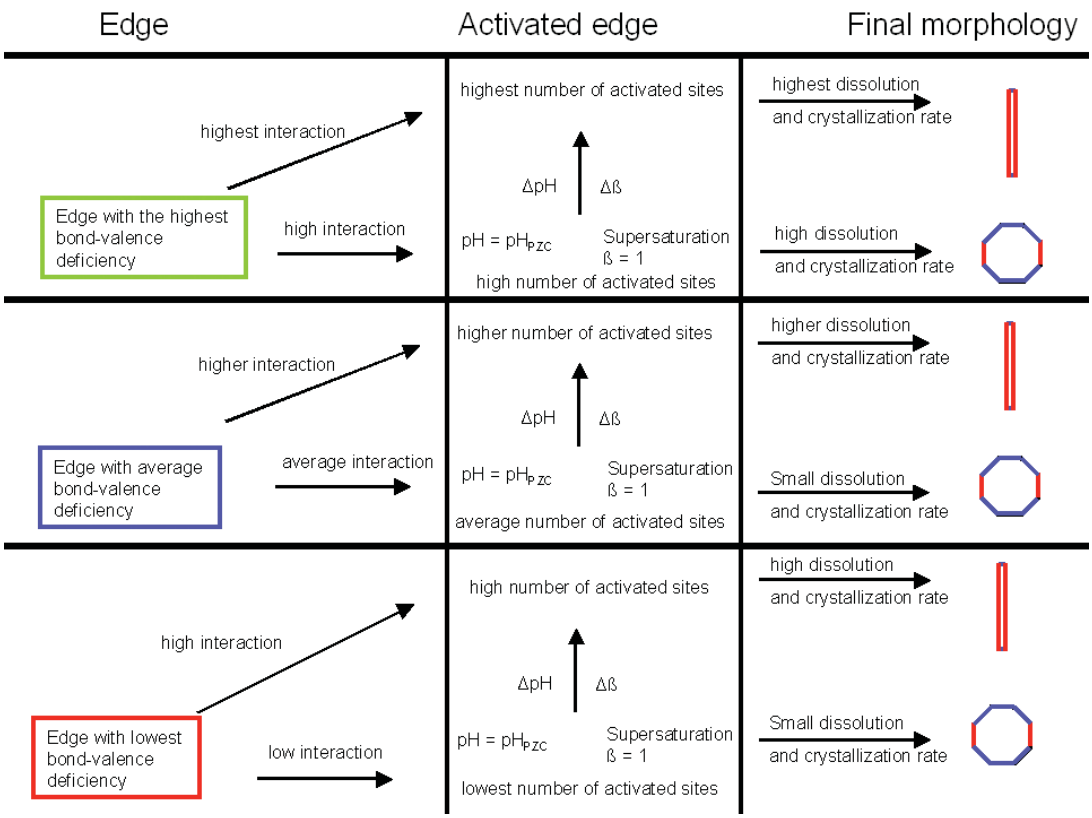

FIG. 6. The left column lists the possible types of edges: edges with lowest, average and highest bond-valence deficiencies are indicated in red, blue and green, respectively. The central column schematically indicates the increase in activated sites with (a) the initial bond-valence deficiency of the edge, (b) the difference between the pH of the solution and the pH_{pzc} of the edge (indicated as ΔpH), and (c) the difference between the supersaturation, β, of a solution and the supersaturation at equilibrium, with β = 1 (indicated as Δβ). The increase in ΔpH and Δβ is indicated by an arrow. The right column lists the corresponding rates of dissolution and crystal growth, and the final morphologies of a theoretical (001) face. The colors of the edges indicate the corresponding bond-valence deficiencies of the edges.

at low Δβ, one would expect edges of low and average bond-valence deficiency.

Change in morphology with stacking sequences of layers

An edge terminates one layer and can be characterized by a chain of polyhedra in the layer. A face crossing the layers terminates more than one layer, and this surface is characterized by chains of polyhedra that terminate the different layers. If adjacent layers are shifted relative to each other, the face can be terminated by different types of chains. Figure 7a shows sequence of layers with or without a shift between the layers. There are interstitial cations, (H_2O) or (OH) groups between each layer.

Arrangements (1) to (3) (Fig. 7) show three layers that are terminated by one type of chain of polyhedra. The chain indicated by a yellow rectangle has a lower bond-valence deficiency than the chains indicated by green rectangles, and hence edges in arrangements (1) and (3) are more stable than edges in arrangement (2). In arrangements (4) to (6), the layers contain the same type of chains of polyhedra. However, the central layer is shifted by one polyhedron relative to the adjacent layers. In this case, two chains of high bond-valence deficiency and one chain of low bond-valence deficiency terminate the edges in arrangement (4). Edges on a face that are terminated by chains of high and low bond-valence deficiencies have different growth and dissolution rates. Hence, in Figure 7a, the upper and lower layers grow faster than the central layer. This growth mechanism results in arrangement (5), in which only chains of lower bond-valence deficiency terminate an edge. Thus, edges in arrangement (5) are more stable than edges in arrangement (4). Arrangement (5) con-

tains one major kink-site with interstitial complexes above and below. The rates of growth and dissolution at this kink-site are therefore not only characterized by the bond-valence deficiency of the chain; they are also controlled by the acidity of the interstitial complex. This is in contrast to arrangement (1), in which the rates of growth and dissolution are determined only by the bond-valence deficiency of the chains. Thus, edges in arrangement (5) are less stable than edges in arrangement (1).

Figure 7b shows the same type of arrangements as in Figure 7a, but with chains of average and high bond-valence deficiency (indicated by pink and green rectangles, respectively). The stabilities of edges in the corresponding arrangements are the same, *i.e.*, edges in arrangement (7) have a higher stability than edges in arrangement (11). The difference in bond-valence deficiency can now be used to compare the stability of edges that have a similar shift between their layers. Edges in arrangement (1) have a lower bond-valence deficiency than edges in arrangement (7), and therefore, the former are more stable and have lower rates of dissolution and growth than the latter (Fig. 7c). In the same way, edges in arrangement (5) are more stable than edges in arrangement (11), and therefore the former also have lower rates of dissolution and growth than the latter (Fig. 7c).

The kink sites of arrangements (5) and (11) are characterized by the acidity of the adjacent interstitial com-

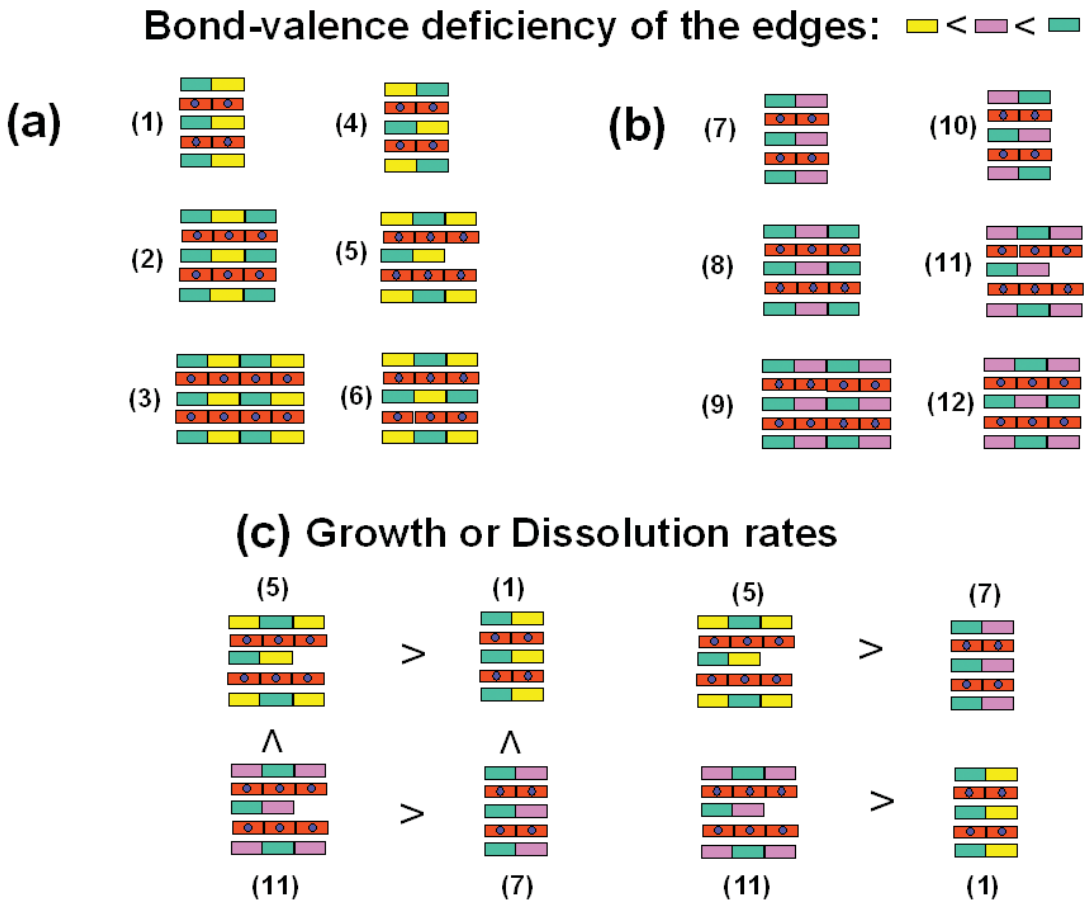

FIG. 7. Schematic representation of different sequences in the stacking of layers, with chains of different bond-valence deficiencies. (a) Chains are indicated as yellow (low bond-valence deficiency) and green (high bond-valence deficiency) rectangles, and interstitial complexes are indicated with red rectangles and blue circles. Arrangements (1) to (6) display growth sequences of edges with identical chains but with different shifts between the layers. (b) Arrangements (7) to (12) are identical to arrangements (1) to (6) owing to the shift between the layers, but have chains of average and low bond-valence deficiency (indicated as pink and green rectangles). (c) Growth and dissolution rates among the different arrangements (for details, see text).

plexes and by the bond-valence deficiency of the chain of polyhedra. Hence, there are three components at these kink sites that interact with the aqueous species. The corresponding edges thus interact more extensively with the aqueous solution than edges in arrangements (1) and (3). Hence, we predict that edges in arrangements (5) and (11) have lower stability than edges in arrangements (1) and (7).

Change in morphology with change in arrangement of interstitial complexes

A change in morphology of the basal face with change in arrangement of the interstitial complex can be observed in minerals with identical structural units, identical shifts between the layers, but different arrangements of their interstitial complexes. This is the case for becquerelite, $^{[7]}Ca(H_2O)_4[(UO_2)_3O_2(OH)_3]_2(H_2O)_4$, and billietite, $^{[10]}Ba(H_2O)_4[(UO_2)_3O_2(OH)_3]_2\ (H_2O)_3$. Figures 8a and 8b show the arrangements of the interstitial cations Ca and Ba in becquerelite and billietite, respectively. The interstitial Ca atoms in becquerelite are arranged in rows parallel to [010], whereas the interstitial Ba atoms in billietite are arranged in rows parallel to [100]. Evaluation of the bond-valence deficiencies (taking into account the shift between the layers in each structure) indicates that [100] and [110] are the most stable edges, whereas edges such as [100], [210], [130] and [310] are less stable. Hence, we predict that the edges [100] and [110] invariably occur, independent of pH and saturation, whereas all other edges occur only close to the pH_{pzc} and at saturation.

Becquerelite and billietite crystals strongly resemble each other in color and form. The edges [100] and [110] invariably occur on their (001) face, in good agreement with our predictions. Only becquerelite crystals are reported as elongate parallel to [010], whereas billietite crystals can be elongate parallel to [100] [Figs. 8a and 8b; Perloff (1998); http://www.trinityminerals.com/sm2001/uranium.shtml]. This implies that the occurrence of edges and their dominance on the final morphology may be also controlled by the arrangement of the interstitial complexes. We may summarize the above discussion as follows: (a) If we consider only the struc-

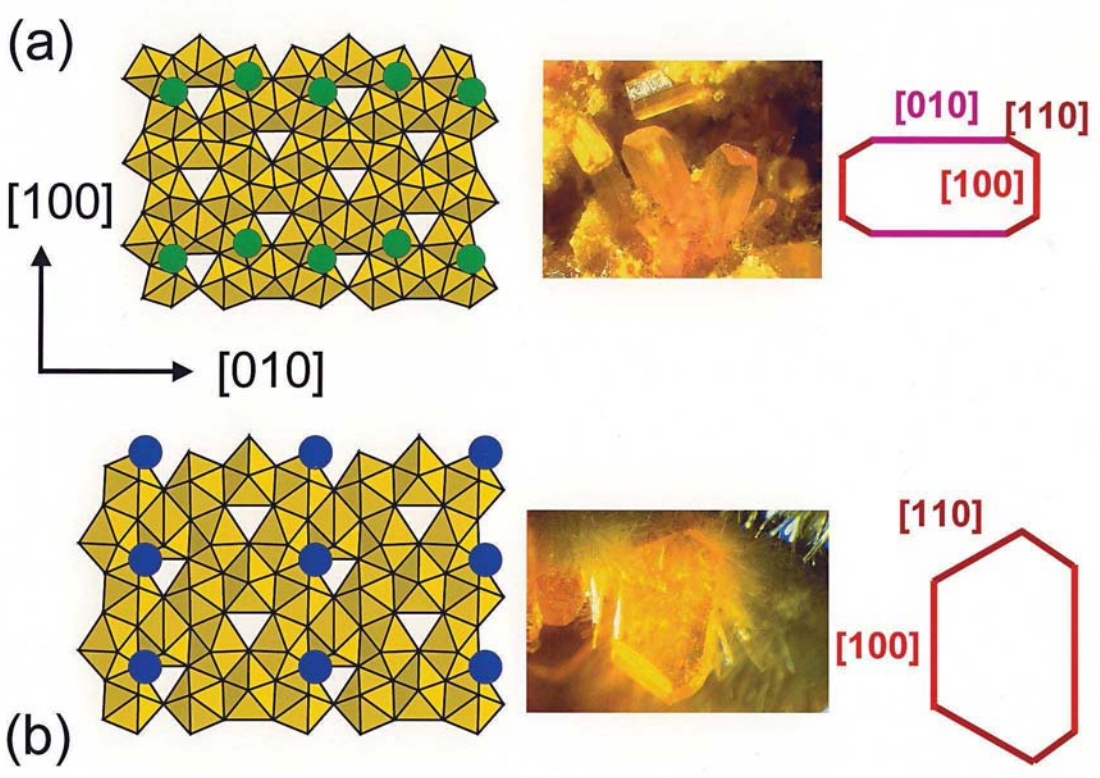

FIG. 8. Left: polyhedron illustrations of layers in (a) becquerelite, and (b) billietite, showing the positions of the interstitial Ca (green circles) and Ba (blue circles). Right: examples of the corresponding (001) face morphologies on becquerelite and billietite crystals (for details, see text).

tural information of the uranyl sheets, we can predict the occurrence (or non-occurrence) of edges with the lowest and highest bond-valence deficiencies. (b) If we consider also the pH_{pzc}, pH, degree of saturation and the arrangement of the interstitial complex, we can predict the occurrence of edges with average bond-valence deficiency.

Calculation of bond-valence deficiency along chains of polyhedra

In order to predict the occurrence of different edges, we must consider the different types of linear periodic chains of polyhedra parallel to an edge. Figure 9 shows linear periodic chains of polyhedra parallel to [100] in schoepite. Depending on whether one considers the surface on the right or left side of the figure, one can construct (linear periodic) chains of polyhedra with different types of terminations (Figs. 9a, c). Terminations of linear periodic chains that terminate the layer to the right or left side are called *right terminations* or *left terminations*, respectively.

The linear periodic chain of polyhedra parallel to [100] has a repeat distance of 14.377 Å. Let us designate the left termination of this chain as *a1*: there are two $^{[7]}$U–OH terminations and four $^{[7]}$U–OH–$^{[7]}$U terminations (Fig. 9a). The average bond-valence of $^{[7]}U^{6+}$–O in schoepite is 0.47 *vu*, and the average O–H bond-valence is 0.80 *vu* (Brown 1981). The oxygen atoms of the two [1]-coordinated and the four [2]-coordinated (OH) groups receive $(2 \times 1 \times 0.47 + 2 \times 0.8) = 2.54$ *vu*, and $(4 \times 2 \times 0.47 + 4 \times 0.8) = 6.96$ *vu*, respectively. The resulting bond-valence deficiency at the oxygen atoms in the chain is the difference between their formal valence and their incident bond-valence sum. For example, the oxygen atoms of the two [1]-coordinated (OH) groups in the repeat unit of the chain have a formal charge of 4^-, and they accept 2×0.47 *vu* from equatorial U–O bonds and 2×0.80 *vu* from O–H bonds. The sum of the incident bond-valence is 2.54 *vu*, result-

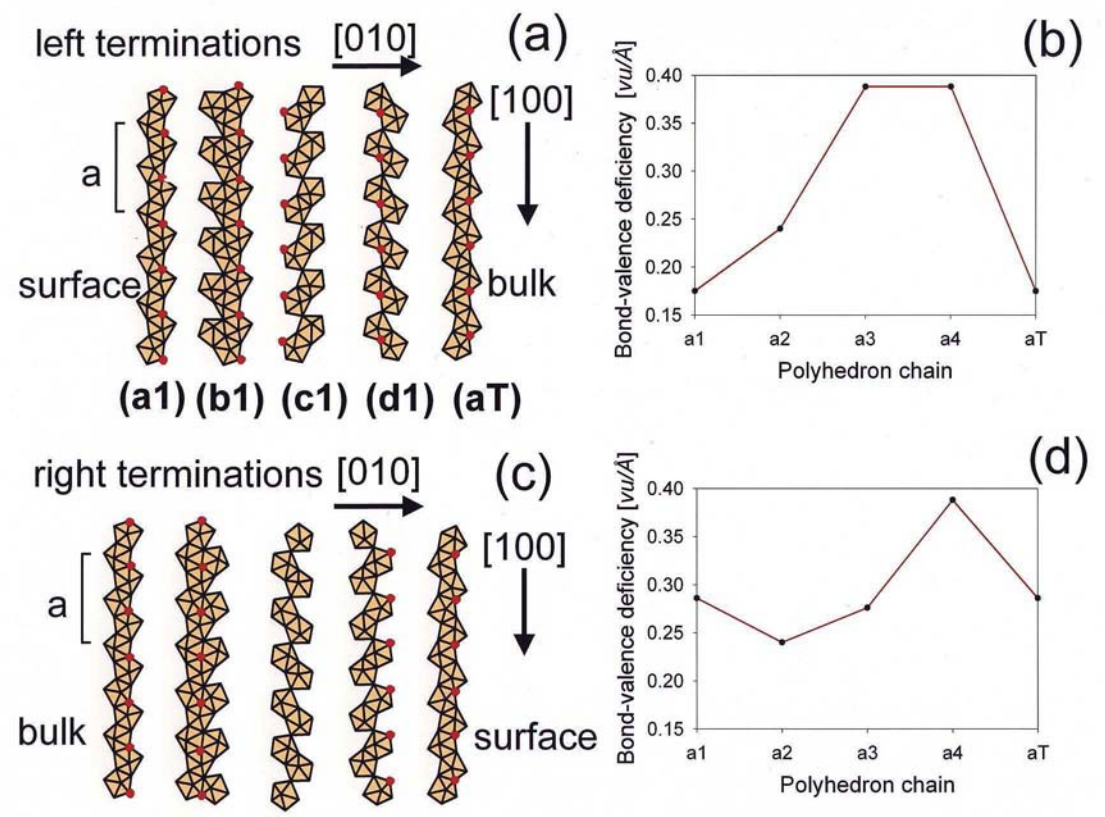

FIG. 9. (a) The left form of chain termination for different chains parallel to the [100] edge in the uranyl sheet of schoepite; the positions of the O^{2-} anions are indicated by red circles. At each chain, the bulk structure continues to the left, and the surface occurs at the right side. (b) The calculated bond-valence deficiency per unit length (*vu* / Å) of anion terminations on chain terminations of the left form. (c) The right form of chain terminations for different chains parallel to the [100] edge. (d) The corresponding bond-valence deficiency per unit length of the anion terminations on chain terminations of the right form.

ing in an aggregate bond-valence deficiency of 4 – 2.54 = 1.46 *vu*. The bond-valence deficiency of the four [2]-coordinated oxygen atoms is 1.04 *vu*. The bond-valence deficiency of the oxygen atoms in the repeat distance of the chain of polyhedra is 1.46 + 1.04 = 2.50 *vu*, and normalized to the length of the chain: 2.50 / 14.337 = 0.1744 *vu* / Å.

The bond-valence deficiency of such a chain depends on the type and number of anion terminations. A high bond-valence deficiency occurs where the chain contains a high number of negatively charged terminations, such as U–OH (–0.5), U–O–U (–1.0) or U–O (–1.5 *vu*), and a low bond-valence deficiency occurs if the chain contains a high number of the formally neutral U–OH–U terminations. Here, the number of kink sites along the chain controls the number of U–φ and U–φ–U terminations.

Summary

(1) The bond valence of an anion termination on a terminating chain of polyhedra correlates with the intrinsic acidity-constant, *pKa*, and with the free energy, ΔG_{at}, of the corresponding acid–base reaction.

(2) The bond-valence deficiency of a linear periodic chain of polyhedra parallel to an edge correlates with the type and number of activated sites on an edge.

(3) Processes of crystal growth and dissolution on an edge are catalyzed by the activated sites and increase with their number and the strength of the bonds between the corresponding anion terminations and the aqueous species.

(4) The interaction between activated sites and aqueous species is minimized where the pH of the solution is at the pH_{pzc} of the edge and where the solution is close to saturation with respect to the mineral.

(5) Interaction of an edge with the aqueous solution during crystal growth and dissolution depends also on the shift between the layers and the arrangement of the interstitial complexes between the layers.

(6) One can use the latter parameters and the bond-valence deficiency of a polyhedron to predict the occurrence of edges on the basal face of uranyl-sheet minerals.

Acknowledgements

We thank referees Mike Hochella and Cornelis Woensdregt and Editor Bob Martin for their comments, which added considerably to the clarity of this paper. MS and AP thank the Deutsche Forschungsgemeinschaft for an Emmy Noether Fellowship and grant P153/10-1, respectively. FCH was supported by a Canada Research Chair in Crystallography and Mineralogy and by a Discovery Grant from the Natural Sciences and Engineering Research Council of Canada.

References

Atkins, P.W. (1996): *Physikalische Chemie* (zweite Auflage). VCH Verlagsgesellschaft, Weinheim, Germany.

Bargar, J.R., Brown, G.E., Jr., & Parks, G.A. (1997a): Surface complexation of Pb(II) at oxide–water interfaces. 1. XAFS and bond-valence determination of mononuclear and polynuclear Pb(II) sorption products on aluminum oxides. *Geochim. Cosmochim. Acta* **61**, 2617-2637.

_____, _____ & _____ (1997b): Surface complexation of Pb(II) at oxide–water interfaces. 2. XAFS and bond-valence determination of mononuclear and polynuclear Pb(II) sorption products and surface functional groups on iron oxides. *Geochim. Cosmochim. Acta* **61**, 2639-2652.

_____, Towle, S.N., Brown, G.E. & Parks, G.A. (1997c): XAFS and bond-valence determination of the structures and compositions of surface functional groups and Pb(II) and Co(II) sorption products on single-crystal α-Al_2O_3. *J. Colloid Interface Sci.* **185**, 473-492.

Bickmore, B.R., Rosso, K.M., Nagy, K.L., Cygan, R.T. & Tadanier, C.J. (2003): Ab initio determination of edge surface structures for dioctahedral 2:1 phyllosilicate: implications for acid–base reactivity. *Clays Clay Minerals* **51**, 359-371.

Brown, G.E., Jr., & Parks, G.A. (2001): Sorption of trace elements on mineral surfaces: modern perspectives from spectroscopic studies, and comments on sorption in the marine environment. *Int. Geol. Rev.* **43**, 963-1073.

Brown, I.D. (1981): The bond-valence method: an empirical approach to chemical structure and bonding. *In* Structure and Bonding in Crystals II (M. O'Keeffe & A. Navrotsky, eds.). Academic Press, New York, N.Y. (1-30).

_____ & Altermatt, D. (1985): Bond-valence parameters obtained from a systematic analysis of the inorganic crystal structure database. *Acta Crystallogr.* **B41**, 244-247.

_____ & Shannon, R.D. (1973): Empirical bond-strength – bond-length curves for oxides. *Acta Crystallogr.* **A29**, 266-282.

Burns, P.C. (1999): The crystal chemistry of uranium. *In* Uranium: Mineralogy, Geochemistry and the Environment (P.C. Burns & R. Finch, eds.). *Rev. Mineral.* **38**, 23-90.

Dzombak, D.A. & Morel, F.M.M. (1990): *Surface Complexation Modeling: Hydrous Ferric Oxide*. John Wiley & Sons, New York, N.Y.

Faure, G. (1998): *Principles and Applications of Geochemistry* (2nd ed.). Prentice Hall, Upper Saddle River, New Jersey.

Finch, R.J., Cooper, M.A., Hawthorne, F.C. & Ewing, R.C. (1996): The crystal structure of schoepite, $[(UO_2)_8O_2(OH)_{12}](H_2O)_{12}$. *Can. Mineral.* **34**, 1071-1088.

HARTMAN, P. & PERDOK, W.G. (1955a): On the relations between structure and morphology of crystals I. *Acta Crystallogr.* **8**, 49-52.

_____ & _____ (1955b): On the relations between structure and morphology of crystals II. *Acta Crystallogr.* **8**, 521-524.

_____ & _____ (1955c): On the relations between structure and morphology of crystals III. *Acta Crystallogr.* **8**, 525-529.

HAWTHORNE, F.C. (1985): Towards a structural classification of minerals: the $^{vi}M^{iv}T_2\varphi_n$ minerals. *Am. Mineral.* **70**, 455-473.

_____ (1986): Structural hierarchy in $^{VI}M_x^{III}T_y\varphi_z$ minerals. *Can. Mineral.* **24**, 625-642.

_____ (1990): Structural hierarchy in $M^6T^4\varphi_n$ minerals. *Z. Kristallogr.* **192**, 1-52.

_____ (1994) Structural aspects of oxides and oxysalt crystals. *Acta. Crystallogr.* **B50**, 481-510.

_____ (1997): Structural aspects of oxide and oxysalt minerals. *In* Modular Aspects of Minerals (S. Merlino, ed.). *Eur. Mineral. Union, Notes in Mineralogy* **1**, 373-429.

HIEMSTRA, T., VENEMA, P. & VAN RIEMSDIJK, W.H. (1996): Intrinsic proton affinity of reactive surface groups of metal (hydr)oxides: the bond valence principle. *J. Colloid Interface Sci.* **184**, 680-692.

LEWIS, G.N. (1916): The atom and the molecule. *J. Am. Chem. Soc.* **38**, 762-785.

MOLL, H., REICH, T. & SZABÓ, Z. (2000): The hydrolysis of dioxouranium (VI) investigated using EXAFS and ^{17}O-NMR. *Radiochim. Acta* **88**, 411-415.

PERLOFF, L. (1998): *The Photo-Atlas of Minerals* (A.R. Kampf & G. Gerhold, eds.). The Gem and Mineral Council, Los Angeles County Museum of Natural History, Los Angeles, California.

RUFE, E. & HOCHELLA, M., JR. (1999): Quantitative assessment of reactive surface area of phlogopite dissolution during acid dissolution. *Science* **285**, 874-876.

SCHINDLER, M. & HAWTHORNE, F.C. (2001a): A bond-valence approach to the structure, chemistry and paragenesis of hydroxy-hydrated oxysalt minerals. I. Theory. *Can. Mineral.* **39**, 1225-1242.

_____ & _____ (2001b): A bond-valence approach to the structure, chemistry and paragenesis of hydroxy-hydrated oxysalt minerals. II. Crystal structure and chemical composition of borate minerals. *Can. Mineral.* **39**, 1243-1256.

_____ & _____ (2001c): A bond-valence approach to the structure, chemistry and paragenesis of hydroxy-hydrated oxysalt minerals. III. Paragenesis of borate minerals. *Can. Mineral.* **39**, 1257-1274.

_____ & _____ (2004): A bond-valence approach to the uranyl-oxide hydroxy-hydrate minerals: chemical composition and occurrence. *Can. Mineral.* **42**, 1601-1627.

_____, _____ & BAUR, W.H. (2000): A crystal-chemical approach to the composition and occurrence of vanadium minerals. *Can. Mineral.* **38**, 1443-1456.

STUMM, W. (1992): *Chemistry of the Solid–Water Interface*. John Wiley & Sons, New York, N.Y. (428).

SUNAGAWA, I. (1987): Morphology of minerals. *In* Morphology of Crystals (I. Sunagawa, ed.). Terrapub, Tokyo, Japan (509-587).

Received August 12, 2003, revised manuscript accepted September 7, 2004.

The Canadian Mineralogist
Vol. 42, pp. 1651-1666 (2004)

PREDICTION OF CRYSTAL MORPHOLOGY OF COMPLEX URANYL-SHEET MINERALS. II. OBSERVATIONS

MICHAEL SCHINDLER[§] AND ANDREAS MUTTER

Institut für Mineralogie, Universität Münster, Corrensstr. 24, D-48149 Münster, Germany

FRANK C. HAWTHORNE

Department of Geological Sciences, University of Manitoba, Winnipeg, Manitoba R3T 2N2, Canada

ANDREW PUTNIS

Institut für Mineralogie, Universität Münster, Corrensstr. 24, D-48149 Münster, Germany

ABSTRACT

The morphology of basal faces of uranyl-sheet minerals is predicted by considering the bond-valence deficiency of the chains of polyhedra, the shift between the layers, and the arrangement of the interstitial complexes between the layers. The sheet structural units of schoepite, $[(UO_2)_8O_2(OH)_{12}](H_2O)_{12}$, and fourmarierite, $Pb[(UO_2)_4O_3(OH)_4](H_2O)_4$, have the same underlying anion-topology. The stabilities of their edges differ because adjacent layers in schoepite are shifted by one chain of polyhedra, whereas adjacent layers are not shifted in fourmarierite. The minerals becquerelite, $^{[7]}Ca(H_2O)_4[(UO_2)_3O_2(OH)_3]_2\ (H_2O)_4$, compreignacite, $^{[7]}K_2(H_2O)_3\ [(UO_2)_3O_2(OH)_3]_2(H_2O)_4$, billietite, $^{[10]}Ba(H_2O)_4[(UO_2)_3O_2(OH)_3]_2\ (H_2O)_3$, protasite, $^{[10]}Ba(H_2O)_3[(UO_2)_3O_3(OH)_2]$, and masuyite, $^{[10]}Pb(H_2O)_3[(UO_2)_3O_3(OH)_2]$, all have structural units with the same basic anion-topology. The stabilities of their edges differ because of the different arrangements of interstitial species. In becquerelite, the interstitial cations are arranged in rows parallel to [010], whereas in billietite and compreignacite, the interstitial cations are arranged in rows parallel to [100]. For masuyite and protasite, the stability of their edges is defined by large differences in the bond-valence deficiencies of the chains of polyhedra with left and right terminations. The stabilities of edges in curite, $Pb_3[(UO_2)_8O_8(OH)_6](H_2O)_3$, are dictated by the low bond-valence deficiencies of the chains of polyhedra parallel to [001] and [011], and by the arrangement of cations in rows parallel to [001]. Minerals of the carnotite group contain the structural unit $[(UO_2)_2(V_2O_8)]^{2-}$, and the stability of the edges of their sheets is determined by the low bond-valence deficiency of chains of polyhedra parallel to [010 and [110]. Minerals of the uranophane group are based on the $[(UO_2)SiO_3(OH)]^-$ sheet, and the stabilities of their edges are more strongly affected by the bond-valence deficiency of the chains of polyhedra than by the arrangement of the interstitial cations, and by the shift in the sheets. All predictions are compared with the corresponding morphologies of crystals recorded by Atomic Force Microscopy (AFM), on images of crystals, and on crystal drawings from the (mainly older) mineralogical literature. All predictions are in good agreement with the observed morphology of the basal faces.

Keywords: uranyl minerals, morphology, surface structure, crystal growth, dissolution, bond valence.

SOMMAIRE

Nous prédisons la morphologie des faces de base des minéraux contenant des feuillets à polyèdres uranylés en considérant le déficit en valences de liaison des chaînes de polyèdres, le décalage entre les feuillets, et l'agencement des complexes interstitiels entre les couches. Les unités structurales en feuillets de la schoepite, $[(UO_2)_8O_2(OH)_{12}](H_2O)_{12}$, et de la fourmariérite, $Pb[(UO_2)_4O_3(OH)_4](H_2O)_4$, possèdent la même topologie anionique de base. La stabilité de leurs bordures diffère en fonction du décalage de feuillets adjacents équivalent à une chaîne de polyèdres dans la schoepite, tandis que les feuillets adjacents ne sont pas décalés dans la fourmariérite. Les minéraux becquerelite, $^{[7]}Ca(H_2O)_4[(UO_2)_3O_2(OH)_3]_2\ (H_2O)_4$, compreignacite, $^{[7]}K_2(H_2O)_3\ [(UO_2)_3O_2(OH)_3]_2(H_2O)_4$, billietite, $^{[10]}Ba(H_2O)_4[(UO_2)_3O_2(OH)_3]_2\ (H_2O)_3$, protasite, $^{[10]}Ba(H_2O)_3[(UO_2)_3O_3(OH)_2]$, et masuyite, $^{[10]}Pb(H_2O)_3[(UO_2)_3O_3(OH)_2]$, possèdent tous des unités structurales ayant la même topologie anionique de base. La stabilité de la bordure de leurs feuillets diffère à cause des divers arrangements des espèces interstitielles. Dans la becquerelite, les cations interstitiels sont agencés en rangées parallèles à [010], tandis que dans la billietite et la compreignacite, les cations interstitiels

§ *Current address*: Department of Geological Sciences, University of Manitoba, Winnipeg, Manitoba R3T 2N2, Canada.
E-mail address: mschindl@lakeheadu.ca

sont agencés en rangées parallèles à [100]. Dans le cas de la masuyite et la protasite, la stabilité de leurs bordures dépendrait des différences majeures des déficits en valences de liaison des chaînes de polyèdres ayant des terminaisons gauche et droite. La stabilité des bordures des feuillets de la curite, $Pb_3[(UO_2)_8O_8(OH)_6](H_2O)_3$, est régie par le faible déficit en valences de liaison associé aux chaînes de polyèdres parallèles à [001] et [011], et par l'agencement des cations en rangées parallèles à [001]. Les minéraux du groupe de la carnotite contiennent l'unité structurale $[(UO_2)_2(V_2O_8)]^{2-}$, et la stabilité de la bordure de leurs feuillets dépendrait du faible déficit en valences de liaison des chaînes de polyèdres parallèles à [010] et [110]. Les minéraux du groupe de l'uranophane contiennent le feuillet $[(UO_2)SiO_3(OH)]^-$, et la stabilité de la bordure de leurs feuillets est plus fortement affectée par le déficit en valences de liaison des chaînes de polyèdres que par l'agencement des cations interstitiels, et par le décalage des feuillets. Toutes nos prédictions sont comparées avec la morphologie correspondante de cristaux étudiés par microscopie en force atomique (AFM), des images de cristaux disponibles, et des dessins de cristaux tirés surtout de la littérature plus ancienne. Toutes nos prédictions s'avèrent concordantes avec la morphologie observée de la face de base de ces minéraux.

Mots-clés: minéraux d'uranyle, morphologie, structure de surface, croissance cristalline, dissolution, valences de liaison.

Introduction

Uranyl-oxide minerals are common at many oxidized uranium deposits, and play a key role in the paragenesis of minerals that form where uraninite has been exposed to oxidizing meteoric water (Frondel 1958, Deliens 1977, Finch *et al.* 1992, Finch & Ewing 1992, Finch & Murakami 1999). Uranyl minerals have also been identified as corrosion products of UO_2 and spent nuclear fuel (Wadsen 1977, Wang & Katayama 1982, Forsyth & Werme 1992, Sunder *et al.* 1992, Wronkiewicz *et al.* 1992, 1996, Buck *et al.* 1997, 1998). Recently, the formation of schoepite, $[(UO_2)_8O_2(OH)_{12}](H_2O)_{12}$ has been observed on used depleted-uranium ammunition in Kosovo (United Nations Environmental Program 2001).

Chemical reactions on the surfaces of uranyl-sheet minerals are an important issue, as they result in the release of $(UO_2)^{2+}$ to natural waters. Therefore, a detailed atomic-scale understanding of the surface chemistry of uranyl-sheet minerals is desirable. Uranyl-sheet minerals contain layers of polymerized uranyl-polyhedra with uranium in [6], [7] and [8] coordination as tetragonal, pentagonal and hexagonal bipyramids, respectively. In these polyhedra, strong U–O uranyl bonds are not involved in linkage between uranyl polyhedra; they extend orthogonal to the sheet, whereas weaker equatorial U–φ bonds link the polyhedra in the plane of the sheet [φ: O^{2-}, $(OH)^-$, (H_2O)]. The equatorial O-atoms in the sheet of polyhedra can participate in acid–base reactions through protonation and deprotonation. Hence, edge surfaces on uranyl minerals are much more reactive than the corresponding basal surfaces because equatorial O-atoms on the edge surface almost always bond to fewer U^{6+} atoms than oxygen atoms in the sheet, and hence must satisfy their individual bond-valence requirements through a higher degree of protonation.

The Periodic Bond-Chain (PBC) theory (Hartman & Perdok 1955a, b, c) defines the basal face parallel to the sheets of uranyl polyhedra as an F face (flat face) because the sheet contains more than one periodic bond-chain. A PBC is an uninterrupted chain of strong bonds between building units. The basal face slowly grows, and therefore dominates the morphology of sheet-structure uranyl-oxide minerals. The morphology of the basal face itself is controlled by the faster-growing S faces (step faces), which contain only one type of periodic bond-chain.

Schindler *et al.* (2004a) showed that these periodic bond-chains can be represented by polyhedron chains in the sheet structural units of uranyl-oxide minerals. Parallel chains of polyhedra in the translation unit perpendicular to the basal face define the surface of an *edge*. The interaction of the surface of an edge with the aqueous species controls surface processes such as crystal growth and dissolution. These interactions depend on the surface structure of an edge, the pH value and the saturation index with respect to the mineral. Schindler *et al.* (2004a) also showed that the surface structure of an edge is characterized by the bond-valence deficiency of anion terminations along chains of polyhedra parallel to the edge, and by the shift and orientation of adjacent layers. Furthermore, they showed that the stability of edges also depends on the arrangement of the interstitial cations between the layers. In this paper, we will use this approach to predict the morphology of the basal faces of uranyl-oxide minerals, and will compare our predictions with AFM observations on synthetic crystals and morphological observations on natural crystals of uranyl-oxide minerals.

Experimental

Crystal growth, atomic-force microscopy and X-ray powder diffraction

In order to increase the database on the morphology of basal faces of uranyl-oxide crystals, we examined the crystal growth of uranyl-oxide minerals on the (001) face of dehydrated schoepite with an atomic-force microscope. The crystals of dehydrated schoepite were synthesized according to the procedure of Schindler *et al.* (2004a). After synthesis, 0.1 g of crystals were washed and brought in contact with 0.25 mol L^{-1} $BaCl_2$, KCl and $PbNO_3$ salt solutions at 25°C for 24 h. The

(001) face of the schoepite crystals was examined with the atomic force microscope (Digital Instruments Nanoscope III, Dimensional 3000). The surface was scanned in contact mode, and the images were analyzed with the Nanoscope Software package. The samples were subsequently examined by X-ray powder diffraction (Philips PW3040 powder diffractometer with Cu$K\alpha$ X-radiation) in order to identify the phases grown on the crystals of dehdyrated schoepite.

Collection of morphology data of basal faces of uranyl-oxide minerals

In order to determine the occurrence of edges on schoepite crystals and other uranyl-sheet minerals, we have examined images of crystals recorded by atomic force microscopy (AFM), or images (both photographs and sketches) drawn from the (mainly older) mineralogical literature. For the literature data, the indices of edges or the corresponding faces were determined by optical goniometry. In the case of AFM and images from Perloff (1998) and the internet, we indexed the edges by measuring the angles between the edges on the image and comparing them with corresponding angles derived from structural data.

The (001) Face of Schoepite

In schoepite, $[(UO_2)_8O_2(OH)_{12}](H_2O)_{12}$, there are eight crystallographically distinct sites occupied by U^{6+}, two of which are [7]-coordinated by two apical uranyl O-atoms and five equatorial (OH) groups, and six of which are [7]-coordinated by two apical uranyl O-atoms, one equatorial O-atom and four equatorial (OH)-groups (Finch *et al.* 1996). Schoepite has space-group symmetry $P2_1ca$ (orthorhombic), with a 14.337, b 16.813, c 14.731 Å. Figure 1 shows part of a (001) layer in schoepite, in which the pentagonal bipyramidal poly-

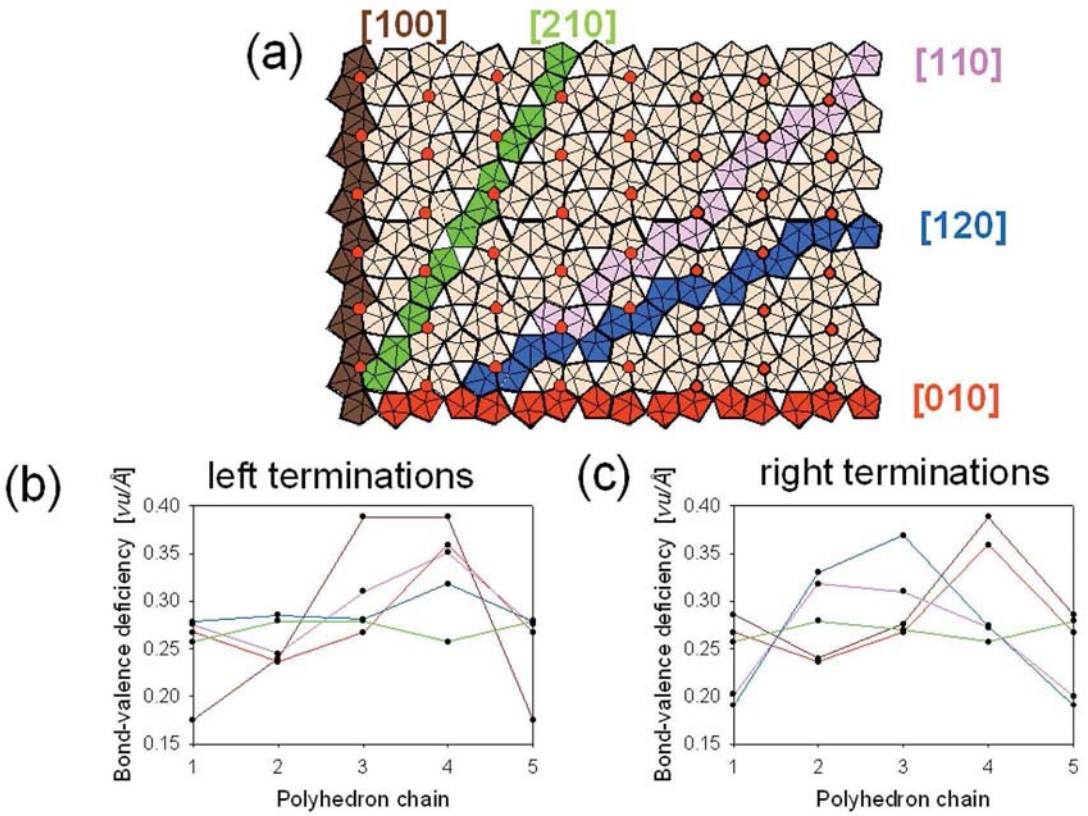

FIG. 1. (a) Polyhedron representation of the uranyl-oxide hydroxy-hydrate sheet in schoepite, $[(UO_2)_8O_2(OH)_{12}](H_2O)_{12}$; chains of polyhedra parallel to [100], [010], [120], [110] and [210] are shown in dark brown, red, blue, violet and blue-green, respectively. Equatorial O^{2-} anions of the uranyl polyhedra are shown as red-brown octagons, equatorial edges are shown as heavy black lines. (b), (c) Calculated bond-valence deficiencies for left and right anion-terminations on chains parallel to the [100], [010], [120], [110] and [210] edges in the uranyl sheet of schoepite. Bond valences were calculated using the curves of Brown & Altermatt (1985). The colors of the plots correspond to the colors of the different [*hk*0] directions in the schoepite sheet.

hedra share edges involving equatorial O- and (OH)-anions. The additional (H_2O) groups occur between the layers and link them together with weak hydrogen bonds.

Bond-valence deficiencies of chains of polyhedra in schoepite

Figure 1a shows selected chains of polyhedra parallel to [100], [010], [110], [120] and [210] in the schoepite sheet. Figures 1b and c show the change in bond-valence deficiency for the different chains. It is apparent that chains parallel to [100], [010], [110] and [120] have lower bond-valence deficiencies than chains parallel to [210]. The bond-valence deficiencies of the chains parallel to [210] are invariably high, whereas chains parallel to [100], [010], [110] and [120] have both low and high bond-valence deficiencies. Chains with low bond-valence deficiencies result in a low concentration of activated sites on the corresponding edges.

Orientation and shift of layers

Finch *et al.* (1996) showed that the positions of U^{6+} atoms and equatorial O-atoms in the structure of schoepite obey space-group symmetry *Pbca*. Adjacent layers are therefore related *via* a pseudo-two-fold screw axis parallel to [001]. Hence, right and left terminations of each chain of polyhedra occur on the same edge.

There is a shift between the layers parallel to the edges [100], [120], [110] and [210]. At those edges, therefore, chains of polyhedra of low bond-valence deficiency are parallel to chains of polyhedra with high bond-valence deficiency. For example, the chain of polyhedra parallel to [100] with the lowest minimum in bond-valence deficiency, 0.174 *vu* / Å, is parallel to a chain of polyhedra with a minimum in bond-valence deficiency of 0.276 *vu* / Å. Both chains could define an edge without an additional kink-site, but the large deficiency of one of the chains of polyhedra will produce a higher number of activated sites during crystal growth. This results in a higher growth-rate perpendicular to the chain of polyhedra, which produces a kink site (Schindler & Hawthorne 2004) between the adjacent layers on the [100] edge. Schindler *et al.* (2004a, Figs. 7a, b, c) predicted that this type of arrangement is less stable than an arrangement with chains of polyhedra of similar bond-valence deficiency along an edge. This is the case for adjacent layers (with no kink site) at the edge parallel to [010] (Schindler *et al.* 2004a, Fig. 7b); each layer is terminated by a chain of polyhedra with a bond-valence deficiency of 0.236 *vu*.

We are now able to predict the growth or dissolution rates of the different edges: they increase in the sequence [010] << [100] < [120] = [110] << [210], where "<" indicates a higher rate of growth of the corresponding edge. We predict that the edges [010] and [100] should invariably occur, independent of ΔpH and $\Delta\beta$, whereas the occurrence of the edges [120] and [110] depends on ΔpH and $\Delta\beta$, and the [210] edge should never occur.

Morphology of schoepite crystals

Figure 2a shows an AFM image of a schoepite crystal grown on the (104) surface of calcite (Schindler & Putnis 2004, who described in detail the relations between morphology and conditions of crystallization). The corresponding indices of the edges in the image are [120], [110], [100] and [010]. Figure 2b is an AFM image of schoepite crystals where the (001) face is defined by the [100] and [010] edges. Figure 2c shows a schoepite crystal from Katanga, Democratic Republic of Congo, with a prominent (001) face slightly elongate along [010] (http://www.trinityminerals.com/sm/uranium.shtml). The edges defining the (001) face have indices [120], [110], [100] and [010]. Figure 2d shows a drawing of a prismatic crystal of schoepite from Katanga on which the [100], [010] and [110] edges define the (001) face, and [120] edges occur between the (210) and (211) faces (indicated as m and P, respectively, in Fig. 2d; Walker 1923). Figure 2e shows typical rectangular crystals of schoepite from Katanga (http://webmineral.com/data/schoepite.shtml). The morphology of their (001) face is characterized primarily by [100] and [010] edges and, to a lesser extent, by the [110] edge (Palache 1934, Palache *et al.* 1944). These crystals are nearly identical to crystals grown under basic conditions (Fig. 2b, Schindler & Putnis 2004). Hence, they may have grown in a solution at low supersaturation and large differences between pH and pH_{pzc} (the pH of a solution in which a surface has zero net proton-charge: Stumm 1992, p. 18). These examples show that the morphology of schoepite crystals from growth experiments and from mineral samples are in good agreement with our predictions.

The (001) Face of Fourmarierite

Fourmarierite, $Pb[(UO_2)_4O_3(OH)_4](H_2O)_4$, has space-group symmetry $Bb2_1m$ (orthorhombic) with *a* 13.986, *b* 16.400, *c* 14.293 Å (Piret 1985). The uranyl sheet in fourmarierite has the composition $[(UO_2)_4O_3(OH)_4]^{2-}$, and its topology is identical to the topology of the uranyl sheet in schoepite (Burns 1999). The Pb^{2+} cations and (H_2O) groups occur between the uranyl sheets.

Figure 3a shows details of the uranyl sheet in fourmarierite. The equatorial O^{2-} ions are shown as black and red circles; the latter circles are identical to the O^{2-} positions in the schoepite sheet. However, in contrast to schoepite, there is no shift between the layers of polymerized uranyl-polyhedra in fourmarierite. However, adjacent layers are rotated by 180° to each other, which means that left and right terminations of the polyhedron chains occur on one edge. The interstitial cations are homogeneously distributed between

these layers and are not arranged in specific rows parallel an edge, such as in becquerelite and billietite (see Schindler *et al.* 2004a). Thus, the stability of edges should depend only on their individual bond-valence deficiencies and not on the arrangement of the layers or the distribution of cations in the interstices. Calculation of bond-valence deficiencies on chains of polyhedra in schoepite shows that the deficiency along each chain strongly depends on the number of O^{2-} anions. Inspection of the O^{2-} sites in the fourmarierite sheet shows that O^{2-} anion terminations occur on all chains parallel to [010], but not on all chains parallel to [100]. As a result, we expect that chains of polyhedra parallel to [100] have lower minima of bond-valence deficiency than chains parallel to [010]. This is indeed the case: the calculated bond-valence deficiencies for chains of polyhedra parallel to [100], [010], [120], [120] and [110] clearly show that the chain parallel to [100] has the lowest minimum in bond-valence deficiency (Fig. 3, right and left terminations). There are small differences between minima in bond-valence deficiency of chains parallel to [120] and [110]. Thus, we predict the probability of occurrence of edges to be [100] > [110] = [120] > [210] > [010]. This means that the (001) face of fourmarierite crystals grown in a solution close to equilibrium and at a pH close to the pH_{pzc} of the edges might be defined by the [100], [110], [120] and [210] edges. In a solution with a higher supersaturation with respect to fourmarierite and with a pH very different from the pH_{pzc}, we would expect elongate crystals parallel to

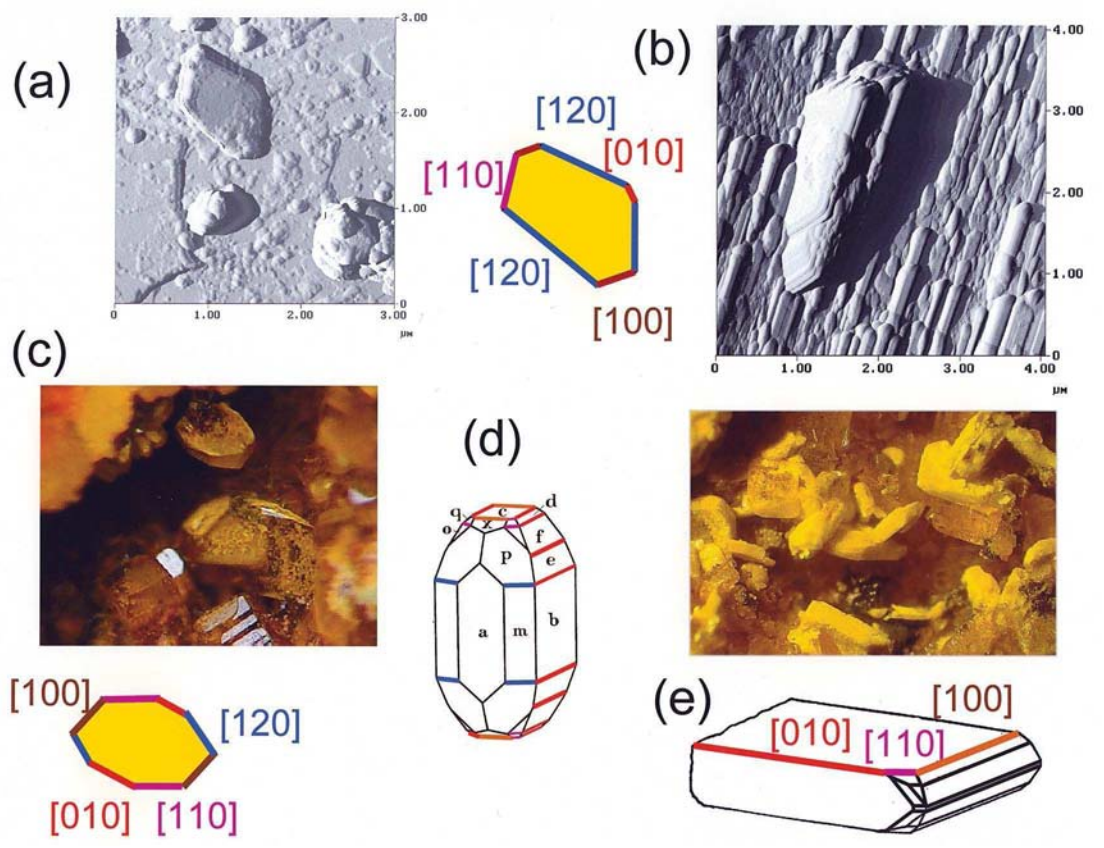

FIG. 2. (a) AFM image of a schoepite crystal grown in a weak acidic solution on the calcite (104) surface; the (001) face is defined by the [120], [110], [100] and [010] edges. (b) AFM image of schoepite crystals formed in a weak basic solution on the (104) surface of a calcite; their morphology is similar to that of crystals from Kasolo, Katanga, Democratic Republic of Congo (Walker 1923, Palache 1934). (c) Schoepite crystals with a prominent (001) face defined by the [120], [110], [100] and [010] edges (Perloff 1998). (d) Prismatic crystals of schoepite with a (001) face defined by [100], [010] and [110] edges; [120] edges occur between the (210) and (211) faces [indicated as (m) and P]. (e) Schoepite crystals from Kasolo, Democratic republic of Congo (Perloff 1998), together with a sketch of a crystal showing a dominant (001) face with [100], [010] and minor [110] edges (Palache *et al.* 1944).

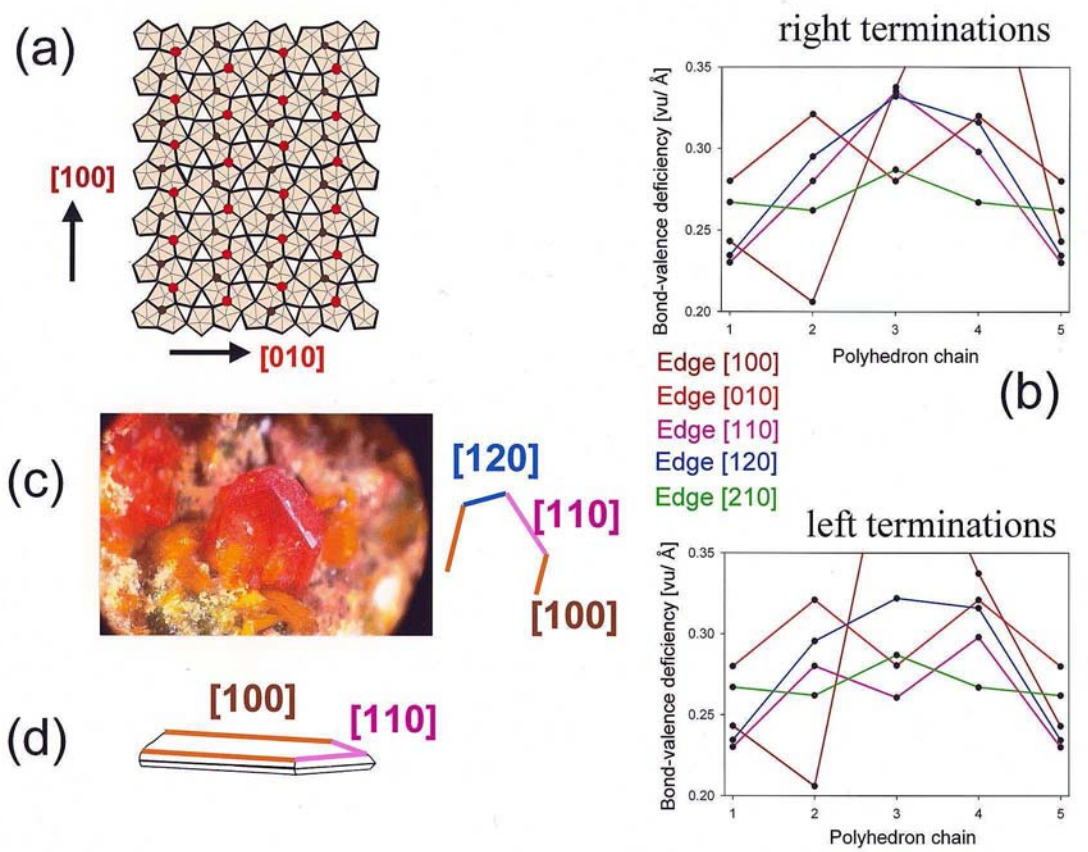

FIG. 3. (a) The $[(UO_2)_4O_3(OH)_4]^{2-}$ sheet as the structural unit in fourmarierite; the equatorial O^{2-} anions are identical to those in the analogous positions in the schoepite sheet and are shown as red circles, whereas the anions unique to fourmarierite are shown as brown circles. (b) Calculated bond-valence deficiencies of the right- and left-form chain-terminations on chains parallel to the [100], [010], [210], [110] and [120] edges. (c) A thick tabular orange crystal of fourmarierite from the Shinkolobwe mine, Democratic Republic of Congo (Perloff 1998), with a (001) face defined by the [100], [110] and [120] edges. (d) Morphology of fourmarierite crystals from Katanga, Democratic Republic of Congo, with a (001) face defined by [100] and [110] edges.

[100], and with a prominent (001) face that is defined only by the [100] and [110] or [120] edges.

Morphology of fourmarierite crystals

Figure 3c shows a thick tabular orange crystal of fourmarierite from the Shinkolobwe mine, Democratic Republic of Congo (Perloff 1998). Its (001) face is bounded mainly by the [100], [110] and [120] edges. Buttgenbach (1924) examined the morphology of fourmarierite crystals from Katanga, Democratic Republic of Congo, and described the crystals as elongate on [100], with dominant (001), (110) and (111) faces (based on the orientation of Piret 1985) (Fig. 3d). The (001) face in fourmarierite is bounded by the [100] and [110] edges, in good agreement with our predictions.

THE (001) FACE OF MINERALS OF THE BECQUERELITE GROUP

Minerals of the becquerelite group are becquerelite, $^{[7]}Ca(H_2O)_4[(UO_2)_3O_2(OH)_3]_2(H_2O)_4$, compreignacite, $^{[7]}K_2(H_2O)_3\ [(UO_2)_3O_2(OH)_3]_2(H_2O)_4$, billietite, $^{[10]}Ba(H_2O)_4[(UO_2)_3O_2(OH)_3]_2\ (H_2O)_3$, $^{[8]}K_2(^{[9]}Ca,Sr)(H_2O)_5[(UO_2)_3O_3(OH)_2]_2$, and rameauite, $K_2Ca[(UO_2)_6O_4(OH)_6]\ (H_2O)_6$. The chemical composition of their (sheet) structural unit is $[(UO_2)_3O_2(OH)_3]^-$, in which U^{6+} occurs in [7]-coordination (Fig. 4a). The topology of the sheet differs from that of sheets in fourmarierite and schoepite. The structures of becquerelite, compreignacite and billietite have orthorhombic symmetry, but the space-group symmetry and unit-cell dimensions vary with the type of interstitial cation and the number

of interstitial (H_2O) groups. We calculated the bond-valence deficiencies of the different chain-terminations of unit length *a* 13.8378 / 2 = 6.919, *b* 12.3781 Å from the crystal-structure data on becquerelite (Pagoaga *et al.* 1987), and will describe the crystal morphologies of becquerelite, billietite and compreignacite crystals on the basis of these cell dimensions and in the orientation given in Figure 4a.

In becquerelite, billietite and compreignacite, adjacent layers are rotated by 180° relative to each other. Hence, the left and right terminations of the same type of chain define the corresponding edges of two adjacent layers.

Interstitial complexes in becquerelite and billietite are arranged in rows parallel to [010] and [100], respectively. The corresponding crystals of both minerals are elongate in these directions. In compreignacite, the interstitial complexes are arranged in rows parallel to [100], and the interstitial K is highly disordered in those complexes (Burns 1998). Thus, we would expect similar morphologies for the (001) face in billietite and compreignacite.

Figure 4b shows the calculated bond-valence deficiencies of the chain terminations of the different chains of the uranyl sheet. It is apparent that the [110] and [100] edges contain chains with the lowest minima in bond-valence deficiency, and that the differences in minima are very small for chains parallel to [010], [210], [310] and [130]. Considering only the bond-valence deficiencies and not the arrangement of the interstitial species, we predict that the probability of occurrence of edges decreases in the sequence [110] = [100] >> [310] = [210] > [110] = [130].

Morphology of becquerelite, billietite and compreignacite

Figures 5a and 5b show an image of becquerelite crystals from Shinkolobwe, Democratic Republic of Congo (Perloff 1998) and the indices of the correspond-

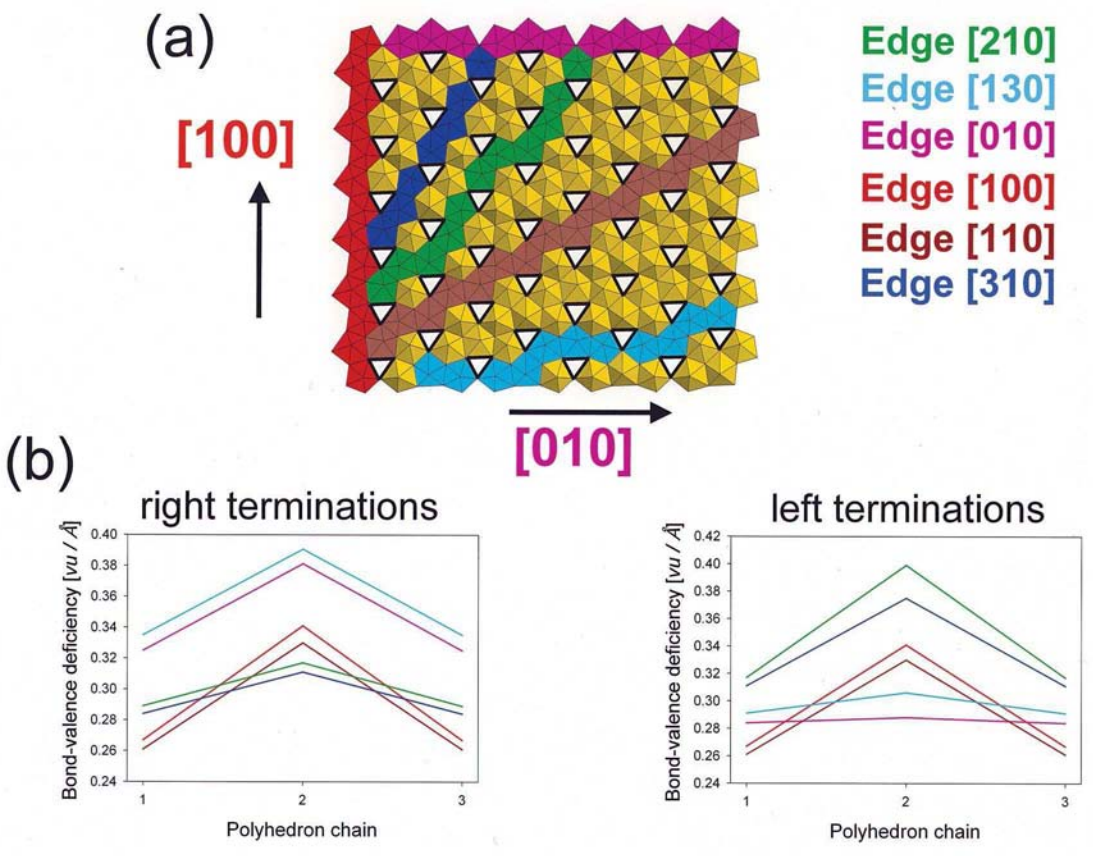

FIG. 4. (a) The $[(UO_2)_3O_2(OH)_3]_2^{2-}$ sheet as the structural unit in minerals of the becquerelite group. (b) Calculated bond-valence deficiencies of the left and right forms of chain terminations on chains parallel to the edges [100], [010], [310], [110], [130] and [210]. The positions of the (OH) groups are shown as vertices of a black triangle (Fig. 5a), and the chains parallel to the edges are indicated in the same colors as in Figure 4b.

ing edges: [110], [100] and [010]. Figures 5c and 5d show AFM images of becquerelite crystals grown on the (104) surface of calcite (Schindler *et al.* 2004b). Figure 5c shows an aggregate of small crystals of becquerelite grown in uranyl acetate + $NaCO_3$ solution for one month at a pH of 7.5–8.5. Figure 5d shows a parallel aggregate of larger crystals of becquerelite crystals in uranyl acetate solution at 100°C for 3 days at a pH of 5–6. In both cases, the indices of the edges are [110], [100] and [010] (Fig. 5e).

Figures 5f shows a crystal of billietite from Shinkolobwe, Democratic Republic of Congo (http://trinityminerals.com/sm2001/uranium.shtml); the indices of the edges present are [100], [010] and [110] (Fig. 5h). Figure 5g shows an AFM image of billietite crystals on the (001) surface of dehydrated schoepite; these crystals may be twinned on [110] (Fig. 5i). Twinning of billietite crystals is common on [111] and [110]; the latter twinning is particularly common and produces pseudohexagonal crystals (Schoep & Stradiot 1948; Fig. 5i).

Compreignacite was described in the same orientation as billietite. Protas (1964) reported equant crystals on which the (001) face is bounded by [100], [010], [110] and [310] edges (Fig. 5j). He also reported compreignacite crystals twinned on [110], for which the (001) face is not bounded by the [100] or [110] edges (Fig. 5k). The [100] and [110] edges, which are defined

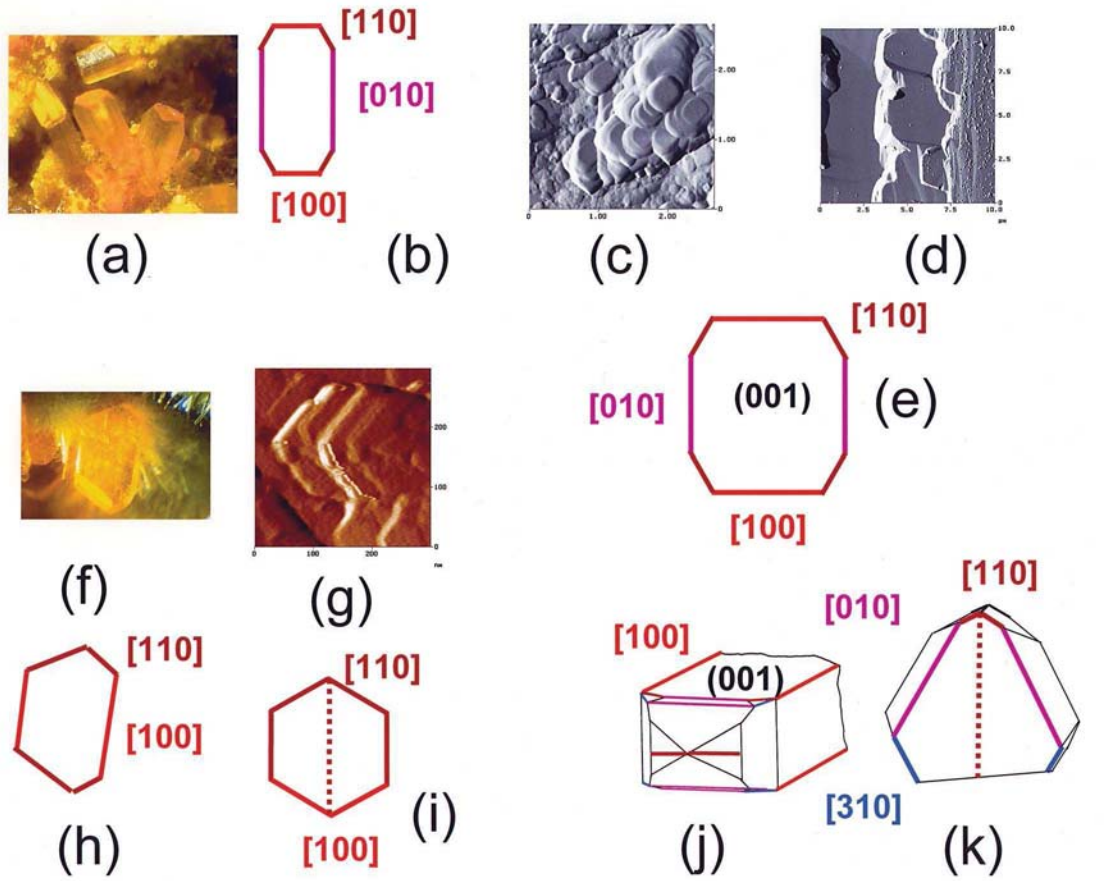

FIG. 5. (a, b) Crystals of becquerelite from Shinkolobwe, Democratic Republic of Congo (Perloff 1998) with a (001) face defined by the [110], [100] and [010] edges. (c, d) AFM images and (e) sketch of becquerelite crystals grown on the calcite (104) surface with (001) faces defined by the [110], [100] and [010] edges. (f) Crystal of billietite from Shinkolobwe, Democratic Republic of Congo (Perloff 1998) and (h) the corresponding sketch of the (001) face defined by the [100] and [110] edges. (g) AFM image of billietite crystals on the (001) surface of dehydrated schoepite. (i) Sketch of a crystal twinned by reflection on (110), with a (001) face defined by the [100] and [110] edges. (j) Bulky crystals of compreignacite with a (001) face defined by the [100], [110], [310] and [010] edges. (k) Compreignacite crystals twinned by reflection on [110] with a (001) face defined by the [010] and [310] edges.

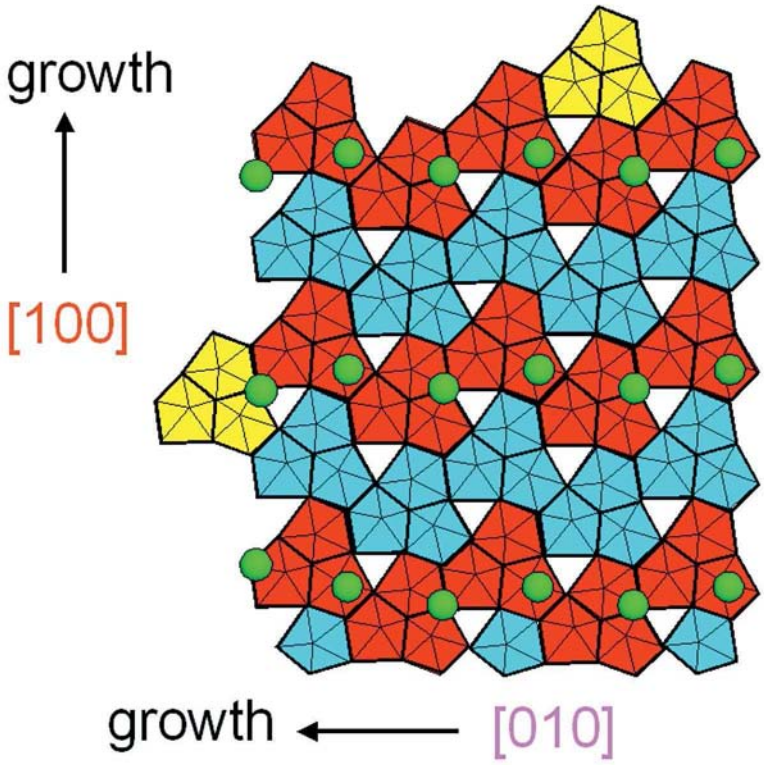

FIG. 6. The layer of polymerized uranyl-bearing polyhedra in becquerelite; this layer can be constructed of clusters of three polymerized pentagonal bipyramids (indicated in red and blue). These clusters are structurally identical to the principal aqueous species $[(UO_2)_3(OH)_5(H_2O)_5]^+$ in a weakly acidic solution. The position of the interstitial complex is indicated by the Ca atoms in the interlayer (green circles). Clusters attached on the [100] and [010] edges are indicated in yellow (see text for details).

by chains with the lowest bond-valence deficiencies, almost always occur on crystals of the becquerelite-group minerals. Except for twinned billietite and compreignacite, such crystals are elongate parallel to the rows of interstitial complexes in the interlayer. Hence, crystals of the becquerelite-group minerals grow parallel to the arrangement of interstitial complexes (which are only bonded to each other by weak hydrogen bonds). This is surprising, as it contradicts the basic ideas of PBC theory. One possible explanation of this phenomenon is illustrated in Figure 6, which shows the possible attachment of a cluster of three polymerized pentagonal bipyramids to the [010] and [100] edges in becquerelite [note that the (001) layer can be entirely constructed of such clusters]. Growth parallel to [100] corresponds to attachment of a cluster at the [010] edge. This attached cluster shares five ligands with the corresponding kink-site. If there is no layer above or below this layer, ligands (mainly O-atoms of the uranyl group) of the attached cluster do not receive bonds from the interstitial complex. If the cluster is attached to the [100] edge, there would be only four common ligands between cluster and kink site, but the ligands of the cluster would accept bonds from the interstitial complex.

THE (001) FACE OF MINERALS OF THE MASUYITE GROUP

The minerals of the masuyite group are protasite, $^{[10]}Ba(H_2O)_3[(UO_2)_3O_3(OH)_2]$, and masuyite, $^{[10]}Pb(H_2O)_3[(UO_2)_3O_3(OH)_2]$. They both have the (sheet) structural unit $[(UO_2)_3O_3(OH)_2]^{2-}$, which has the same topology as the sheet in minerals of the becquerelite group (Burns 1999; Figs. 4a, 7a). Both structures have space-group symmetry *Pn* (monoclinic), and the bond-valence deficiency of the chain terminations are calculated for the masuyite sheet with *a* 12.241, *c* 6.983 Å (Burns & Hanchar 1999). Reorientation of the axes (*c* = *a*, *a* = *b*) results in edge indices identical to those in the minerals of the becquerelite group.

The (OH) positions in the masuyite sheet differ from those in the isochemical sheet of richetite, $^{[6]}M_x$ $^{<[8.4]>}$ $Pb_{8.57}(H_2O)_{24}[(UO_2)_{18}O_{18}(OH)_{12}](H_2O)_{17}$ (Burns 1999). Compared to the sheet in minerals of the becquerelite group, one of the three (OH) groups is missing (Figs. 4a, 7a). This results in loss of mirror planes through the triangles parallel to [110] and [100] (Fig. 7a). As a result, we expect a high variation in bond-valence deficiencies on the right and left terminations of chains parallel to [110] and [100]. This is indeed the case: the minima in bond-valence deficiencies are lower on the left termination than on the right termination (Fig. 7b). This indicates the highly anisotropic character of the corresponding edges during dissolution and crystal growth. There is no shift between the layers either in masuyite or protasite, and the interstitial complexes are more or less homogeneously distributed in the interlayer of both minerals (Burns & Hanchar 1999, Pagoaga *et al.* 1987). Thus we have to consider only the average minima in bond-valence deficiencies for both terminations. Based on these minima, we predict that the probability of occurrence of edges decreases in the sequence [110] > [100] >> [130] > [310] = [010] > [210].

Morphology of masuyite and protasite

Vaes (1947) and Pagoaga *et al.* (1987) observed sector twinning with a 60° rotation of the twin plane around [001] in masuyite and protasite; the corresponding twin planes are [100] and [110]. Figure 7c shows a twin on [110], where the (001) face is bounded by the [100] and [110] edges (Vaes 1947). These observations indicate that the twin planes occur parallel to the missing mirror planes orthogonal to [100] and [110]. Instead of the predicted anisotropic growth of crystals, masuyite and protasite crystals show extensive twinning on [100] and [110]. This extensive twinning may be a result of the

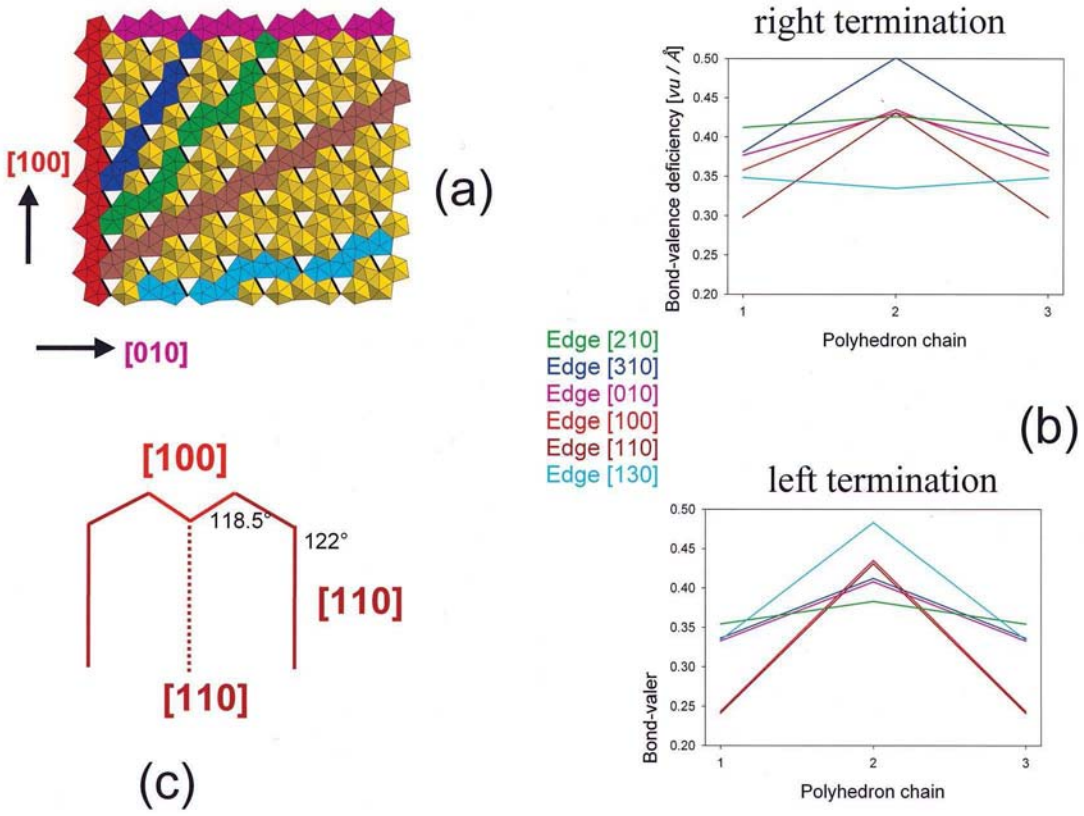

FIG. 7. (a) The $[(UO_2)_3O_3(OH)_2]^{2-}$ structural unit in minerals of the masuyite group. (b) Calculated bond-valence deficiencies of the left and right forms of chain terminations on chains parallel to the edges [100], [010], [310], [110], [130] and [210]. (c) Twins of masuyite (or protasite) crystals across [110], with the (001) face defined by the [100] and [110] edges.

large differences in the minima of the bond-valence deficiencies of the corresponding chains.

The (100) Face of Curite

Curite, $Pb_3[(UO_2)_8O_8(OH)_6](H_2O)_3$, has space-group symmetry *Pnam*, with *a* 12.551, *b* 13.003, *c* 8.390 Å (Taylor *et al.* 1981). The (sheet) structural unit is parallel to (100) and contains pentagonal and tetragonal biypramids. The arrangement of polyhedra produces slabs parallel to [001] that are linked *via* equatorial (OH) groups (Fig. 8a). In space-group symmetry *Pnam*, adjacent layers are related by a two-fold screw axis, and therefore are rotated by 180° relative to each other. Hence, left and right terminations of the chains of polyhedra occur together on the corresponding edges. The interstitial complexes are arranged in rows parallel to [001]. Similar to the minerals of the becquerelite group, an attached cluster or polyhedron at the [100] edge will accept bonds from the interstitial complex above or below the corresponding kink-site. Hence, the arrangement of interstitial complexes along [001] may promote growth in this direction. Figure 8b shows the calculated bond-valence deficiency for chains of polyhedra parallel to the edges [001], [012], [021], [011] and [010], where the [021] chain is a linear combination of the [001] and [011] chains, and the [012] chain is a combination of the [011] and [010] chains. There are many other possible chains that are a linear combination of either [001] and [011] or [010] and [011]. In the first case, we can indicate the chains with the general indices [0*k*>*l*], and in the second case with the general indices [0*k*<*l*]. On the basis of the bond-valence deficiencies of the chains of polyhedra parallel to [001], [011] and [010], one would expect that the chains of polyhedra parallel to [0*k*>*l*] have lower deficiencies than chains of polyhedra parallel to [0*k*<*l*]. This is indeed the case; chains of polyhedra parallel to [021] have a lower mini-

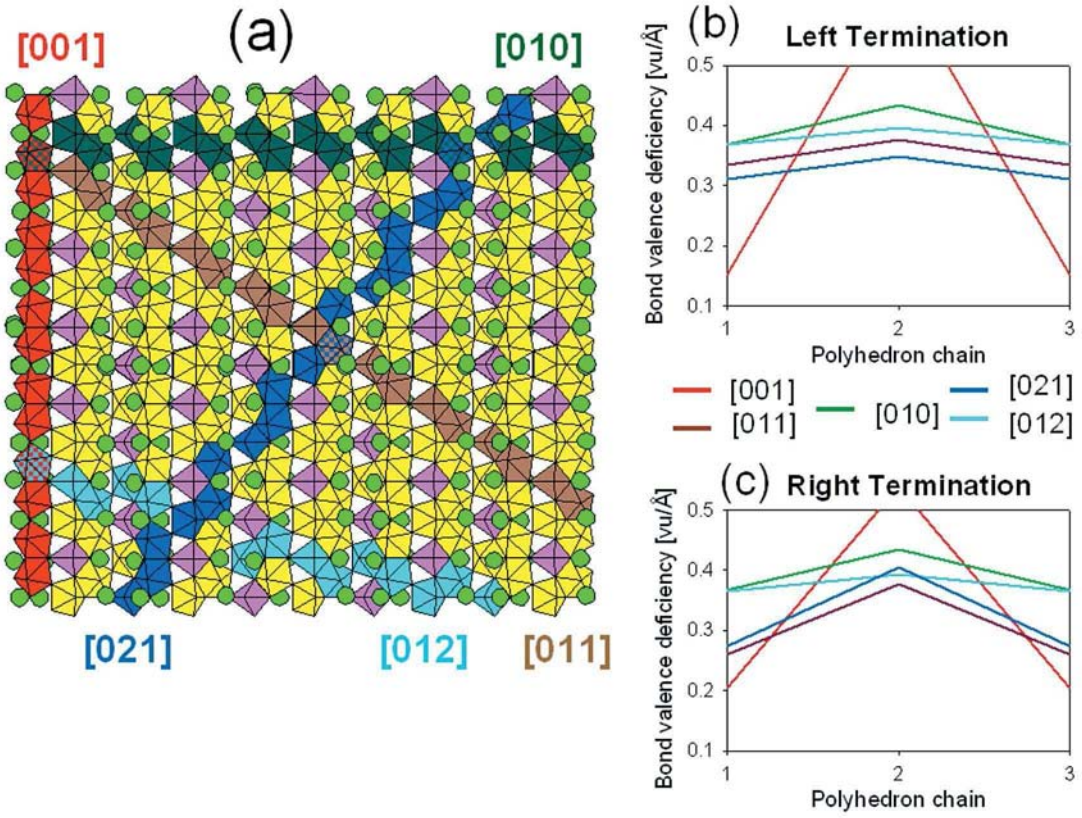

FIG. 8. (a) The $[(UO_2)_8O_8(OH)_6]^{2-}$ structural unit in curite and the chains of polyhedra parallel to [001] (red), [011] (brown), [010] (dark green), [021] (dark blue) and [012] (light blue). The positions of the Pb atoms are indicated with large green circles. (b) Calculated bond-valence deficiencies of the left and right forms of chain terminations on chains parallel to the edges [001], [010], [011], [012] and [021].

mum in bond-valence deficiency than chains of polyhedra parallel to [012] (Figs. 8b, c).

The minima in bond-valence deficiency of chain terminations in the right and left form indicate that the probability of occurrence of edges decreases in the sequence [001] > [011] = [0*k*>*l*] > [0*k*<*l*] > [010]. Because the minima in bond-valence deficiency indicate a high stability of the [001] edge and because the interstitial complexes are arranged parallel to this edge, we predict that the (001) face will be prominent on curite crystals, which will be dominated by the [001] edge.

Figures 9a, b show curite crystals obtained by synthesis (Schindler *et al.* in prep.) and from a mineral sample from the Shinkolobwe mine, Democratic Republic of Congo. Both crystals are elongate parallel to [001] (Perloff 1998), but the synthetic crystal is defined by [011] and [0*k*>*l*] edges (with $k = 4$ and $l = 3$), whereas the crystals of the mineral sample are exclusively defined by the [011] and [001] edges (Fig. 9d). Elongation of the crystals parallel to the [001] edge indicates the predicted dominance of that edge, and the occurrence of the [011] and [0*k*>*l*] edges also is in agreement with our predictions.

The (001) Face of Minerals of the Carnotite Group

The minerals of the carnotite group contain the structural unit $[(UO_2)_2(V_2O_8)]^{2-}$, a sheet containing (UO_7) pentagonal bipyramids and ($V^{5+}O_5$) square pyramids. The ($V^{5+}O_5$) square pyramids share common edges and form a [V_2O_8] dimer, which shares corners with dimers of edge-sharing (UO_7) pentagonal bipyramids (Fig. 10a).

Five-coordinated vanadium in ($V^{5+}O_5$) square pyramids is characterized by the occurrence of one or two strong vanadyl bonds. Schindler *et al.* (2000) indicated the number of vanadyl bonds by a three-part coordination number in which the number of bonds are listed in the order *vanadyl*, *equatorial* and *trans*. In the minerals of the carnotite group, V^{5+} is in [1+4] coordination (*i.e.*, there is one vanadyl bond, four equatorial bonds and no

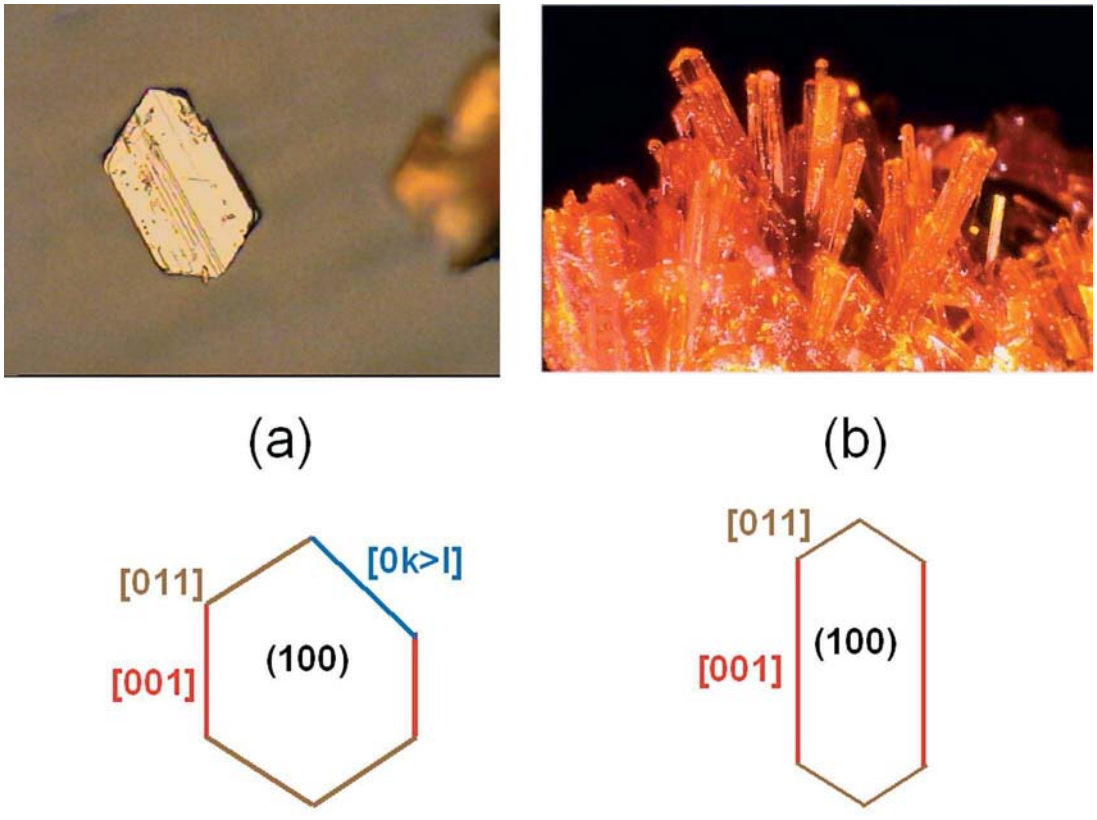

FIG. 9. (a) Synthetic crystal of curite, and (b) red crystals of curite from the Shinkolobwe mine, Democratic Republic of Congo (Perloff 1998), with a (100) face defined by [001], [0*k*>*l*] (with $k = 4$ and $l = 3$) and [011] edges.

trans bonds), and the average equatorial V^{5+}–O bond-valence is 0.79 *vu* (Schindler *et al.* 2000).

Depending on the interstitial complex, the minerals of the carnotite group have orthorhombic or monoclinic symmetry. Structural data of minerals of the carnotite group are available for francevillite (Mereiter 1986), curienite (Borène & Cesbron 1971), and sengierite (Piret *et al.* 1980). The structural data show that there are no shifts between the layers, and that the interstitial complexes are more or less equally distributed between the layers of these minerals. The bond-valence deficiencies of the different chain-terminations are calculated with the cell *a* 10.419, *b* 8.510 Å taken from the structure refinement of francevillite, $^{[9]}Ba(H_2O)_5[(UO_2)_2(V_2O_8)]$ (Mereiter 1986). Figure 10b shows the calculated bond-valence deficiencies of chain terminations parallel to several edges. Inspection of the corresponding minima in bond-valence deficiency shows that the probability of occurrence of edges decreases in the sequence [010] > [110] >> [100] = [120] > [210].

Morphology of minerals of the carnotite group

Minerals of the carnotite group form large idiomorphic crystals. Figure 10c shows green crystals of sengierite, $^{[6]}Cu_2(OH)_2(H_2O)_6[(UO_2)_2(V_2O_8)]$, from the Luiswishi mine, Democratic Republic of Congo (Perloff 1998) and yellow crystals of tyuyamunite, $Ca[(UO_2)_2(V_2O_8)](H_2O)_8$, from the Marie mine, Montana (http://www.dakotamatrix. com/GalleryImages/Rare/tyuy1b.jpg). Figure 10d shows the general morphology of the (001) basal face on almost all crystals of minerals of the carnotite group (Frondel 1958). The (001) face is bounded primarily by the [010] and [110] edges, with

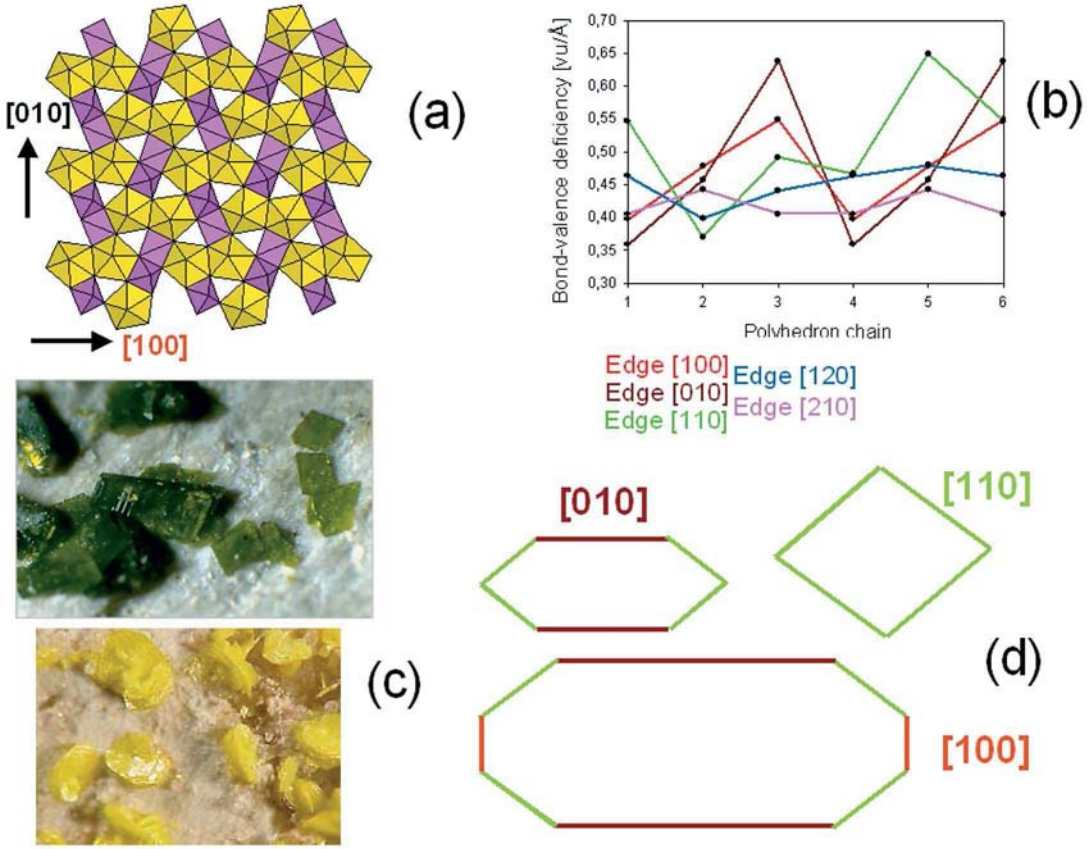

FIG. 10. (a) The $[(UO_2)_2(V_2O_8)]^{2-}$ structural unit in minerals of the carnotite group. (b) Calculated bond-valence deficiencies of chain terminations on chains parallel to the edges [100], [010], [110], [120] and [210]. (c) Green crystals of sengierite from the Luiswishi mine, Democratic Republic of Congo (Perloff 1998) and yellow crystals of tyuyamunite from the Marie mine, Montana (http://www.dakotamatrix.com/galleryimages/rare/tyuy1b.jpg). (d) Characteristic morphologies of the basal (001) face, with dominant [010] and [110] and minor [100] edges.

small [100] edges. These observations are in agreement with our predictions. The geometrical arrangement of interstitial cations is similar in all minerals of the carnotite group, and hence the different types of interstitial cations have minor or negligible effect on the stability of specific edges on the $[(UO_2)_2(V_2O_8)]^{2-}$ sheet.

The (010) Face of Minerals of the Uranophane Group

The minerals of the uranophane group are based on $[(UO_2)SiO_3(OH)]^-$ sheets, which contain $(U^{6+}\varphi_7)$ pentagonal bipyramids and acid $[SiO_3(OH)]$ groups (Fig. 11a). The pentagonal bipyramids share edges to form chains connected by $(Si\varphi_4)$ tetrahedra. The (OH) groups are located at the free apices of the $(Si\varphi_4)$ tetrahedra and form hydrogen bonds to interstitial (H_2O) groups. The minerals of the uranophane group are monoclinic and triclinic. The structural data on these minerals indicate that between the layers, there is a minimum shift that does not exceed one chain-width, and this small shift may not affect the stability of the corresponding edges. Interstitial complexes are homogeneously distributed between the layers in minerals with the α-uranophane structure-type (Burns 1999). For the β-uranophane structure, the interstitial complexes are arranged in rows parallel to [100] (Fig. 11a). Each interstitial complex occurs above and below the uranyl chain parallel to [001]. An attached pentagonal bipyramid on this chain will not accept any bonds from the interstitial complex. Hence, the interstitial complex cannot promote cluster attachment at the [001] edge, and the arrangement of interstitial cations in β-uranophane may not significantly influence growth of the crystals. The bond-valence deficiency of the chain terminations are calculated with the cell *a* 6.632, *c* 13.966 Å of β-uranophane (re-

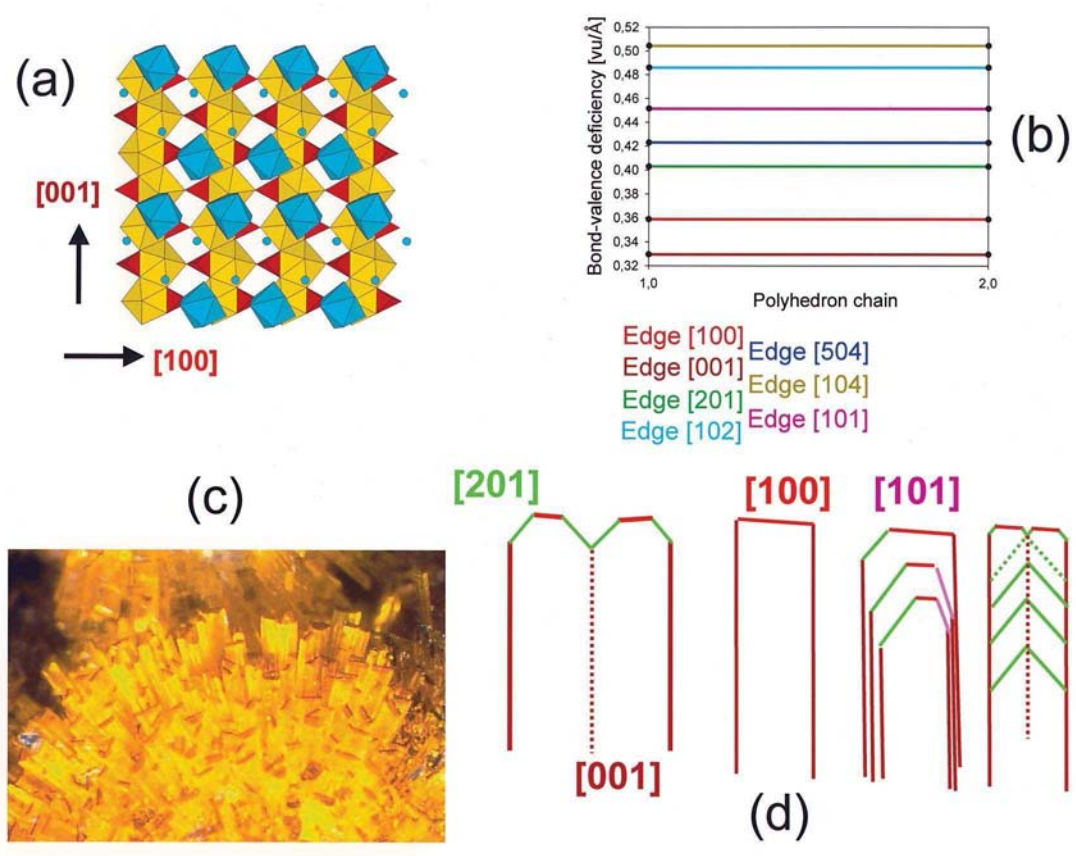

FIG. 11. The $[(UO_2)SiO_3(OH)]^-$ structural unit in minerals of the uranophane group, with the interstitial $(Ca\varphi_8)$ polyhedra indicated in light blue. (b) Calculated bond-valence deficiencies of chain terminations on chains parallel to the edges [001], [100], [201], [504], [101], [102] and [104]. (c) Yellow prisms of β-uranophane from the Rossing mine, Namibia (Perloff 1998). (d) Morphology of β-uranophane crystals with a (010) face defined by the [001] and [100] edges; the "edges" [201] and [101] occur mainly as growth zones.

oriented from *abc* to *cba*, Viswanathan & Harneit 1986) and with an average bond-valence of 1.0 *vu* for the equatorial Si–O bond. In $[(UO_2)SiO_3(OH)]^-$, if one considers chains of polyhedra that do not contain silicate tetrahedra with more than one free equatorial ligand, every [*h0l*] edge has only one possible chain-termination. Figure 11b shows the corresponding bond-valence deficiency of the single chain-termination parallel to each edge. The minima in deficiency indicate that the probability of the occurrence of edges decreases in the sequence [001] >> [100] >> [201] >> [504] >> [101] >> [102] >> [104].

Morphology of minerals of the uranophane group

All minerals of the uranophane group form prismatic to acicular crystals parallel to [001] and with a prominent (010) basal face. Figure 11c shows yellow prisms of β-uranophane, $^{[8]}Ca(H_2O)_5[(UO_2)(SiO_3OH)]_2$, from the Rossing mine, Namibia (Perloff 1998). Steinocher & Nováček (1939) and Branche *et al.* (1951) showed that the termination of β-uranophane crystals is bounded by the [100], [201] and [101] edges. The latter two edges occur mainly on growth zones, but almost disappear in the last stages of crystallization (Fig. 11d). These observations on β-uranophane show for the first time the direct relation between growth rate and bond-valence deficiency on the corresponding chains of polyhedra in uranyl-oxide minerals: the chain parallel to [100] has a lower minimum in bond-valence deficiency than the chains parallel to the faster-growing [201] and [101] edges. The observed morphology is thus in agreement with our predictions.

Summary

We can predict the occurrence of edges on the basal faces of uranyl-oxide minerals using the bond-valence deficiency of anion-terminations along chains of polyhedra, the shift and orientation of adjacent layers, and the arrangement of interstitial cations (Schindler & Hawthorne 2004). These predictions are in agreement with observation on minerals with different interstitial complexes and with different sheets as structural units.

Acknowledgements

We thank referees Mike Hochella and Cornelis Woensdregt and Editor Bob Martin for their comments, which added considerably to the clarity of this paper. MS thanks the Deutsche Forschungsgemeinschaft for an Emmy Noether Fellowshp. FCH was supported by a Canada Research Chair in Crystallography and Mineralogy and by a Discovery Grant from the Natural Sciences and Engineering Research Council of Canada.

References

Borène, J. & Cesbron, F. (1971): Structure cristalline de la curiénite, $Pb(UO_2)_2(VO_4)_2 \cdot 5H_2O$. *Bull. Soc. fr. Minéral. Cristallogr.* **94**, 8-14.

Branche, G., Chervet, J. & Guillemin, C. (1951): Nouvelles espèce uranifères françaises. *Bull. Soc. Fr. Minéral. Cristallogr* **74**, 457-488.

Brown, I.D. & Altermatt, D. (1985): Bond-valence parameters obtained from a systematic analysis of the inorganic crystal structure database. *Acta Crystallogr.* **B41**, 244-247.

Buck, E.C., Finch, R.J., Finn, P.A. & Bates, J.K. (1998): Np in dehydrated schoepite. In Scientific Basis for Nuclear Waste Management XXI (I.A. McKinley & C. McCombie, eds.). *Mater. Res. Soc. Proc.* **506**, 87-94.

_____, Wronkiewicz, D.J., Finn, P.A. & Bates, J.K. (1997): A new uranyl oxide hydrate phase derived from spent fuel alteration. *J. Nucl. Mater.* **249**, 70-76.

Burns, P.C. (1998): The structure of boltwoodite and implications for the solid-solution toward sodium boltwoodite. *Can. Mineral.* **36**, 1069-1075.

_____ (1999): The crystal chemistry of uranium. *In* Uranium: Mineralogy, Geochemistry and the Environment (P.C. Burns & R. Finch, eds.). *Rev. Mineral.* **38**, 23-90.

_____ & Hanchar, J.M. (1999): The structure of masuyite, $Pb[(UO_2)_3O_3(OH)_2](H_2O)_3$, and its relationship to protasite. *Can. Mineral.* **37**, 1483-1491.

Buttgenbach, H. (1924): La fourmariérite, nouvelle espèce minérale. *Ann. Soc. Géol. Belg.* **47**, 41.

Deliens, M. (1977): Associations de minéraux secondaires d'uranium à Shinkolobwe (région du Shaba, Zaïre). *Bull. Soc. fr. Minéral. Cristallogr.* **100**, 32-38.

Finch, R.J., Cooper, M.A., Hawthorne, F.C. & Ewing, R.C. (1996): The crystal structure of schoepite, $[(UO_2)_8O_2(OH)_{12}](H_2O)_{12}$. *Can. Mineral.* **34**, 1071-1088.

_____ & Ewing, R.C. (1992): The corrosion of uraninite under oxidizing conditions. *J. Nucl. Mater.* **190**, 133-156.

_____, Miller, M.L. & Ewing, R.C. (1992): Weathering of natural uranyl oxide hydrates: schoepite polytypes and dehydration effects. *Radiochim. Acta* **58/59**, 433-443.

_____ & Murakami, T. (1999): Systematics and paragenesis of uranium minerals. *In* Uranium: Mineralogy, Geochemistry and the Environment (P.C. Burns & R.J. Finch, eds.). *Rev. Mineral.* **38**, 91-179.

Forsyth, R.S. & Werme, L.O. (1992): Spent fuel corrosion and dissolution. *J. Nucl. Mater.* **190**, 3-19.

Frondel, C. (1958): Systematic mineralogy of uranium and thorium. *U.S. Geol. Surv., Bull.* **1064**.

HARTMAN, P. & PERDOK, W.G. (1955a): On the relations between structure and morphology of crystals I. *Acta Crystallogr.* **8**, 49-52.

_____ & _____ (1955b): On the relations between structure and morphology of crystals II. *Acta Crystallogr.* **8**, 521-524.

_____ & _____ (1955c): On the relations between structure and morphology of crystals III. *Acta Crystallogr.* **8**, 525-529.

MEREITER, K. (1986): Crystal structure refinements of two francevillites, (Ba,Pb)[$(UO_2)_2V_2O_8$]•$5H_2O$. *Neues Jahrb. Mineral., Monatsh.*, 552-560.

PAGOAGA, M.K., APPLEMAN, D.E. & STEWART, J.M. (1987): Crystal structures and crystal chemistry of the uranyl oxide hydrates becquerelite, billietite, and protasite. *Am. Mineral.* **72**, 1230-1238.

PALACHE, C. (1934): Crystallography of the uranium oxides. *Am. Mineral.* **19**, 309-315.

_____, BERMAN, H. & FRONDEL, C. (1944): *The System of Mineralogy*. **1**. *Elements, Sulfides, Sulfosalts, Oxides*. John Wiley and Sons, New York, N.Y. (p. 627).

PERLOFF, L. (1998): *The Photo Atlas of Minerals* (A.R. Kamp & G. Gerhold, eds.). The Gem and Mineral Council, Los Angeles County Museum of Natural History, Los Angeles, California.

PIRET, P. (1985): Structure cristalline de la fourmariérite, $Pb(UO_2)_4O_3(OH)_4$•$4H_2O$. *Bull. Minéral.* **108**, 659-665.

_____, DECLERCQ, J.-P. & WAUTERS-STOOP, D. (1980): Structure cristalline de la sengiérite. *Bull. Minéral.* **103**, 176-178.

PROTAS, J. (1964): Une nouvelle espèce minérale: la compreignacite, K_2O•$6UO_3$•$11H_2O$. *Bull. Minéral.* **87**, 365-371.

SCHINDLER, M. & HAWTHORNE, F.C. (2004): A bond-valence approach to uranyl oxysalt minerals. I. Crystal structure and chemical composition. *Can. Mineral.* **42**, 1601-1627.

_____, _____ & BAUR, W.H. (2000): Crystal-chemical aspects of vanadium: polyhedral geometries, characteristic bond-valences and polymerization of (VO_n) polyhedra. *Chem. Mater.* **12**, 1248-1259.

_____, _____, PUTNIS, C. & PUTNIS, A. (2004b): Growth of uranyl-hydroxy-hydrate and uranyl-carbonate minerals on the (104) calcite surface. *Can. Mineral.* **42**, 1683-1697.

_____, MUTTER, A. HAWTHORNE, F.C. & PUTNIS, A. (2004a): Prediction of crystal morphology of complex uranyl-sheet minerals. I. Theory. *Can. Mineral.* **42**, 1629-1649.

_____ & PUTNIS, A. (2004): Crystal growth of schoepite on the (104) surface of calcite. *Can. Mineral.* **42**, 1667-1681.

SCHOEP, A. & STRADIOT, S. (1948): Additional data on the properties of becquerelite and billietite. *Am. Mineral.* **33**, 503-507.

STEINOCHER, V. & NOVÁČEK, R. (1939): On β-uranotile. *Am. Mineral.* **24**, 324-338.

STUMM, W. (1992): *Chemistry of the Solid–Water Interface*. John Wiley & Sons, New York, N.Y. (p. 428).

SUNDER, S., SHOESMITH, D.W., CHRISTENSEN, H. & MILLER, N.H. (1992): Oxidation of UO_2 fuel by the products of gamma radiolysis of water. *J. Nucl. Mater.* **190**, 78-86.

TAYLOR, J.C., STUART, W.I. & MUMME, I.A. (1981): The crystal structure of curite. *J. Inorg. Nucl. Chem.* **43**, 2419-2423.

UNITED NATIONS ENVIRONMENT PROGRAM (2001): Depleted Uranium in Kosovo (2001). Post-conflict environmental assessment.

VAES, J.F. (1947): Six nouveaux minéraux d'urane provenant de Shinkolobwe (Katanga). *Ann. Soc. Géol. Belg.* **70**, 212-230.

VISWANATHAN, K. & HARNEIT, O. (1986): Refined crystal structure of β-uranophane $Ca(UO_2)_2(SiO_3OH)_2$•$5H_2O$. *Am. Mineral.* **71**, 1489-1493.

WADSEN, T. (1977): The oxidation of polycrystalline uranium dioxide in air at room temperature. *J. Nucl. Mater.* **64**, 315.

WALKER, T.L. (1923): Schoepite, a new uranium minerals from Kasolo, Belgian Congo. *Am. Mineral.* **8**, 67-69.

WANG, R. & KATAYAMA, J.B. (1982): Dissolution mechanism for UO_2, and spent fuel. *Nucl. Chem. Waste Management* **3**, 83-90.

WRONKIEWICZ, D.J., BATES, J.K. GERDING, T.J., VELECKIS, E. & TANI, B.S. (1992): Uranium release and secondary phase formation during unsaturated testing of UO_2 at 90°C. *J. Nucl. Mater.* **190**, 107-127.

_____, _____, WOLF, S.F. & BUCK, E.C. (1996): Ten year results from unsaturated drip tests with UO_2 at 90°C: implications for the corrosion of spent nuclear fuel. *J. Nucl. Mater.* **238**, 78-95.

Received August 12, 2003, revised manuscript accepted September 8, 2004.